(4)

Technical Report 1154
June 1990
Volume III

Assessment of $Li/SOCl_2$ Battery Technology: Reserve, Thin-Cell Design

P. A. Mosier-Boss
S. Szpak

NAVAL OCEAN SYSTEMS CENTER
San Diego, California 92152-5000

J. D. FONTANA, CAPT, USN
Commander

R. M. HILLYER
Technical Director

ADMINISTRATIVE INFORMATION

The work described in this report was performed for the Office of the Chief of Naval Research, Arlington, VA 22217, and the Independent Exploratory Development Programs (IED), NOSC. The work described was performed by members of the Propulsion and Hydrodynamics Branch, Code 634, NOSC.

Released by
L. A. Parnell, Head
Propulsion and
Hydrodynamics Branch

Under authority of
R. H. Moore, Head
ASW Technology
Division

MA

CONTENTS

TECHNICAL PAPERS

PRESENTATIONS

1.0 INTRODUCTION

In choosing and developing a battery system, extensive research, i.e., computer modeling and electrochemistry experiments, is required. The kinetics of chemical and electrochemical reactions determine the operational characteristics of a battery, including discharge rate capability and shelf storage life. This in turn affects power output. Battery design also affects battery output, i.e., distance between the bipolar plates, thickness of the electrodes and spacers, materials used, uniformity of electrolyte flow, etc. To maximize the performance of a battery system, therefore, one must do basic research to identify the electrochemical and chemical process occurring within the battery. Too often this has not been done with the expected results.

With regards to the $Li/SOCl_2$ battery development program described in Volume I of TR 1154, this volume contains a compilation of technical papers and is a continuation of Volume II of TR 1154. These papers have appeared in refereed journals and books. In addition, abstracts of presentations given at meetings and a table of contents for the previous two volumes of TR 1154 are included. This work was performed as part of the Naval Ocean Systems Center Independent Exploratory Development program and constitutes a portion of a program whose goal is to establish a technology base for high-discharge rate $Li/SOCl_2$ batteries.

This page intentionally left blank.

2.0 TECHNICAL PAPERS

This section contains technical papers that support the Li/$SOCl_2$ battery development program described in Volume I of TR 1154. These papers have appeared in refereed journals and books.

RESEARCH NOTE

RESOLUTION OF VIBRATIONAL BANDS INTO VOIGT PROFILES

The traditional role of vibrational spectroscopy (e.g. i.r. absorption or Raman scattering) has been the identification of chemical groups and molecular symmetry. With modern instrumentation, not the least of which is inexpensive computation time, other aspects of molecular dynamics can be examined. Information on bond properties as well as inter- and intramolecular interactions can be assessed from frequencies and their shifts, band intensities, depolarization ratios and excitation profiles.

In practice, it is often necessary to resolve a complex band into its components. Such separation is not a new problem and various procedures have been employed. As a rule, this resolution is based on an arbitrarily assumed lineshape, usually a Lorentzian distribution modified by an auxiliary function [1, 2] or an inverse polynomial [3]. Moreover, the selection of the modifying functions has been made based on computation cost without an apparent physical justification.

Quantum mechanical arguments specify conditions under which a system comprised of Raman or i.r. active molecules, perturbed by an interaction with a radiation field, yields the Lorentzian lineshape [4]. These conditions are: a continuum of energy levels for each species and a decay time of the initial state due to the perturbing radiation that is long compared with the lifetime of the initial state. Concomitantly, the lifetime of the initial state must be long so that the indeterminancy of the initial level is small compared to the transition frequency. However, a purely Lorentzian profile is never attainable because of the Gaussian component associated with either the Doppler effect [4] or molecular interactions of a dispersive type.

While the width of the Lorentzian line is an intrinsic property of a molecule, depending on the ratio of the decay time to the lifetime of the initial state, the Gaussian distribution is related to the interaction with the environment, particularly with the nearest neighbors of the excited molecule. The observed excitation profiles arise from the convolution of the Lorentzian and Gaussian contributions and assume the form of the Voigt profile, Eqn. (1)

$$f(\nu, \nu_o, \Delta\nu_L, \Delta\nu_G) = \frac{2\ln 2}{\pi^{3/2}} \frac{\Delta\nu_L}{\Delta\nu_G^2} \int_{-\infty}^{\infty} \frac{e^{-y^2}}{a^2 + (\omega - y)^2} dy \quad (1)$$

where $a = \Delta\nu_L \sqrt{(\ln 2)}/\Delta\nu_G$, $\omega = 2(\nu - \nu_o)\sqrt{(\ln 2)}/\Delta\nu_G$ and ν_o, $\Delta\nu_L$ and $\Delta\nu_G$ are, respectively, the center frequency, and the full widths at half maximum of the Lorentzian and Gaussian distributions that characterize the line [4].

In a dynamic system composed of N number of species, the experimentally observed spectral band, $S(\nu)$, is ideally a superposition of N lines and can be approximated by the expression:

$$I(\nu) = C_o(\nu - \alpha) + \sum_{i=1}^{N} C_i f(\nu, \nu_{oi}, \Delta\nu_{Li}, \Delta\nu_{Gi}) \quad (2)$$

where the function $f(\ldots)$ is defined in Eqn. (1). Because $f(\ldots)$ is normalized, the C_i can be interpreted as the areas of the fundamental Lorentzian lines. To account for sloping baseline as well as for the tails of distant lines, a linear term, $C_o(\nu - \alpha)$, has been added.

The least square fit of Eqn. (2) to the experimental data is constructed by minimizing the test function, F, given by Eqn. (3):

$$F = \sum_{j=1}^{M} [S(\nu_j) - I(\nu_j)]^2/(M - P) \quad (3)$$

where M is the number of data points in the measured spectrum $S(\nu)$ and P is the number of variable parameters characterizing the spectral intensity calculated by Eq. (2). The minimization of F [Eqn. (3)] was carried out using the NELDER–MEAD algorithm [5]. The number of lines N is selected from consideration of the vibrational mode under investigation, the chemical nature of the components, as well as from the minimization procedure. Constraining the line widths to be greater than the data point separation and including the factor $(M - P)$ in Eqn. (3), places an upper limit on the value of N that will minimize F. The integral appearing in Eqn. (1) was evaluated by the method of ROMBERG quadrature [6] where the $+\infty$ and $-\infty$ limits were replaced by $+3$ and -3. Computational round off errors, truncation errors in evaluation of Eqn. (1), and scatter in the intensity data broaden the minimum in F, occasionally making it difficult to select the global minimum from several local minima. Except for the truncation error, this difficulty is not specific to the Voigt profile, nor to the NELDER–MEAD algorithm, but is characteristic of nonlinear optimization.

To illustrate, the band resolution and deconvolution procedures have been applied to two test cases: Raman scattering of $C_6H_5CH_3$ in the region 980–1040 cm^{-1} and the absorption of the CD_3CN–CCl_4 system in the region 2220–2310 cm^{-1}. Toluene was selected because it represents an inert solvent [7]. In contrast, owing to the clustering of CD_3CN molecules as well as interactions between CD_3CN and CCl_4 molecules [8, 9], the CD_3CN–CCl_4 system is clearly not an inert system. Carbon-13 NMR studies of the CH_3CN–CCl_4 system indicate the presence of $(CH_3CN)_2$, CH_3CNCCl_4, $(CH_3CN)_2CCl_4$ as well as monomeric CH_3CN [9]. Deconvolution of the CN stretch of a dilute solution of CH_3CN in CCl_4 was not done since the CN stretch, ν_2, of CH_3CN is complicated by a $\nu_3 + \nu_4$ combination band in Fermi resonance with it [12]. The C–H bending modes of toluene occur at 1004 and 1031 cm^{-1} and are not affected by combination bands, overtones, hot bands or Fermi resonance. The results of the deconvolution of the Raman lineshape are presented in Fig. 1 and tabulated in Table 1. The CD_3CN–CCl_4 system is more complex. The separation of the observed band into three Voigt profiles is shown in Fig. 2 and the results of deconvolution are summarized in Table 2.

A comparison of the Lorentzian and Gaussian widths of toluene and CD_3CN shows that the toluene bands have a greater Gaussian contribution whereas the CN stretch of CD_3CN shows a greater Lorentzian component. The difference between CD_3CN and toluene may simply reflect the kind of forces acting in the system. Toluene has a low dipole moment, 0.36 D [10]; consequently, the forces are primarily dispersive thus affecting the Gaussian component. On the other hand, CD_3CN has a large dipole moment, 3.92 D [10]; therefore, substantial dipole–dipole and dipole-induced dipole interactions occur in the CD_3CN–CCl_4 system. The

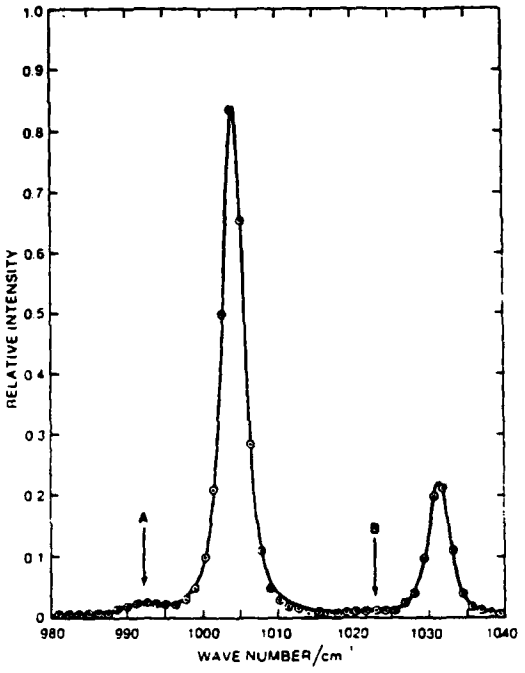

Fig. 1. Raman scattering in the C–H bending modes of toluene. Points indicate measured data, solid line is the computer generated fit (*cf.* Table 1). Arrow A—breathing mode of the benzene ring; arrow B—unidentified impurity.

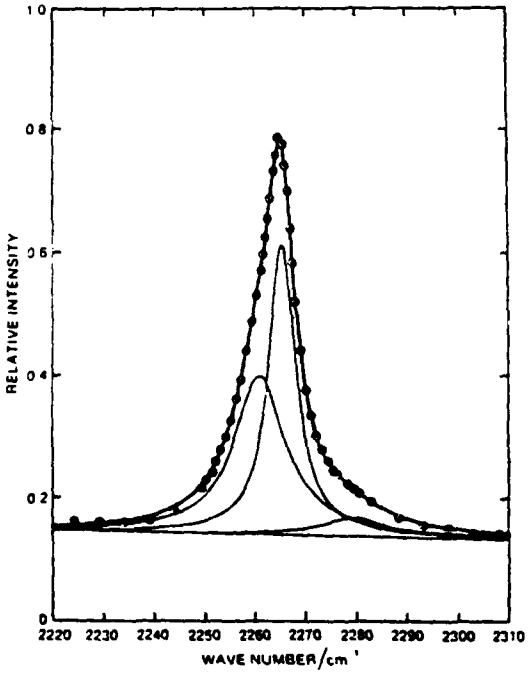

Fig. 2. Infrared absorption in the C≡N stretching region of CD_3CN–CCl_4 system. Points indicate measured data, heavy line is the computer generated peak, light lines are the Voigt profiles of the spectral band components calculated using Eqn. (2).

Table 1. Computer analysis of the C–H bending mode of toluene

ν_0 (cm^{-1})	$\Delta\nu_G$ (cm^{-1})	$\Delta\nu_L$ (cm^{-1})	C
0*	1.737	1.527	—
991.7	2.066	4.950	0.415
	1.120†	3.423†	
1004.1	2.285	1.964	3.939
	1.485†	0.437†	
1022.3	1.799	3.577	0.021
	0.470†	2.050†	
1031.2	2.215	2.019	1.045
	1.375†	0.492†	

* Voigt profile of the Rayleigh scattered line to determine the instrument function.

† The $\Delta\nu_G$ and $\Delta\nu_L$ have been corrected for the instrument function as follows

$$\Delta\nu_G = \sqrt{((\Delta\nu_{G,m})^2 - (\Delta\nu_{G,i})^2)}$$

$$\Delta\nu_L = \Delta\nu_{L,m} - \Delta\nu_{L,i}$$

(Subscripts i and m refer to the instrument function and the uncorrected values, respectively.)

Table 2. Computer analysis of the CN stretch of CD_3CN in CCl_4

	ν_0 (cm^{-1})	$\Delta\nu_G$ (cm^{-1})	$\Delta\nu_L$ (cm^{-1})	C
a	2260.7	0.725	12.48	1280
	2265.2	0.194	6.37	1189
	2278.9	1.172	14.15	161
b	2262.4	0.779	13.71	1990
	2265.4	0.184	5.14	683
c	2264.2	0.854	10.41	2528

a—three line fit, $F = 0.905$;
b—two line fit, $F = 3.92$;
c—one line fit, $F = 40.5$.

broadening of the lineshape by permanent dipoles has been shown to have a Lorentzian form [11]. Examination of Table 2 shows that the relative Gaussian contribution in each of the peaks composing the CN stretch differs. This may reflect the difference in the environment of the nitrile group in each of the species occurring in solution which should aid in line assignment. Line fitting alone, however, is insufficient to determine the molecular dynamics and additional information is required for this purpose.

The use of a Voigt profile has several advantages over other proposed lineshapes; formost, (i) a possible physical interpretation, secondarily, (ii) a requirement of only three "non-linear" parameters per line, and for emission spectra only [13], (iii) an easy subtraction of the instrument contribution to the calculated lineshape, if the instrument function has also a Voigt profile. However, as with any technique, there are disadvantages. These include: (i) the computer time required to evaluate the integral in Eqn. (1), and (ii) the lack of generality in the attainable lineshapes. However, since this integral is a convolution, a fast Fourier transform algorithm could be used to speed up its evaluation [6] and, while inverse polynomials may yield better fits, parameters having little, if any, physical significance may have been introduced by such a procedure.

Naval Ocean Systems Center, San Diego, CA 92152-5000, U.S.A.

C. J. Gabriel
P. A. Mosier-Boss
S. Szpak

REFERENCES

[1] A. R. DAVIS, D. E. IRISH, R. B. RODEN and A. J. WEERHEIM, *Appl. Spectrosc.* **26**, 384 (1972).

[2] B. FAHYS, D. RENDOT and J. MIGNOT, *Spectrochim. Acta* **34A**, 889 (1978).

[3] C. BAKER, W. F. MADDAMS, J. G. GRASELLI and M. A. S. HAZLE, *Spectrochim. Acta* **34A**, 761 (1978).

[4] B. DIBARTOLO, *Optical Interactions in Solids*. Wiley, New York (1968).

[5] J. C. NASH, *Compact Numerical Methods for Computers: Linear Algebra and Function Minimization*. Wiley, New York (1979).

[6] R. BARAKAT, *The Computer in Optical Research. Methods and Applications* (edited by B. R. FRIEDMAN). Springer, Berlin (1980).

[7] O. POPOVYCH, *Nonaqueous Solution Chemistry*. Wiley, New York (1981).

[8] J. YARWOOD, R. ARNDT and G. DOGE, *Chem. Phys.* **25**, 387 (1977).

[9] P. A. MOSIER-BOSS and A. I. POPOV, *J. Am. chem. Soc.* **107**, 6168 (1985).

[10] *Handbook of Chemistry and Physics*, 65th edn. (edited by R. C. WEAST). Chemical Rubber, Cleveland (1984).

[11] R. G. BREENE, JR., *The Shift and Shape of Spectral Lines*. Pergamon Press, New York (1961).

[12] S. L. DUNCAN, D. C. MCKEAN, F. TULLINI, G. D. NIVELLINI and J. P. PENA, *J. molec. Spectrosc.* **69**, 123 (1978).

[13] Y. S. CHANG and J. H. SHAW, *Appl. Spectrosc.* **31**, 213 (1977).

Reprinted from JOURNAL OF THE ELECTROCHEMICAL SOCIETY
Vol. 134, No. 11, November 1987
Printed in U.S.A.

Comments on Electroreduction of $SOCl_2$

M. J. Madou*

SRI International, Menlo Park, California 94025

J. J. Smith*

Naval Weapons Center, China Lake, California 93555-6001

S. Szpak*

Naval Ocean Systems Center, San Diego, California 92152-5000

ABSTRACT

The complexity of the electroreduction of $SOCl_2$ on inert electrode surfaces is examined. Comments concerning the reaction path are based on rest potential measurements, cyclic voltammetry, *in situ* IR spectroscopy, and response of the electrode electrolyte interphase to illumination. Experimental difficulties due to film formation are emphasized.

In recent years, primarily due to its importance in battery technology, the electroreduction of $SOCl_2$ has been discussed extensively. A number of reaction paths have been proposed (1-4), unfortunately, without irrefutable experimental evidence offered in support. Theoretical modeling (5) defined the cell operational parameters as a function of electrode reaction kinetics and the physicochemical properties of the system. In particular, the nature of the prepassive film, the morphology of the LiCl precipitate, as well as its induction period and growth rate, appear to dominate the cell performance.

In this communication, we examine selected aspects of the $SOCl_2$ reduction, and comment specifically on the properties of prepassive and passive films, in the presence and absence of $AlCl_3$ and/or catalytic substances, e.g., metal phthalocyanines. As a part of this discussion, we describe the photoeffects reported earlier for the C/$SOCl_2$, and extend this observation to Pt/$SOCl_2$ and Au/$SOCl_2$ interphases as well. We illustrate the effect of the excess of $AlCl_3$ on the reaction path through the use of *in situ* IR spectra. We conclude this communication emphasizing the complexity of the electroreduction and the need for including other than purely electrochemical steps in the description of cells employing $SOCl_2$. It is our intent to put forth some new thoughts on the mechanism and processes accompanying the electroreduction of $SOCl_2$. These thoughts, while speculative, offer guidelines for further exploration.

Experimental

The description of the electrochemical cell, apparatus, and preparation of solutions employed in this investigation has been given previously (7). The *in situ* infrared data were taken using the cell and experimental arrangement described in Ref. (8). Data on the effect of phthalocyanines are based on cyclic voltammograms and ac impedance measurements. The photoeffects were observed using conventional photoelectrochemical techniques.

The effect of the addition of $AlCl_3$ and of Co-phthalocyanine (Co-Pc) on the rest potential was examined in a U-cell provided with two compartments separated by a fritted glass disk. In this cell, one compartment contained a Li reference electrode immersed in neutral electrolyte, the other contained a test electrode immersed in an electrolyte modified by addition of either $AlCl_3$, Co-Pc, or both.

Results

Rest potential.—As shown in Table I, the addition of $AlCl_3$ causes the rest potential of carbon and molybdenum electrodes to become about 300 mV more positive, while the Li electrode potential remains unaffected. The addition of Co-Pc also shifted the rest potential in the positive direction, but by only 100 mV. When both substances were added simultaneously, the potential shift was about 400 mV, i.e., the observed potential displacement was additive. The Li electrode always remained at the same potential, irrespective of solution composition. Consequently, the Li electrode can serve as a good reference electrode, while both C and Mo immersed in $SOCl_2$ based electrolytes behave as electrodes of the first kind.

Current/potential relation.—The effect of the addition of $AlCl_3$ on the current/potential relationship is illustrated in Fig. 1. In particular, curve a is a voltammogram recorded in a 1*M* $LiAlCl_4$ solution in $SOCl_2$. Curves b and c are voltammograms in solutions containing 0.07*M* $AlCl_3$ + 0.93*M* $LiAlCl_4$ in $SOCl_2$, and 0.6*M* $AlCl_3$ + 0.4*M* $LiAlCl_4$ in $SOCl_2$, respectively.

The addition of $AlCl_3$, even in small amounts, generates a new peak, peak A, located approximately 200 mV positive with respect to the $SOCl_2$ reduction peak in neu

*Electrochemical Society Active Member

Table I. Open-circuit potential measurements in a U-type cell, between two Li electrodes, and between Li and C, and Li and Mo

	1.6*M* $LiAlCl_4$	1.6*M* $LiAlCl_4$ + di-Li-Pc	1.6*M* $LiAlCl_4$ + CoPc	1.6*M* $LiAlCl_4$ + $AlCl_3$	1.6*M* $LiAlCl_4$ + $AlCl_3$ + CoPc
Li/Li	0	0	0	0	0
Li/C	3.6	3.6	3.7	3.9	4
Li/Mo					

tral solutions, peak B. The height and position of peaks A and B depend, in a complex way, on the concentration and the ratio of $AlCl_3/LiAlCl_4$. Specifically, as the ratio $AlCl_3/LiAlCl_4$ increases, peaks A and B become broader, their separation increases, and they are displaced in the cathodic direction, curve c, Fig. 1. Voltammograms exhibiting similar features were recorded for the reduction of $SOCl_2$ on smooth Pt electrodes in neutral and acidic electrolytes (Fig. 2, curves a and b, respectively). Peaks associated with the reduction of $SOCl_2$ and SO_2 are more pronounced here.

The appearance of a new reduction peak in electrolytes containing an excess of $AlCl_3$ can arise from a number of factors, the most likely being a change in the reaction path resulting from the formation of different molecular species in acidic electrolytes. The appearance of different species and their participation in the electroreduction is demonstrated by *in situ* IR spectra and the difference exhibited within the 500-800 and 1100-1300 cm^{-1} wave number regions (Fig. 3).

The addition of Me-Pc to a neutral solution causes the peak current to increase and the peak potential to shift in the anodic direction. The magnitude of the peak current and its position depend on the complexed central ion. This dependence is illustrated in Fig. 4, where voltammograms obtained in electrolyte containing Co-Pc, Fe-Pc, and Cu-Pc are shown alongside the voltammogram in 1*M* $LiAlCl_4$ solution only (curves d, c, b, and a, respectively). Although the peak current and potential depend on the complexed central ion, the total charge transferred in the period between the initiation of reduction and passivation of the electrode surface, is about the same.

The catalytic activity of the Me-Pc can be demonstrated using ac impedance measurements. Figure 5 shows a Nyquist plot for neutral solution (curve a) and for the same solution containing Fe-Pc (curve b). The addition of Fe-Pc yields a semicircle, but its radius is substantially smaller, indicating that the interfacial transfer resistance is less in the presence of the catalyst (Co-Pc behaves similarly, while Cu-Pc shows only negligible effect).

Prepassive film.—The potential region where the electrode surface remains free from a prepassive film is relatively narrow (70 mV). Within this region, the reaction is kinetically controlled (7). It is noteworthy that, when Bu_4NPF_6 (Bu for butyl) is substituted for $LiAlCl_4$, the electrode surface remains free from filming through the range of overpotentials where the prepassive film is normally generated. We did not observe any current limitations within the range of our instrument, *i.e.*, up to 1A. In such an electrolyte, kinetic studies can, thus, be extended over a much wider range of overpotentials.

The removal of passive films can be accomplished by either mechanical means, or by holding the electrode at potentials positive to the rest potential, *e.g.*, at 4.5V *vs.* Li reference. The restoration of the electrode surface to its original state, by mechanical means, is more difficult when such films are formed in the presence of dissolved Me-Pc; there is no effect on the electrochemical removal.

Illumination of the passivated electrode surface with UV radiation enhanced the electroreduction of $SOCl_2$ on all surfaces investigated (Fig. 6). The largest effect was observed on the carbon electrode, curve a, the smallest on an Au electrode, curve d (Fig. 6). The enhancement depends on the electrode potential, alternatively, on passive film thickness, as demonstrated by comparing curve b with c, curve c being deeper into the passive region.

Discussion

The necessary condition for the initiation of an electrochemical process is the intimate contact between the reactive species and a phase boundary where the charge transfer occurs. This requirement implies that an approach step must precede the charge transfer step and, furthermore, it suggests that an electrocatalyst may affect more than one of the elementary processes comprising the overall reaction pathway. Electrocatalysis may be viewed as a special case of heterogeneous catalysis, inasmuch as the catalyst must be in contact with an electronically conductive substrate which functions as either electron source or sink. When the catalyst is applied in the form of a thin film, it must be sufficiently conductive to prevent substantial ohmic losses. Alterna-

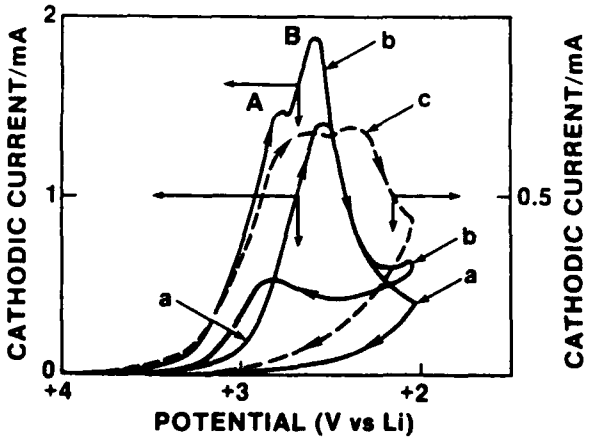

Fig. 1. Cyclic voltammograms on glassy carbon: scan rate—50 mV s^{-1}, electrode area—0.312 cm^2, and electrolyte—curve a (1M $LiAlCl_4$ in $SOCl_2$), curve b (0.93M $LiAlCl_4$ + 0.07M $AlCl_3$ in $SOCl_2$), and curve c (0.4M $LiAlCl_4$ + 0.6M $AlCl_3$ in $SOCl_2$).

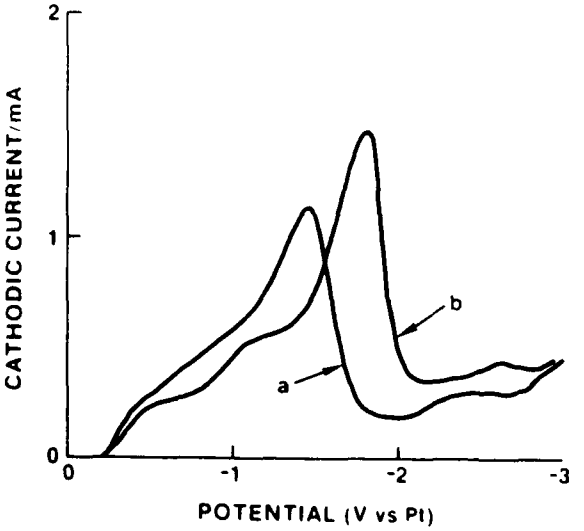

Fig. 2. Cyclic voltammograms on smooth platinum: scan rate—50 mV s^{-1} and electrolyte—curve a (1.5M $LiAlCl_4$ in $SOCl_2$), and curve b (0.75M $LiAlCl_4$ + 1.5M $AlCl_3$ in $SOCl_2$). Pt-reference electrode.

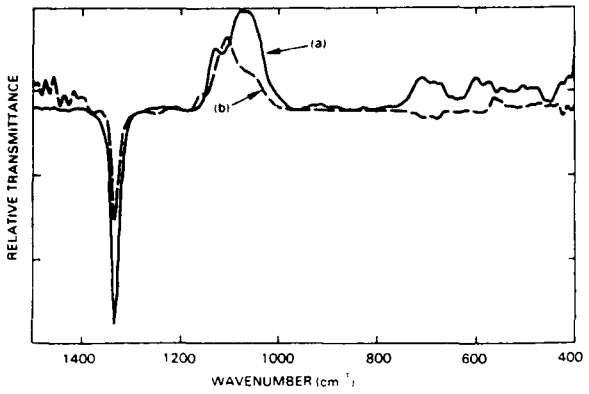

Fig. 3. *In-situ* IR adsorption spectrum: electrode—smooth platinum and electrolyte—curve a (0.75M $LiAlCl_4$ + 0.75M $AlCl_3$ in $SOCl_2$, at 1.8V vs. Pt reference), and curve b (1.5M $LiAlCl_4$ in $SOCl_2$, at 1.8V vs. Pt-reference).

tively, the electrocatalytic substance may be dissolved in the electrolyte. In such a case, active sites may be created on an otherwise inactive substrate by chemisorbed active material.

The formation of various complexes in $SOCl_2$ based electrolytes and their involvement in the electroreduction has been established, however, their properties are, at the present time, not entirely known. Furthermore, complexation involving reaction products such as SO_2 cannot be excluded (9, 10). The combination of these factors precludes detailed evaluation at this time.

Rest potential.—An Evans type representation of the log i *vs.* V curves for the reduction and oxidation of the $SOCl_2$-$LiAlCl_4$ solution implies that the rest potential observed on glassy carbon electrodes is an example of mixed potential (7). The displacement of the rest potential upon the addition of $AlCl_3$ to a neutral solution arises from differences in reactants and products, as illustrated in Fig. 7. In the presence of excess $AlCl_3$, the potential displacement is due to the formation of a more stable product, $LiAlCl_4$, while in neutral solutions it is due to the formation of LiCl. Theoretical calculations predict the displacement of ΔE_r between 530 and 630 mV, depending upon the value of the equilibrium constant, K, for the reaction

$$LiCl + AlCl_3 \overset{K}{\rightleftharpoons} LiAlCl_4 \qquad [1]$$

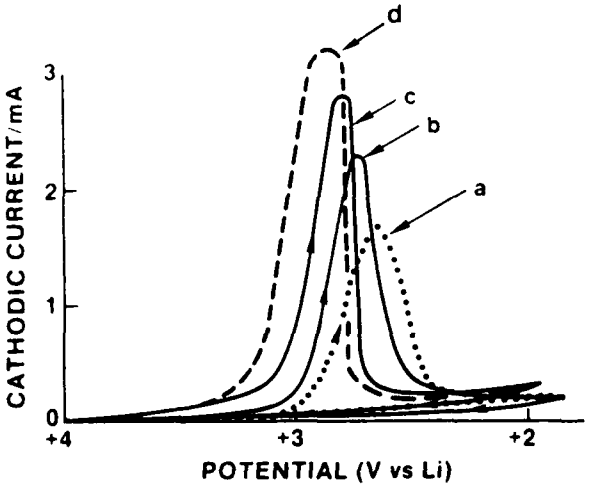

Fig. 4. Cyclic voltammograms on glassy carbon: scan rate—50 mV s^{-1}, electrode area—0.314 cm^2, and electrolyte—1.0M $LiAlCl_4$ in $SOCl_2$. Curve a (no additives), curve b (saturated with Cu-Pc), curve c (saturated with Fe-Pc), and curve d (saturated with Co-Pc).

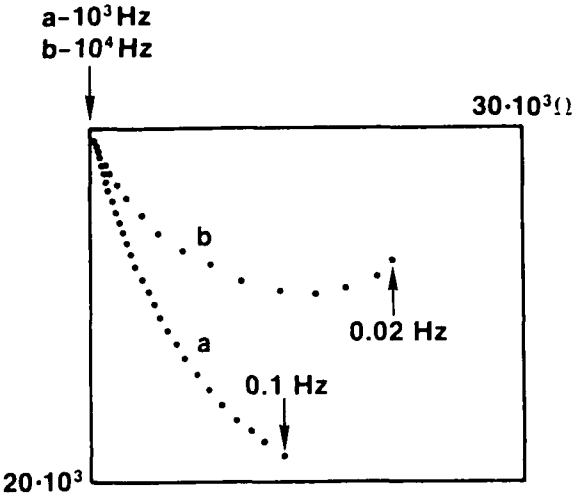

Fig. 5. Nyquist plot: electrode (glassy carbon) and electrolyte (1M $LiAlCl_4$ in $SOCl_2$), curve a (no additive), and curve b (saturated with Fe-Pc).

In acid solutions, $AlCl_3 \cdot SOCl_2$ adducts are the reactants, *i.e.*, the rest potential should be less by ΔE_r arising from reaction [2]

$$SOCl_2 + AlCl_3 \overset{K_1}{\rightleftharpoons} AlCl_3 \cdot SOCl_2, (n = 1,2) \qquad [2]$$

Unfortunately, the K_1 value for reaction [2] is not known. However, by taking the complexation of $SOCl_2$ into account, a more stable reactant is made, *i.e.*, ΔG, and, therefore, ΔE will also be lowered, with respect to the situation where no complexation is assumed. The complexation, therefore, accounts for the lower than theoretically expected value for V_{oc}, listed in Table I.

The observed shift of the electrode rest potential associated with the addition of Co-Pc is consistent with the concept of a mixed potential, inasmuch as the presence of a catalyst cannot affect a true reversible potential. The additivity of the rest potential shift by 100 mV suggests a complex reaction path, with the Me-Pc affecting that ele-

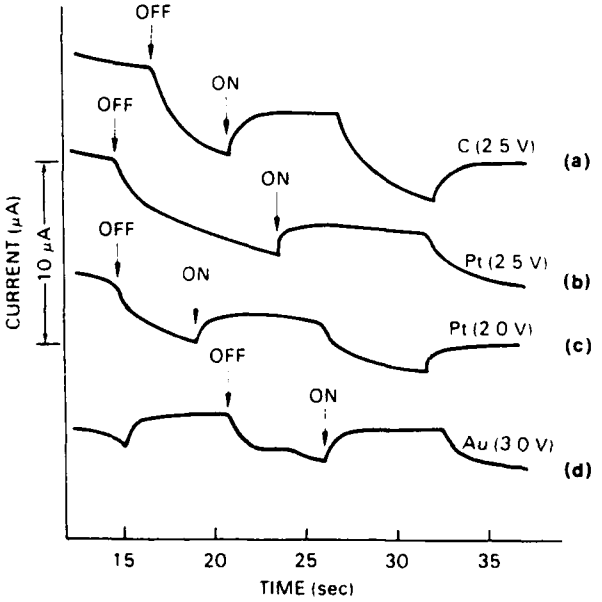

Fig. 6. Effect of illumination on reduction of $SOCl_2$: a—glassy carbon electrode at 2.5V, b—platinum electrode at 2.5V, c—platinum electrode at 2.0V, and d—gold electrode at 3.0V. All potentials vs. Li reference electrode.

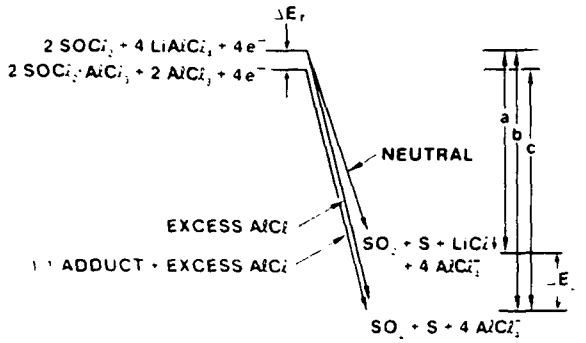

Fig. 7. Energetics of the $LiCl-AlCl_3-SOCl_2$ system

mentary process whose rate depends on bulk composition. Alternatively, by analogy to a redox couple, the shift in positive direction indicates either an increase in the concentration of oxidizing, or a decrease in reducing species arising from, *e.g.*, interaction of these species with solvent molecules. The latter view is in agreement with the findings reported by Myers *et al.* (11), namely, that $SOCl_2$ reacts with Me-Pc (Me = Cr^{II}, Mn^{II}, Fe^{II}, and Co^{II}) to form oxidized species, but not with Me = Cu. It is noteworthy that the total effect of Me-Pc on the $SOCl_2$ electroreduction is more complex than indicated by the 100 mV shift (12).

Effect of excess $AlCl_3$.—The presence of a second peak in neutral solutions was first reported by Doddapaneni (13) and interpreted as evidence of a two-step process in the reduction of $SOCl_2$. However, he observed the additional peak only under special circumstances, namely, on stress-annealed graphite electrodes, on dry surfaces, and during the first cycle. Blomgren *et al.* (14) has also reported the appearance of a second peak in neutral solutions. A similar behavior is seen in Fig. 2. Evidently, the appearance of additional peaks in neutral solutions is related to the state of electrode surface. In contrast to the results in neutral solutions, the peaks in acid solutions were always reproducible in successive voltammograms. At present, we attribute the appearance of two peaks in acid solutions to the change in properties of the electrolyte phase, primarily to the formation of an $AlCl_3 \cdot SOCl_2$ adduct.

The dependence of voltammograms on $AlCl_3$ concentration, shown in Fig. 1, is difficult to analyze in view of the complexity of the $LiCl-AlCl_3-SOCl_2$ system (9, 10). With the addition of $AlCl_3$, not only does the conductivity of the electrolyte change, but so does its structure. The ion-ion and ion-solvent interactions, as well as formation of yet unidentified aggregates (10), make a definite interpretation of the voltammograms impossible at the present time. Nevertheless, certain conclusions can be drawn. First, the appearance of an additional peak in acid solutions cannot be due to two-step reduction of $SOCl_2$ because, in such a case, a merger of these peaks would not have occurred at higher $AlCl_3$ concentrations. Second, peak A cannot be associated with the observed step-like change in the voltage-time curves of a discharging $Li/SOCl_2$ cell, attributed to the exhaustion of $AlCl_3$ (15), since peak A is reproduced in consecutive cycles. Third, peak A cannot be due to SO_2 reduction because it occurs at higher potentials (*i.e.*, at 2.4V, as in Fig. 2). This latter conclusion has also been verified by *in situ* IR spectroscopy (17).

The complexity of the $SOCl_2$ reduction path is further illustrated by examining the IR spectral region, shown in Fig. 3. This region contains the principal vibrational frequencies for the major constituents of the electrolyte, *viz.*, $SOCl_2$, $AlCl_3$, and $LiAlCl_4$, as well as complexes involving reactants and reaction products. In a separate investigation we have been examining the electroreduction of thionyl chloride electrolyte solutions using the spectroscopic technique, SNIFTERS (16). The resultant spectra reveal several important features of the thionyl chloride reduction process. Figure 3 shows the SNIFTERS spectra for the electroreduction of (a) 1.5*M* $AlCl_3$ + 1.5*M* LiCl and (b) 1.5*M* $AlCl_3$ + 0.75*M* LiCl thionyl chloride solutions, neutral and acid, respectively. In both cases, the most identifiable product, increased absorption, is sulfur dioxide, which yields the characteristic absorption at 1339 cm^{-1}. The apparent reactant(s), decreased absorption, is, however, different for the neutral and acidic solutions, as shown by the distinct differences in absorption in the 1000 to 1200 and 400 to 800 cm^{-1} regions. The strong feature near 1100 cm^{-1}, in both cases, likely involves complexed thionyl chloride. We have previously shown that the absorption in this region for the acidic solution is due, in part, to the $AlCl_3 \cdot SOCl_2$ complex, and results from a perturbation of the sulfur-oxygen stretching frequency of the thionyl chloride (17). Figure 3 clearly shows that this complex is one of the principal reactive species in acid solution, an observation which is consistent with the results of Tsaur and Pollard (5). The species responsible for the decreased absorption near 1100 cm^{-1} in neutral solution has not been identified conclusively. At present, we believe this reactant to be a thionyl chloride complex, possibly with Li^+ ion; the observed frequency is due to a moderately perturbed sulfur-oxygen stretching vibration. Such complexes have been reported earlier from Raman spectroscopic investigations (18). A portion of the rich vibrational spectra below 800 cm^{-1} is also due to the thionyl chloride complexes. While a complete assignment of the absorptions in this region has yet to be made, Fig. 3 does show the difference in behavior between acid and neutral electrolytes in this frequency range.

Even this qualitative description of the effect of excess $AlCl_3$ on the process of $SOCl_2$ electroreduction points out, rather clearly, the complexity of the reaction path. Thus, it is not surprising that the cell modeling predicts a correct behavior only prior to the onset of kinetic control and/or film formation (19). Results of an extensive analysis of the $SOCl_2$ electroreduction based on the survey of the IR spectra will be given elsewhere.

Effect of Me-Pc.—Examination of Fig. 1 and 4, together with information assembled in Table I, leads us to conclude that the participation of Me-Pc in the electroreduction of $SOCl_2$ differs fundamentally from that of $AlCl_3$. In both cases, however, the kinetically controlled region is relatively narrow. Thus, the usual requirements concerning selection of a suitable reference point for comparison of electrocatalytic activities (20) is especially important here. In principle, the determination can be carried out, either by comparing currents at a fixed overpotential within a region where reaction is under kinetic control, or by measuring the electron transfer resistance at the open circuit. A catalyzed reaction will lead to small resistance or larger exchange current density.

The observed catalytic activities of Me-Pc, where Me = Co, Fe, Cu, and Li, decrease in the following order: Fe > Co >> Cu > Li (with no activity associated with Li-Pc), *i.e.*, in the same order as reported for the electroreduction of oxygen (21, 22). This observation, in turn, was offered as indication of the weakening of the S=O bond arising from the interaction of the $SOCl_2$ molecule with the central metal ion of the N_4 chelates. A word of caution, in contrast to the reduction of O_2 (21, 22), details of the reaction path for the reduction of $SOCl_2$ are not known. Furthermore, because $SOCl_2$ is a weak donor [0.4 on the Gutmann scale (23)], it may form complexes with the reaction products and catalytic activities may not be limited to the charge transfer reaction, but, may directly or indirectly, affect other elementary processes as well.

The nature of the prepassive film.—Chakhov *et al.* (6) reported that vitreous carbon and pyrolytic graphite, when immersed in $SOCl_2$ based electrolytes, behave like p-type semiconductors with a 2 eV bandgap. They attributed this behavior to the formation of a surface compound, presumably a solid film, leading to the electrode passivation through a decrease in the concentration of

free electrons in the surface layers. Upon illumination of the surface, there is an increase in the concentration of free electrons, and, hence, an increase in reduction of $SOCl_2$. However, since these effects are also seen on metallic electrodes (*e.g.*, Pt and Au), any model relying exclusively on involvement of carbon corrosion products is, therefore, incomplete.

A common factor associated with observed photoeffects is the presence of LiCl film. A stoichiometric LiCl film is an insulator with a 9.0 eV bandgap; consequently only a presence of nonstoichiometric film, Li_xCl_y, could account for the observed response to illumination. In particular, the presence of cation vacancies in the LiCl film can provide a narrow space charge region at the electrode/LiCl interphase to allow for electron tunneling (24). The flow of electrons into the conduction band, or into localized states within the LiCl film, would be enhanced by illumination. Whether or not corrosion of the electrode material modifies the solid LiCl structure and allows for semiconducting properties, cannot be stated at this time. Noting the magnitude of the photoeffect, and correlating it with the stability of electrode material in the $SOCl_2$ electrolyte, we would have to admit that it is possible, except that the Au/$SOCl_2$ interphase is stable in this electrolyte (25), thus leaving the explanation of Chakhov *et al.*, involving participation of corrosion products, in doubt.

Concluding Remarks

The electroreduction of $SOCl_2$ on an electrode surface is a complex process. A number of possible pathways have been proposed, but none have been fully supported by experimental evidence. It is increasingly clear that the S=O group plays an important role in the electroreduction process. The evidence has been presented, implying that the presence of reactive species perturbs the S=O bond strength. In particular, we offer the following comments.

1. The kinetics of electroreduction can be examined only within a narrow range of overpotentials.

2. The electrode rest potential is a mixed potential. An excess of $AlCl_3$ and the presence of Me-Pc shifts the rest potential in positive direction, by 300 and 100 mV, respectively. The additivity of this shift suggests that $SOCl_2$ molecules interact differently with $AlCl_3$, than with Me-Pc.

3. The IR absorption spectra demonstrate the participation of $AlCl_3 \cdot SOCl_2$ complexes in the charge transfer process in acidic solutions. Furthermore, it shows that a different reaction path occurs in neutral electrolytes.

4. Prepassive films formed during the $SOCl_2$ reduction on glassy carbon, platinum, and gold electrodes exhibit semiconducting properties. This behavior is attributed to the modification of the structure of the LiCl film.

Acknowledgment

This work was supported, in part, by the Naval Sea Systems Command 63R3 and, in part, by the Office of Naval Research.

Manuscript submitted Sept. 8, 1986; revised manuscript received April 3, 1987.

Naval Ocean Systems Center assisted in meeting the publication costs of this article.

REFERENCES

1. N. Doddapaneni, Abstract 315, p. 505, The Electrochemical Society Extended Abstracts, Vol. 82-2, Detroit, MI, Oct. 17-21, 1982.
2. B. Carter, R. Williams, F. Tsay, A. Rodriques, and H. Frank, Paper 829110 presented at the Proceedings of the 17th IECEC Conference, Los Angeles, CA (1980).
3. W. A. Bowden and A. N. Dey, *This Journal*, **127**, 1419 (1980).
4. W. K. Istone and R. J. Brodd, *ibid.*, **129**, 1863 (1982).
5. K. C. Tsaur and R. Pollard, *ibid.*, **131**, 975, 984 (1984), K. C. Tsaur and R. Pollard, ibid., **133**, 2296 (1986).
6. N. I. Chakhov, Yu. M. Povarov, and Yu. V. Pleskov, *Elektrokhimiya*, **16**, 1445 (1980).
7. M. J. Madou and S. Szpak, *This Journal*, **131**, 2421 (1984).
8. A. Bewick, K. Kunimatsu, B. S. Pons, and J. W. Russell, *J. Electroanal. Chem.*, **160**, 47 (1984).
9. Y. Bedfer, J. Corset, M. C. Dhamelincourt, F. Wallart, and P. Barbier, *J. Power Sources*, **9**, 267 (1983).
10. S. Szpak and H. V. Venkatasetty, *This Journal*, **131**, 961 (1984).
11. J. F. Myers, G. W. R. Canham, and A. B. P. Lever, *Inorg. Chem.*, **14**, 461 (1975).
12. J. J. Smith, S. Szpak, and W. A. West, Power Source 11, Proceedings of the 15th International Power Sources Symposium, Brighton, England, Sept. 1986.
13. N. Doddapaneni, ERADCOM-TR-81-0381-F, Final Report.
14. G. E. Blomgren, V. Z. Leger, M. L. Krunenberg, T. Kalnooki-Kis, and R. J. Brodd, in "Power Sources 7," J. Thompson, Editor, Academic Press, New York.
15. K. A. Klinedinst and M. J. Domeniconi, *This Journal*, **127**, 530 (1980).
16. J. W. Foley, C. Korzeniewski, J. Daschback, and S. Pons, in "Electroanalytical Chemistry," A. J. Bard, Editor, Marcel-Dekker, New York, To be published.
17. J. J. Smith, S. Pons, J. Li, W. West, and S. Szpak, Paper Nr SW-2 presented at the Third International Meeting on Li-Batteries, Kyoto, Japan, May 1986.
18. G. Mairesse, Doctoral Thesis, University of Lille, Lille, France (1978).
19. J. R. Driscoll, R. Pollard, J. J. Smith, and S. Szpak, Power Sources 10, Proceedings of the 14th International Power Sources Symposium, Brighton, England, Sept. 1984.
20. D. D. McDonald and M. C. H. McKubre, in "Modern Aspects of Electrochemistry," Vol. 14, J. O'M. Bockris, B. E. Conway, and R. E. White, Editors, Chapter 2, Plenum Press, New York (1982).
21. E. Yeager, *This Journal*, **128**, 160 (1981).
22. G. Sandstede, "From Electrocatalysis to Fuel Cells," University of Washington Press, Seattle, WA (1972).
23. V. Gutmann, "Coordination Chemistry in Non-Aqueous Solutions," Springer-Verlag, Wien-New York (1968).
24. F. M. Delnick, W. R. Cieslak, D. E. Peebles, and J. W. Rogers, Jr., Abstract 40, p. 63, The Electrochemical Society Extended Abstracts, Vol. 86-2, San Diego, CA, Oct. 19-24, 1986.
25. J. R. Driscoll, Private communication (1986).

QUALITY ASSESSMENT OF UNACTIVATED CELLS BY A.C. IMPEDANCE TECHNIQUES

J. R. DRISCOLL*

Altus Corporation, San Jose, CA 95112 (U.S.A.)

S. SZPAK**

Naval Ocean Systems Center, Code 633B, San Diego, CA 92152-5000 (U.S.A.)

(Received October 1, 1985; in revised form November 25, 1985)

Summary

A.C. impedance measurements are demonstrated to be very effective in assessing the quality of reserve activated battery cells during fabrication. The impedance of four-cell bipolar batteries was measured over the frequency range 0.1 - 20 kHz. A parallel *RC* circuit was determined to be a good model for the unactivated cells. Capacitance is a sensitive measure of cell spacing consistency. Uniform and defect-free cells have a variation of ±3% in capacitance, and a sensitivity analysis of capacitance to cell spacing shows that this is equivalent to a ±1.5% variation in cell spacing. Bode plots identify defective cells with high resistance shorts not detectable through capacitance measurements.

Introduction

The development of high energy and high power batteries has received a great deal of attention in the last few years, particularly with the emergence of lithium-based systems. One design for high power applications is a bipolar reserve activated construction in which the basic unit contains a large number of series-connected cells. The final battery configuration may contain as many as 1000 or more cells with individual cell thickness in the submillimeter range. With this number of closely spaced cells, there is a clear need for a method of assuring cell quality both during and after fabrication in order to meet both electrical performance and safety goals. The requirement for cell quality assurance is not limited to systems of this design for it can be extended to other systems as well.

*Present address: Lockheed Palo Alto Research Laboratories, Palo Alto, CA 94304, U.S.A.

**Author to whom correspondence should be addressed.

One measure of cell quality during fabrication is the d.c. resistance of the dry cell. While this procedure will detect some defects, primarily internal shorts, it is not sensitive to other potential problems such as incorrect cell spacing or incorrect components. On the other hand, capacitance measurements [1, 2] have been used successfully as a measure of cell quality. In general, cell capacitance is sensitive to both low resistance internal shorts and cell spacing, but is insensitive to intermediate-level shorts.

Given the complimentary nature of the resistance and capacitance data, it was decided to explore the possibilities of using the more general a.c. impedance methods where both can be determined simultaneously in order to improve further the techniques of cell quality assessment. Should this prove useful, a computer based data aquisition system would make cell quality assessments reliable, rapid, and routine. This communication presents the results of an initial exploration.

Experimental

Test vehicle

Impedance measurements were made as a function of frequency on four-cell bipolar stacks. The nickel bipolar plates were 0.114 m in diameter and 5.1×10^{-5} m thick. Porous cathodes were fabricated from Shawinigan carbon black. In place of an active anode material stainless steel sheets were used. These were cut to the same dimensions and were 7.6×10^{-5} m thick. In the results reported here two separator systems were examined: a single layer of ceramic paper and a composite of three layers consisting of a layer of fibrous hemp against the cathode, a layer of 2.5×10^{-4} m unwoven glass fiber paper, and a layer of microporous polypropylene. Only three of the four cells in any one stack could be measured since one end of the stack had a plastic plate used for visual observations in other experiments.

Instrumentation

An Hewlett-Packard 4276A LCZ analyzer was used for the measurements. This instrument has a frequency range of 0.1 - 20 kHz. Spring clip probes were connected to small tabs spot welded onto the individual bipolar plates. The magnitudes of the impedance and phase angle were recorded at 13 frequencies between 0.1 and 20 kHz.

Results and discussion

Discussion of the experimental results will be in terms of the relation between cell capacitance and cell uniformity and the effect of cell defects on the overall impedance characteristics. The determination of these depends on the equivalent electrical circuit which, in turn, can be estimated from the frequency dependent behavior of the cell.

Equivalent circuit

An unwetted cell would be expected to behave as a parallel *RC* combination, since, in essence, it consists of two electronic conductors separated by a dielectric. Data from defect free cells confirm this expectation. Figure 1 is a plot in the admittance plane of the data for three defect-free cells and shows a linear correlation between the imaginary and real components with the angle of the lines to the real axis slightly less than 90°. This is in accordance with the frequency response of a parallel *RC* circuit. There is some departure from ideal *RC* behavior in the system. The admittance plots have a slight curvature at low frequencies and the angle of the lines to the real axis is not exactly 90°. This non-ideal behavior can be attributed to frequency dependent energy loss mechanisms in a real system which are not due solely to d.c. resistivity [3 - 5].

All the cell data showed similar behavior and thus, initially, a simple parallel *RC* network was taken as a reasonable basis for further analysis of the data.

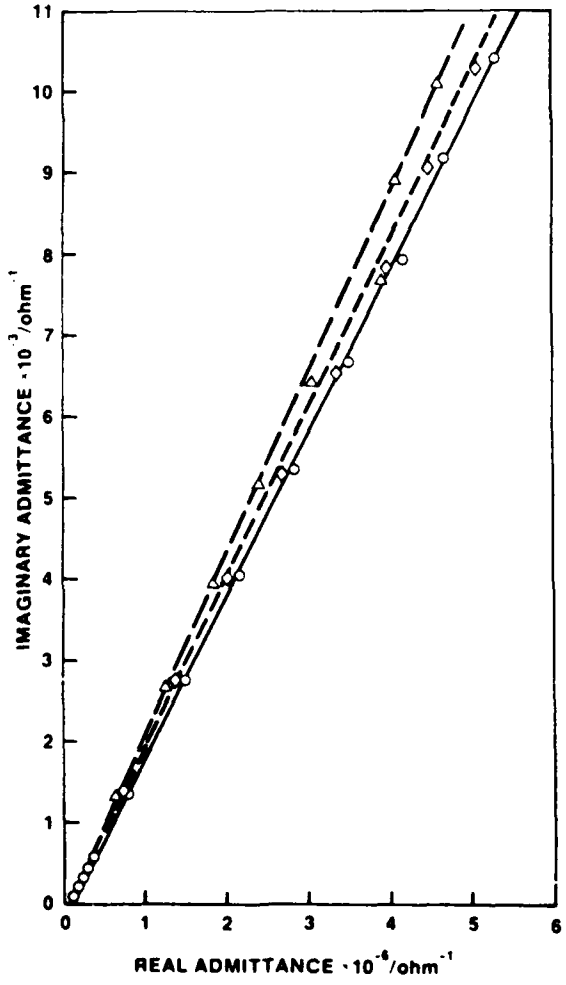

Fig. 1. Data for 3 identical cells plotted in the admittance plane. The nearly vertical lines indicate the cell can be modelled with a parallel *RC* circuit. (Note scale change between ordinate and abscissa.) ○, Cell 25-1; △, cell 25-2; ◇, cell 25-3.

Capacitance and cell uniformity

Given the parallel *RC* network model, capacitance is directly calculated from the impedance and phase angle as

$$C = \sin \theta / \omega Z \tag{1}$$

where C is the capacitance in farads, θ is the phase angle, ω is the radial frequency and Z is the magnitude of the impedance in ohms. The capacitance for a set of defect-free cells of the same design is quite consistent at all frequencies, with a standard deviation of about 3%. This is shown in Table 1 for data measured at 20 kHz. The excellent capacitance reproducibility for identically constructed cells is encouraging as a measure of consistency. This alone is important, but it is also important in establishing the sensitivity of the method to anomalous cell spacings.

An estimate of the sensitivity of capacitance to total cell spacing is obtained from the basic equation for capacitance and the cell data. Assuming the dielectric constant of the separator and the cell area remain constant as a function of cell thickness, the capacitance is given by the standard equation:

$$C = \epsilon_0 \epsilon A / (t - m) \tag{2}$$

where C is the capacitance in farads, ϵ_0 is the permittivity of free space, ϵ is the insulator dielectric constant, t is the total cell thickness, m is the thickness of the electrodes, and the term $(t - m)$ represents the dielectric thickness. The sensitivity of capacitance to changes in total cell thickness is given by eqn. (3), which is derived from eqn. (2) by taking the derivative of capacitance with respect to total cell thickness, dividing by eqn. (2) and rearranging.

$$dC/C = [-t/(t - m)]\, dt/t \tag{3}$$

The magnitude of the term $-t/(t - m)$ establishes the sensitivity of capacitance to cell thickness. The value of m was not experimentally measurable in these cells but was determined, on the assumption that the electrodes are incompressible at the specified cell dimensions, by rearranging eqn. (2) to eqn. (4) and performing a linear regression analysis.

TABLE 1

Capacitance of unwetted cells with composite separator

Cell spacing ($m \times 10^4$)	Capacitance (nF)	Standard deviation	Number of cells
4.70	0.641	0.017	6
4.45	0.717	0.017	9
4.19	0.828	0.019	6
3.94	0.915	0.020	7
3.68	1.02	0.039	5

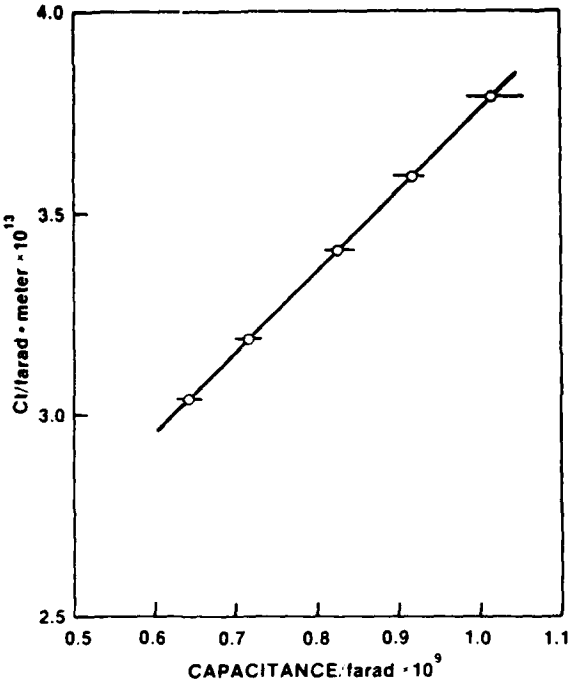

Fig. 2. A plot of the capacitance–thickness data according to eqn. (4) in the text for the determination of m and $\epsilon_0 \epsilon A$. The correlation coefficient of the linear fit is 0.986.

$$Ct = mC + \epsilon_0 \epsilon A \tag{4}$$

The values of m and $\epsilon_0 \epsilon A$ were calculated from the 33 data points of capacitance *versus* cell spacing summarized in Table 1. The result shows a good correlation, as illustrated in Fig. 2, with the values of m and $\epsilon_0 \epsilon A$ of 1.98×10^{-4} m and 1.77×10^{-13} farad-meter, respectively. These values are reasonable for the system. Since the anode thickness was 7.6×10^{-5} m, the cathode thickness in the compressed cell is the difference between this and $m - 1.22 \times 10^{-4}$ m. The dielectric constant of the compressed separator calculated from the value of $\epsilon_0 \epsilon A$ is 2.97, based on the electrode area of 6.7×10^{-3} m^2 and ϵ_0 equal to 8.9×10^{-12} farad/m.

Substitution of this value of m into eqn. (4) indicates that, for the range of cell thicknesses in these experiments, the relative change in capacitance is 1.7 - 2.2 times the relative change in cell thickness. Thus, capacitance is a sensitive measure of cell spacing uniformity. For example, the standard deviation of ±3% observed in the experimental cells translates to thickness deviations of about ±1.5%. It is clear, then, that anomalies which affect cell spacing, *e.g.*, the insertion of an extra component or the omission of a component, are detectable.

This analysis assumes an invariant dielectric constant for the separator, since variations in the separator, *e.g.*, porosity and composition, also will affect the measured cell capacitance. This implies that prior to cell fabrication the uniformity of the separators must be assured, which can easily be done with a.c. measurements in a standard test fixture.

Effect of cell defects

Determination of capacitance does not take full advantage of the information available with the a.c. method. High resistance shorts do not necessarily affect the capacitance but do affect the overall impedance behavior of the cell. This is illustrated in Fig. 3 where a Bode plot of the data from three cells with the ceramic paper are presented. The capacitance of all three cells was essentially identical, the average was 0.971 with an average deviation of ±0.020 nF. The Bode plots of the two defect-free cells have slopes of approximately −1 over the range of accessible frequencies, indicating that the impedance is dominated by the capacitive reactance down to at least 100 Hz. With no detectable contribution from the d.c. resistance, it is only possible to put a lower bound of approximately 3 MΩ on the actual cell resistance. If the cell resistance was less than this, the low frequency data points would begin to deviate from the linear relationship. This is illustrated by the behavior of the defective cell.

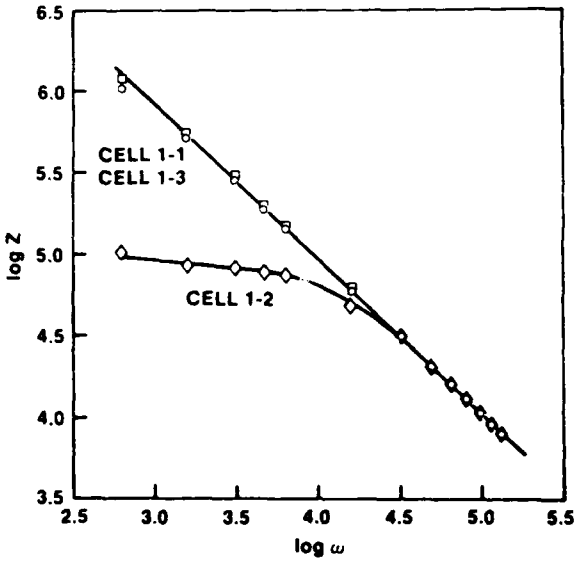

Fig. 3. Bode plot of the impedance data for 3 cells from battery #1. Cells 1 and 3 are defect free, thus the plots are linear with a slope of −1. Cell 3 has a high resistance short of 0.1 MΩ which dominates at the low frequencies. ○, Cell 1-1; □, cell 1-3; ◇, cell 1-2.

The Bode plot of the defective cell has an initial slope of −1 at the high frequencies, which is identical to the behavior of other cells. At lower frequencies, however, the slope gradually changes to 0, indicating dominance by the d.c. resistance of 100 kΩ. Post-test examination of the defective cell revealed a small perforation in the separator allowing the formation of a carbon track between the cathode and anode. This procedure identified all cells which were defective due to an internal short.

Conclusions

This exploratory investigation has shown that a.c. impedance techniques are valuable tools for assessing the quality of dry cells. One of the

advantages of the method is that it not only locates defective cells but also helps identify the nature of the problem. Moreover, it has been shown that capacitance is a sensitive function of cell spacing. Over the frequency range investigated, Bode plots of the data provide a good method of distinguishing shorted from unshorted cells. Unshorted cells have a slope of −1; deviations from this indicate a short in the cell which may not be indicated by the capacitance. Only lower bounds could be determined for the resistance of defect-free cells.

Acknowledgement

This work was funded by Naval Sea Systems Command (NAVSEA 63R3). We thank Mr Frank Romano for his interest and support.

References

1 K. L. Hampartzumian, in J. Thompson (ed.), *Power Sources 9*, Academic Press, New York, 1982.
2 Final Tech. Rep. — Advanced Lithium Battery Program, *Contract N00024-81-C-6124*, Altus Corp., 30 May, 1984.
3 A. K. Jonscher, *J. Mater. Sci., 13* (1978) 553.
4 K. S. Cole and R. H. Cole, *J. Chem. Phys., 9* (1941) 341.
5 J. R. MacDonald, *J. Appl. Phys., 34* (1963) 538.

Reprinted from JOURNAL OF THE ELECTROCHEMICAL SOCIETY
Vol. 135, No. 1, January 1988
Printed in U.S.A.

Photoeffects on Polarized Electrodes in the $SOCl_2$-$LiAlCl_4$ System

M. Madou,* T. Otagawa,* and S. Gaisford

SRI International, Menlo Park, California 94025

J. J. Smith*

Naval Weapons Center, China Lake, California 93555-6001

S. Szpak*

Naval Ocean Systems Center, San Diego, California 92152-5000

In 1980, Chakhov et al (1) reported that the C/$SOCl_2$-$LiAlCl_4$ interphase, while under cathodic polarization, exhibits p-type semiconductor behavior when illuminated. They attributed this behavior to the formation of an unspecified surface compound—presumably a solid film—containing corrosion products of the carbon surface. Furthermore, they suggested that within this film, upon illumination, the concentration of free electrons increases and, hence, the rate of the $SOCl_2$ reduction increases. Recently, Madou et al (2) extended these observations to other substrates, viz. Pt and Au and concluded that any model relying excusively on the involvement of carbon corrosion products is incomplete and that the precipitation of the LiCl film is the only common factor, ie, the presence of the LiCl film is a necessary condition for the observed cathodic photoeffect.

Pure LiCl is an insulator with an energy gap of 8.6 eV (3), while the light effective for increasing $SOCl_2$ reduction has a wavelength corresponding to a band gap of 2.0 eV. To reconcile this difference, we note that recent work (4) related to the growth of LiCl films accompanying the electroreduction of $SOCl_2$ invoked the existence of a narrow space charge region to allow for electron tunneling and the flow of electrons into localized states within this film. This flow of electrons would be enhanced by illumination.

This communication extends observations on the effect of illumination to the Si/$SOCl_2$-$LiAlCl_4$ interphase with n- type Si electrodes and provides further evidence that the presence of the LiCl film is a necessary condition for the cathodic photoeffects. Due to the preliminary nature of this investigation the discussion is mostly qualitative.

RESULTS

Cyclic voltammetry.--Figure 1 compares the cyclic voltammograms obtained in 1.0 M $LiAlCl_4$ in $SOCl_2$ electrolyte on n- type Si and Pt electrodes, curves a and b, respectively. The effect of illumination for n- Si is also included, curve a'. Switching of illumination on and off results instantaneously in curve a' or a, respectively. Note the very substantial photoeffect on the anodic branch of the current/potential curve, a large overpotential for the $SOCl_2$ reduction and a reduced potential for the oxidation of $SOCl_2$ on n- Si electrodes. Moreover, it is seen that illumination does not effect the $SOCl_2$ reduction regime. Anodic current can be maintained indefinitely whereas cathodic currents result in the passivation of the electrode surface. This current is not associated with a prior cathodic scan.

Time effects.--Figure 2 shows the current-time relation of a cathodically polarized electrode/electrolyte interphase. As illustrated, the response of the C/$SOCl_2$-$LiAlCl_4$ interphase to illumination is sluggish (3 to 5 seconds, curve a), being somewhat faster for the Pt/. . .(curves b and b' at potentials 2.5 and 2.0 V vs Li-ref, respectively) and Au/. . .(curve c) interphases but still lower than commonly observed for the relaxation of a typical semiconductor/electrolyte interphase. In summary, cathodic photoeffects are associated with C, Au and Pt and anodic photoeffects with n- Si. Moreover, the latter is much larger and exhibits a faster response time.

Passivation of the electrode surface.--The difference in the amount of transferred charge needed for the complete passivation of the electrode surfaces is shown in Fig. 3. It is seen that 4×10^{-4} coulombs, which is roughly equivalent to the formation of one monolayer of Li Cl, are required to passivate the Pt electrode, curve a, and ten times more to passivate an equal area of the Si surface, curve b. A slight etching of the Si electrode surface was visually observed.

DISCUSSION

Two types of photoeffects are seen. On C, Au and Pt electrodes there is a photo-enhanced reduction of $SOCl_2$ while on n-Si the photo enhancement is associated with $SOCl_2$ oxidation. The occurrence of photoeffects on other than C/$SOCl_2$-$LiAlCl_4$ interphases casts serious doubt concerning the conclusion reached by Chakhov et al. While corrosion products might contribute to the observed photoeffects on carbon surface, the degree of their participation is not clear. The most plausible explanation is the presence of a LiCl film which acts as a diffusion barrier

*Electrochemical Society Active Member.

barrier which becomes less effective upon illumination. Specifically, we propose the film to be non-stoichiometric LiCl film containing localized states which, upon illumination, enhance flow of electrons from the metal to the $SOCl_2$ electrolyte. The results on n- type Si, ie, no response to illumination of the cathodically polarized electrode, Fig. 1 -curves a and a', and an excessive amount of transferred charge to passivate its surface, Fig. 3 -curve b, show rather convincingly that the origin of the observed cathodic photoeffect must be attributed to the presence of the LiCl film on electrode surfaces and their absence on silicon.

In view of the rather limited solubility of LiCl in the electrolyte and the excessive amount of charge required for passivation, we conclude that the Si- electrode is not inert and, in effect, prevents the formation of the LiCl film, most likely by undergoing chemical oxidation by $SOCl_2$ to form $SiCl_4$ with further complexation to yield $SiCl_6^{2-}$. The dissolution of Si, ie, the removal of covalently bound atoms requires substantial expenditure of energy involving the participation of holes (5). It is a parasitic reaction which, over long periods of time, will consume both Si and $SOCl_2$. Specifically, during the course of $SOCl_2$ reduction, the Si^{4+} ions produced by corrosion compete effectively with Li^+ ions for Cl^- ions, thus delaying the onset of precipitation of LiCl.

CONCLUDING REMARKS

1. Cathodic photoeffects observed upon illumination of electrode/$SOCl_2$-$LiAlCl_4$ interphase are due to the presence of non-stoichiometric LiCl films.

2. The photo-electrochemistry of the Si/$SOCl_2$-$LiAlCl_4$ interphase is analogous to that of a Si electrode in other electrolytes.

3. The onset of passivation of a Si surface is considerably delayed, when compared with Pt, Au or C surfaces, due to the formation of soluble $SiCl_6^{2-}$ species.

Acknowledgement. This work was, in part, supported by the Office of Naval Research.

This was Paper 497 presented at the Philadelphia Meeting of the Society, May 1987.

REFERENCES

1. N. I. Chakhov, Yu. M. Povarov and Yu. V. Pleskov, Electrokhimiya, *16*, 1445 (1980).
2. M. J. Madou, J. J. Smith and S. Szpak, This Journal submitted.
3. A. J. Decker, Solid State Physics, Prentice Hall, Inc.
4. F. M. Delnick, R. W. Cieslak, D. E. Peebles and J. N. Rogers, The Electrochemical Society Fall Meeting, San Diego, CA, 1986.
5. H. Gerischer, *Semiconductor Electrochemistry* in *Physical Chemistry, An Advanced Treatise*, Vol. IX A, H. Eyring, D. Henderson and W. Jost, eds. Academic Press, New York-London, 1970.

Manuscript submitted June 5, 1987; revised manuscript received Sept. 4, 1987.

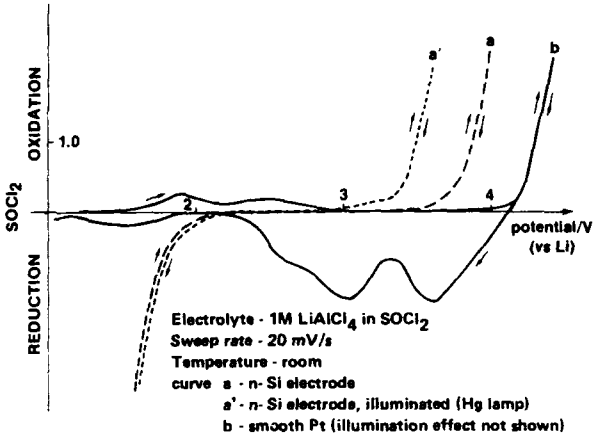

Figure 1. Cyclic voltammograms in $SOCl_2$-$LiAlCl_4$ system.

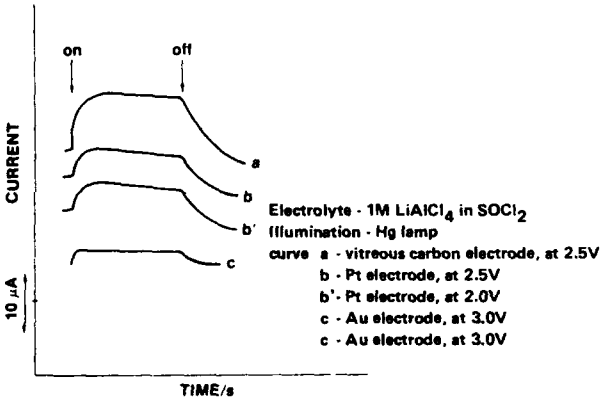

Figure 2. Response of electrode/electrolyte interphase to illumination.

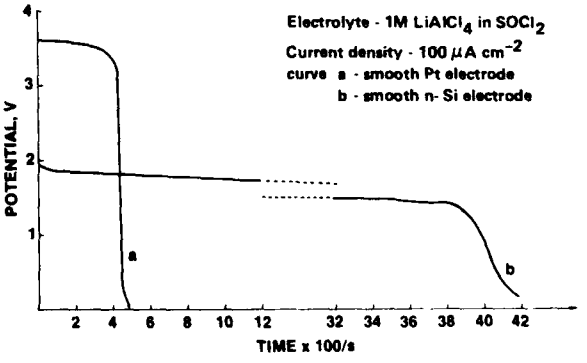

Figure 3. Potential/time curves for $SOCl_2$ reduction at constant current.

The Naval Ocean Systems Center assisted in meeting the publication costs of this article.

ROLE OF Fe–Pc IN A DISCHARGING Li–$SOCl_2$ CELL

R. J. NOWAK

Office of Naval Research, Arlington, VA 22217-5000, U.S.A.

D. R. ROLISON

Naval Research Laboratory, Washington, D.C. 20375-5000, U.S.A.

J. J. SMITH

Physics Division, Research Department, Naval Weapons Center, China Lake, CA 93555-6001, U.S.A.

and

S. SZPAK

Naval Ocean Systems Center, San Diego, CA 92152-5000, U.S.A.

(*Received* 23 *November* 1987; *in revised form* 9 *February* 1988)

Abstract—The concept of electrocatalysis is examined for energy conversion devices employing a liquid catholyte which yield insoluble products upon charge transfer reaction. The model developed by Tsaur and Pollard for Li–$SOCl_2$ cells is used to assess the effect of additives, in particular, iron phthalocyanine, on the performance characteristics of this cell. Limitations of this model as applied to the predictions of cell lifetime and voltage are discussed.

INTRODUCTION

Various additives, including metallic platinum[1] and copper[2], the transition metal halides[3] and the transition metal N4 chelates, *eg*, Co–, Fe– and Cu–phthalocyanines[4, 5], have been employed in lithium–$SOCl_2$ batteries to increase battery lifetime and discharge rate capabilities. The mechanism(s) by which these additives affect battery performance has yet to be elucidated. It has been suggested that some (*eg* Cu, $CuCl_2$, BrCl, *etc*) function as intermediates in the reduction process, more specifically, they form a shuttle mechanism within the cell.

Other additives such as the metal phthalocyanines, Me–Pc, have been proposed to act as catalysts, *ie*, as substances that accelerate the relevant charge transfer reaction. While the concept of electrocatalysis is straightforward when the electrode reactions are kinetically controlled throughout the entire discharge period, this is not the case in lithium–$SOCl_2$ batteries. In this system, a non-conductive solid-state phase (LiCl) is formed and the porous electrode structure produces a strongly non-linear charge transfer current density. Here, an expansion of the definition of the additive effects beyond that of traditional catalysis is necessary.

In this communication, the effects of iron phthalocyanine (Fe–Pc) addition on the performance characteristics of lithium–$SOCl_2$ cells are examined and compared with the expected behavior of catalytic activities as predicted by modelling. Disagreements are discussed. The basis for prediction and for cell description is the model of Tsaur and Pollard[6, 7], in which the cell operational parameters are stated as a function of the electrode reaction kinetics and the physicochemical properties of the system.

EXPERIMENTAL AND OBSERVATIONS

Experiments were performed in a thin cell of standard design, shown schematically in Fig. 1. It consisted of a lithium foil, 0.25 mm thick, a 92% porous glass separator, 0.25 mm thick, and a Teflonated, 80% porous carbon (Shawinigan black) cathode structure. These components were sandwiched between nickel current collectors.

Galvanostatic discharge curves

The efficacy of an additive is customarily measured in terms of its impact on cell voltage and lifetime. The effect of the addition of Fe–Pc on cell performance is illustrated in Fig. 2, where curves a and b are plots of cell voltage *vs* time for the cell without and with Fe–Pc (2.0 mg cm^{-3} dissolved in the electrolyte), respectively. Qualitatively, the behavior is similar in both cases: each exhibits the initial voltage "hump" associated with the presence of excess $AlCl_3$ in the electrolyte[6, 7]. The presence of Fe–Pc does, however, increase the open-circuit potential by 100 mV[8] and the cell operating voltage by *ca* 200 mV. Furthermore, the cell lifetime is doubled[5] and the slope of the voltage–time curve, Fig. 2, is less than that for the reference cell.

The effect of Fe–Pc on cell lifetime diminishes as the discharge current increases and becomes insignificant

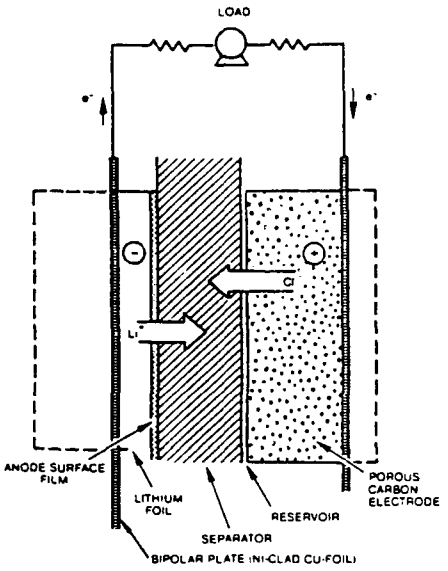

Fig. 1. Cross section of Li–$SOCl_2$ schematic.

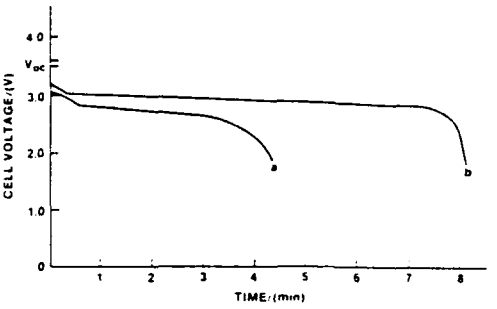

Fig. 2. Effect of Fe–Pc addition on Li–$SOCl_2$ cell discharge curves. Curve (a); 0.5 M $LiAlCl_4$ + 1.0 M $AlCl_3$ in $SOCl_2$. curve (b); same with 2.0 mg cm^{-3} of Fe–Pc dissolved in electrolyte. Discharge current, 80 mA cm^{-2}.

at current densities above 100 mA cm^{-2}[9]. Other metal phthalocyanines yield qualitatively the same results, although Fe–Pc is the most effective. A related observation, reported by Venkatasetty[4] and confirmed by Madou *et al.*[8, 10, 11], is that the exchange current density is only moderately affected by Fe–Pc addition while the transfer coefficients are unaffected.

LiCl *growth forms*

Scanning electron microscopic (SEM) examination of spent cathodes reveals a variety of growth forms for the precipitated LiCl reaction product produced during the discharge of uncatalysed cells. Examples are shown in Fig. 3a, b and c. The crystallites vary from a fused mass. Fig. 3a, through a carpet-like deposit of submicron size, Fig. 3b, to well developed columnar growth, Fig. 3c. The specific morphology of these crystals is determined by the local current density, degree of supersaturation and concentration gradients within the cell[12]. Presence of Fe–Pc tends to produce crystals with the columnar growth structure of Fig. 3c. Madou *et al.*[10] have shown that the films produced in the presence of Fe–Pc are also tougher and more adherent to the electrode surface. To a lesser

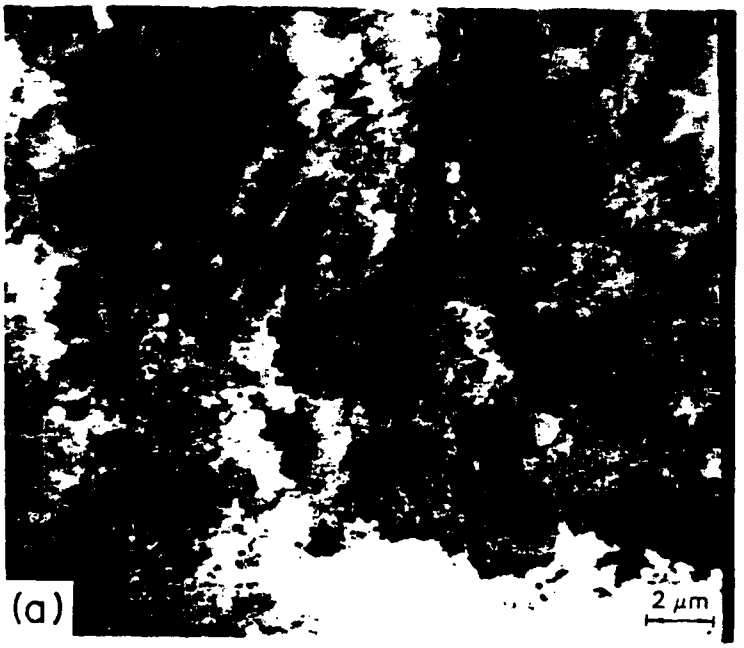

Fig. 3.

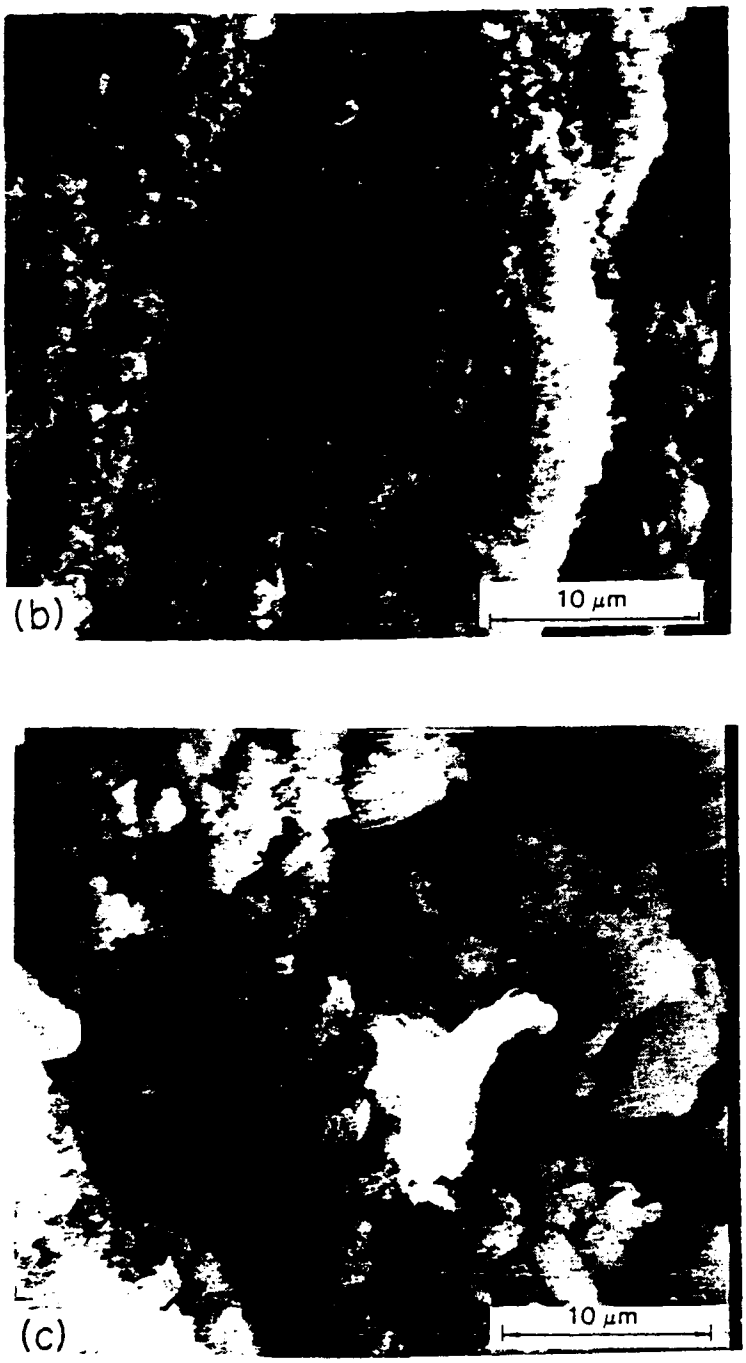

Fig. 3. SEM photographs illustrating the variety of morphological features of LiCl deposits. (a) Fused crystallites; (b) carpet-like deposits (c) columnar growth.

degree, the growth form depends on the transition metal central ion. In either case, the effect on the morphology of the precipitate is greatest at low overpotentials and diminishes as the discharge current increases.

Termination mode

The SEM photograph shown in Fig. 4 is a cross section of a discharged cathode from a cell containing Fe–Pc. The light region on the right-hand side of the photograph indicates the presence of a compact LiCl

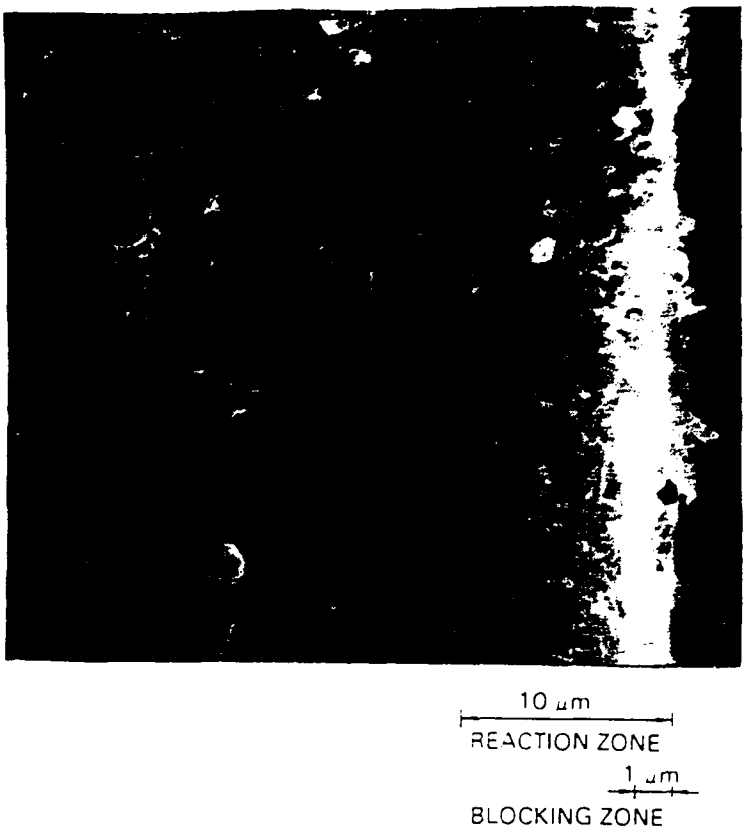

Fig. 4. Cross section of a discharged cathode. Electrolyte: 1.8 M $LiAlCl_4$ + 0.5 M $AlCl_3$ in $SOCl_2$ containing 1.5 % (w/w) Fe–Pc. Temperature: 23°C, discharge current density, 120 mA cm^{-2}.

deposit. Evidently, the termination of cell operation has occurred because of choking of the front face of the cathode structure in much the same manner as occurs in the absence of catalyst. The thickness of the blocking zone varies with the discharge rate and is *ca* 100 μm thick for a discharge rate of 40 mA cm^{-2} and *ca* 5 μm for 120 mA cm^{-2}. The blocking zone thickness also depends, to a lesser degree, on the electrolyte composition and the preparation of the cathode structure. These compact layers formed in all cells that were discharged at current densities in excess of 40 mA cm^{-2}.

DISCUSSION

Electrocatalysis is a special case of heterogeneous catalysis where the catalyst is in contact with an electronically conducting substrate whose surface acts as either an electron source or sink for the charge transfer process. The catalytic effect is manifested through an increase in the exchange current density, requiring for elucidation, a knowledge of the reaction path and the rate-determining step. In systems, including Li–$SOCl_2$, containing a liquid catholyte, the set of constraints imposed by the structure of the positive electrode must also be considered.

The electrical circuit analog for an operating Li–$SOCl_2$ cell is represented by Fig. 5. Starting with the lithium electrode (*ie*, the source of electrons and lithium ions), the always present protective LiCl film offers a resistance R_f to the current flow. Its thickness is governed by the electrolyte composition and the discharge current[6, 13], with the maximum thickness determined by the extent of $SOCl_2$ transport across it[6]. Further to the right, the ionic current passes through a separator. No LiCl precipitation has been

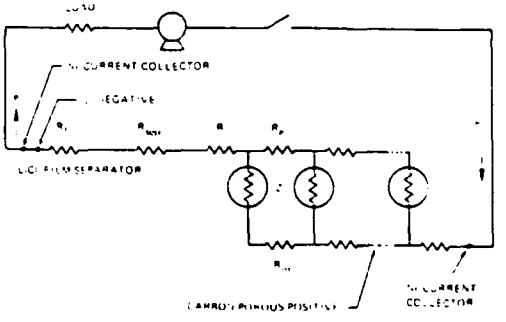

Fig. 5. Electrical circuit analog of an operating Li–$SOCl_2$ cell.

observed in this region, so the resistance to current flow, R_{sep}, remains approximately constant during the whole discharge period. Finally, the ionic current enters the confines of the porous structure of the positive electrode whose surface acts as an electron sink with a highly non-linear distribution of the charge transfer current density. The distribution of this current density is determined by the interplay of various elementary processes, such as diffusion, adsorption, solvent–solute interactions[14] and the charge transfer. It is within this functional element of the cell where the effect of Fe–Pc addition on performance must be examined.

The analysis presented here is based on a consideration of the changes associated with the addition of Fe–Pc on the open-circuit potential, the current–potential relation, the state of the electrode–electrolyte interphase and the growth forms of LiCl crystallites.

Electroreduction of $SOCl_2$

In recent years, a number of reaction paths for the electroreduction of $SOCl_2$ have been proposed[10]. At present, the experimental evidence is insufficient to select one of the proposed paths: this complicates the interpretation of the effect of a catalytic additive. However, certain conclusions are possible based on the fact that the open-circuit potential and the quasi-exchange current density increase upon the addition of Me–Pc without a significant change in the transfer coefficients.

Addition of a catalyst cannot change the position of an equilibrium for a reversible reaction, as the forward and reverse reactions are affected to the same degree. The observed shift in the open-circuit potential by 100 mV upon addition of Fe–Pc is consistent with the concept of a mixed potential[8]. By analogy to a redox system, the observed potential shift in a positive direction can indicate either an increase in the concentration of oxidizing species or a decrease in the concentration of reducing species. A change in reactant concentration might arise from an interaction of adsorbed species with solvent molecules. This view is supported by the results of Myers *et al.*[15], namely, that $SOCl_2$ reacts with Me–Pc to form oxidized species. Further discussion of the mechanistic aspects of Fe–Pc interaction with $SOCl_2$ is beyond the scope of this paper. In addition, the usual effect of an increase in j_0 is not consistent with observation inasmuch as an increase in the exchange current density would reduce the cell lifetime if LiCl precipitates from the liquid phase.

Electrode–electrolyte interphase

Two recent investigations, one on the effect of illumination[11] and one on the growth rate of the passive film as a function of applied potential and temperature[16], have confirmed the importance of the LiCl film in the electroreduction process. Consequently, any effect that Fe–Pc exerts on film growth should be manifested in the observed kinetics of the electroreduction.

During the electroreduction of $SOCl_2$ the electrode surface remains free of LiCl deposits within a relatively narrow range of overpotentials and only within this range is the reaction kinetically controlled[8, 10]. At higher potentials, a transition from kinetic to transport control occurs. However, the amount of charge transferred prior to passivation is not affected by Fe–Pc.

In both the catalysed and uncatalysed cases, the prepassive and passive films can be removed from the electrode surface either by mechanical means or by holding the electrode at the potentials positive of the open-circuit potential[10]. Mechanical removal of these films is, however, more difficult when the films are formed in the presence of Fe–Pc. This implies that Fe–Pc affects the mechanical properties of the film, yet does not affect the chemical nature of the deposit. Thus, the mechanism for the role of Fe–Pc in the electroreduction must include this effect on the formation of the LiCl film.

Growth forms

A consequence of the formation of the modified solid LiCl phase in the presence of Fe–Pc is a change in the specific surface area of the porous electrode. The great variety of morphological forms seen in Fig. 3a, b and c indicates that growth occurs in the electrolyte phase where the shape of the growing crystallites is affected by two factors: mass transport and interfacial kinetics. Interfacial processes are the probable cause for the non-spherical shape of the precipitate[17]; an anisotropic growth mechanism is operative long before the onset of diffusional control. The relative contributions of these two mechanisms determine the growth pattern of the precipitates.

The solution–precipitation path is a common occurrence in operating cells[18–20]. To sustain the current flow in these cells, reactants must be brought to the reaction layer and the products removed. As the local charge transfer increases, LiCl solubility limits are exceeded, the nucleation process commences and proceeds with the rate given by Equation (1)[7]:

$$r_n = k_n[(c_1c_2) - K_s], \tag{1}$$

where k_n is the rate constant for the nucleation process, (c_1c_2) represents the local supersaturation (c_1 and c_2 are the local concentrations of lithium ions and chloride ions, respectively) and K_s is the solubility product. With further passage of current, the growth of crystallites and the formation of new nuclei occur simultaneously. Following Tsaur and Pollard[7], crystallite growth obeys Equation (2):

$$r_g = k_g v^m[(c_1c_2) - K_s], \tag{2}$$

so that the precipitation rate parameter for the formation of the solid phase and, *ipso facto*, for the removal of Cl^- from the reaction space is given by Equation (3):

$$k = k_n + k_g v^m. \tag{3}$$

The term v^m is the volume fraction of LiCl in the cathode and describes the crystal surface available for growth. The exponent m reflects the morphology of the growing crystallites: large values of m correspond to crystallites with a small surface-to-volume ratio and *vice versa*, *ie*, spherical particles are characterized by a large m while a small m is associated with needle- and plate-like growths. The form of Equation (3) is the same for either surface kinetic control or for mass

transport control; *ie*, the difference lies only in the numerical value of k_g. The observed change in the growth form, Fig. 3a, b and c requires m to be a position-dependent parameter.

Cell potential

As stated earlier, Madou *et al.*[10] measured an open-circuit potential shift of 100 mV while the observed difference in the operating cell voltage was about 200 mV, as shown in Fig. 2. Thus, Fe–Pc affects more than just a change in the free energy of reaction. The most likely cause of the difference in the cell operating voltage is a reduction in Cl^- concentration at the electrode surface relative to that in a cell without Fe–Pc; this effect is quantified in Equation (31) of Tsaur and Pollard[7].

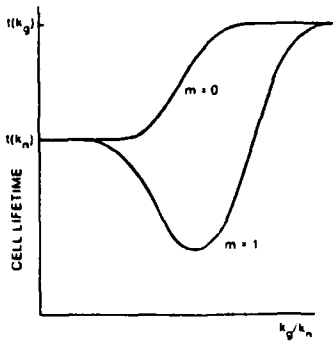

Fig. 6. Cell lifetime as a function of k_g/k_n ratio. Curve (a) $m = 0$; curve (b) $m = 1$.

Cell lifetime

The picture of Fe–Pc activity most consistent with the observed cell behavior during discharge is one in which Fe–Pc molecules are initially adsorbed on the electrode surface and subsequently serve as preferred reaction and nucleation sites. As a result, the LiCl precipitation occurs at specific sites on the electrode surface. No effect of Fe–Pc on the main transport in the electrolyte phase is expected.

With a delayed precipitation of LiCl, the cell lifetime is affected by three factors, *viz* nucleation rate (rate constant, k_n), growth rate (rate constant, k_g) and precipitate morphology (morphology factor, m). Growth of LiCl crystallites within the interphase region can produce locally complex concentration gradients that affect the growth form. For this to occur, Fe–Pc has to facilitate the rate of precipitation of LiCl, primarily through an increase in the nucleation rate constant, k_n, and secondarily through changes in the growth rate are constant, k_g, and the morphology factor m.

At low growth rates, irrespective of the m value, the cell lifetime is controlled by the nucleation rate. As the growth rate increases, it dominates the cell lifetime. This transition is illustrated schematically in Fig. 6: it is seen that for $m = 0$, the cell lifetime changes monotonically between two limiting cases, *ie*, between nucleation and growth control. However, as m increases, a minimum in the cell lifetime develops with its magnitude depending on the ratio of k_g/k_n. Moreover, since the concentration of Cl^- at the electrode surface depends on the rate of precipitation, the ratio k_g/k_n influences in the cell operating potential.

Calculations[7] show that in systems where a solid product is formed in the course of the charge transfer reaction occurring in a porous electrode employing liquid reactants, the cell lifetime can be altered by a factor of 2, or more, simply by changing the rate of precipitation. In the Li–$SOCl_2$ system, a change in the rates of nucleation and growth affects both the operating cell voltage and cell lifetime.

Circuit analysis of the porous electrode

Further support for this interpretation of the influence of Fe–Pc on cell discharge can be derived from an analysis of the electrical circuit analog in Fig. 5. In this analog, the behavior of the porous electrode is represented by two sets of factors that determine the distribution of the charge transfer current density. The first set, collected in R_e, accounts for those processes in solution that contribute to ionic transport in the direction normal to the electrode surface: these are longitudinal diffusion, migration, and convective flow. The second set, the interphase impedance, denoted by Z, represents processes occurring within the electrode–electrolyte interphase. A large value of Z promotes a more uniform distribution of the charge transfer current density, while an increase in the solution resistivity, R_e, tends to shift the reaction zone toward the electrode surface facing the separator.

An extension of cell lifetime is usually attributed to achieving a more uniform distribution of the charge transfer current density which permits a more complete utilization of reactants stored within the electrode structure. In terms of the electrical circuit analog, the addition of Fe–Pc acts to increase the total interphase impedance which, for a complex reaction, is a sum of the impedances of all of the in-series elementary processes comprising the overall electrode reaction[21]. Thus, although j_0, the quasi-exchange current density is increased or the impedance of the electrode process, Z_e, is decreased, the total impedance of the interphase,

$$Z = Z_e A + \sum_i Z_i,$$

may increase upon addition of Fe–Pc.

Because of formation of the prepassive film and growth from the solution phase, the effect of Fe–Pc addition will manifest itself through the change in the electrode surface area which, as stated earlier, is governed by the rate of nucleation and growth. The ionic transport resistance in the electrolyte phase affects the current density distribution. A small amount of additive is not expected to alter this resistance to an appreciable extent. This lesser slope of the $V(t)$ curve (Fig. 7) indicates film formation and growth in the proximity of the charge transfer surface, or, alternatively, an expansion of the electrode structure due to the pressure expected by the growing crystallites. Both of these effects have been reported.

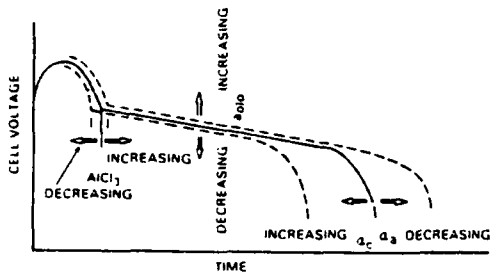

Fig. 7. Schematic representation of a galvanostatic discharge curve: effect of change in kinetic parameters.

Other factors

The importance of other possible factors in the performance characteristics of the Li-$SOCl_2$ cell can be determined from the modelling predictions. The effects of the various input parameters derived under the restrictive conditions of immediate precipitation are summarized in Fig. 7. The calculated discharge curve is for the cell employing an acid electrolyte. The slope of the $V(t)$ curve in the central region reflects the growth characteristics of the LiCl crystallites generated by the discharge process occurring within the positive electrode porous structure. The slope and operating voltage are rather insensitive to the value of the pre-exponential factor in the Butler-Volmer current-potential relation. In contrast, the cell lifetime is very sensitive to this factor, primarily through the expression adopted for the change in the specific surface area, which contains the morphology parameter.

CONCLUSION

The addition of Me-Pc's to a Li-$SOCl_2$ cell, either dissolved in the electrolyte or adsorbed on the electrode surface, raises the operating cell voltage and extends its lifetime. In practical terms, the presence of Me-Pc increases cell power output, as well as the extractable energy content, at moderate current densities.

The exact extent of the Me-Pc effect on the reaction is uncertain: results show that the beneficial effects diminish with an increase in discharge current. The presence of Fe-Pc increases the open-circuit potential and affects the rate of the nucleation process and the resultant crystallite morphology. Such behavior is not commonly expected for a catalyst, in the classical definition of the term.

The final resolution of the role that Fe-Pc or other additives play in the course of Li-$SOCl_2$ cell discharge awaits more definitive information on the mechanism of $SOCl_2$ electroreduction. Regardless, additives improve cell lifetime and do so through a modification of the LiCl precipitation process.

The practical implication of this discussion is that the electroreduction process is represented by a complex path that cannot be described unambiguously. Thus, it is not surprising that even small changes in manufacturing processes may result in unexpected, and often, undesirable performance characteristics.

Acknowledgements—This work was supported, in part, by the Office of Naval Research and by the Naval Sea Systems Command. The authors wish to acknowledge helpful discussions with W. A. West and J. R. Driscoll.

REFERENCES

1. K. A. Klinedinst, *J. electrochem. Soc.* **128**, 250 (1981).
2. L. R. Giattino, U.S. Patent 4,167,608 (1979).
3. W. K. Behl, *J. electrochem. Soc.* **128**, 939 (1981).
4. H. V. Venkatasetty, U.S. Patent 4,279,973 (1981).
5. N. Doddapaneni, Ext. Abst. 360, The Electrochem. Soc. Meeting, Detroit, MI (1982).
6. K.-C. Tsaur and R. Pollard, *J. electrochem. Soc.* **131**, 975, 984 (1984).
7. K.-C. Tsaur and R. Pollard, *J. electrochem. Soc.* **133**, 2296 (1986).
8. M. J. Madou and S. Szpak, *J. electrochem. Soc.* **131**, 2471 (1984).
9. J. P. Descroix, Private Communication (1986); J. Bouet, F. Richard, V. Danel, and J. P. Descroix, Abst. No. 34, The Electrochem. Soc. Fall Meeting, San Diego, CA (1986).
10. M. J. Madou, J. J. Smith, and S. Szpak, *J. electrochem. Soc.* **134**, 2794 (1987).
11. M. J. Madou, J. J. Smith, and S. Szpak, *J. electrochem. Soc.* **135**, 262 (1988).
12. S. Szpak and J. R. Driscoll, *J. Power Sources*, **10**, 343 (1983).
13. J. Brossan, A. de Guibert, and G. Fuellade, Extended Abstract, F.3, 31st ISE Meeting, Venice, Italy, (1980).
14. S. Szpak and T. Katan, Proc. Electrode Materials and Processes, The Electrochem. Soc. 776, 770 (1977).
15. J. F. Meyers, G. W. Rayner Canham, and A. B. P. Lever, *Inorg. Chem.* **14**, 46 (1975).
16. F. M. Delnick, W. A. Cieslak, D. E. Pebbles, and J. W. Rogers, Jr., Abst. Nr 40, The Electrochem. Soc. Fall Meeting, San Diego, CA (1986).
17. S. K. Chan, H. H. Reimer, and M. Kahlweit, *J. Cryst. Growth* **32**, 30 (1976).
18. S. Szpak, A. Nedoluha, and T. Katan, *J. electrochem. Soc.* **122**, 105 (1975).
19. T. Katan, S. Szpak, and D. N. Bennion, *J. electrochem. Soc.* **120**, 883 (1973).
20. S. Szpak and C. J. Gabriel, *J. electrochem. Soc.* **126**, 1914 (1979).
21. R. de Levie, in *Advances in Electrochemistry and Electrochemical Engineering* (Edited by P. Delahay), Vol. 6, Interscience (1967).

POWER LOSSES IN BATTERIES WITH A COMMON ELECTROLYTIC PATH

C. J. GABRIEL and S. SZPAK*

Naval Ocean Systems Center, San Diego, CA 92152-5000 (U.S.A.)

(Received April 22, 1988; in revised form November 21, 1988)

Summary

The distribution of power losses in an operating electrochemical power source of pile construction provided with a common manifold is discussed. The developed relationships yield information that can guide the battery design to meet *a priori* specified requirements. Selected illustrative examples pertain to the $Li/SOCl_2$ system.

Introduction

Two types of designs for high-power-output, energy-dense, electrochemical systems are under active development: (i) the flowing electrolyte and (ii) the static electrolyte, reserve type, thin cell approach. Both designs utilize a modular concept and both have a common manifold which provides the means for maintaining forced flow of the electrolyte or activating the battery.

In the course of an assessment of the battery operational capabilities, information on power output and efficiency are often required. Calculations yielding this information are relatively simple for single cells or batteries without a common electrolytic path, but they are more difficult when a common manifold is employed. In such designs, the optimization procedure must consider all losses, including those attributed to the intercell currents, a consideration only rarely treated in the literature [1].

This communication examines only the effect of intercell currents on the power density and efficiency of an operating electrochemical system. The method is general — the examples to illustrate the selected points pertain to the $Li/SOCl_2$ batteries. The assumptions underlying the treatment are identical with those used in ref. 2.

General consideration

An electrochemical cell is a constrained system that reacts spontaneously as the constraints are removed. In principle, the removal of constraints, *i.e.*,

*Author to whom correspondence should be addressed.

the cell discharge, can be carried out reversibly; in practice, however, irreversible processes do occur, thus reducing the extractable energy content. As a rule, the analysis of energy conversion is performed under restrictive conditions of a constant pressure and temperature. Under these conditions, by combining the first and second laws of thermodynamics, eqns. (1) and (1a) hold for a single cell

$$(U - V)J_1 = T \sum_{k=1}^{K} (\mathrm{d}_i S)_k \tag{1}$$

or

$$(U - V)J_1 = J_1^2 R_z \tag{1a}$$

where terms on the right side of eqns. (1) and (1a) account for the rate of heat generation by the K irreversible processes associated with the flow of current, J_1. As written, R_z in eqn. (1a) is the cell internal impedance, *i.e.*, it includes losses due to anodic and cathodic overpotentials (ref. 2, eqns. (11) and (13)). Consequently, eqn. (1) is the basis for the examination of the effect of intercell currents on both the power delivered to the load and the cell/battery efficiency. Furthermore, as written, eqn. (1) states that the difference between the cell/battery own power and that delivered to the load appears in the form of Clausius uncompensated heat, which must be removed to maintain constant temperature [3]. Here, the battery own power is equivalent to the power of irreversibility, as defined by van Rysselberghe [4]. Moreover, for a single cell, or in the absence of intercell currents, eqn. (2) applies

$$I_{c,n} = I_{a,n} = J_1 \tag{2}$$

because the electrode currents, $I_{a,n}$ and $I_{c,n}$, are also equal to the load current, J_1.

From Fig. 1, where the potential distribution across the discharging cell is schematically illustrated, we have

$$U = U_c - U_a \tag{3}$$

and

$$V = V_c - V_a \tag{3a}$$

Substitution of eqns. (2) and (3) into eqn. (1) yields, after rearrangement, eqn. (4)

$$(U_c I_c - U_a I_a) - (V_c I_c - V_a I_a) = T \sum_{k=1}^{K} (\mathrm{d}_i S)_k \tag{4}$$

Identifying the first term in eqn. (4) as the cell own power, P_b, and the second term as the power into the load, P_l, we can now examine the effect of the presence of intercell current, I_n, on the power output as well as cell/battery efficiency through the relationship, eqn. (5), see Fig. 2.

$$I_{c,n} = I_n + I_{a,n} \tag{5}$$

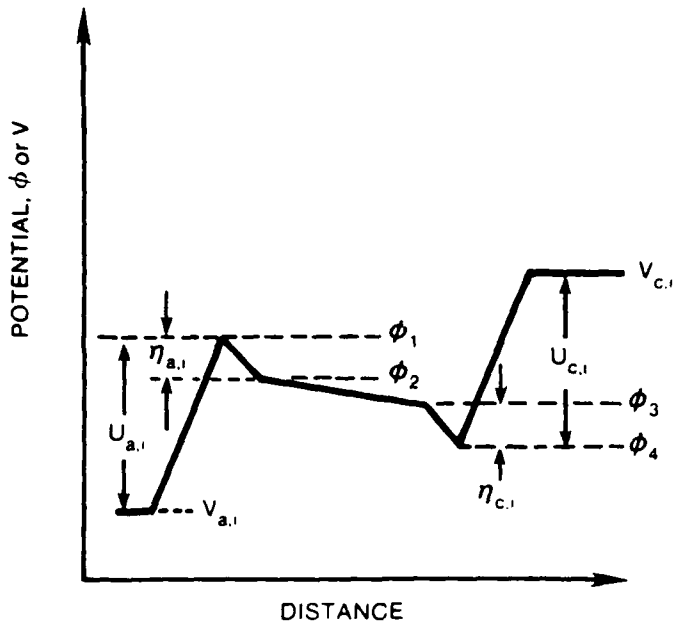

Fig. 1. Idealized distribution of electric potential within a cell, where the sign conventions used here for $U_{a,c}$ and $\eta_{a,c}$ are defined by: $U_a = V_a - \Phi_1$, $U_c = V_c - \Phi_4$; $\eta_a = \Phi_1 - \Phi_2$; $\eta_c = \Phi_3 - \Phi_4$; $J_1 R_2 = \Phi_2 - \Phi_3$.

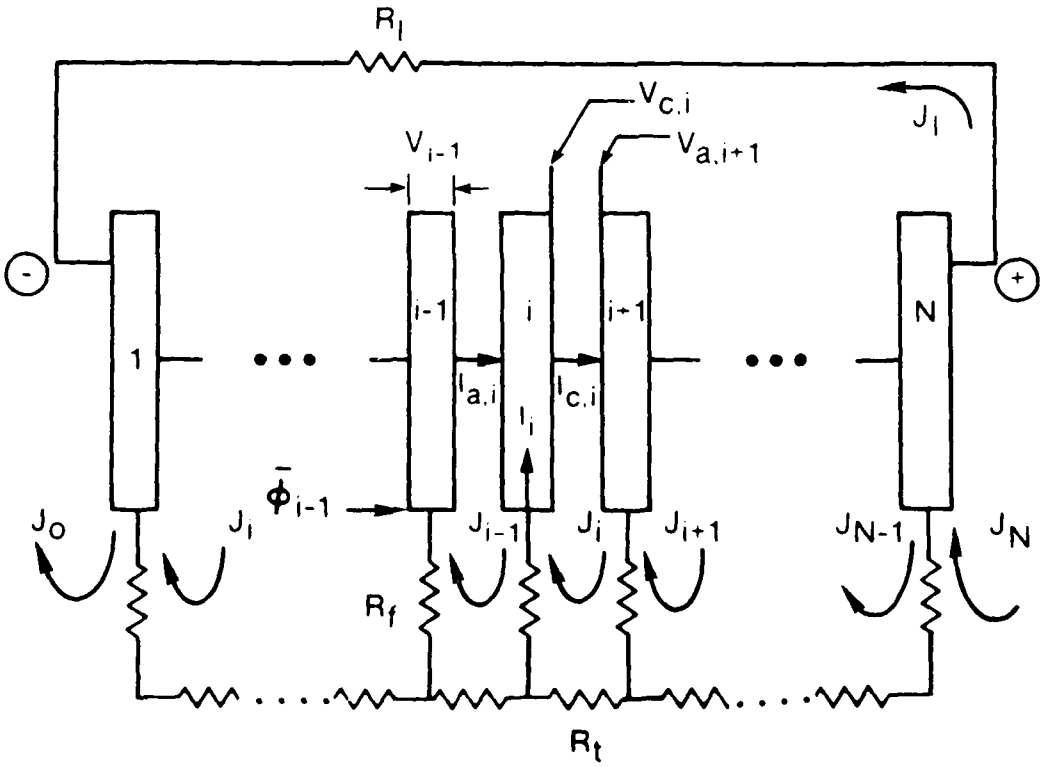

Fig. 2. Module representation by electric circuit analog. V_{i-1}, cell voltage; Φ_{i-1}, potential at inlet to $(i-1)$th cell; $I_{a,i}$, $I_{c,i}$ and I_i, anode, cathode and intercell current, respectively; J_i, circulating current; J_l, loop current in external resistor, R_l; R_f, manifold feed-line resistor; R_t, equivalent fill tube resistor.

However, the right hand side of the generalization of eqn. (4) will no longer have the simple dependence on J_1 indicated in eqn. (1a), because it must include losses in the manifold as well as losses within cells themselves generated by intercell currents.

Power losses

Limiting the discussion to losses associated with the presence of a common electrolytic path, we have, for the arrangement shown in Fig. 2, the battery own power and the power delivered to the load, given by the relationships, eqns. (6) and (6a), respectively

$$P_b = \sum_{n=1}^{N} (U_{c,n} I_{c,n} - U_{a,n} I_{a,n}) \tag{6}$$

and

$$P_l = \sum_{n=1}^{N} (V_{c,n} I_{c,n} - V_{a,n} I_{a,n}) \tag{6a}$$

In the case of a battery employing identical cells with constant parameters, using relationships derived previously [2], *viz.*

$$\sum_{n=1}^{N} I_n = 0$$

and

$$\sum_{n=1}^{N} I_{a,n} = NJ_1 + \sum_{n=1}^{N} J_n$$

eqns. (6) and (6a) become eqns. (7) and (7a)

$$P_b = U\left(NJ_1 + \sum_{n=1}^{N} J_n\right) \tag{7}$$

and

$$P_l = J_1 \sum_{n=1}^{N} V_n \tag{7a}$$

Using eqn. (8)

$$\sum_{n=1}^{N} J_n = \frac{NU - J_1(R_l + NR_z)}{R_z} \tag{8}$$

and expressing J_1 in terms of battery voltage and design parameters, ref. 2, eqn. (28), we obtain

$$P_b = \frac{NU^2}{R_z}\left[\frac{N(1-\zeta)R_z + R_l\zeta}{N(1-\zeta)R_z + R_l}\right] \tag{9}$$

Similarly, using the relationship

$$\sum_{n=1}^{N} V_n = R_l J_l$$

we have for the power delivered to the load, eqn. (10)

$$P_l = \left[\frac{N(1-\zeta)U}{R_l + N(1-\zeta)R_z}\right]^2 R_l \tag{10}$$

The battery power consumed in all processes, including the presence of intercell currents, is obtained upon subtracting eqn. (10) from eqn. (9). The result in a dimensionless form is given by eqn. (11)

$$\Pi = \frac{1-\zeta+\zeta\rho}{1-\zeta+\rho} - \rho\left[\frac{1-\zeta}{1-\zeta+\rho}\right]^2 \tag{11}$$

where the two terms on the right are dimensionless powers, $\Pi_\alpha = R_z P_\alpha / NU^2$ with α = b, l, respectively, and the dimensionless resistance $\rho = R_l/NR_z$.

The parameter ζ, appearing in eqns. (9) - (11), is related to the battery design as well as to the electrochemical system employed [2]. This relationship is given by eqn. (12)

$$\zeta = \frac{R_z}{R_t + R_z}\left[1 - \frac{(\lambda^N - 1)(\lambda + 1)}{N(\lambda^N + 1)(\lambda - 1)}\right] \tag{12}$$

where

$$\lambda = 1 + \frac{R_t + R_z}{2R_f^*} + \left[\frac{R_t + R_z}{2R_f^*}\left(2 + \frac{R_t + R_z}{2R_f^*}\right)\right]^{1/2} \tag{12a}$$

and

$$R_f^* = R_f + R_p - R_z\left(\frac{\sigma^2}{\sigma_a \sigma_c}\right) \tag{12b}$$

The respective resistances are identified in Fig. 2 except for the R_p which is the distributed resistance at the port entrance of the cell.

A plot of the dimensionless quantities Π_α as a function of log ρ, eqns. (9) and (10), is shown in Fig. 3. Evidently, the power into the load exhibits a maximum at $\rho = 1 - \zeta$, while the battery own power decreases monotonically with an increasing ρ and, in the limit, as $\rho \to \infty$, $\Pi_b \to \zeta$.

Equation (11), the measure of all losses associated with the battery operation, including those due to the presence of the common electrolytic path, can be examined with the aid of Fig. 3. For a given ζ, this power consumption, $\Pi_b - \Pi_l$ increases from ζ to 1 with decreasing ρ. For ρ less

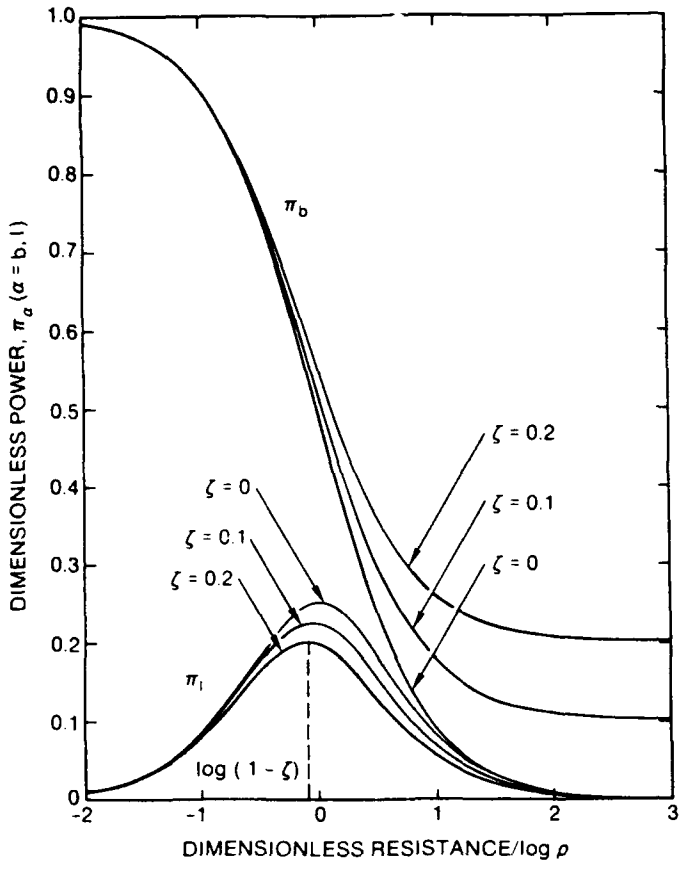

Fig. 3. Plot of dimensionless power, Π_α, with α = l, b as a function of dimensionless resistance, ρ, for ζ = 0, 0.1 and 0.2, as indicated.

than $1 - \zeta$, it increases rapidly becoming, in effect, independent of whether or not a common electrolytic path is maintained.

Distribution of power losses

The distribution of power losses can be conveniently examined with the aid of eqns. (4), (6) and (6a). Considering Fig. 2, the total losses are separated into their components by an assumed electric circuit analog; in eqn. (4) these losses are expressed by the term

$$T \sum_{k=1}^{K} (d_i S)_k$$

We can now identify:

(i) losses occurring within the cells, with or without intercell currents present, eqn. (13);

(ii) losses in the manifold tube, eqn. (14);

(iii) losses in the feed lines, eqn. (15)

$$P_z = P_b - P_l - P_t - P_f \qquad (13)$$

where

$$P_t = R_t \sum_{i=1}^{N} J_i^2 \tag{14}$$

and

$$P_f = \sum_{i=1}^{N} I_i^2 R_{f,i} \tag{15}$$

When there are no intercell currents, eqn. (2) holds and, under the conditions leading to eqn. (1), eqn. (13) would become eqn. (16)

$$P_z = J_1^2 \sum_{i=1}^{N} R_{z,i} \tag{16}$$

This equation, along with eqns. (14) and (15), would then provide the cell-to-cell distribution of power losses, because each term in these equations can be assigned to a particular location in the battery. However, in the presence of intercell currents, the total power loss specified by eqn. (13) cannot be distributed among the cells without additional assumptions. These assumptions are required by the application of the trapezoidal rule to certain integrals in the model of ref. 2, eqns. (A-4) - (A-7). Consequently, the intercell currents, I_i, in eqn. (15) consider only the current and conductivity distribution on the electrodes and not the details of the complicated current and conductivity distributions that actually exist in the region near the entrance port.

The results of a sample calculation using the data from Table 1, ref. 2, applied to a 40-cell $Li/SOCl_2$ battery being discharged through an external load of 20 Ω with the load current J_1 = 6.727 A, are given in Table 1. In this example, the total unaccounted power loss of 1.3 W, which is attributed to the intercell current flow into the cells, is a small fraction of the total power loss. The difference between eqns. (13) and (16) cannot be calculated with the present model for a particular cell; furthermore, in situations where the intercell currents are large, eqn. (16) should not be used.

Experience shows that often in the course of the discharging of an $Li/SOCl_2$ battery, in addition to normal changes taking place within a cell, dendritic Li growths appear in the feed lines at the negative end of the battery and corrosion damage is found localized at the positive end [2]. The dendritic growth occurring in the feed lines reduces resistance in the electrolyte, causing a shift in the distribution of intercell and circulating currents (ref. 2, Fig. 9). This shift affects both the profile and the magnitude of the dissipative processes in the manifold. An example of this time dependence, calculated as in ref. 2, for the above 40 cell battery, is shown in Fig. 4 where the profiles of the power dissipation in the manifold at τ = 0, τ = 0.15, and near the end of cell lifetime, *i.e.*, at τ = 0.9, Fig. 4(a), (b) and (c), respectively, are displayed. It is seen that at τ = 0, this profile is symmetrical with the maximum dissipation occurring at the battery ends and showing minima at the 5th and 35th cells. With the passage of time, however, the

TABLE 1

Power dissipation in a 40 cell $Li/SOCl_2$ module*
(Input data, ref. 2, Table 1.)

Design parameters		
$\lambda = 1.159$		
$\zeta = 7.236 \times 10^{-4}$		
$\rho = 14.36$		
$R_z = 3.482 \times 10^{-2}\ \Omega$		
$R_t = 31.83\ \Omega$		
$R_f = 1457\ \Omega$		
$R_f^* = 1463\ \Omega$		
Power distribution		
Battery own power	P_b, eqn. (9)	987.7 W
Power into load	P_l, eqn. (10)	905.0 W
Power into manifold tube	P_m, eqn. (14)	7.096 W
Power into feedlines	P_f, eqn. (15)	2.302 W
Power dissipated within a cell	P_z, eqn. (16)	63.03 W
Unaccounted power**		3.32×10^{-2} W/cell

*Data from Table 1, ref. 2, used in this calculation.
**Difference between P_z calculated from eqn. (13) and eqn. (16).

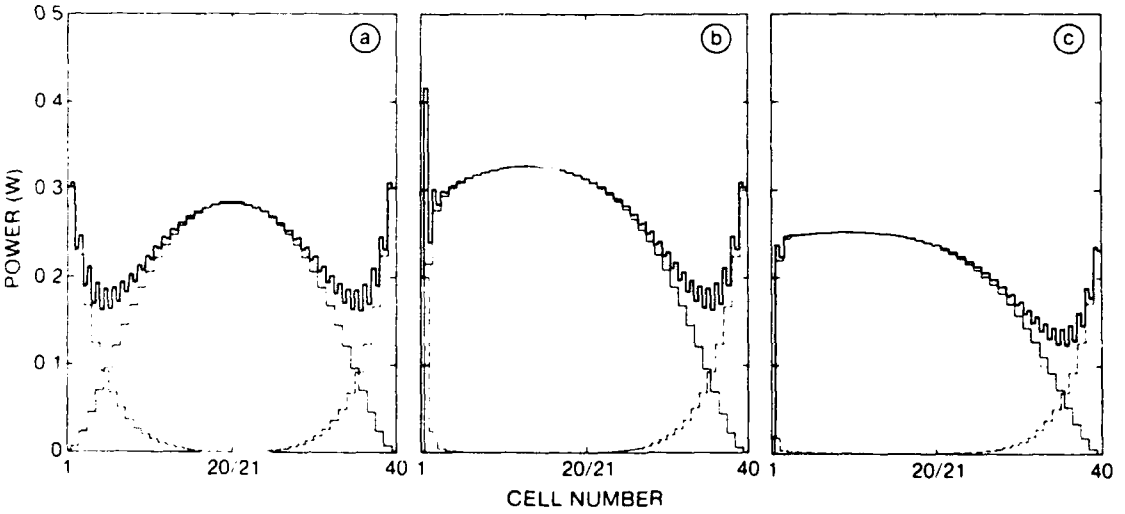

Fig. 4. Distribution of power losses in a 40 cell module, with a 20 Ω load. (a) at $\tau = 0$; $J_l = 6.727$ A; $P_b = 978.7$ W; $P_z = 64.36$ W; $P_l = 905.0$ W. (b) at $\tau = 0.15$; $J_l = 6.701$ A; $P_b = 819.2$ W; $P_z = 67.75$ W; $P_l = 898.1$ W. (c) at $\tau = 0.9$; $J_l = 5.804$ A; $P_b = 846.3$ W; $P_z = 164.2$ W; $P_l = 673.6$ W; P_z calculated from eqn. (13); P_f, dashed lines; P_t, light solid lines; $P_f + P_t$, heavy solid lines.

distribution of the dissipative processes shifts toward the battery negative end and increases somewhat in magnitude because of the increased dissipation in the manifold tube. Very small changes are observed at the positive

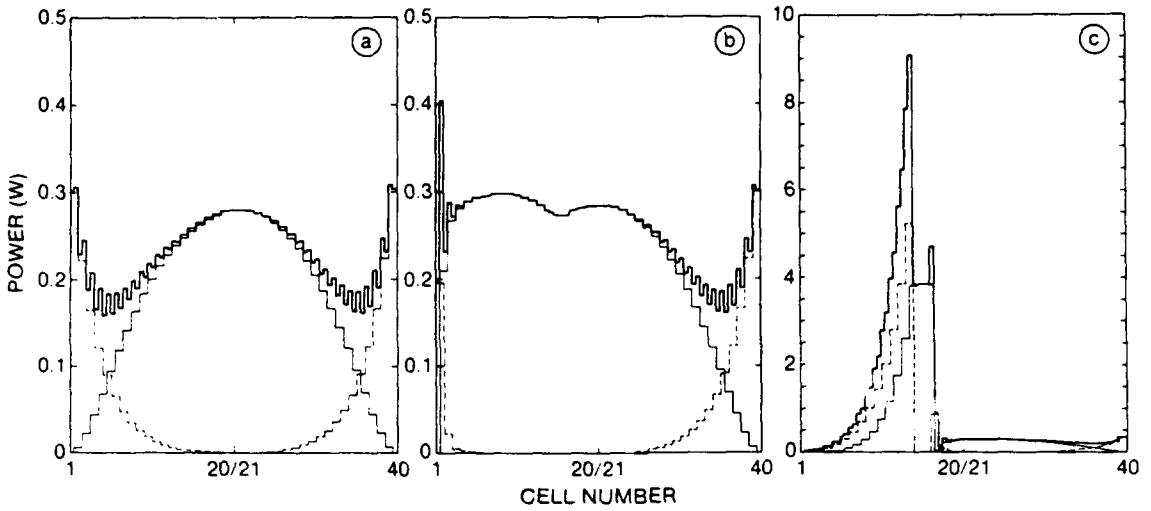

Fig. 5. Discharge time dependent distribution of power losses in a 40 cell module with a 20 Ω load and having defective central cells. (a) at $\tau = 0$; $J_1 = 6.685$ A; $P_b = 972.7$ W; $P_z = 69.56$ W; $P_l = 893.9$ W. (b) at $\tau = 0.15$; $J_1 = 6.509$ A; $P_b = 948.9$ W; $P_z = 91.21$ W; $P_l = 847.2$ W. (c) at $\tau = 0.3$; $J_1 = 0.3472$ A; $P_b = 47.83$ W; $P_z = 1.251$ W; $P_l = 2.412$ W. Deficiency factor $w = 0.2$ for cells 14, 15 and 16; P_z calculated from eqn. (13); P_f, dashed line; P_t, light solid line; $P_f + P_t$, heavy solid line.

end. At the end of the discharge, *i.e.*, at $\tau > 1$, not shown, the residual dissipative losses become small.

Another example of a manifold power loss profile is illustrated in Fig. 5. In this example, it is assumed that in the 40 cell module, the 14th, 15th and 16th cells are defective, with $w = 0.2$. Here, w denotes the computational deficiency factor introduced to account for cell component variation [2]. It is seen that a defective cell or a series of such cells, can cause a concentration of dissipative processes and, therefore, produce a localized heat source of a substantial magnitude. Obviously, creation of such heat sources is undesirable because they may lead to catastrophic events [5].

Condition for trade-off between the P_l and extractable energy

As shown in Fig. 3, in the absence of intercell currents, $\zeta = 0$, the maximum power delivered to the load occurs when $\rho = 1$, *i.e.*, when the battery internal resistance equals the external load, $R_l = NR_z$. Under this condition, half of the stored energy is delivered to the load. In the presence of intercell currents, the maximum power is realized when $\rho = 1 - \zeta$, with only the fraction, $(1 - \zeta)/2(1 + \zeta)$, of the stored energy delivered to the load.

In practice, it is often desired to discharge a battery under conditions that maximize the use of stored energy. These conditions are summarized in Fig. 6 where it is seen that in the absence of intercell currents, the load ρ should be as large as practical since the ratio P_l/P_c increases monotonically with ρ. However, with intercell currents present, this ratio has a maximum when $\rho = (1 - \zeta)\zeta^{-1/2}$. As ρ increases beyond this point, the power dissipation

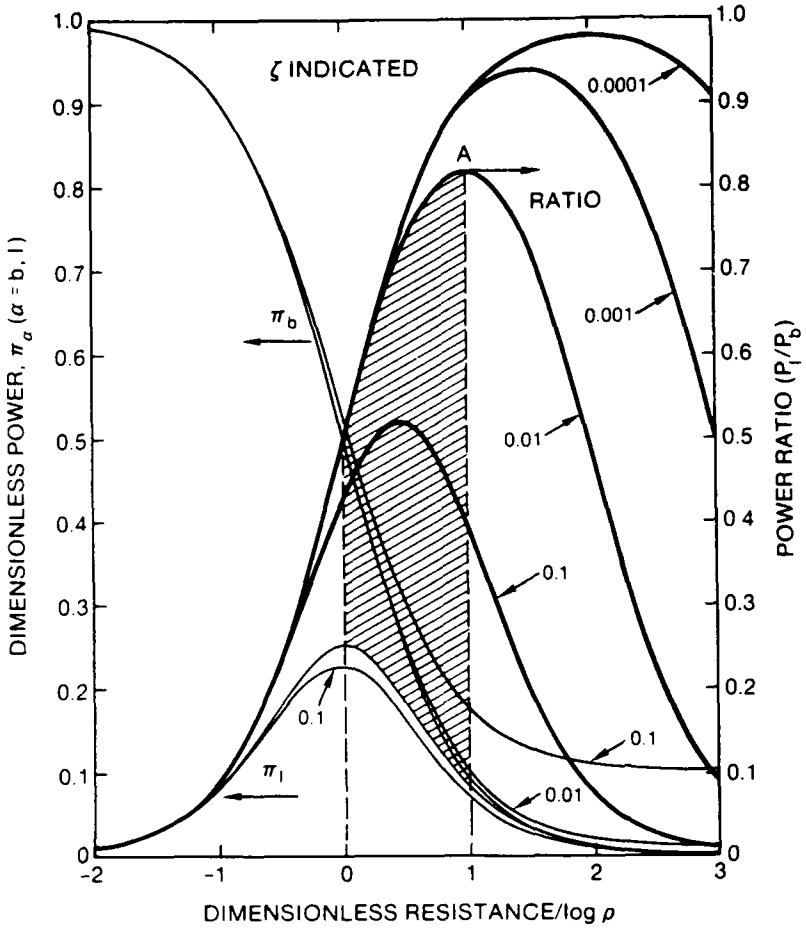

Fig. 6. Conditions for choosing the load resistance for either maximum P_l or minimum battery power dissipation. Point A, max P_l/P_b for $\zeta = 0.01$. Shaded area indicates the region of ρ where an inverse relation exists between P_l and P_l/P_b for $\zeta = 0.01$.

TABLE 2

Values of dimensionless quantities at the trade-off limits

ρ	$1-\zeta$	$(1-\zeta)\zeta^{-1/2}$
$\frac{P_l}{P_b}$	$\frac{1-\zeta}{2(1+\zeta)}$	$\frac{1-\zeta^{1/2}}{1+\zeta^{1/2}}$
Π_l	$\frac{1-\zeta}{4}$	$\zeta^{1/2}\frac{(1-\zeta^{1/2})}{1+\zeta^{1/2}}$
Π_b	$\frac{1+\zeta}{2}$	$\zeta^{1/2}$
L_M	2ζ	$\frac{2\zeta^{1/2}}{1+\zeta^{1/2}}$
L_P	ζ	—

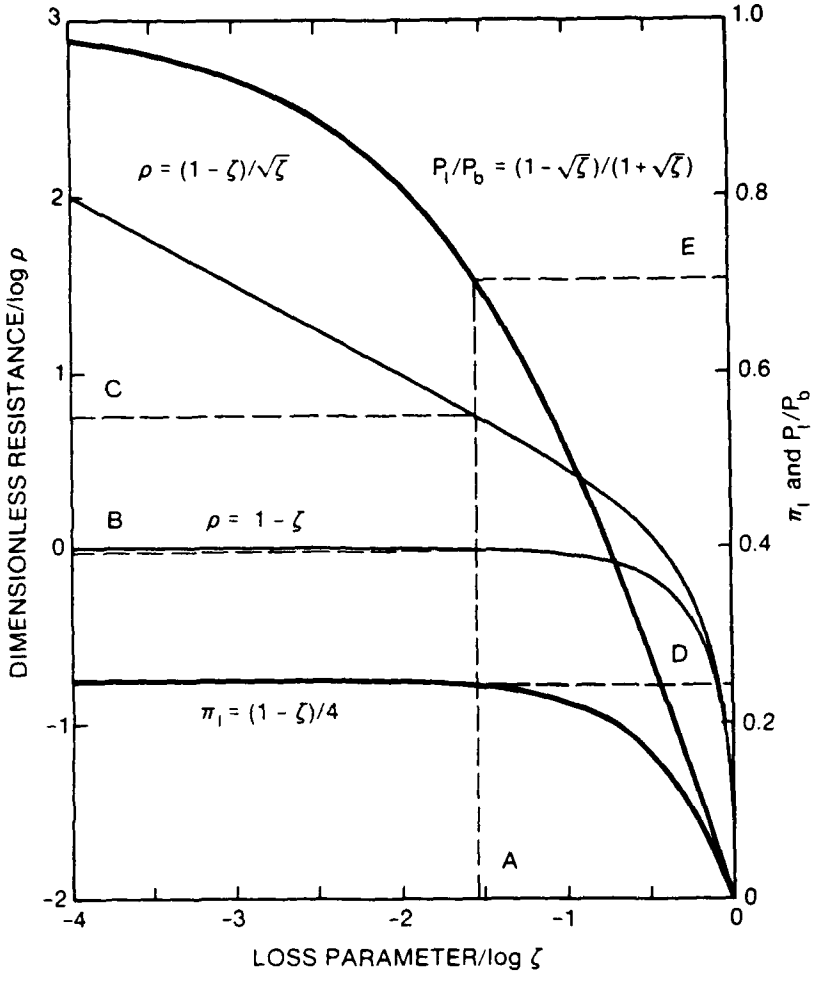

Fig. 7. Plot of design criteria listed in Table 2. Points B, C, D and E are values obtained for the value of ρ indicated by point A. Heavy curves have ordinate scale on the right.

by intercell currents decreases less rapidly than that delivered to the load. Consequently, the design range to trade-off power into load against the material utilized is $1 - \zeta < \rho < (1 - \zeta)\zeta^{-1/2}$. Outside this range both power and stored energy delivered to the load decrease.

The information given in Table 2, and illustrated in Fig. 7, can be used in two ways. First, a range of load resistances can be determined from the knowledge of ζ, *e.g.*, point A; so that at the lower end, *e.g.*, point B, the maximum power is delivered; and at the upper end, *e.g.*, point C, the maximum amount of material is used. These maxima, respectively points D and E, can be found as well. Second, the factor ζ can be designed to provide either a specified maximum power delivery or a specified material utilization. For example, requiring either the maximum power delivery or material use to be greater than that indicated by points D and E, respectively, would limit $\log \zeta$ to be less than the value indicated by point A. Additionally, L_M the relative loss of maximum material use, and L_P the relative loss of power delivery, are listed in Table 2. Evidently, the presence of intercell currents produces a greater relative decrease in material use than in power delivery.

For example, if $\zeta = 0.01$, L_M is 0.18 at maximum material use and 0.02 at maximum power delivery; while L_P, defined only for maximum power delivery, is 0.01.

Conclusions

(i) A simple model devised for the analysis of intercell currents in batteries of pile construction with a common manifold accounts for dissipative losses occurring during discharge and gives their distribution for small intercell currents.

(ii) The initial distribution of dissipative processes is symmetrical. However, in the course of battery discharge, a shift in the distribution occurs. Its magnitude is governed by the charge transfer reactions and the design of manifold.

(iii) Defective cells may create highly localized heat sources which, in turn, may initiate a catastrophic event.

(iv) The use of active material cannot be indefinitely increased by increasing the load resistance, and the relative loss in use of active material exceeds the relative loss in power delivery.

Acknowledgement

This work was supported, in part, by both the Office of Naval Research and the Naval Sea Systems Command and constitutes a fraction of a program to establish a technology base for high discharge rate Li/$SOCl_2$ batteries.

List of symbols

I	Intercell current (A)
J	Loop current (A)
L	Relative loss
N	Number of cells
P	Power (W)
R	Resistance (Ω)
S	Entropy, JK^{-1}
T	Temperature (K)
U	Cell voltage at zero current (V)
V	Cell voltage (V)
w	Cell deficiency factor
α	Index
ζ	Loss parameter
η	Overpotential (V)
λ	Design parameter

Π Dimensionless power
ρ Dimensionless resistance
σ Cell conductivity (S cm^{-2})

Subscripts
a Anodic
b Battery own
c Cathodic
f Manifold feed line
i Running index
k Running index
M Material
n Running index
p Cell port
P Power (W)
l Load
t Manifold tube
z Cell
* Refers to equivalent quantities

References

1 N. D. Koshel and O. S. Ksenzhek, *Elektrokhimiya, 7* (1971) 850.
2 S. Szpak, C. J. Gabriel and J. R. Driscoll, *J. Electrochem. Soc., 131* (1984) 1996.
3 P. van Rysselberghe, *Electrochim. Acta, 11* (1966) 125.
4 P. van Rysselberghe, *Thermodynamics of Irreversible Processes*, Hermann (Paris) and Blaisdell Publ. Co, (New York).
5 S. Szpak, C. J. Gabriel and J. R. Driscoll, *Electrochim. Acta, 32* (1987) 239.

J. Chem. Soc., Faraday Trans. 1, 1989, **85**(1), 11–21

Raman and Infrared Spectroscopy of the $AlCl_3$–$SOCl_2$ System

Pamela A. Mosier-Boss, Roger D. Boss, Cedric J. Gabriel and Stanislaw Szpak
Naval Ocean Systems Center, San Diego, CA 92152-5000, U.S.A.

Jerry J. Smith
Naval Weapons Center, China Lake, CA 93555-6001, U.S.A.

Robert J. Nowak
Office of Naval Research, Arlington, VA 22217-5000, U.S.A.

The structural aspects of the $AlCl_3$–$SOCl_2$ system have been examined by vibrational spectroscopy. The $SOCl_2$ molecule exhibits amphoteric character, *i.e.* it can act simultaneously as a donor through the oxygen atom and as an acceptor through the sulphur atom. The liquid state contains loosely bound, open-chain dimers/oligomers, $(Cl_2SO)_n$ with $n \geqslant 2$. The dissolution of Al_2Cl_6 in $SOCl_2$ occurs dissociatively with the formation of $Cl_2SO \rightarrow AlCl_3$ adducts. At higher $AlCl_3$ concentrations, an increase in solution electrical conductivity is attributed to the reaction:

$$2\,Cl_2SO \rightarrow AlCl_3 \rightleftharpoons [Cl_2Al(\leftarrow OSCl_2)_2]^+ + AlCl_4^-$$

Hecht,[1] followed by Spandau and Brunneck[2] proposed the existence of 1:1 and 2:1 $AlCl_3$–$SOCl_2$ adducts. In the early 1960s, Long and Bailey[3] examined the structural features of these adducts and concluded that complexation occurred through the oxygen atom of $SOCl_2$. A few years later, Auborn and co-workers[4] employed this system in the construction of Li galvanic cells of highest practical energy densities. Their work prompted further inquiry into the nature, structure and reactivity of the various $SOCl_2$ complexes associated with the Li–$SOCl_2$ cell operation.[5–8]

Here, we discuss the structure of neat $SOCl_2$ and is reactivity through interaction with a set of selected miscible liquids. We include an analysis of the structural changes and species produced by the addition of Al_2Cl_6 to $SOCl_2$.[8]

Experimental

Chemicals

Thionyi chloride was refluxed under an argon or helium atmosphere to remove dissolved HCl and SO_2 with the end point indicated by pH paper located in the gas exit stream. The $SOCl_2$ was then distilled and the middle fraction was collected and stored under argon. Aluminium chloride, benzene, carbon tetrachloride and hexanes, all of spectroscopic grade (Fluka), and toluene and methylene chloride (Aldrich, gold label) were used as received.

Solutions

All solutions were prepared in a glove bag by diluting known volumes of $SOCl_2$ with CCl_4, CH_2Cl_2, C_6H_{14} or $C_6H_5CH_3$. The $AlCl_3$–$SOCl_2$ solutions were prepared from known amounts of Al_2Cl_6 and filtered through a glass-fibre filter prior to use.

Instrumentation

Infrared spectra were obtained on a Nicolet 5DXB FT-IR spectrometer with a resolution of $2\,cm^{-1}$. Standard demountable cells with NaCl windows were used throughout. The pathlength was maintained at 2.5×10^{-5} m; spectra were subtractively normalized to compensate for solvent absorption.

The Raman spectra were recorded on a system comprising a Lexel model 85 Ar-ion laser emitting at 488 nm, which was chopped at 20 Hz, a sample chamber with coupling and collecting optics, a Spex model 1400–11 scanning double monochromator with photon-counting preamplifier and line driver, a photon-counting integrator[9] and a digital synchronous detector. The samples were contained in a Helma model 162 F stoppered quartz cell. The cell chamber was flushed with dry nitrogen to prevent condensation on the cell windows when operating below room temperature. Temperatures were controlled to within ± 0.1 °C. Most of the spectra were recorded at a laser power of 50 mW.

Resolution of Spectral Bands

The recorded infrared absorption and Raman-scattering bands were computer-analysed and decomposed into their component Voigt profiles using a previously described procedure.[10] In a dynamic system, comprising a number of species, N, with overlapping spectral lines, the experimentally observed spectral band intensity, $I(\nu)$, is a superposition of at least N lines, and can be approximated by eqn (1)

$$I(\nu) = C_0(\nu - \alpha) + \sum_{i=1}^{N} C_i f_i(\ldots) \tag{1}$$

where α, C_0 and C_i are adjustable parameters and $f(\ldots)$ is defined by eqn (2)

$$f(\nu, \nu_0, \Delta\nu_L, \Delta\nu_G) = \frac{2\ln 2}{\pi^{\frac{3}{2}}} \frac{\Delta\nu_L}{\Delta\nu_G^2} \int_{-\infty}^{\infty} \frac{\exp(-y^2)}{a^2 + (y-\omega)^2} dy \tag{2}$$

where $$a = \Delta\nu_L \sqrt{(\ln 2)/\Delta\nu_G}, \quad \omega = 2(\nu - \nu_0)\sqrt{(\ln 2)/\Delta\nu_G},$$

and ν_0, $\Delta\nu_L$ and $\Delta\nu_G$ are, respectively, the centre frequency, and the full widths at half maximum of the Lorentzian and Gaussian distributions that characterize the line. The linear term $C_0(\nu - \alpha)$ has been added to account for a sloping baseline.

Molecular-orbital Calculations

Calculations were performed using AMPAC, a general purpose, semi-empirical molecular-orbital package developed at the University of Texas (Austin, TX). These calculations yield information on electronic and core–core repulsion energies, heats of formation and vibrational frequencies.

Results and Discussion

The molecular structure of a liquid arises from interactions between neighbouring molecules. This premise allows us to follow structural changes as the molecules adapt themselves to the changing environment, *e.g.* to changes in solution composition or temperature. For example, $SOCl_2$, being an amphoteric molecule, may form dimers/oligomers. In the more complex $AlCl_3$–$SOCl_2$ system, such interactions can lead to the formation of molecular adducts and ionic species.[8]

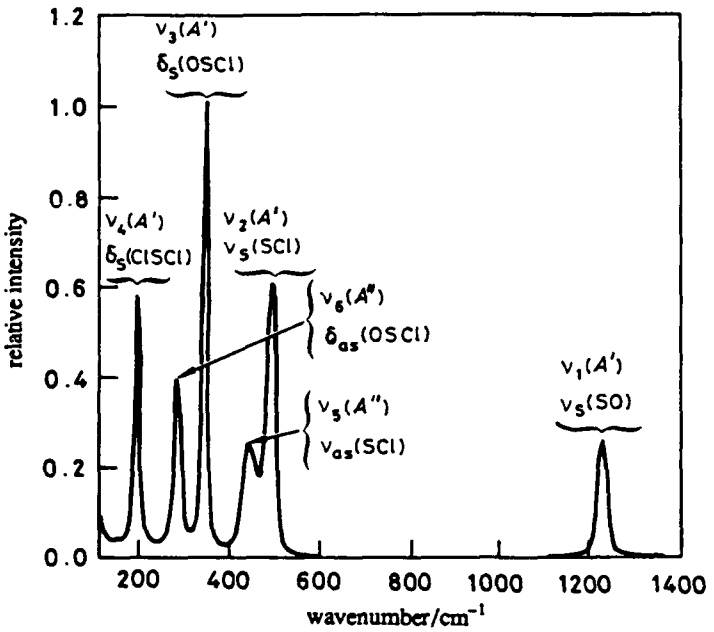

Fig. 1. Raman spectrum of neat $SOCl_2$: vibrational modes and assignments.

Method of Analysis

The $SOCl_2$ molecule is of the ZXY_2 type and a member of the C_s symmetry point group.[11] It has six normal modes of vibration, all Raman and infrared active. The Raman spectrum of neat $SOCl_2$ and the assignments are shown in fig. 1. The structural characteristics of $SOCl_2$ in the liquid state as well as the $AlCl_3$–$SOCl_2$ system are ascertained by examining the position and lineshape of $\nu_1(A')$, the symmetric S—O stretching vibration at 1231 cm^{-1} and the $\nu_2(A')$ and $\nu_5(A')$ symmetric and asymmetric S—Cl stretching vibrations at 492 and 455 cm^{-1}, respectively; these vibrational modes are sensitive to changes in the charge distribution arising from molecular interactions.

The S=O bond of $SOCl_2$ has partial double bond character which results from the superposition of $p\pi \rightarrow d\pi$ back-bonding from O to S upon the $S \rightarrow O$ σ bond.[12] According to the valence-shell electron-pair repulsion (VSEPR) model, bonding through the oxygen atom should lessen the $p\pi \rightarrow d\pi$ back-bonding and, hence, lower the S=O bond-order and stretching frequency. Conversely, bonding through the sulphur atom increases the $p\pi \rightarrow d\pi$ back-bonding, thus raising the S—O stretching frequency. Withdrawal of electron density from the S=O bond will decrease the repulsion between the lone pair of electrons on the sulphur and the chlorine atoms of $SOCl_2$, which, in turn, strengthens the S—Cl bonds and shifts the symmetric and asymmetric S—Cl stretching vibrations to higher frequency. Moreover, coordination through the sulphur atom will reduce the repulsion between the sulphur lone pair of electrons and the chlorines, also shifting the symmetric and asymmetric S—Cl stretching vibrations to higher frequencies. Examples of this kind of behaviour have been reported for the metallic complexes of $(CH_3)_2SO$, in which complexation with Zn^{2+}, Al^{3+}, Ni^{2+}, Co^{2+}, Fe^{2+} and Fe^{3+} ions occurs through the oxygen atom while complexation with Pd^{2+} and Pt^{2+} occurs through the sulphur atom.[13]

Thionyl Chloride in the Liquid State

In the liquid state, the S—O stretching frequency is at 1231 cm^{-1}; whereas, in the gaseous state it occurs at 1251 cm^{-1}.[14] This rather small shift to lower frequency upon

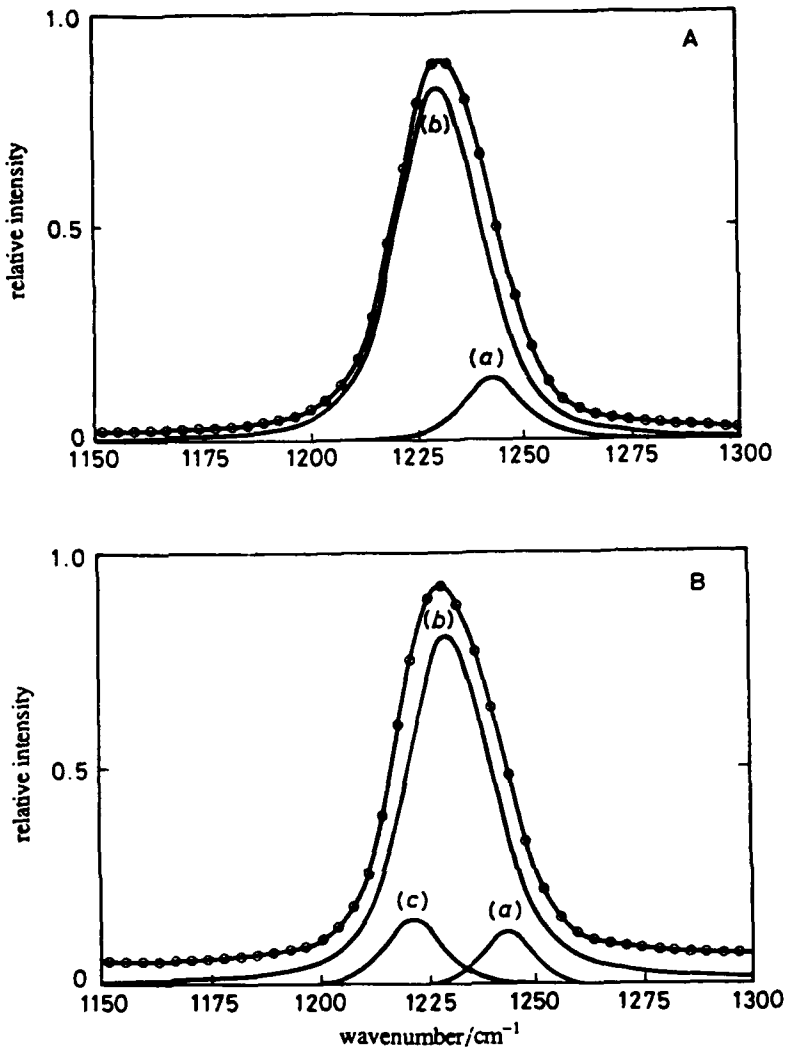

Fig. 2. Decomposition of S—O stretching spectral band of neat $SOCl_2$ into Voigt profiles: A, 23.5 °C; B, −20.0 °C.

condensation of $SOCl_2$ implies that the intermolecular interactions are weak. At 23.5 °C the S—O stretch of neat $SOCl_2$ at 1231 cm^{-1}, shown in fig. 2, is actually a composite band which has been resolved into two Voigt profiles with peaks at 1242.6 and 1230.5 cm^{-1}, profiles (*a*) and (*b*) respectively. However, at −20 °C the S—O stretch of neat $SOCl_2$ can be resolved into three Voigt profiles with peaks at 1243.5, 1230.8 and 1221.5 cm^{-1}, profiles (*a*), (*b*) and (*c*), respectively, in fig. 2. This band structure suggests that pure $SOCl_2$ is a weakly associated liquid, which, in view of the rather low latent heat of vaporization and the numerical value of the slope of the fluidity as a function of specific volume,[8] indicates the presence of small, interacting molecular clusters.

The existence of the association implies that the $SOCl_2$ molecule is amphoteric, *i.e.* it acts simultaneously as a donor through the oxygen atom, and as an acceptor through the sulphur. Thionyl chloride may self-associate in two ways; *via* sulphur-to-oxygen bonding in either a cyclic-dimer form, or an open chain form, which may contain more than two members, and *via* sulphur–sulphur association. In longer chains, a cooperative effect may increase the donor character of the S=O bond.

Dilution experiments were performed to determine the structure of the associated

species of $SOCl_2$. Infrared spectroscopy was used to examine the changes in the lineshape and position of the S—O stretching vibrational band upon dilution in three types of solvents: (*a*) poor acceptors (inert solvents), *e.g.* C_6H_{14} and CCl_4; (*b*) π-interacting solvents, *e.g.* $C_6H_5CH_3$; and (*c*) a polar liquid, *e.g.* CH_2Cl_2 (with $\mu = 1.6$ D†).[15] On the basis of the VSEPR model, as well as more general donor–acceptor considerations,[16] the following characteristics of the S—O stretch of the monomer and associated species of $SOCl_2$ are expected. For a monomer, the S—O stretching vibrational peak should be fairly narrow and its peak position should be solvent dependent. The cyclic dimer, should also exhibit a fairly narrow peak but its position should be relatively solvent independent. Furthermore, because of the decrease in repulsion between the lone pair of electrons on the sulphur atom and the negative charge on the chlorine atoms, the separation between the S—Cl symmetric and asymmetric stretches, ν_2 and ν_5, respectively, should be less than that for the monomer. For an open chain dimer/oligomer, the peak position of the S—O stretching frequency is expected to be solvent dependent and the peak should be broader than that of the monomer. The open-chain dimer probably has two different S=O bonds. The extent to which these differ will depend on the strength of the interaction within the dimer. If the strength of the interaction were on the order of an ionic or covalent bond then both these S=O vibrational bands would be observed. However, as the strength of the interaction decreases, the separation between these two bands would also decrease eventually resulting in one broad band. This would be the expected result for dipole–dipole and dipole–induced-dipole interactions. Finally, the separation between ν_2 and ν_5 is expected to be greater for the open dimer than for the monomer due to increased repulsion between the chlorines and lone pair of electrons on the sulphur atom.

Results of dilution experiments are as follows. In all solvents, within the $SOCl_2$ concentration range studied, the S—O Voigt profile at 1221.5 cm^{-1}, $\nu(c)$ in fig. 2, is not observed. For this reason and the fact that it is observed only in neat $SOCl_2$ at low temperatures, this band is attributed to higher aggregates, *i.e.* to trimers, tetramers *etc.* Furthermore, it is seen that the peak position of the other two Voigt profiles is solvent dependent. In CCl_4 and hexanes, which are considered to be 'inert' solvents, the high-frequency peak, $\nu(a)$, is narrower than the low-frequency peak, $\nu(b)$. In these solvents, the association of $SOCl_2$ is expected to be the dominant reaction. Therefore the high frequency peak, $\nu(a)$ is assigned to the monomer and the low frequency peak, $\nu(b)$, to dimer. The ratio of the areas of these peaks is consistent with these assignments. Since $\nu(b)$ is broader than $\nu(a)$, we conclude that the dimer is one of the open type as shown in fig. 3(*a*). Further evidence for an open structure can be found in the separation between the symmetric and asymmetric S—Cl stretches, ν_2 and ν_5. In the gaseous state this separation is 37 cm^{-1}, whereas in the liquid state, it is 47 cm^{-1}.[14]

In methylene chloride, both $\nu(a)$ and $\nu(b)$ of the S—O stretching bands are very broad. With a dipole moment of 1.60 D, CH_2Cl_2 is a weakly polar solvent; thus one expects dipole–dipole interactions to occur between CH_2Cl_2 and $SOCl_2$. Such interactions have been observed for $(CH_3)_2SO$ and $CHCl_3$.[15,16] The behaviour of the S—O stretching composite band of $SOCl_2$ solutions in $C_6H_5CH_3$ is similar to that observed in CCl_4 and C_6H_{14}; *i.e.* $\nu(a)$ is fairly narrow and $\nu(b)$ is broader. From this we conclude that any interactions between $SOCl_2$ and $C_6H_5CH_3$ are very weak and that self-association of $SOCl_2$ is the dominant reaction.

The results of the MO calculations provide additional insights into the possible structures of neat $SOCl_2$ in the liquid state. In particular, calculations have been performed for dimeric $SOCl_2$ using the structures S—O—S—O in cyclic form and in open chain, as well as the O—S—S—O type of association. The calculations showed that the oxygen–sulphur associated dimers are favoured, fig. 3. The sulphur–sulphur

† 1 D = 3.33564×10^{-30} C m.

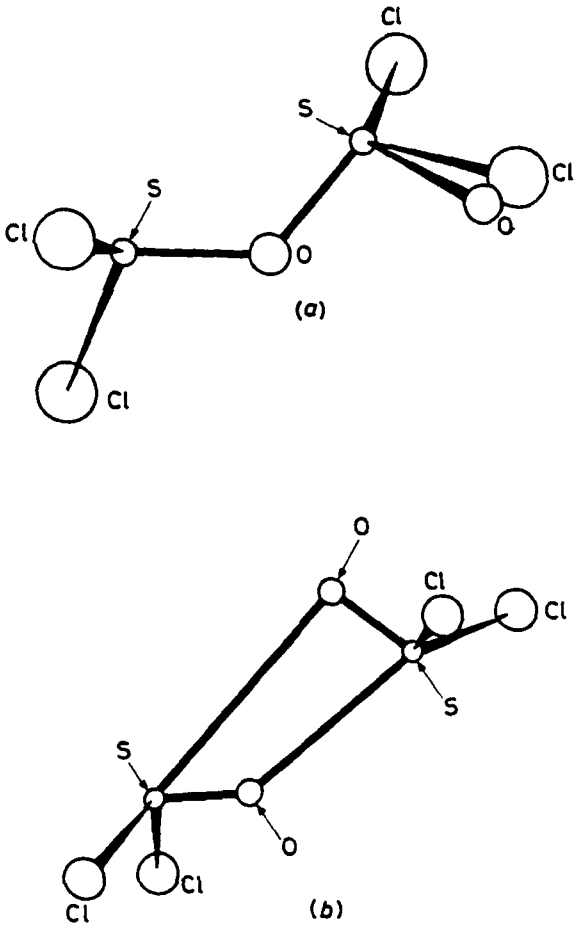

Fig. 3. MO-optimized structures: (*a*) open dimer; (*b*) cyclic dimer.

associated species gives an S—S bond length exceeding 6 Å (6×10^{-10} m) thereby suggesting little or no association *via* this bonding arrangement. Furthermore, the MO calculations indicate that ordered dimeric structures, as well as longer oligomeric structures, can exist in the liquid state with essentially the same stability as the molecular $SOCl_2$ itself, and, yet, are not of significantly different stability so as to dominate the structure of the liquid $SOCl_2$.

The dilution experiments supported by molecular-orbital calculations indicate the presence of dimers with the open-chain spatial arrangement illustrated in fig. 3(*a*) rather than the cyclic form, fig. 3(*b*). In fact, calculations of cyclic dimer structures invariably led to optimized geometries in which the cyclic dimer opened to form an open-chain dimer. These MO calculations yield structures whereby the lone pairs of the sulphurs are directed away from one another. This implies that the repulsion between the lone pair of electrons on the sulphur atom is principally responsible for molecular structure of $SOCl_2$ dimers. Similar arguments for the formation of the cyclic dimers results in a highly improbable structure; the repulsion between the lone pair of electrons with the simultaneous requirement for the charge transfer for $O_1 \rightarrow S_2$ and $O_2 \rightarrow S_1$, creates a distorted arrangement.

In summary, $SOCl_2$ in the liquid state consists of weakly associated species having an open structure. The presence of cyclic dimers, which could be possible, is excluded on a basis of MO calculations.

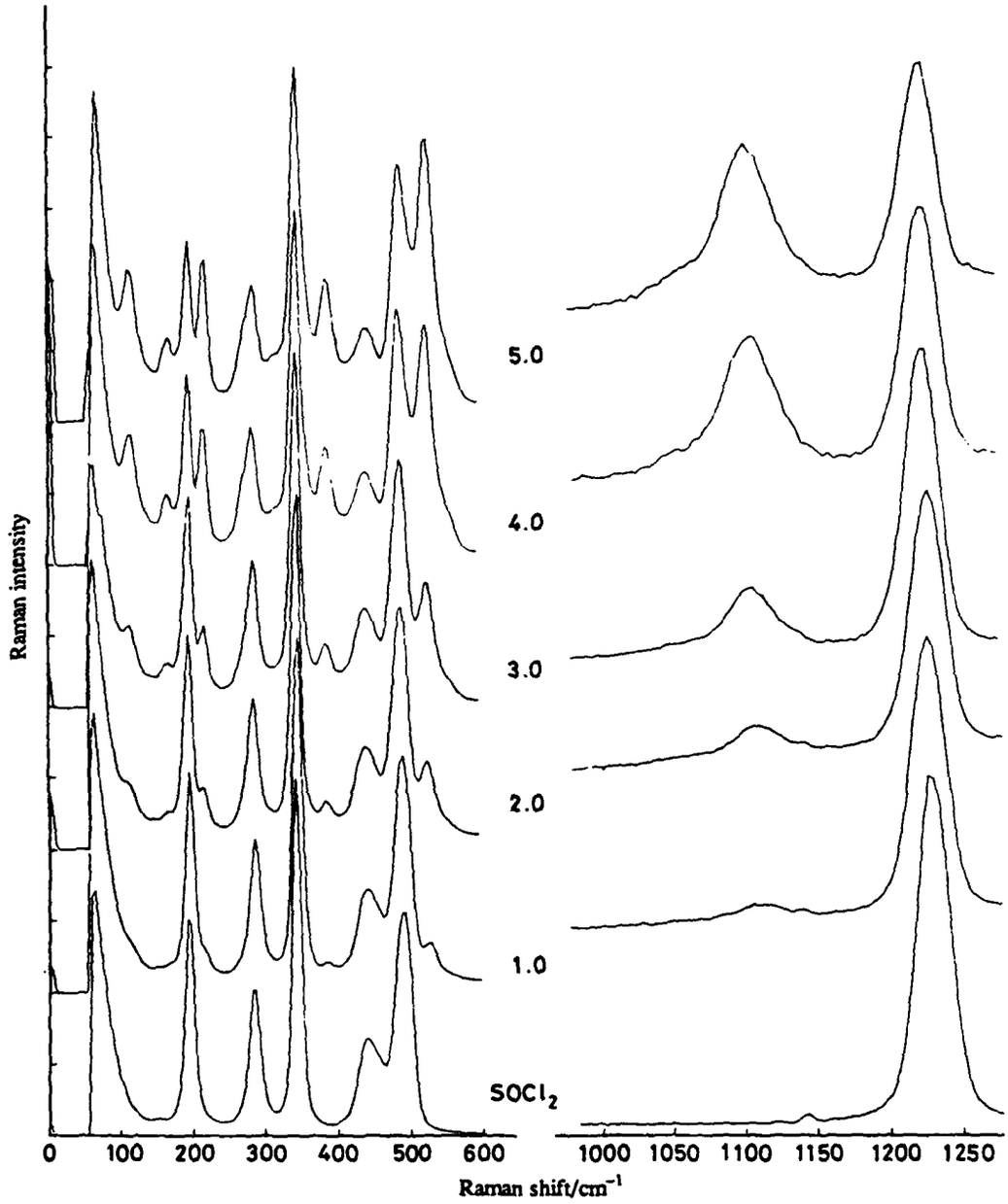

Fig. 4. Evolution of Raman Spectra as a function of $AlCl_3$ concentration (mol dm^{-3}).

The $AlCl_6$–$SOCl_2$ System

With the addition of Al_2Cl_6, a covalent compound containing halogen bridges, a new set of Raman bands appears and indicates the formation of adduct(s). In the course of 1:1 adduct formation, the Al—Cl—Al bonds of the acceptor molecular must first be broken. The improvement in coordination makes the formation of the 1:1 adduct energetically favourable. The progressive changes in the Raman spectra are shown in fig. 4. Upon the addition of Al_2Cl_6 the Raman spectra become more complex. In addition to bands at 1108, 523, 383, 217, 167 and 114 cm^{-1}, a band at *ca.* 1055 cm^{-1} emerges, and gains in intensity with increasing Al_2Cl_6 concentration. It is noteworthy that the appearance of this band is accompanied by an increase in the solution conductivity.[8]

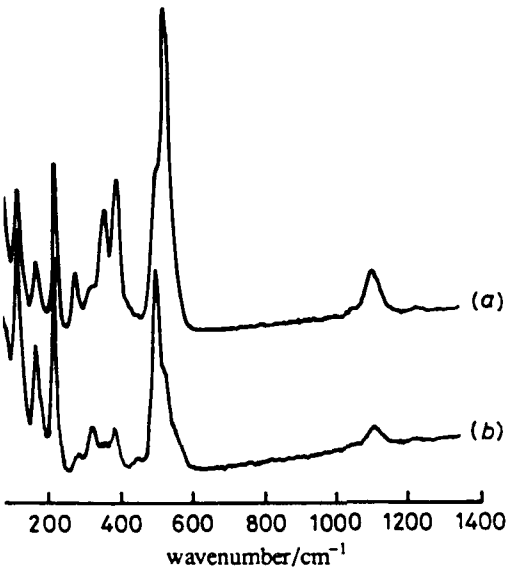

Fig. 5. Polarized (*a*) and depolarized (*b*) Raman Spectra of the equimolar $AlCl_3$–$SOCl_2$ solution.

The polarized and depolarized Raman spectra of the equimolar $AlCl_3$–$SOCl_2$ solution are shown in fig. 5. The most significant changes are the disappearance of the band at 1231 cm^{-1} the S—O stretching vibration of neat $SOCl_2$, and an emergence of a new band at *ca.* 1108 cm^{-1}. Such a change in the S—O stretching frequency accompanied by the shift observed in the symmetric and asymmetric S—Cl stretches to higher frequencies (*i.e.* from 492 to 523 and from 455 to 500 cm^{-1}, respectively) is consistent with complexation of $AlCl_3$ through the oxygen atom of $SOCl_2$. The observed vibrational modes of the $AlCl_3$–$SOCl_2$ complex(es) and their assignments are shown in table 1. These assignments correspond with those made for the $AlCl_3$ complexes with tetrahydrofuran, C_4H_8O[18,19] and nitromethane, CH_3NO_2.[20]

Species and Equilibria

An examination of the 1000–1300 cm^{-1} spectral region, fig. 4, indicates the formation of, at least, two distinct species. The first species, with the S—O stretching vibrational frequency $\nu_1(A')$ at 1108 cm^{-1}, has been attributed to the 1:1 adduct, $Cl_2SO \rightarrow AlCl_3$. The identification of the species exhibiting a broad band at 1055 cm^{-1} is less certain. For example, the broadness of this peak as well as the shift of $\nu_1(A')$ to lower frequency indicates further electron withdrawal from the oxygen atom perhaps from the formation of a 1:2 complex, $Cl_2SO(AlCl_3)_2$ by the reaction

$$2\,Cl_2SO \rightarrow AlCl_3 \rightleftharpoons Cl_2SO \rightarrow (AlCl_3)_2 + SOCl_2. \qquad (I)$$

Such a conclusion is consistent with the existence of 1:2 complex in the solid state.[3] Spectroscopically, this equilibrium requires that the ratio of the area of the band at 1055 cm^{-1} to the area of the 1108 cm^{-1} band should increase with increasing $AlCl_3$ concentration. However, it is observed that this ratio is nearly constant at 0.3 ± 0.1 for all concentrations of $AlCl_3$ in which the two bands can be resolved. Fig. 6 shows the decomposition of the S—O stretch of the $AlCl_3$ adducts. Furthermore, an increase in the solution electrical conductivity which coincides with the appearance of this band offers an alternative interpretation, namely that of formation of ionic species.

Molecular adducts are neutral molecules. Formation of ions from the $Cl_2SO \rightarrow AlCl_3$

Table 1. Vibrational assignments and calculated frequencies for the Raman spectrum of the 1:1 $AlCl_3$–$SOCl_2$ complex and other observed vibrations for the 1:1 solution

vibrational mode	ν_{obsd}/cm^{-1} observed frequency	ν_{calcd}/cm^{-1} calculated frequency
O—Al—Cl bending of complex	< 110	35,101
$AlCl_3$ rocking of complex	114	116
$AlCl_3$ bending of complex	—	121
$AlCl_3$ bending of complex	167	157
Cl—Al—Cl bending of $AlCl_4^-$	181 (w)	—
deformation of complex	—	184
SCl_2 bending of free $SOCl_2$	194[a] (p)	167
SCl_2 bending of complex	217	192
Al—O—S bending of complex	274	283
$SOCl_2$ torsion of free $SOCl_2$	282	—
$SOCl_2$ torsion of complex	318	—
$SOCl_2$ deformation of free $SOCl_2$	344 (p)	340
$SOCl_2$ deformation of complex, Al—Cl symmetric stretching of $AlCl_3$ and $AlCl_4^-$	355	335
Al—O stretching of complex	383	503
Al—O stretching[b]	419 (w)	—
Al—O stretching[b]	428 (w)	—
S—Cl asymmetric stretching of free $SOCl_2$	455[a]	566
Al—Cl asymmetric stretching of complex	—	395,566
S—Cl asymmetric stretching of free $SOCl_2$	492[a] (p)	615
S—Cl asymmetric stretching of complex	500	608
S—Cl symmetric stretching of complex	523	645
$AlCl_3$ degenerate stretching of complex[c]	560 (w)	588
S—O stretching[b]	1055	—
S—O stretching of complex	1108 (p)	1330
S—O stretching of free $SOCl_2$	1231 (p)	1374

(w) weak. (p) polarized. [a] not observed in the equimolar solution. [b] band due to either $Cl_2(SO) \rightarrow (AlCl_3)_2$ or $Cl_2Al(\leftarrow OSCl_2)_2^+$. [c] compare with 525 cm^{-1} for the 1:1 $AlCl_3$: tetrahydrofuran complex, 532 cm^{-1} for the 1:1 $AlCl_3$: nitromethane complex, and both bands are weak in the Raman.

adduct can occur either *via* the halide ion transfer or the internal exchange route, eqn (II) and (III), respectively.

$$Cl_2SO \rightarrow AlCl_3 \rightleftharpoons SOCl^+ + AlCl_4^- \quad \text{(II)}$$

$$2\,Cl_2SO \rightarrow AlCl_3 \rightleftharpoons Cl_2Al(\leftarrow OSCl_2)_2^+ + AlCl_4^-. \quad \text{(III)}$$

Of these ions, the presence of the $AlCl_4^-$ ions is documented by a weak band at 181 cm^{-1}, and attributed to the Cl—Al—Cl bending mode, fig. 5. The stronger bands associated with a $AlCl_4^-$, complex ion, *i.e.* the bands at 122 and 350 cm^{-1}, are obscured by vibrational modes of the free and complexed $SOCl_2$. The $AlCl_4^-$ ion also has a band at 495 cm^{-1} which is strong in the i.r.[23] An attempt was made to see this band by adding LiCl to 4.0 mol dm^{-3} $AlCl_3$ in $SOCl_2$. Such a solution would contain $AlCl_4^-$ as well as $Li(SOCl_2)_2^+$. Owing to the overlapping S—Cl vibrational bands of neat $SOCl_2$ as well as $SOCl_2$ complexed by $AlCl_3$ and Li^+, it was not possible to discern the 495 cm^{-1} band of $AlCl_4^-$. There is no spectroscopic evidence for the positively charged $SOCl^+$ species, as required by eqn (II) and suggested by others.[1-3] On the other hand, the evidence for the

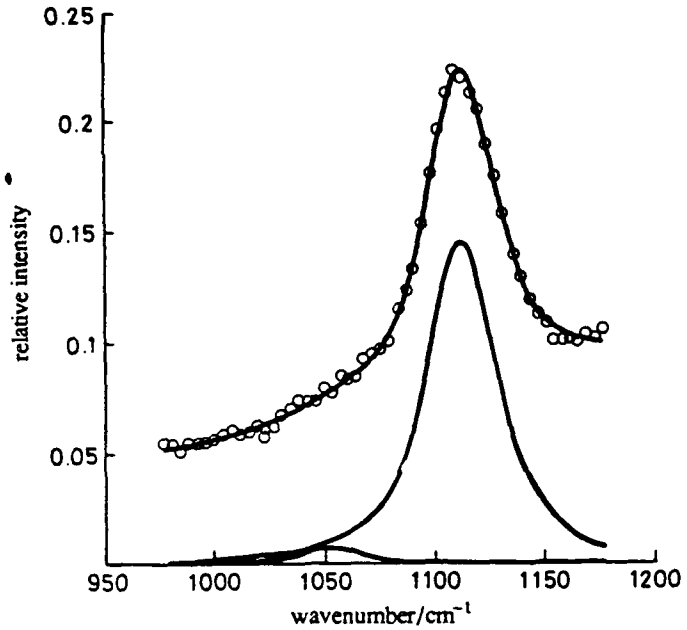

Fig. 6. Decomposition of the S—O stretching spectral band associated with the aluminium complex of 4.0 mol dm^{-1} $AlCl_3$ in $SOCl_2$ at −20.0 °C into Voigt profiles.

presence of the $[Cl_2Al(\leftarrow OSCl_2)_2]^+$ ions, eqn (III), is as follows. The S=O bond in the onium ion must be weakened due to the reduced $p\pi \rightarrow d\pi$ back-bonding, thus lowering the vibrational frequency *vs.* that of a neutral adduct. The appearance of a new band at 1055 cm^{-1} supports its presence. Furthermore, because the $[Cl_2Al(\leftarrow OSCl_2)_2]^+$ would have a positive charge on the Al atom, its Al—O bond would be stronger than that for a neutral complex. This, in turn, would shift the Al—O stretching vibrations to higher frequencies. Indeed, in the neutral adduct the Al—O stretching mode occurs at 383.3 cm^{-1} while in the conductive, equimolar $AlCl_3$–$SOCl_2$ solution, new weak bands attributed to the ionic complex, were found at 419 and 428 cm^{-1}. In addition, eqn (III) requires that the concentration of the $AlCl_4^-$ ion must be equal to that of the $Cl_2Al(\leftarrow OSCl_2)_2^+$ ion. The equilibrium constant expression may be rearranged to give eqn (IV):

$$[Cl_2Al(\leftarrow OSCl_2)_2]^+ = K[Cl_2SO \rightarrow AlCl_3] \qquad \text{(IV)}$$

which requires that the areas of the bands at 1055 and 1108 cm^{-1} be in constant proportion, *i.e.* independent of the $AlCl_3$ concentration, as observed.

The results of the MO calculations of relative stabilities of the mono- and di-solvated onium complex favour the latter as the dominant species responsible for the increase in solution conductivity. The suggested structure is a tetrahedral arrangement about the Al with $SOCl_2$ coordination through the oxygen, *i.e.* consistent with eqn (IV).

On the basis of the argument presented, the 1055 cm^{-1} band is assigned to the $[Cl_2Al(\leftarrow OSCl_2)_2]^+$ ion.

Conclusions

(*a*) Neat $SOCl_2$ is an associated liquid which forms open chain dimers/oligomers $(Cl_2SO)_n$ with $n = 2, 3, 4 \ldots$; (*b*) aluminium chloride dissolves dissociatively in $SOCl_2$ *i.e.* as $AlCl_3$ not Al_2Cl_6; (*c*) complexation of $SOCl_2$ with $AlCl_3$ occurs through the oxygen to form the adduct, $Cl_2SO \rightarrow AlCl_3$; (*d*) the $Cl_2SO \rightarrow AlCl_3$ adduct dissociates to yield the ionic species $[Cl_2Al(\leftarrow OSCl_2)_2]^+$ and $AlCl_4^-$.

This work was in part supported by the Office of Naval Research.

References

1 H. Hecht, *Z. Anorg. Chem.*, 1947, **254**, 44.
2 H. Spandau and E. Brunneck, *Z. Anorg. Chem.*, 1952, **270**, 201; 2.
3 D. A. Long and R. T. Bailey, *Trans. Faraday Soc.*, 1963, **59**, 594.
4 J. J. Auborn, K. W. French, S. I. Lieberman, V. K. Shah and A. Heller, *J. Electrochem. Soc.*, 1973, **120**, 1613.
5 K. C. Tsaur and R. Pollard, *J. Electrochem. Soc.*, 1984, **131**, 975; 984; 1986, **133**, 2296.
6 M. J. Madou, J. J. Smith and S. Szpak, *J. Electrochem. Soc.*, 1987, **134**, 2794.
7 J. R. Driscoll, R. Pollard, J. J. Smith and S. Szpak, in *Power Sources 11* (Academic Press, 1987).
8 S. Szpak and H. V. Venkatasetty, *J. Electrochem. Soc.*, 1984, **131**, 961.
9 S. A. Miller, *Rev. Sci. Instr.*, 1968, **39**, 1923.
10 P. A. Mosier-Boss, C. J. Gabriel and S. Szpak, *Spectrochim. Acta, Part A*, 1987, **43**, 1293.
11 R. A. Suthers and T. Henshall, *Z. Anorg. Allg. Chem.*, 1972, **388**, 269.
12 F. A. Cotton and R. Francis, *J. Am. Chem. Soc.*, 1960, **82**, 2986.
13 J. Selbin, W. E. Bull and L. H. Holmes Jr, *J. Inorg. Nucl. Chem.*, 1961, **16**, 219.
14 D. E. Martz and R. T. Lagemann, *J. Chem. Phys.*, 1954, **22**, 1193.
15 W. Lin and S. Tsay, *J. Phys. Chem.*, 1970, **74**, 1037.
16 A. L. McChellan, S. W. Nicksic and J. C. Guffy, *J. Mol. Spectrosc.*, 1963, **11**, 340.
17 M. Dalibart, J. Derouault, P. Granger and S. Chapelle, *Inorg. Chem.*, 1982, **21**, 1040.
18 J. Derouault and M. T. Forel, *Inorg. Chem.*, 1977, **16**, 3207.
19 J. Derouault, P. Granger and M. T. Forel, *Inorg. Chem.*, 1977, **16**, 3214.
20 M. Dalibart, J. Deroault and P. Granger, *Inorg. Chem.*, 1982, **21**, 2241.
21 I. Lindquist, *Inorganic Adduct Molecules of Oxo-compounds* (Academic Press, New York, 1963).
22 V. Gutmann, *The Donor–Acceptor Approach to Molecular Interactions* (Plenum Press, New York, 1978).
23 J. E. H. Jones and J. L. Wood, *Spectrochim. Acta, Part A*, 1967, **23**, 2695.

Paper 7/2000; *Received* 10*th November*, 1987

$LiCl-AlCl_3-SOCl_2$ System

Structures, Species, and Equilibria

P. A. Mosier-Boss* and S. Szpak*

Naval Ocean Systems Center, San Diego, California 92152-5000

J. J. Smith*,[1]

Naval Weapons Center, China Lake, California 93555-6001

R. J. Nowak*

Office of Naval Research, Arlington, Virginia 22217-5000

ABSTRACT

The addition of LiCl to the $AlCl_3$-$SOCl_2$ binary system results in the destruction of the $Cl_3Al \leftarrow OSCl_2$ adduct and onium ion, $[Cl_2Al(\leftarrow OSCl_2)_2]^+$, to form solvated $Li(\leftarrow OSCl_2)_2^+$ ion and the complex $AlCl_4^-$ ion. Spectroscopic evidence as well as molecular orbital calculations show that the S—O bond energies of free and complexed $SOCl_2$ can be arranged in a series: $Cl_2SO > (Cl_2SO)_2 > Li(\leftarrow OSCl_2)_2^+ > Cl_3Al \leftarrow OSCl_2 > [Cl_2Al(\leftarrow OSCl_2)_2]^+$. Structural aspects of the $LiCl$-$AlCl_3$-$SOCl_2$ electrolytes derived from viscosity and conductivity data are in agreement with spectroscopic evidence.

One of the major, as yet unresolved, issues in maximizing $Li/SOCl_2$ cell performance is the mechanism of $SOCl_2$ electroreduction. The available evidence (1), supported by more general considerations (2, 3), suggests the importance of the composition as well as structural aspects of bulk electrolyte on the kinetics of the charge transfer process. Madou *et al.* (1) have provided some evidence for the participation of more than one $SOCl_2$-bearing species. Venkatasetty (4), in discussing the role of transition metal phthalocyanines in the charge transfer process, viewed the rate enhancement as due to the formation of thionyl chloride adducts with phthalocyanines.

Recently, the structural aspects of the $AlCl_3$-$SOCl_2$ system have been examined by Mosier-Boss *et al.* (5). This communication reports on changes that occur within this system upon the addition of LiCl, examines structures of the electrolyte constituents by molecular orbital (MO) calculations, and concludes by comparing results with those obtained earlier from transport properties, *viz.* viscosity and conductivity (6).

Experimental

All solutions were prepared in a controlled atmosphere by dissolving known amounts of spectroscopic grade Al_2Cl_6 and LiCl in freshly distilled $SOCl_2$. Raman spectra were obtained on a system comprised of an Ar-ion laser emitting at 488 nm with a power of 50 mW. The samples were contained in a quartz cell with provisions for temperature control to within 0.2°C and covering the range of −20° to 40°C. The investigation was limited to the xM LiCl-3M $AlCl_3$ in $SOCl_2$ with $0 \leq x \leq 3.0$. In addition, a special case of 1:1:2 $LiCl:AlCl_3:SOCl_2$ was included.

The MO calculations were performed using AMPAC, a general purpose, semi-empirical molecular orbital package developed at the University of Texas, Austin, Texas. These calculations yield information on the size, shape, and charge distribution within molecules and complexes. The recorded S—O stretching vibrations of neat and complexed $SOCl_2$ were computer analyzed and decomposed into their component Voigt profiles using a previously described procedure (7).

Results and Discussion

The discussion of the mechanism of $SOCl_2$ electroreduction, as applied to $Li/SOCl_2$ cells, invariably assumes that the rate-determining step (rds) is the reaction

$$SOCl_2 + e^- \rightarrow SOCl^* + Cl^- \qquad [1]$$

which is followed by a series of steps involving the SOCl* radical (8-10). The proposed mechanisms ignore the fact that the $SOCl_2$ molecule has been shown to form adducts with $AlCl_3$ (5, 11-14) and is able to enter the solvation sheet of ionic species either initially present or generated in the course of the charge transfer process. Furthermore, these mechanisms ignore the fact that neat $SOCl_2$ itself is an associated liquid, $(SOCl_2)_n$ with $n \geq 2$ (5). Thus, taking as a starting point a premise that the composition of the electrode/electrolyte interphase is related to the bulk, Eq. [1], as written, does not identify which $SOCl_2$ molecules reside in the reaction space and participate in the charge transfer process.

*Electrochemical Society Active Member.

[1] Present address: Department of Energy, ER 13, Washington, DC 20545.

Raman spectroscopy of the LiCl-$AlCl_3$-$SOCl_2$ system.—In the liquid state, the $SOCl_2$ molecules form clusters having an open zig-zag structure (5). Their Raman spectra are relatively simple. Upon addition of $AlCl_3$, these spectra become more complex, as illustrated in Fig. 1, spectra a, b, and c, for neat $SOCl_2$, 2.0 and 4.0*M* $AlCl_3$ solutions, respectively. In addition to bands at 194, 282, 344, 455, 492, and 1231 cm^{-1} for neat $SOCl_2$, new bands appear at 114, 167, 217, 274, 318, 383, 523, 560, and 1108 cm^{-1}. Assignments of these new spectral bands have been discussed elsewhere (5) with the conclusion that the addition of $AlCl_3$ results in the formation of the $Cl_2SO \rightarrow AlCl_3$ adduct. The observed shift in the $\nu_1(A')$ vibrational mode to lower frequency indicates that complexation occurs through the oxygen atom of $SOCl_2$. The bands at 114, 167, and 560 cm^{-1} are assigned to the $AlCl_3$ moiety of the $Cl_2SO \rightarrow AlCl_3$ adduct while those at 274 and 383 cm^{-1} have been assigned to the Al-O-S bending and Al-O stretching vibrations of the adduct, respectively. Uncomplexed $AlCl_3$ has bands occurring at 151, 183, 394, and 615 cm^{-1} (15).

The 100-600 cm^{-1} spectral region displays vibrational modes due to both $AlCl_3$ and $SOCl_2$, as illustrated in Fig. 1, making this region difficult to analyze because of numerous overlapping bands. In contrast, the vibrations observed in the region between 1000 and 1300 cm^{-1} are due to the S—O stretching vibrations of neat and complexed $SOCl_2$. This vibration is very sensitive to any change in charge distribution resulting from molecular interactions. Redistribution of electronic charge affects both the position and shape of the S—O vibrational band, $\nu_1(A')$, of the interacting $SOCl_2$ molecule.

The addition of $AlCl_3$ results in the formation of $Cl_2SO \rightarrow AlCl_3$ adducts. As the $AlCl_3$ concentration is increased, a new vibrational band appears at 1055 cm^{-1}, as shown in Fig. 1. This new band is very broad and is due to a S—O stretching vibration of a second $AlCl_3$-$SOCl_2$ species. The broadness of this band as well as the shift of the S—O stretching vibration to lower frequency indicates further electron withdrawal from the oxygen atom perhaps from the formation of a 1:2 complex, $Cl_2SO(AlCl_3)_2$, as suggested by others (11, 12). Such a conclusion is consistent with the existence of a 1:2 complex in the solid state (11). However, an increase in the solution conductivity coincides with the appearance of this band (6). Since molecular adducts are neutral and, as such, are nonconductive, this new band occurring at 1055 cm^{-1} is due to an ionic species and not to $Cl_2SO(AlCl_3)_2$. This ionic species has been identified as the onium ion, $[Cl_2Al(\leftarrow OSCl_2)_2]^+$, for reasons discussed elsewhere (5), which forms via the internal exchange reaction

$$2Cl_2SO \rightarrow AlCl_3 \rightleftarrows [Cl_2Al(\leftarrow OSCl_2)_2]^+ + AlCl_4^- \qquad [2]$$

yielding not only a positive onium complex $[Cl_2Al(\leftarrow OSCl_2)_2]^+$ but also a negative $AlCl_4^-$ ion (5). Since the ratio of the areas of the 1055 cm^{-1} peak, due to the onium ion, and the 1108 cm^{-1} peak, due to the neutral adduct, is very small, the degree of ionization is also very small.

The effect of LiCl addition on the structural features of the $AlCl_3$-$SOCl_2$ system is demonstrated in Fig. 2. Upon the addition of LiCl, the bands at 114, 167, 217, 383, 523, 560, and 1108 cm^{-1} disappear and new bands at 118, 178, 299, 358, 464, and 1215 cm^{-1} appear. The assignments of these

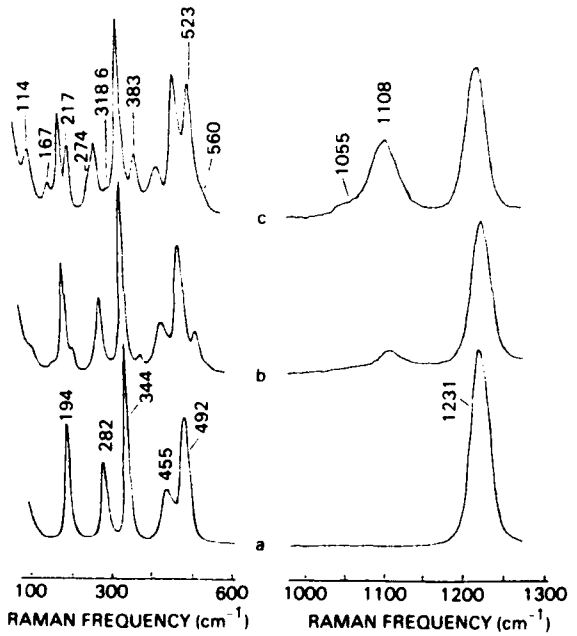

Fig. 1. Raman spectra of $AlCl_3$-$SOCl_2$ system: (a) neat $SOCl_2$; (b) 2.0M $AlCl_3$ in $SOCl_2$; (c) 4.0M $AlCl_3$-$SOCl_2$.

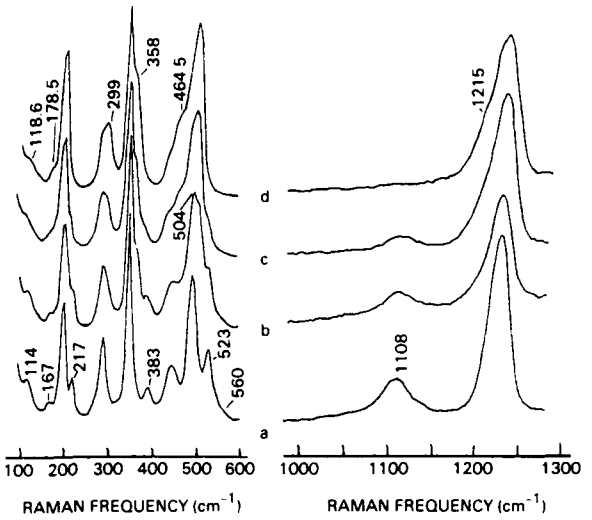

Fig. 2. Raman spectra of LiCl-$AlCl_3$-$SOCl_2$ system: (a) 3.0M $AlCl_3$ in $SOCl_2$; (b) 3.0M $AlCl_3$ and 1.0M LiCl in $SOCl_2$; (c) 3.0M $AlCl_3$ and 2.0M LiCl in $SOCl_2$; (d) 3.0M $AlCl_3$ and 3.0M LiCl in $SOCl_2$.

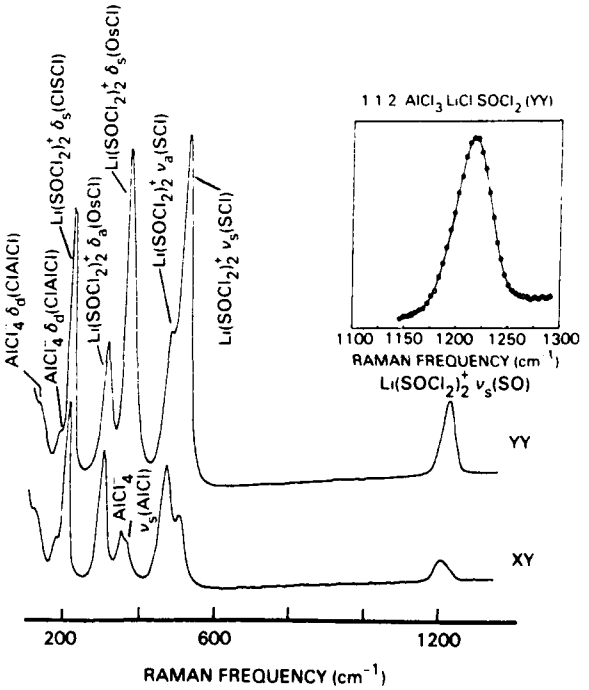

Fig. 3. Polarized and depolarized Raman spectra of 1:1:2 LiCl: $AlCl_3$:$SOCl_2$ solution. Insert: decomposition of S—O stretching vibration into Voight profiles.

Table I. Vibrational modes of free and complexed $SOCl_2$

Neat $SOCl_2$	$Cl_2SO \leftarrow AlCl_3$	$Li(\leftarrow OSCl_2)_2^+$	$Cl_2Al(\leftarrow OSCl_2)_2^+$	Assignment
194p	217p	201.1p	—	SCl_2 bending
284	318	299.1	—	Torsion
344p	355p	347.8p	—	$OSCl_2$ deformation
455	500	464.5	—	S—Cl asymmetric stretch
492p	523p	504.4p	—	S—Cl symmetric stretch
—	—	1211.0	—	S—O asymmetric stretch
1231p	1108p	1220.0p	1055	S—O symmetric stretch

p—polarized.

new bands are shown in Fig. 3. Qualitatively, the addition of LiCl causes the destruction of the $Cl_2SO \rightarrow AlCl_3$ adduct, indicated by Eq. [3]

$$nSOCl_2 + Cl_2SO \rightarrow AlCl_3 + LiCl \rightleftarrows (n-1)\,SOCl_2 + Li(\leftarrow OSCl_2)_2^+ + AlCl_4^- \quad [3]$$

In particular, for $n = 1$, *i.e.*, for the 1:1:2 molar ratio of $LiCl:AlCl_3:SOCl_2$, no free $SOCl_2$ should be present. Accordingly, as seen in Fig. 3, the spectral bands associated with the $Cl_2SO \rightarrow AlCl_3$ adduct and the free $SOCl_2$ disappear and those characteristic of $AlCl_4^-$ and the solvated Li^+ ion are present. The positions of the vibrational modes of neat $SOCl_2$ and $SOCl_2$ associated with Li^+ and $AlCl_3$ are shown in Table I.

The S—O stretching band of the solvated Li^+ ion can be decomposed into two peaks occurring at 1211 and 1220 cm^{-1}, as seen in Fig. 3. By measuring the polarization ratio, ρ, of a Raman line, which is defined as the ratio of the intensity of the parallel to perpendicular components of the Stokes line (16), it is possible to determine the symmetry of the vibration. It is found, by measuring ρ, that the peak at 1220 cm^{-1} is polarized whereas the one at 1211 cm^{-1} is depolarized. Accordingly, these peaks are assigned to the symmetric and asymmetric S—O stretching modes, respectively, of the solvated Li^+ ion. Since the Li—O bond is electrostatic in nature, the Li—O vibrations are not Raman active. Calculations indicate that this vibration should occur at *ca.* 400 cm^{-1} (17).

The vibrational modes of free and complexed $SOCl_2$ are given in Table I. It is seen that within the 100-600 cm^{-1}

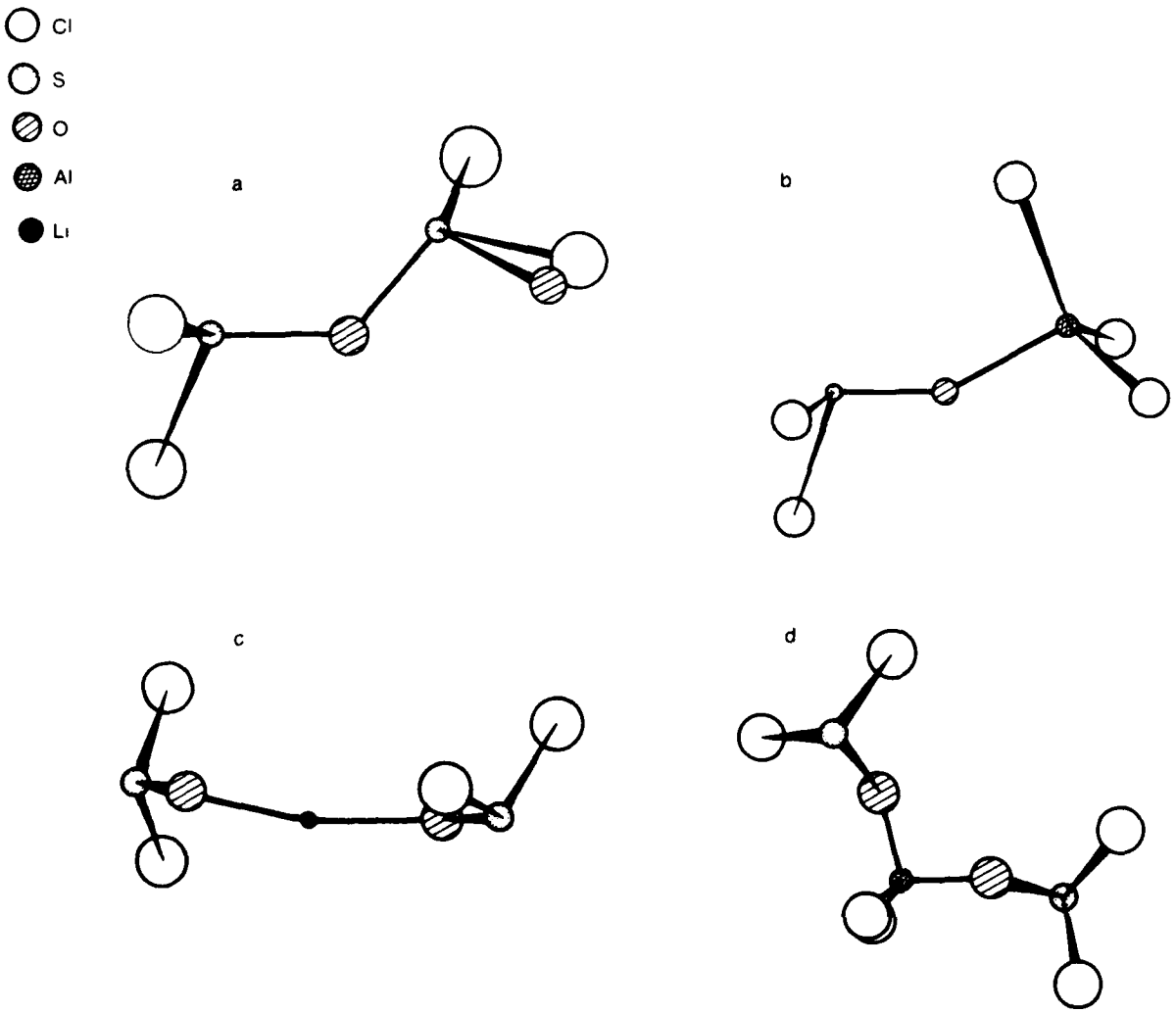

Fig. 4. Computer generated structures: (a) $(SOCl_2)_2$-open chain; (b) $Cl_3Al\leftarrow OSCl_2$ adduct; (c) $Li(\leftarrow SOCl_2)_2^+$ solvated species; (d) $[Cl_2Al(\leftarrow OSCl_2)_2]^+$ onium ion.

spectral region, the vibrational modes of the Li^+ complexed $SOCl_2$ occur at higher frequencies than those in neat $SOCl_2$. Furthermore, the separation between the symmetric and asymmetric S-Cl stretches of $SOCl_2$ decreases upon complexation with Li^+. This indicates that the repulsion between the sulfur lone pair of electrons and the Cl's of $SOCl_2$ are lessened upon complexation with Li^+. Such behavior is consistent with coordination through the oxygen atom, as required by the valence shell electron pair repulsion (VSEPR) model as well as the more general bond lengthening rule (18). Typically, Li^+ has a solvation number of four; in the 1:1:2 $LiCl:AlCl_3:SOCl_2$ solution the other two coordination sites can be filled by the ion pairing with $AlCl_4^-$. In the presence of excess $SOCl_2$, these sites are likely filled with $SOCl_2$ molecules. This conjecture is in analogy to the situation found in the system: Li^+/DMSO/1-methyl-2-pyrrolidone where two sites are occupied by DMSO and two by 1-methyl-2-pyrrolidone molecules (19).

A comparison of the frequencies for the S—O stretching vibration allows the various species in the $LiCl-AlCl_3-SOCl_2$ system to be arranged with respect to the strength of the S—O bond of the interacting $SOCl_2$ molecule in the following order of diminishing strength: $Cl_2SO > (Cl_2SO)_n$ (n = 2,3) > $Li(\leftarrow OSCl_2)_2^+$ > $Cl_3Al(\leftarrow OSCl_2)$ > $[Cl_2Al(\leftarrow OSCl_2)_2]^+$. Thus, if the rate of the charge transfer reaction is related to the S—O bond strength, the effect of the $AlCl_3$ concentration on the electrode rest potential (1) is readily explained.

Molecular orbital calculations.—In the $LiCl-AlCl_3-SOCl_2$ system, the $SOCl_2$ molecules are present in energetically different states, as evidenced by the S—O bond strength. In an attempt to answer which $SOCl_2$-bearing species will be preferentially affected by the electrode surface, one must consider the size, shape, and electrical charge distribution for each type of molecular species. The need for such considerations is evident from the results reported by Madou *et al.* (1) and Venkatasetty's interpretation of the role of iron and cobalt phthalocyanines in the observed enhancement of the $SOCl_2$ electroreduction on carbon electrodes (4). In the first case, the appearance of a second peak during the voltammetric sweep and its dependence on the $AlCl_3$ concentration could indicate that the reduction of $SOCl_2$ occurs sequentially from two different $SOCl_2$-bearing species. In the second case, Venkatasetty argued that the enhancement in the exchange current density, j_o, arises because of an interaction with the metal phthalocyanines. Specifically, because of the tetrahedral arrangement of electron pairs, the $SOCl_2$ molecule can participate through the filled p-orbitals of its sulfur atom with the empty d-orbitals of the central metal atom, resulting in adduct formation. A strong metal-sulfur interaction would weaken the S—Cl bonding thus facilitating electron transfer.

The MO calculations were undertaken to guide the interpretation of spectral data and to assist in deciding which species are most likely to be present under a given set of experimental conditions. While these calculations probably are not sufficiently accurate for unequivocally establishing structures and related properties, nevertheless the results based on relative comparison among the various species are, most likely, valid.

The structures, shown in Fig. 4, are optimized structures. Calculations reproduce the structures of $SOCl_2$, $AlCl_3$, and $AlCl_4^-$ within 5% on all bonds and angles. In an attempt to resolve the structure of neat $SOCl_2$ in the liquid state, we examined the relative stabilities of $SOCl_2$ and $(SOCl_2)_n$, in both cyclic and open chain structures, for n = 2 and oligomers, i.e., for $n > 2$. The total energy for each of these structures is quite similar, *e.g.*, -1259.05 and -1259.06 eV for $SOCl_2$ and an open chain $(SOCl_2)_2$, respectively; both molecular species are of equal stability. The calculated heats of formation are -22 and -47 kcal mol^{-1} for monomer and open chain dimer, respectively. The latter compares rather well with the experimental value of 48 kcal mol^{-1} for liquid $SOCl_2$ (20). It is noted, in passing, that all attempts to calculate a true cyclic $SOCl_2$ dimer always led to an open chain structure as the favored geometry. On this basis we conclude that neat $SOCl_2$ in the liquid state readily associates, albeit, weakly to form open chain aggregates.

Calculations suggest only slight structural changes upon complexation of $SOCl_2$ with itself or $AlCl_3$. Results tabulated in Table II show bond lengthening in the range of 0.02-0.05Å. The most significant change has occurred when forming an onium ion, $[Cl_2Al(\leftarrow OSCl_2)_2]^+$. Here, the two $SOCl_2$ molecules are affected somewhat differently. Similarly, the bond angles are relatively unchanged by complexation and vary by *ca.* 2 degrees.

In general, complexation of $SOCl_2$ leads to an increase in the positive charge on the sulfur atom. The largest redistribution occurs when $SOCl_2$ is complexed with the Al atom, either $AlCl_3$ or the onium ion. In most instances this redistribution is shared with the oxygen and chlorine atoms. For the onium ion, the Al, S, and Cl atoms, all share the additional positive charge.

The MO calculations agree with the interpretation of spectral data and support the conclusion that $SOCl_2$ forms weak adducts with itself and $AlCl_3$, and that complexation only slightly modifies the structural and vibrational characteristics of the $SOCl_2$ molecules. Although such small changes in the charge distribution may profoundly affect their reactivity (18), we do expect the reduction process to take place within the same overpotential range.

Comparison with transport properties.—Szpak and Venkatasetty (6) measured selected transport properties, *viz.* viscosity and conductivity in an attempt to explore structural aspects of the $LiCl-AlCl_3-SOCl_2$ system. In what follows, we re-examine their conclusions in light of spectroscopic evidence. The Batschinski-Hildebrand equation, Eq. [4], (21, 22) relates the fluidity, ϕ, to the ratio of occupied to unoccupied volume, $(v-v_o)/v_o$

$$\phi = B(v-v_o)/v_o \qquad [4]$$

The B constant is a property of a liquid measuring its ability to absorb momentum generating the newtonian flow. Thus, its value depends on the molecular size and shape and, qualitatively, yields information on the molecular structure. For neat $SOCl_2$ the Batschinski-Hildebrand plot yields a B value of 11.2 cP^{-1}, which is characteristic of molecular liquids. This is in agreement with the slight spectroscopic shifts of the S—O stretching frequency, indicating a weak self-association (5). Such weak associations will not dominate the response of a liquid to the applied pressure gradient. The addition of $AlCl_3$ does not substantially change the B constant, indicating that the newly formed species have about the same volume as the dimerized $SOCl_2$. On the other hand, the addition of LiCl breaks up the $Cl_3Al\leftarrow OSCl_2$ adduct which contributes to the reduction in the B value through both a volume effect and presence of ionic species. This is also in agreement with spectroscopic evidence.

Additional information not available earlier concerns the slight increase in conductivity upon the addition of $AlCl_3$. This increase in the conductivity is due to the internal exchange reaction, at high $AlCl_3$ concentrations, to form a positively charged onium ion $[Cl_2Al(\leftarrow OSCl_2)_2]^+$ and $AlCl_4^-$ and not due to the formation of higher anionic complexes.

Conclusions

1. Thionyl chloride, in the liquid state, forms open chain dimers and/or oligomers having an open chain, zig-zag structure.

2. Dissolution of Al_2Cl_6 results in the formation of adducts, $Cl_3Al\leftarrow OSCl_2$. At higher Al_2Cl_6 concentrations these adducts undergo an internal exchange reaction to form onium ions, $[Cl_2Al(\leftarrow OSCl_2)_2]^+$, and $AlCl_4^-$ ions. Since the area of the peak due to the onium ion, at 1055 cm^{-1}, is much less than that of the adduct, at 1108 cm^{-1}, implies that the degree of ionization in the $AlCl_3-SOCl_2$ system is very small.

3. Addition of LiCl causes the destruction of adducts and onium ions with the formation of solvated $Li(\leftarrow OSCl_2)_2^+$ ions and complex $AlCl_4^-$ ions.

4. The S—O bond strength of the free and complexed $SOCl_2$ diminishes as follows

Table II. Bond lengths and charge distribution obtained from MO calculations for $SOCl_2$, $(SOCl_2)_2$, $Cl_3Al \leftarrow OSCl_2$, $[Cl_2Al(\leftarrow OSCl_2)_2]^+$ and $[Li(\leftarrow OSCl_2)_2]^+$

$SOCl_2$

Atom	Charge	Bond	Length (Å)
S	1.2349	S—O	1.468
O	−0.5500	S—Cl_1	2.037
Cl_1	−0.3424	S—Cl_2	2.038
Cl_2	−0.3425	—	—

$(SOCl_2)_2$, open dimer

Atom	Charge	Bond	Length (Å)
S_1	1.256	S_1—O_1	1.470
S_2	1.2701	O_1—S_2	3.313
O_1	−0.5983	S_2—O_2	1.470
O_2	−0.570	S_1—Cl_1	2.034
Cl_1	−0.3289	S_1—Cl_2	2.034
Cl_2	−0.3287	S_2—Cl_3	2.040
Cl_3	−0.3501	S_2—Cl_4	2.040
Cl_4	−0.3501		

$Cl_3Al \leftarrow OSCl_2$

Atom	Charge	Bond	Length (Å)
S	1.3293	S—O	1.496
O	−0.6238	S—Cl_1	2.020
Al	0.9616	S—Cl_2	2.018
Cl_1	−0.2235	O—Al	1.845
Cl_2	−0.2217	Al—Cl_3	2.103
Cl_3	−0.4382	Al—Cl_4	2.107
Cl_4	−0.3975	Al—Cl_5	2.127
Cl_5	−0.3861		

$[Cl_2Al(\leftarrow OSCl_2)_2]^+$

Atom	Charge	Bond	Length (Å)
Al	1.1016	S_1—O_1	1.506
O_1	−0.6868	S_1—Cl_1	2.010
O_2	−0.6836	S_1—Cl_2	2.103
S_1	1.3343	Al—O_1	1.7951
S_2	1.3265	Al—Cl_3	2.093
Cl_1	−0.1579	Al—Cl_4	2.096
Cl_2	−0.1711	Al—O_2	1.7847
Cl_3	−0.3666	O_2—S_2	1.510
Cl_4	−0.3691	S_2—Cl_5	2.009
Cl_5	−0.1585	S_2—Cl_6	2.012
Cl_6	−0.1686		

$[Li(\leftarrow OSCl_2)_2]^+$

Atom	Charge	Bond	Length (Å)
Li	1.000	S_1—O_1	1.480
S_1	1.2509	S_1—Cl_1	2.028
S_2	1.2508	S_1—Cl_2	2.027
O_1	−0.6753	Li—O_1	3.484
O_2	−0.6770	Li—O_2	3.470
Cl_1	−0.2884	S_2—O_2	1.481
Cl_2	−0.2854	S_2—Cl_3	2.028
Cl_3	−0.2878	S_2—Cl_4	2.028
Cl_4	−0.2877		

$$Cl_2SO > (Cl_2SO)_2 > Li(\leftarrow OSCl_2)_2^+ > Cl_3Al \leftarrow OSCl_2 > [Cl_2Al(\leftarrow OSCl_2)_2]^+$$

5. The MO calculations provide information on size, shape, and charge distribution of $SOCl_2$-bearing species. There is substantial agreement with the interpretation of spectral data.

6. Spectral data, results of MO calculations, and the viscosity and conductivity measurements are in agreement. The Raman data and Batschinski-Hildebrand plots indicate that neat $SOCl_2$ is a weakly associated liquid. The addition of Al_2Cl_6 results in the formation of a neutral complex which is nonconductive. At higher $AlCl_3$ concentrations, the solution conductivity slightly increases due to the formation of onium ions and $AlCl_4^-$. The viscosity and conductance measurements as well as the Raman data indicate that the degree of ionization in the $AlCl_3$-$SOCl_2$ system is small. With the addition of LiCl, the $AlCl_3$-$SOCl_2$ species are destroyed and $Li(\leftarrow OSCl_2)_2^+$ and $AlCl_4^-$ are formed as shown by the Raman spectra, the decrease in the B value of the Batschinski-Hildebrand plots, and the substantial increase in solution conductivity.

Acknowledgments

This work was supported by Office of Naval Research. The authors wish to acknowledge discussions with Dr. R. D. Boss, Naval Ocean Systems Center, San Diego, California, Dr. J. R. Driscoll, Lockheed, Palo Alto Research Laboratory, Palo Alto, California, and Dr. M. Madou, SRI International, Menlo Park, California.

Manuscript submitted Jan. 19, 1988; revised manuscript received *ca.* Oct. 3, 1988.

The U.S. Naval Ocean Systems Center assisted in meeting the publication costs of this article.

REFERENCES

1. M. J. Madou, J. J. Smith, and S. Szpak, *This Journal*, **134**, 2794 (1987), and references therein
2. P. Van Rysselberghe, in "Modern Aspects of Electrochemistry," Vol. 4, Chap. 1, Plenum Press, New York (1966).
3. J. O. M. Bockris and A. K. N. Reddy, "Modern Electrochemistry," Plenum Press, New York (1972).
4. H. V. Venkatasetty, U.S. Pat. 4,252,875 (1981).
5. P. A. Mosier-Boss, R. D. Boss, C. J. Gabriel, S. Szpak, J. J. Smith, and R. J. Nowak, *Trans. Faraday Soc. 1*, **85**, 11 (1989).

6. S. Szpak and H. V. Venkatasetty, *This Journal*, **131**, 961 (1984).
7. C. J. Gabriel, P. A. Mosier-Boss, and S. Szpak, *Spectrochim. Acta*, **43A**, 1293 (1987).
8. W. K. Istone and R. J. Brodd, *This Journal*, **131**, 2467 (1984).
9. S. S. Kim, B. J. Carter, and F. D. Tsay, *ibid.*, **132**, 33 (1985).
10. W. L. Bowden and A. N. Dey, *ibid.*, **127**, 1419 (1980).
11. D. A. Long and R. T. Bailey, *Trans. Faraday Soc.*, **59**, 594 (1963).
12. H. Hecht, *Z. Anorg. Chem.*, **254**, 44 (1947).
13. H. Spandau and E. Brunneck, *ibid.*, **270**, 201 (1952).
14. I. Lindquist, "Inorganic Adduct Molecules of Oxycompounds," Academic Press, Inc., New York (1963).
15. R. G. S. Pong, A. E. Shirk, and J. S. Shirk, *Ber. Bunsenges. Phys. Chem.*, **82**, 79 (1978).
16. R. S. Drago, "Physical Methods in Chemistry," W. B. Saunders, Co., Philadelphia, PA (1977).
17. S. S. Chang, M. W. Siverson, and P. P. Schmidt, *J. Phys. Chem.*, **89**, 2892 (1985); *ibid.*, **90**, 1046 (1986).
18. V. Gutmann, "The Donor-Acceptor Approach to Molecular Interactions," Plenum Press, New York (1978).
19. J. L. Wuepper and A. J. Popov, *J. Am. Chem. Soc.*, **92**, 1493 (1969).
20. "International Critical Tables," Vol. 5, p. 179, McGraw-Hill, Inc., New York (1929).
21. J. A. Batschinski, *Z. Phys. Chem.*, **84**, 643 (1913).
22. J. H. Hildebrand, *Science*, **174**, 490 (1971); *Faraday Discuss. Chem. Soc.*, **66**, 151 (1978).

Reprinted from JOURNAL OF THE ELECTROCHEMICAL SOCIETY
Vol. 136, No. 9, September 1989
Printed in U.S.A.

Electroreduction of $SOCl_2$

I. $AlCl_3$-$SOCl_2$ System on Pt Electrode

P. A. Mosier-Boss* and S. Szpak*

Naval Ocean Systems Center, San Diego, California 95152-5000

J. J. Smith

Department of Energy, Washington, DC 20545

R. J. Nowak*

Office of Naval Research, Arlington, Virginia 22217-5000

ABSTRACT

The mechanism of $SOCl_2$ reduction on Pt electrodes is examined by linear sweep voltammetry and IR reflectance spectroscopy with the interpretation aided by molecular orbital calculations. The present model emphasizes structural aspects of bulk electrolyte as well as the electrode/electrolyte interphase region. Initially this region is enriched by preferential adsorption of $[Cl_2Al(\leftarrow OSCl_2)_2]^+$ ions occurring through the S atom of the complexed $SOCl_2$ molecule. Further enhancement is noted at low cathodic overpotentials. At higher overpotentials, SO_2 and unidentified species, P_1 and P_2, are observed. The model requires stability of both P_1 and P_2 when in an adsorbed state. The acceptance of the first electron is an irreversible process while the acceptance of the second electron is quasi-reversible. The formation of final reaction products, *viz.*, Cl^-, S, and SO_2 occurs within the reaction layer.

Early discussion of the mechanism of $SOCl_2$ electroreduction centered around events involving isolated $SOCl_2$ molecules, *i.e.*, disregarding molecular interactions (1-4). This approach was criticized by Madou *et al.* (5) based on the shape of voltammograms, particularly in practical electrolytes containing excess $AlCl_3$. The complexity of the reaction path was indicated by the formation of prepassive surface films long before the onset of passivation (6) and further emphasized by the role played by the various additives, *e.g.*, Fe-Pc (7). However, the best evidence for the complex reaction pathway was provided by the spectroscopic examination of the Pt/$AlCl_3$-LiCl-$SOCl_2$ interphase region (8, 9).

In an attempt to provide better understanding of events associated with the cell discharge and, in particular, those occurring at the positive electrode, studies into the structural aspects of $SOCl_2$-based electrolytes were undertaken (10-12). Specifically, structural features were derived from the analysis of the Walden product (10) and from Raman and IR spectra for the $AlCl_3$-$SOCl_2$ and LiCl-$AlCl_3$-$SOCl_2$ systems, respectively (11, 12). Here, we report on the extension of this effort and concentrate on changes that occur within the reaction zone adjacent to the charge-transfer plane upon polarization of the Pt/$AlCl_3$-$SOCl_2$ system. IR reflectance spectroscopy and linear sweep voltammetry (lsv) were selected as primary experimental tools. The interpretation of experimental observations was aided by molecular orbital (MO) calculations.

Experimental

Procedures employed in the preparation of solutions were reported earlier (11, 12). The spectroscopic examination of the electrode/electrolyte interphase was performed in a modified cell, first described by Pons (13). The linear sweep voltammograms were obtained with the aid of the computer driven potentiostat, PAR Model 173 with a 276 IEEE computer interface. IR transmittance spectra were obtained using a Barnes mount with AgCl windows and a 15 μm Teflon space. The MO calculations were performed using AMPAC, a general purpose, semiempirical molecular orbital package developed at the University of Texas, Austin, Texas. These calculations yield information on the size, shape, and charge distribution within molecules and complexes. The recorded S—O stretching vibrations of complexed $SOCl_2$ were computer analyzed and decomposed into their Voigt profiles using a previously described procedure (14).

Electrochemical cell.—The spectroelectrochemical cell was made of a machinable ceramic material (Macor, Dow Chemical). A removable AgCl window was sealed against the cell body by an O-ring (Kalrez, du Pont). The working electrode was a polished Pt foil permanently attached to a ceramic plunger. The counter- and reference electrodes were a Pt wire and a Ag/AgCl wire in a Teflon sleeve, respectively. A variable distance between the window and electrode surface was provided; however, each set of measurements was carried out at a fixed distance. The cell was placed at a 45° angle using a specular reflectance apparatus—Spectra-Tech, Model 500—inside a 5 DXB Nicolet FT-IR spectrometer. The path lengths were calibrated with neat CCl_4.

Results

IR spectra can be used to identify species present in solution and, to a lesser degree, determine their concentrations. Such an examination by itself can, at best, provide only limited information on the characteristics of the electrode/electrolyte interphase (15); it cannot unequivocally determine the reaction pathway(s). On the other hand, linear sweep voltammetry is a useful tool for exploring complex electrochemical processes since the shape of the lsv curves depends on two parameters related to the thermodynamics of the system and to the kinetics of the charge transfer and associated transport processes. Moreover, the easily adjustable experimental conditions allow the examination of a transition from one dominant process to another.

IR spectroscopy of the electrode/electrolyte interphase.—The evolution of IR spectra reflected from the electrode surface is illustrated in Fig. 1. Detailed examination was restricted to the spectral region 950-1350 cm^{-1}. This region was selected because the S—O stretching vibrations of neat $SOCl_2$, $Cl_3Al(\leftarrow OSCl_2)$ complex and $[Cl_2Al(\leftarrow OSCl_2)_2]^+$ onium ion, which occur in the Raman spectra at 1231, 1108, and 1055 cm^{-1}, respectively, are unobstructed by other absorptions. Also, the S—O stretching vibrations of these species are very sensitive to any changes in the molecular structure (11). For solutions in contact with an electrode surface two additional peaks at 1132 and 1102 cm^{-1} are observed (*vide infra*). The passage of cathodic current results in the disappearance of the 1132 and 1102 cm^{-1} peaks and generates new peaks of which that of SO_2 at 1331 cm^{-1}, is clearly detectable, even at low overpotentials, *e.g.*, 100 mV. At higher overpotentials, new peaks appear at *ca.* 1190, 1170, and 1150 cm^{-1}. Qualitatively, no significant differences are observed in the IR reflectance spectra obtained on Au and Pt electrodes.

lsv curves.—Effect of $AlCl_3$ concentration.—The effect of $AlCl_3$ concentration on the shape of the lsv curves, re-

* Electrochemical Society Active Member.

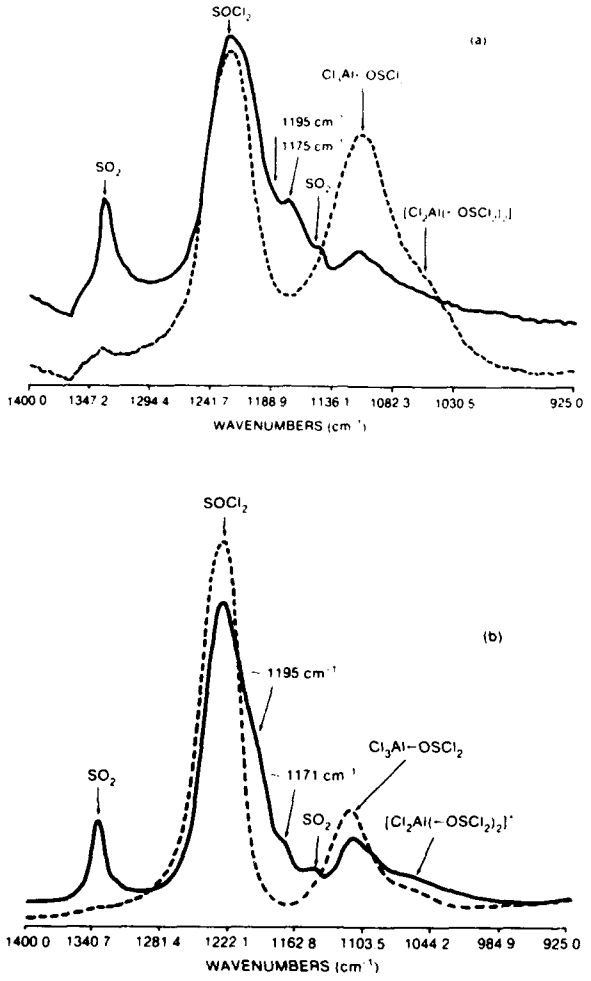

Fig. 1. The 930-1350 cm $^{-1}$ IR spectral region of an electrode/electrolyte interphase at rest and cathodically polarized. (a) Au/4.0M $AlCl_3$ in $SOCl_2$ system; dashed line at $\eta = 0$, solid line at $\eta = -2.5V$. (b) Pt/4.0M $AlCl_3$ in $SOCl_2$ system; dashed line at $\eta = 0$, solid line at $\eta = -3.5V$. Species indicated.

corded for a constant scan rate of 5 mV s $^{-1}$, is illustrated in Fig. 2a-d. A cursory inspection shows a significant difference. On closer examination, however, this difference is in the definition of characteristic points rather than in shape. At concentrations 3.0*M* or less, the forward (reductive) scan consists of two S-shaped segments, followed by a peak current. The current plateaus, j_A and j_B, as well as the peak current, j_p, increase with an increase in $AlCl_3$ concentration. The reverse (oxidative) scan also exhibits two S-shaped segments followed by a rather distinctly different region containing two peaks. All potentials delineating the characteristic segments appear to be concentration independent while the respective currents show a strong dependence.

The situation in a 4.0*M* solution, especially at higher overpotentials, is quite different both on forward and reverse scans. The reductive scan shows only one wave-shaped region at lower overpotentials, becoming a straight line at higher overpotentials. On reverse scan, the $j/V(t)$ curve crosses over the reductive scan, but still retains a peak-shaped region at lower overpotentials.

lsv curves.—Effect of scan rate.—The effect of scan rate on the shape of the lsv curves in a 3.0*M* solution is illustrated in Fig. 3a and b. Qualitatively, the decrease in the scan rate yields better definition of the various regions. Thus, at $\nu = 50$ mV s $^{-1}$, all characteristic features of both reductive and oxidative scans are clearly displayed. Of interest are two features: the merging of the reductive and oxidative waves within the potential range: −500 to −200 mV at the scan rate of 5 mV s $^{-1}$. At still lower rates a cross over of oxidative and reductive waves is observed while at faster rates, a separation of these waves occurs. The second feature of interest is the behavior of peaks, A and B in Fig. 3a. As the scan rate decreases, merging of these points occurs with A shifting in the positive direction and B in the negative, with the displacement of the latter being less.

Discussion

The discussion of experimental results and conclusions reached is aided by considerations of electrolyte composition and associated equilibria and the concept of an electrode/electrolyte interphase.

*Equilibria in the bulk electrolyte.*Mosier-Boss *et al.* (11) reported the following equilibria in the bulk solution

$$(SOCl_2)_n \leftrightarrows (SOCl_2)_{n-1} \quad n = 1, 2, \ldots \qquad [I]$$

$$SOCl_2 + AlCl_3 \leftrightarrows Cl_3Al(\leftarrow OSCl_2) \qquad [II]$$

$$2Cl_3Al(\leftarrow OSCl_2) \leftrightarrows [Cl_2Al(\leftarrow OSCl_2)_2]^+ + AlCl_4^- \qquad [III]$$

The internal exchange reaction, Eq. [III], occurs in the presence of free $SOCl_2$ and the extent of this reaction is expected to be affected by excess $SOCl_2$ with a dependence on the dielectric constant at low $AlCl_3$ concentrations and dominated by the donor properties of the $SOCl_2$ at higher concentrations (16). Significant changes in the governing equilibria and molecular structure occur between 2.0 and 3.0*M* $AlCl_3$ as indicated by difference in IR spectra (8) and a maximum in the electrolyte vapor pressure (17). (Hereafter, for brevity, we use symbols A_0, A_1, and A_2^+ to denote neat $SOCl_2$, complex, and onium ion, respectively).

Concept of an interphase.—A useful concept facilitating the interpretation of experimental data and formulation of a physical model, that of an interphase region, was discussed by van Rysselberghe (18). In the simplest case, it takes the form of the electrical double layer. In more complex cases and, in particular, during charge transfer reaction, it consists of a series of layers, each associated with a participating elementary process. In this representation, the interphase region is an open system which encompasses a number of consecutive elementary processes. A typical set of events is as follows; reactant molecules are brought from the bulk, b, to the electrode surface, s, by diffusion, d, followed by adsorption, a, and, after the charge transfer, products are returned back to the bulk. For A_2^+ as the reacting molecule, the set of events is given by Eq. [IV]

$$A_2^{+,(b)} \rightarrow A_2^{+,(d)} \rightarrow A_2^{+,(a)} + e^{-,(s)} \rightarrow \Sigma \text{ products} \qquad [IV]$$

where the superscripts identify the elementary process considered as well as their position within the interphase.

An interphase region is formed whenever an electrode is in contact with an electrolyte. This region is either in an equilibrium with the bulk electrolyte or in a stationary state leading to a rest potential which is a thermodynamic or a mixed potential, respectively. In the first case, the constituents within the interphase are the same as in the bulk, while in the second case new species are generated by the partial electrode reactions. These new species, depending upon their stability, may or may not have time to diffuse to the bulk.

IR spectroscopy of the interphase region.—In the cell designed for external reflection spectroelectrochemistry, the recorded spectra contain contributions due to bulk electrolyte and the electrode/electrolyte interphase (13). The degree to which the interphase region can be isolated from the bulk, and events associated with the charge transfer process examined, can be assessed by, *e.g.*, varying the path length. The effectiveness of this technique is illustrated by spectra displayed in Fig. 4. Figures 4a and b are the spectra for path lengths of 5 and 10 μm, respectively; relative intensities between the two cases reflect bulk *vs.* interphase concentrations. The peak ratios of complexed species, *i.e.*, onium ion, A_2^+, and complex, A_1, to free $SOCl_2$, increase with decreasing cell path length which is

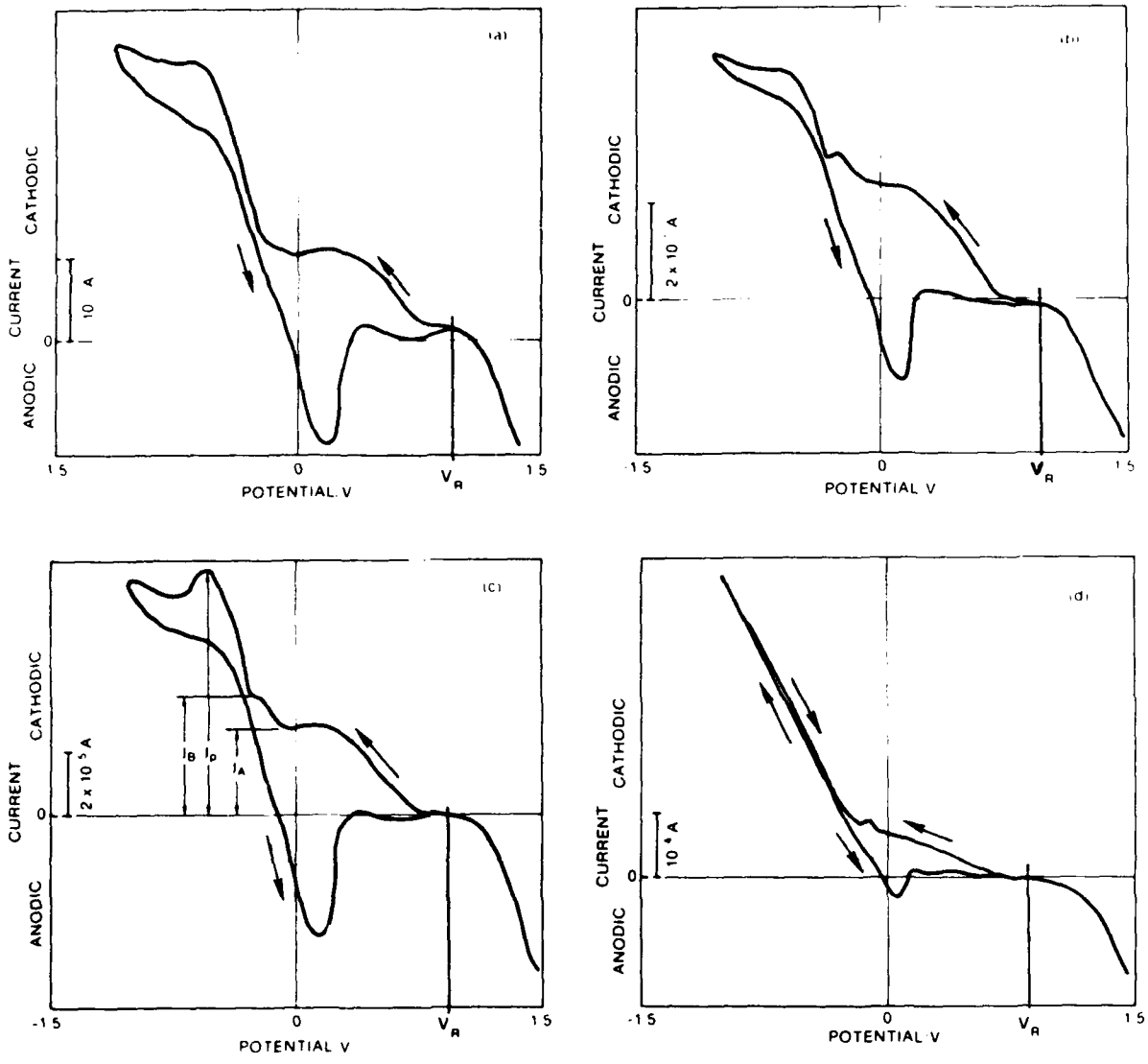

Fig. 2. Effect of $AlCl_3$ concentration on shape of voltammograms. (a) 1.5M; (b) 2.0M; (c) 3.0M; (d) 4.0M $AlCl_3$. Scan rate: $\nu_{red} = \nu_{ox} = 5$ mV s $^{-1}$. Electrode area: 0.15 cm^2. All potentials vs. Ag/AgCl reference in the same solution. V_R indicates rest potential.

indicative of enrichment of the former within the interphase. A more quantitative demonstration of the interphase enrichment can be seen in Fig. 5 and Table I where the resolved Voigt profiles for the S—O vibration band at 1116 cm $^{-1}$ are displayed. It should be noted that both the transmittance and reflectance IR spectra were obtained using AgCl windows. Consequently, the observed effects are due to the electrode/electrolyte interphase and not an artifact of the AgCl windows.

The Voigt profiles show two new peaks at 1132 and 1102 cm $^{-1}$ which are present only within the interphase. These peaks disappear upon cathodic polarization. Two plausible assignments can be made: (i) they can be assigned to the symmetric and asymmetric stretching vibrations of $A_2{}'^{(a)}$ or (ii) to S—O stretching vibrations of $A_1{}^{(a)}$ and $A_2{}'^{(a)}$, respectively. In the first case, these vibrations in the bulk solution are essentially degenerate and appear as a broad band. Case (ii) is consistent with the observation that $A_2{}'$ is more strongly enriched within the interphase than A_1. Further distinction between these two cases cannot be made at the present time. Regardless, since these peaks are shifted to higher frequencies, it follows that the adsorption occurs through the S atom. A shift to higher frequency requires an increase in the force constant of the S—O bond which can only occur if the $p\pi \rightarrow d\pi$ backbonding increases. This conclusion is based on the thoroughly investigated effects of bonding through the S and O atoms of $(CH_3)_2SO$ on the S—O stretching frequencies (19, 20), and further supported by MO calculations. These calculations show that the positive charge rests on the S atom (12). For case (i), the removal of degeneracy would imply that only one of the $SOCl_2$ molecules of the onium ion is actually on the electrode surface.

In summary, the *in situ* IR reflectance spectroscopy clearly indicates that we have a complex electrode/electrolyte interphase. This interphase consists of onium ions (and possibly, 1:1 adduct) adsorbed on the electrode surface in contact with a region of enrichment of onium ions and complex which, in turn, is in contact with the bulk.

Shape of lsv curves.—The tendency of $SOCl_2$ to form adducts and/or to solvate ions further suggests that the electroreduction of $SOCl_2$ in practical electrolytes comprises a complex overall reaction where, most likely, chemical reaction(s) is (are) coupled to a charge transfer. For this reason, the lsv is the experimental technique of choice to assess the complexity of this reaction and elucidate, at least in a qualitative manner, its mechanism. This approach is based on the premise that, for a specific coupling, a characteristic lsv curve is obtained (21, 22). The shape of this curve depends on two parameters: the thermodynamic parameter, $\chi = Kc$, and the kinetic parameter,

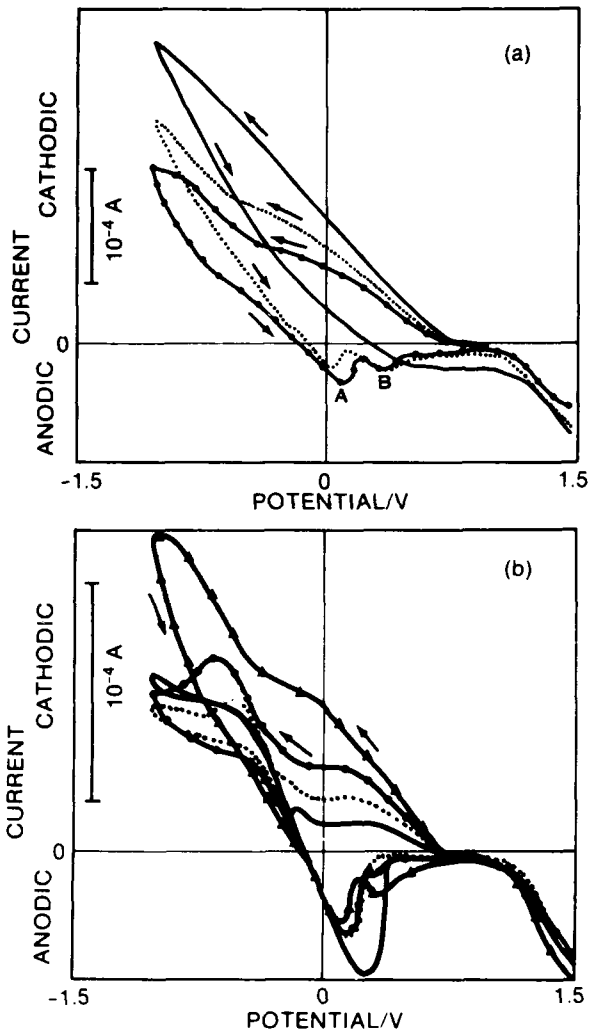

Fig. 3. Effect of scan rate on shape of voltammograms. (a) Scan rates: $\nu_{red} = \nu_{ox} < 50$ mV s^{-1} (———) for 500; (····) for 100, and (–·–·–·–) for 50 mV s^{-1}. (b) Scan rates; $\nu_{red} = \nu_{ox} < 50$ mV s^{-1} (———) for 2; (····) for 5; (–·–·–·–) for 10, and (———) for 50 mV s^{-1}. Electrolyte, 3.0*M* $AlCl_3$. Electrode area: 0.15 cm^2.

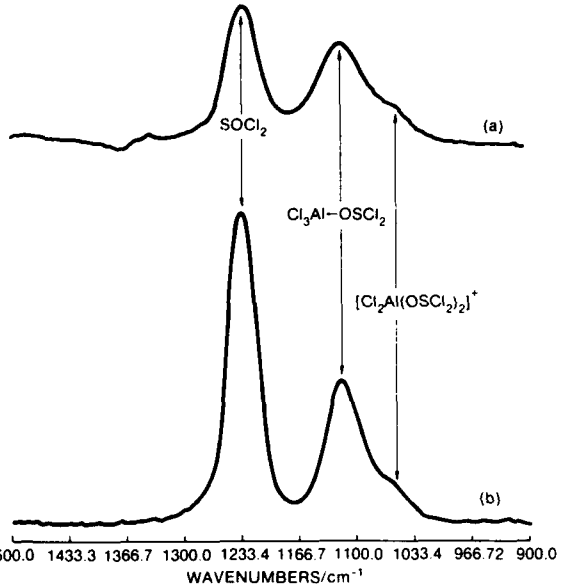

Fig. 4. IR reflectance spectra at rest potential. (a) and (b) Reflectance spectrum as a function of path lengths of 5 and 10 μm, respectively. Electrolyte, 4.0*M* $AlCl_3$ in $SOCl_2$; electrode material, Au.

$\lambda = (RT/nF)\, c(k/\nu)$. These parameters enter as a source/sink term in the mass balance equation, Eq. [1]

$$\frac{\partial c_i}{\partial t} = D_i \frac{\partial^2 c_i}{\partial x^2} - f_i(\chi, \lambda) \qquad [1]$$

where c_i is the concentration of the i-th electroactive species, K is the equilibrium constant, k is the appropriate rate constant, and ν the scan rate. The source/sink function, $f_i(\chi, \lambda)$, is formulated for a specific set of events comprising the overall reaction. Any discussion of the reaction mechanism(s), even a qualitative one, must involve specification of the $f_i(\chi, \lambda)$ function which, in turn, requires an examination of the effect of solution composition and the scan rate. Often, this function is potential dependent and may be simplified by making relevant approximations. Because of the low conductivity of these electrolytes, any attempt for a quantitative evaluation of kinetic factors would not be appropriate (23-25) and, therefore, has not been pursued further. It is emphasized that the shape of the lsv is determined solely by the mass balance equation, Eq. [1]. The resistivity of the electrolyte enters through the λ parameter and affects the position and the symmetry of the peak current as well as its magnitude. In particular, anodic peaks are displaced in the positive direction while the cathodic peaks in the more negative direction (24).

In principle, solution of Eq. [1], subject to appropriate initial and boundary conditions, implies that all pertinent information can be derived from the analysis of a single scan. For complex reactions, however, additional information can be extracted by scan reversal, especially if adsorbed species participate in the charge transfer. This assertion is demonstrated in Fig. 6 where the shape of the j/V curve produced by the reverse scan depends on the point of termination of the forward scan. For example, when the forward scan is reversed at point A, the j/V curves on the forward and reverse scan coincide. At higher cathodic overpotentials, points B, C, and D, the oxidative segments of the j/V curves differ substantially from those on the forward scan. These differences can be used in the formulation of a reaction pathway.

Initial stages of lsv curves.—The rather significant enhancement in the concentration of A_2^- in the vicinity of the electrode surface both at rest potential and while cathodically polarized, is illustrated in Fig. 7, where the reference spectrum obtained at rest potential has been subtracted

Table I. Decomposition of spectral bands of free and adsorbed complexed $SOCl_2$ into Voigt profiles

Method[a]	Symbol[b]	Complex (Bulk)	Onium ion		
			Bulk	Adsorbed state	
T	ν_0	1116.92	1065.55	—	—
	$\Delta\nu_G$	6.085	36.535	—	—
	$\Delta\nu_L$	44.296	61.382	—	—
	I_0	1.137	0.142	—	—
	A	80.175	16.277	—	—
R/Pt	ν_0	1116.96	1064.79	1132.25	1102.97
	$\Delta\nu_G$	9.335	60.260	24.036	26.640
	$\Delta\nu_L$	32.896	6.350	6.302	11.364
	I_0	0.046	0.022	0.018	0.029
	A	2.505	1.589	0.578	1.185
R/Au	ν_0	1116.26	1060.11	1132.92	1101.40
	$\Delta\nu_G$	8.536	57.589	28.128	29.628
	$\Delta\nu_L$	53.452	3.868	8.866	16.616
	I_0	0.080	0.033	0.016	0.037
	A	6.823	2.135	0.647	1.847

[a] T—transmittance
R—reflectance
[b] $\Delta\nu_G$—Gassian width, cm^{-1}
$\Delta\nu_L$—Lorentzian width, cm^{-1}
I_0—peak intensity, Abs
A—band area, Abs cm^{-1}
ν_0—peak position, cm^{-1}

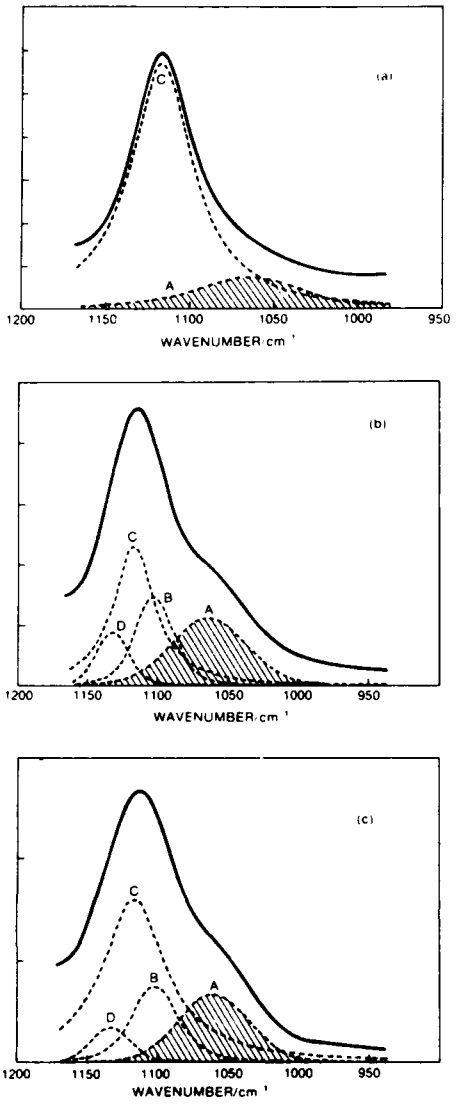

Fig. 5. The 950-1150 cm $^{-1}$ IR special region decomposed into Voigt profiles. (a) Transmittance spectrum, (b) reflectance spectrum from Au electrode, (c) reflectance spectrum from Pt electrode. Both at V_R. A, C, S—O vibrations due to onium and complex in the bulk; B, D, asymmetric and symmetric S—O stretching vibrations of the adsorbed onium ions, respectively, or S—O stretching vibrations of adsorbed onium ion and 1:1 complex, respectively. Electrolyte, 4.0M $AlCl_3$ in $SOCl_2$.

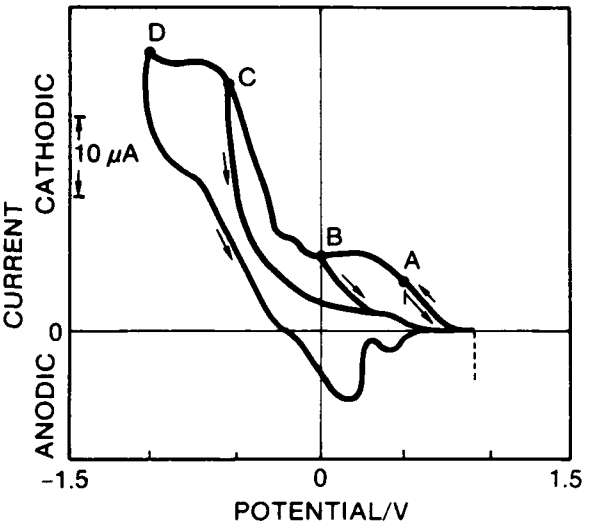

Fig. 6. Effect of scan reversal potential on the shape of $J/V(t)$ curves. Electrolyte, 1.5M $AlCl_3$ in $SOCl_2$; scan rate $\nu_{ox} = \nu_{red} = 5$ mV s $^{-1}$; points; A, B, C, and D indicate scan reversal.

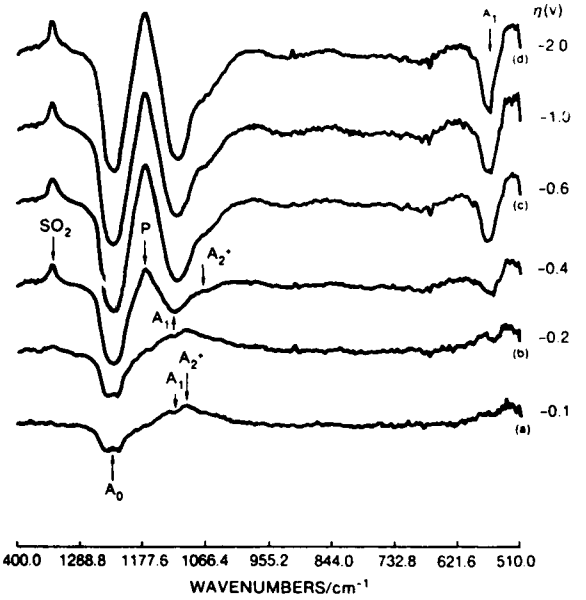

Fig. 7. Effect of applied overpotential on the composition of the interphase by subtractive IR spectroscopy. Electrolyte, 4.0M $AlCl_3$ in $SOCl_2$.

out. (Figure 1 shows the S—O stretching spectral region for the polarized and unpolarized cases, *vide supra.*) There is a corresponding displacement of A_0 and A_1. Evidently, at low overpotentials, *i.e.*, when the charge transfer reaction is insignificant, the major event is the potential dependent shift in the equilibria, Eq. [I]-[III], taking place within the confines of the interphase region. With a further passage of current, new peaks appear, *viz.*, at 1331 and *ca.* 1150 cm^{-1} due to the formation of SO_2 and at 1170 and 1190 cm^{-1} assigned to, as yet, unidentified products containing a S—O bond with the peak at 1170 cm^{-1} appearing first. It is noteworthy that these peaks are not due to SO_2 complexes with either $SOCl_2$ or $AlCl_3$. Concurrently, there is the loss of A_0, A_1, and A_2' species, indicated in Fig. 7 by the negative peaks at 1231, 1108, and 1055 cm^{-1}, respectively. It is not clear, however, whether the $SOCl_2$ in these species are simultaneously reduced or if only one species, *e.g.*, A_2', participates in the reduction process. This ambiguity cannot be resolved by kinetic arguments alone because the species present are coupled to one another via the chemical equilibria, Eq. [II] and [III], and products of the electroreduction of one species may shift the equilibrium to regenerate the electroreducible species. However, assuming the discharge from either species can occur independently, the MO calculations favor the discharge from the A_2' species, Eq. [V]

$$A_2' + e^- \rightarrow P_1 \quad k_1, V^0_1, \alpha_1 \qquad [V]$$

This conclusion is consistent with data asssembled in Tables II-IV. As indicated, the calculated heats of formation for the addition of an electron to A_1 and A_2' are −132 and −299 kcal/mol, respectively. Assuming P_1 to be the initial reaction product, it is likely that the 1190 and/or 1170 cm^{-1} bands in the IR, Fig. 1, are associated with it or with P_2 (*vide infra*, Eq. [VI]). Furthermore, on the basis of the coincidence of the forward and reversed lsv , Fig. 6, point A, we conclude that the charge transfer reaction, Eq. [V], is irreversible.

Development of current plateau(s).—The characteristic feature of the reductive lsv is the appearance of a current

Table II. Bond length and charge density distribution following electron acceptance by neat $SOCl_2$

Reactions

$SOCl_2$; ΔH_f = −22 kcal/mol
$SOCl_2 + e \rightarrow SOCl_2^{\cdot}$; ΔH_f = −111 kcal/mol
$SOCl_2 + e \rightarrow SOCl_2^{2}$; ΔH_f = −48 kcal/mol
(ΔH_f is the MO calculated heat of formation from the elements)

Bond	$SOCl_2$	$SOCl_2$	$SOCl_2^{2}$
	Bond lengths, Å		
S—O	1.468	1.477	1.492
S—Cl_1	2.037	2.160	2.452
S—Cl_2	2.038	2.161	2.453
	Charge density		
Atom	$SOCl_2$	$SOCl_2$	$SOCl_2^{2}$
S	1.2349	0.9203	0.4708
O	−0.5500	−0.5644	−0.7369
Cl_1	−0.3424	−0.6789	−0.8669
Cl_2	0.3425	−0.6790	−0.8670

Table III. Bond length and charge density distribution following electron acceptance by 1:1 complex

Reactions

$Cl_3Al \leftarrow OSCl_2$; ΔH_f = −178 kcal/mol
$Cl_3Al \leftarrow OSCl_2 + e \rightarrow Cl_3Al \leftarrow OSCl_2^{\cdot}$; ΔH_f = −309 kcal/mol
$Cl_3Al \leftarrow OSCl_2 + e \rightarrow Cl_3Al \leftarrow OSCl_2^{2}$; ΔH_f = −309 kcal/mol
(ΔH_f is the MO calculated heat of formation from the elements)

Bond	$Cl_3Al \leftarrow OSCl_2$	$Cl_3Al(\leftarrow OSCl_2)$	$Cl_3Al(\leftarrow OSCl)_2)^2$
	Bond lengths, Å		
S—O	1.496	1.5315	1.560
S—Cl_1	2.020	2.056	2.179
S—Cl_2	2.018	2.055	2.179
O—Al	1.845	1.7436	1.673
Al—Cl_3	2.103	2.154	2.182
Al—Cl_4	2.107	2.143	2.183
Al—Cl_5	2.127	2.137	2.187
	Charge density		
Atom	$Cl_3Al(\leftarrow OSCl_2)$	$Cl_3Al(\leftarrow OSCl_2)$	$Cl_3Al(\leftarrow OSCl)_2)^2$
S	1.3293	0.9872	0.6609
O	0.6238	0.6592	−0.6791
Al	0.9616	0.9859	1.0317
Cl_1	0.2235	0.4461	0.6966
Cl_2	0.2217	0.4472	0.6973
Cl_3	0.4382	0.4884	0.5378
Cl_4	0.3975	0.4718	0.5378
Cl_5	0.3861	0.4604	0.5440

plateau extending over a considerable range of overpotentials, *cf.* Fig. 2. The development of such a current plateau in lsv experiments suggests coupling of chemical reaction(s) to the charge transfer. More specifically, the coupling reaction must either precede or be in parallel with the charge transfer. For the ce-type reaction, the current plateau is proportional to the concentration of the electroactive species, here A_2, but independent of the scan rate. The experimental evidence presented in Fig. 3, is in agreement with the first but not the second condition, if the charge transfer reaction is irreversible. The situation is less clear if the charge transfer reaction is reversible or if it occurs in parallel (21). In the simplest case, the appearance of the current plateau for an exponential $j = f(V)$ relationship, requires that the depletion of the electroactive species is balanced by its production within the zone adjacent to the electrode surface. Otherwise, with an increase in overpotential (and, in the lsv experiments, also with time) the condition $\partial A_2^{\cdot}/\partial t = 0$ cannot be realized.

With the further increase in cathodic overpotentials, yet another current plateau appears, Fig. 2b. This current plateau occurs within a much narrower potential range and is better defined at slower scan rates and lower $AlCl_3$ concentrations. While the coupling of reaction, Eq. [III] with the charge transfer, Eq. [IV], is presumed to be responsible for the development of the first current plateau, the conditions for the development of the second plateau cannot be, at the present time, as clearly stated. However, if the interphase region is considered an open system, the condition of constant affinity exists and can be specified by thermodynamic reasoning, provided that the necessary information is available (18, 26). Analogous to the development of the first plateau, the appearance of the second plateau may be attributed to the coupling of adsorption and charge transfer to the chemical reaction and diffusion. Occurrence of chemical reaction(s) requires the presence of reaction layer, r, sandwiched between the adsorption and diffusion layers.

Table IV. Bond length and charge density distribution following electron acceptance by onium ion

Reactions

$Cl_2Al(\leftarrow OSCl_2)_2^{\cdot}$; ΔH_f = −11 kcal/mol
$Cl_2Al(\leftarrow OSCl_2)_2^{\cdot} + e \rightarrow Cl_2Al(\leftarrow OSCl_2)_2^{2}$; ΔH_f = −310 kcal/mol
$Cl_2Al(\leftarrow OSCl_2)_2 + e \rightarrow Cl_2Al(\leftarrow OSCl_2)_2^{\cdot}$; ΔH_f = −347 kcal/mol
(ΔH_f is the MO calculated heat of formation from the elements)

Bond	$Cl_2Al \leftarrow OSCl_2)_2^{\cdot}$	$Cl_2Al(\leftarrow OSCl_2)_2$	$Cl_2Al(\leftarrow OSCl)_2)_2$
	Bond lengths, Å		
S_1—O_1	1.506	1.496	1.534
S_1—Cl_1	2.010	2.013	2.053
S_1—Cl_2	2.103	2.018	2.049
Al—O_1	1.795	1.844	1.737
Al—Cl_3	2.093	2.108	2.145
Al—Cl_4	2.096	2.121	2.147
Al—O_2	1.785	1.688	1.737
O_2—S_2	1.510	1.534	1.533
S_2—Cl_5	2.009	2.031	2.053
S_2—Cl_6	2.012	2.052	2.050
	Charge density		
Atom	$Cl_2Al(\leftarrow OSCl_2)_2^{\cdot}$	$Cl_2Al(\leftarrow OSCl_2)_2$	$Cl_2Al(\leftarrow OSCl)_2)_2$
Al	1.1016	1.116	1.081
O_1	0.6868	−0.635	−0.6719
O_2	−0.6836	−0.737	−0.6728
S_1	1.3343	1.336	1.007
S_2	1.3265	1.044	1.007
Cl_1	0.1579	−0.225	−0.450
Cl_2	0.1711	−0.218	−0.444
Cl_3	−0.3666	−0.407	−0.480
Cl_4	−0.3691	−0.432	−0.482
Cl_5	−0.1585	−0.3913	−0.450
Cl_6	0.1686	−0.4501	0.444

Reversal of the reductive scan at potentials within the current plateau, *e.g.*, at point B, Fig. 6, results in a decrease in the charge transfer current density which can be attributed to blocking of the electrode surface by an adsorbed species, $P_2^{(a)}$, generated by a slow reduction of P_1, Eq. [VI]

$$P_1^{(a)} + e \rightarrow P_2^{(a)} \qquad k_2 \ll k_2;\ V_2^0,\ \alpha_2 \qquad [VI]$$

The participation of an adsorption step becomes quite evident at higher overpotentials. Qualitatively, the presence of an adsorption step is illustrated in Fig. 6 where a plot of the oxidative lsv is displayed as a function of terminating potential of the reductive scan. The oxidative lsv exhibits two broad peaks whose currents increase with the terminating voltage, without substantial changes in their potentials, however. Such a behavior leads to the following conclusions: (*i*) as the overpotential increases so does the accumulation of reaction product(s) at the electrode surface, and (*ii*) these product(s) are reoxidized within the potential range 200-1000 mV. Thus, the charge transfer reaction, Eq. [VI], is quasi-reversible.

Elementary processes at higher overpotentials.—The current/time relationship, $j(0, t)$, for $V(t) = V_i + |\nu|t$, for the N electroactive species and M adsorption processes, is given by Eq. [2]

$$j(0, t) = \mathbf{F}\left[\sum_{i=1}^{N} n_i L \left.\frac{\partial C_i}{\partial x}\right|_{x=0} + \sum_{m=1}^{M} \Gamma_m \frac{d\theta_m}{dt}\right] \qquad [2]$$

where Γ_m denotes the maximum surface concentration of the m-th species. Both terms in Eq. [2] are time dependent, but in a different way. At slow scan rates, transport of reac-

tants and products between the bulk and the interphase is substantial and the observed lsv is sensitive to the scan rate. At fast scan rates, the condition at the electrode surface is the dominant factor and the contribution due to transport is minimal. As a general observation, the scan rate of $\nu = 100$ mV s^{-1} is taken as the rate separating these contributions (27).

The composition of the interphase region, arising from the interplay between the electrode surface processes and the bulk, is determined by the reductive scan rate and the terminal potential. To illustrate, we selected two scan rates, *viz.*, 5 and 100 mV s^{-1}, with the terminal voltage at −1200 mV. In accordance with Eq. [2], the slower scan includes the effect of transport on surface processes while the faster scan focuses on the processes pertinent to the adsorbed species. Even a cursory examination of Fig. 8a and b, reveals that a slow reductive scan promotes the accumulation of reaction product that can be reoxidized.

The surface condition generated by the slow and fast reductive scan are examined via the analysis of the oxidative lsv. In particular, Fig. 9a-d show the response of the electrode/electrolyte interphase generated at a slow reductive scan and Fig. 10a-d, for fast scans. It is seen that the interphase generated at slow scan rate is insensitive to the oxidative scan rates throughout the potential range. Differences only appear within the potential range of anodic currents The response of the interphase generated at fast scan rate is more complex, *viz.*, high scan rates affect the region of anodic currents while slow rates influence processes immediately after scan reversal. Such a behavior is consistent with fast adsorption of species from the reaction layer.

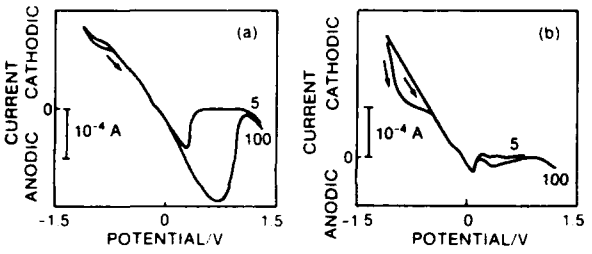

Fig. 8. Effect of reductive scan rate on the composition of the interphase displayed by oxidative lsv at ν_{ox} = 5 and 100 mV s^{-1} (a) for ν_{red} = 10 mV s^{-1}; (b) for ν_{red} = 100 mV s^{-1}. Electrolyte, 3.0M $AlCl_3$ in $SOCl_2$; ν_{ox} indicated.

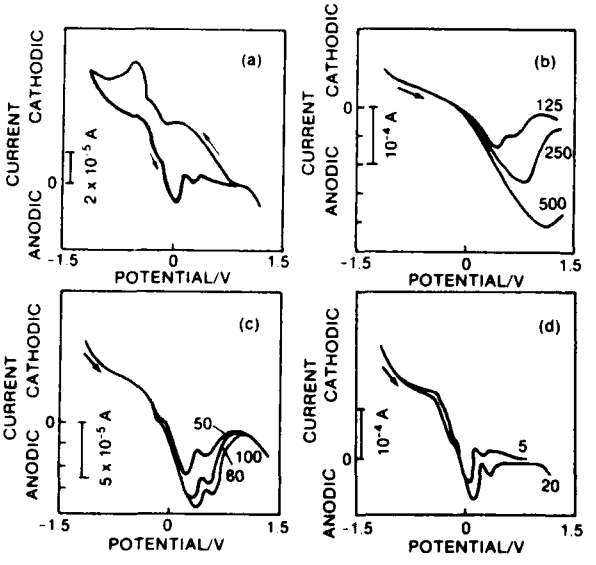

Fig. 9. Effect of ν_{ox} on the shape of oxidative lsv's for ν_{red} = 10 mV s^{-1} and terminated at −1200 mV (vs. Ag/AgCl in the same solution). (a) $\nu_{red} = \nu_{ox}$ = 10 mV s^{-1}; (b) $\nu_{ox} > 125$ mV s^{-1}; (c) 50 < ν_{ox} < 100 mV s^{-1}; (d) $\nu_{ox} < 20$ mV s^{-1}. Electrolyte; 3.0M $AlCl_3$ in $SOCl_2$.

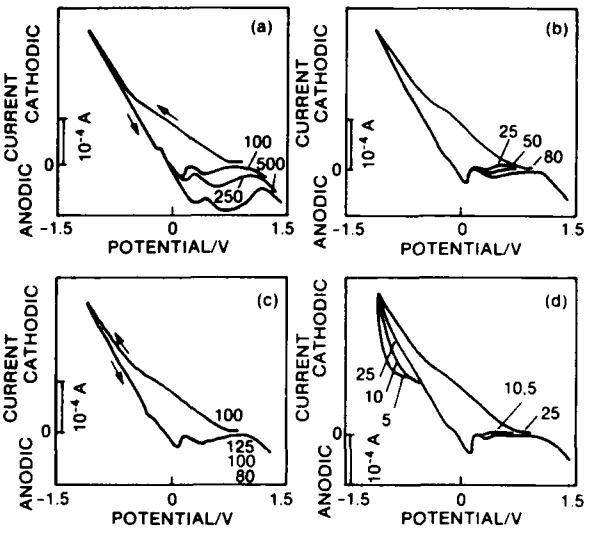

Fig. 10. Effect of ν_{ox} on the shape of oxidative lsv's for ν_{red} = 100 mV s^{-1} and terminated at −1200 mV. Electrolyte, 3.0M $AlCl_3$ in $SOCl_2$.

The common feature of oxidative lsv is the appearance of anodic peak currents. These currents indicate the presence of oxidizable substance(s) in an adsorbed state and, most likely, a reversible character of a charge transfer process, Eq. [V]. Their functional dependence, $j = f(\nu)$, is used in the analysis—a linear relationship is associated with adsorption while the square root dependence usually implies an intervention of a diffusional flux in the overall process. Results summarized in Fig. 11 indicate the dominance of adsorption in a 3.0*M* $AlCl_3$ in $SOCl_2$ electrolyte and the participation of diffusion in a 4.0*M* solution.

Sequence of events, their rates, and the nature of intermediates.—The behavior of the Me/$AlCl_3$-$SOCl_2$ system, subject to cathodic polarization is the result of the participation of, at least, three species, A_2^+, P_1, and P_2. Of these species, the onium ion, A_2^+, is adsorbed rapidly on the

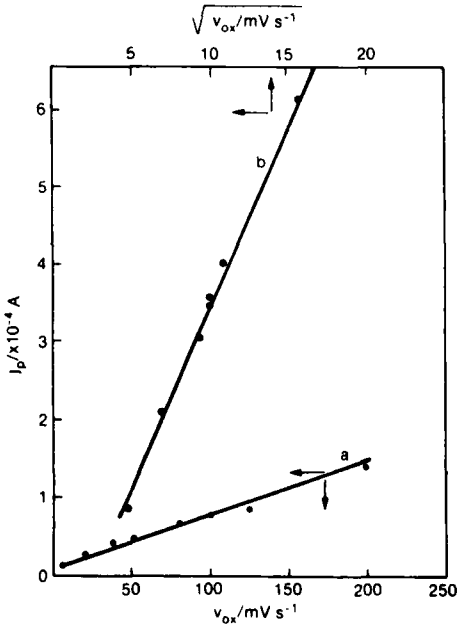

Fig. 11. Plots of anodic peak currents as a function of sweep rate. Curve a, for 3.0M $AlCl_3$ in $SOCl_2$; curve b, for 4.0M $AlCl_3$ in $SOCl_2$.

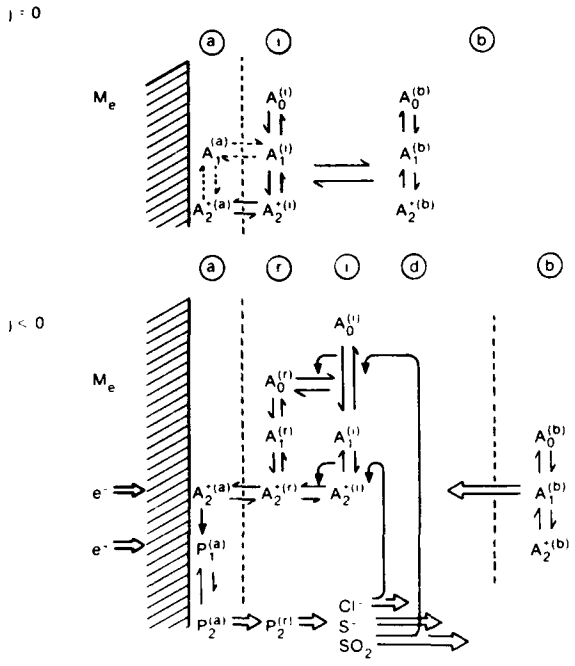

Fig. 12. Summary of participating elementary processes during $SOCl_2$ electroreduction. Superscripts defined in text.

electrode surface, so that its surface concentration is independent of the scan rate. The presence of adsorbed species modifies the j/V relationship which, in turn, makes the interpretation of voltammograms more difficult and the identification of participating processes less certain. The separation of anodic peaks at lower scan rates, shown in *e.g.*, Fig. 10b, is indicative of surface coverage by more than a single species (28). The cross over of the reverse scan, *cf.* Fig. 2d and 3b, implies that the standard potential of reaction, Eq. [VI], is more positive than for the first electron transfer, Eq. [V], *i.e.*, $V_2^0 > V_1^0$.

The summary of events associated with the electroreduction of $SOCl_2$ in the $AlCl_3$-$SOCl_2$ system is presented in Fig. 12. Initially, at rest potential, the interphase is equilibrated with the bulk, Eq. [I]-[III], with a significant enrichment of A_1 and A_2^* in the vicinity of the electrode surface. The interphase consists of adsorption and enrichment layers in contact with the bulk electrolyte.

Upon cathodic polarization, the composition of the interphase includes: $P_1^{(a)}$, $P_1^{(r)}$, $P_2^{(a)}$, $P_2^{(r)}$ with $k_2 > > k_2$. The composition of the interphase is now governed by the charge transfer processes. Eq. [V] and [VI], transport from the bulk and desorption from the electrode surface. The enrichment layer, defined in the absence of the charge transfer, becomes the reaction layer, where species P_1 and P_2, stabilized by the adsorption, undergo chemical reaction(s) to yield stable species Cl^-, S, and SO_2. These species interact with the components of the interphase, diffuse to the bulk where they may affect the established equilibria.

Conclusions

1. Because of the reactivity of $SOCl_2$ molecules, study of its electroreduction must consider the nature of the electrolyte.

2. Reduction occurs via the two-electron transfer of which the first is irreversible while the second is quasi-reversible with $k_2 > > k_2$ and V_2^0 more positive than V_1^0.

3. Adsorption processes play a key role in the reduction mechanism, giving rise to mild autocatalytic effects. Diffusional processes modify the adsorption characteristics.

4. Chemical reactions, including the formation of stable products occur within the interphase region. Desorption destabilizes intermediate species.

Acknowledgments

This work was supported, in part, by the Office of Naval Research. The authors wish to acknowledge discussions with Dr. R. D. Boss, Naval Ocean Systems, San Diego, California and Dr. J. R. Driscoll, Lockheed—Palo Alto Research Laboratory, Palo Alto, California.

Manuscript submitted Sept. 12, 1988; revised manuscript received Jan. 5, 1989.

The Naval Oceans System Center assisted in meeting the publication costs of this article.

REFERENCES

1. N. Doddapaneni, Abstract 315, p. 505, The Electrochemical Society Extended Abstracts, Vol. 82-2, Detroit, MI, Oct. 17-21, 1982.
2. B. Carter, R. Williams, F. Tsay, A. Rodrigues, and H. Frank, in "Proceedings of 17th IECEC Conference," Vol. 2, Paper Nr N.829110, Los Angeles, CA, 1980.
3. W. A. Bowden and A. N. Dey, *This Journal*, **127**, 1419 (1980).
4. W. K. Istone and R. J. Brodd, *ibid.*, **129**, 1863 (1982).
5. M. J. Madou, J. J. Smith, and S. Szpak, *ibid.*, **134**, 2794 (1987).
6. M. J. Madou and S. Szpak, *ibid.*, **131**, 2471 (1984).
7. R. J. Nowak, D. R. Rolison, J. J. Smith, and S. Szpak, *Electrochim. Acta*, **33**, 1313 (1988).
8. J. J. Smith, S. Pons, J. Li, W. West, and S. Szpak, Paper SW-2 presented at 3rd International Meeting on Li Batteries, Kyoto, Japan, May 1986.
9. P. A. Mosier-Boss, S. Szpak, J. J. Smith, and R. J. Nowak, Abstract 487, p. 695, The Electrochemical Society Extended Abstracts, Vol. 88-1, Atlanta, GA, May 15-20, 1988.
10. S. Szpak and H. V. Venkatasetty, *This Journal*, **131**, 961 (1984).
11. P. A. Mosier-Boss, R. D. Boss, S. Szpak, J. J. Smith, and R. J. Nowak, *J. Chem. Soc., Farad. Trans. 1*, **85**, 11 (1989).
12. P. A. Mosier-Boss, S. Szpak, J. J. Smith and R. J. Nowak, This Journal, **136**, 1282 (1989).
13. J. K. Foley and S. Pons, *Anal. Chem.*, **57**, 945A (1985).
14. C. J. Gabriel, P. A. Mosier-Boss, and S. Szpak, *Spectrochim. Acta*, **43A**, 1293 (1987).
15. B. E. Conway, "Theory and Principles of Electrode Processes," The Ronald Press, New York (1965).
16. I. Lindquist, "Inorganic Adducts of Oxo-Compounds," Academic Press, Inc., New York (1963).
17. W. West, J. J. Smith, and S. Szpak, Paper SW-8 presented at 3rd International Meeting on Li Batteries, Kyoto, Japan, May 1986.
18. P. van Rysselberghe, in "Modern Aspects of Electrochemistry," Vol. 4, J. O'M. Bockris, Editor, Plenum Press, New York (1966).
19. F. A. Cotton and R. Francis, *J. Am. Chem. Soc.*, **82**, 2986 (1960).
20. J. Selbin, W. E. Bull, and L. H. Holmes, *J. Inorg. Nucl. Chem.*, **16**, 219 (1961).
21. J. M. Saveant and E. Vianello, *Electrochim. Acta*, **12**, 629 (1967).
22. C. P. Andrieaux, L. Nadjo, and J. M. Saveant, *J. Electroanal. Chem.*, **26**, 147 (1970).
23. D. F. Milner and M. J. Weaver, *Anal. Chim. Acta*, **198**, 245 (1987).
24. E. Ahlberg and V. D. Parker, *J. Electroanal. Chem.*, **121**, 57 (1981).
25. A. S. Hinman, S. Pons, and J. Cassidy, *Electrochim. Acta*, **30**, 89 (1985); *ibid.*, **30**, 95 (1985).
26. P. van Rysselberghe, "Thermodynamics of Irreversible Processes," Hermann, Paris (1963).
27. S. Srinivasan and E. Gileadi, *Electrochim. Acta*, **11**, 321 (1966).
28. E. Laviron, *J. Electroanal. Chem.*, **52**, 355 (1974).

Intercell Currents in Assembly of Modules

S. Szpak* and C. J. Gabriel

Naval Ocean Systems Center, San Diego, California 92152-5000

J. J. Smith

Department of Energy, Washington, DC 20545

J. R. Driscoll

Lockheed Missiles and Space Company, Sunnyvale, California, 94088-3504

ABSTRACT

A method for computing intercell load and nodal currents in a parallel-connected battery assembled from several series-connected modules is described. The method covers systems sharing a common electrolytic path and operating with constant as well as variable parameters such as are encountered in practice. The multimodule $Li/SOCl_2$ battery is selected to illustrate the pertinent points.

Energy and power dense batteries are, of necessity, constructed by arranging individual cells in series and providing a common manifold for electrolyte circulation or battery activation. Whenever an increase in either extractable energy content or power output is required, a number of modules are connected in parallel. For practical reasons, *e.g.*, to maintain simplicity of design or to minimize the use of auxiliary equipment, a continuous electrolytic path is retained. Such an arrangement is expected to modify the distribution of the intercell currents.

The purpose of this communication is to examine the distribution of intercell currents in an assembly of modules sharing a common electrolytic path. The treatment follows closely that given in Ref. (1). Also, the examples selected to illustrate specific points, *e.g.*, energy/power losses and the structural integrity of cells, pertain to $Li/SOCl_2$ batteries that employ a bipolar, thin-cell design.

Intercell Currents

An intercell current is an ionic current that originates in one cell and terminates in another. Its magnitude depends on the module design and the nature and properties of participating processes and is usually evaluated under a set of restrictive conditions. In the present discussion, we retain the basic assumptions and definitions of Ref. (1); *i.e.*, (*i*) the current distribution can be simulated by an equivalent electric circuit analog, shown in Fig. 1; (*ii*) the phenomenological coefficients associated with the ionic current in the segments of the electrolytic path are replaced by equivalent resistances, R_l and R_f, requiring the assumption of uniform current on the cross section of the segments; (*iii*) the potentials in the electrolyte phase at the entrance port to the cell, Φ_i, are uniform and equal to a longitudinal average between equipotential cell electrodes having a potential difference between them of $V_i = V_{c,i} - V_{a,i}$; (*iv*) the bipolar plates are equipotential, *i.e.*, $V_{c,i} = V_{a,i+1}$, $i = 1, 2, \ldots, N-1$; and (*v*) the intercell current is defined as the difference between circulating currents, *i.e.*, $I_i = J_i - J_{i-1}$, where the circulating currents at the terminal cells of the battery are zero.

Multimodule Assembly

An example of a multimodule arrangement is shown in Fig. 2. In general, an assembly can contain either an odd or an even number of modules which, when connected in parallel, share positive/positive, (+/+), and negative/negative, (−/−), interfaces. If an assembly contains an odd number of modules, only one configuration is possible, *i.e.*, one positive and one negative assembly terminal. However, if the assembly contains an even number of modules, two configurations are possible, *viz.* both assembly terminals are either positive or negative. Symbols and conventions employed here are those in Ref. (1). In addition, in each module the cells are counted from 1 to N from the negative to the positive end. Quantities associated with a module are identified by a preceding index in parenthesis; *e.g.*, ${}^{(m)}J_l$ denotes the load current generated by the mth module. For convenience, whenever a direct comparison is made with a corresponding statement in Ref. (1), it is indicated accordingly, *e.g.*, [r.1] refers to Eq. [1] of Ref. (1), and whenever all quantities in an equation have the same module index, the index will be suppressed, provided that no ambiguity exists.

The formulation of appropriate equations is the same as for the single module except for the matching conditions at the (+/+) and the (−/−) interfaces between the neighboring modules. For an $M-$ module battery, Eq. [r.1], expressing the potential across the load, $V = \sum_{i=1}^{N} {}^{(m)}V_i$, becomes Eq. [1]

$$V = R_l \sum_{m=1}^{M} {}^{(m)}J \qquad [1]$$

while Eq. [r.3], applied to the terminal cells of the assembly, becomes ${}^{(1)}J_\mu = {}^{(M)}J_\nu = 0$, where μ and ν are either zero or N depending upon which cell of the module terminates the battery. However, in the terminal cells of a module, *i.e.*, at coupling interfaces between modules, the circulating currents are not necessarily zero; specifically, they are

$${}^{(m-1)}J_N = -{}^{(m)}J_N = J_{(m-1),(m)} \qquad [2a]$$

$${}^{(m)}J_0 = -{}^{(m+1)}J_0 = J_{(m),(m+1)} \qquad [2b]$$

where $J_{(m-1),(m)}$ and $J_{(m),(m+1)}$ are the coupling currents between respective modules. Equation [r.6], denoting the

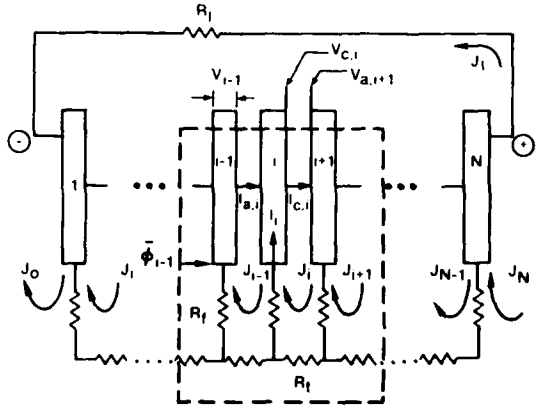

Fig. 1. Module representation by an equivalent electric circuit: V_{i-1}-cell voltage; Φ_{i-1}-potential at manifold inlet to (i − 1) − th cell; J_i-circulating current; J_l-loop current in an external resistor, R_l; R_f-manifold feed-line resistor; and R_t-equivalent feed tube resistor. Control volume indicated by heavy dashed lines.

* Electrochemical Society Active Member.

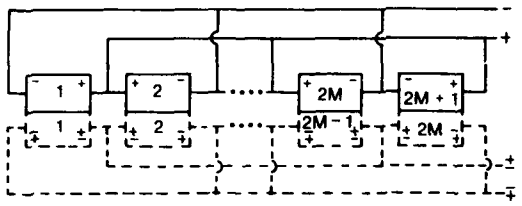

Fig. 2. Multimodule battery representation: (a) solid lines, for an odd number of modules, and (b) doshed lines, for an even number of modules.

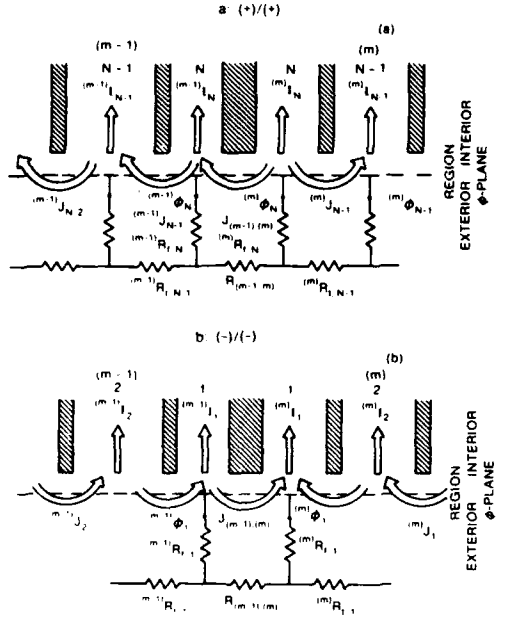

Fig. 3. Module/module coupling representation by an equivalent electric circuit: (a) for the (+)/(+) interface, and (b) for the (−)/(−) interface. Circuit components as in Fig. 1.

equipotential character of bipolar plates, is retained. The load voltage in Eq. [1], in terms of electrode potentials, is

$$V = V_{c,N} - V_{a,1} \qquad [3]$$

where the parallel connection of the modules is denoted by

$$V_{a,1} = {}^{(1)}V_{a,1} = \cdots = {}^{(M)}V_{a,1}$$
$$V_{c,N} = {}^{(1)}V_{c,N} = \cdots = {}^{(M)}V_{c,N} \qquad [3a]$$

as indicated in Fig. 2.

In Ref. (1), the set of N equations [r.15] and [r.17] determined the distribution intercell and circulating currents within a single module. Here, a corresponding set for each module is required and an additional $(M - 1)$ equation is written to account for the presence of coupling between modules.

Conditions at the Module/Module Interfaces

A (+/+) interface between the $(m-1)$-th and mth module, together with the identification of the elements of the electric circuit analog, is shown in Fig. 3a. For convenience, we define a fictious junction at the entrance port of the cells separating the exterior and interior regions of the cell-feedline-loop currents that couple the modules; here, $\Phi_N|_{ex} = \Phi_N|_{in}$. We have for the exterior portion of the coupling-current loop the potential difference

$${}^{(m)}\Phi_N - {}^{(m-1)}\Phi_N|_{ex} = -{}^{(m-1)}(J_{N-1}R_{f,N}) + J_{(m-1),(m)}[{}^{(m-1)}R_{f,N} + R_{(m-1),(m)} + {}^{(m)}R_{f,N}] + {}^{(m)}(J_{N-1}R_{f,N}) \qquad [4]$$

where $R_{(m-1),(m)}$ is the coupling resistance between the two modules.

The development of a corresponding expression for the same potential difference through the interior region is somewhat more complex. In deriving this expression, frequent references to Appendix B, Ref. (1) are required. Examining Fig. 3, we write in an analogy to Eq. [r.B5]

$${}^{(m)}\Phi_N - {}^{(m-1)}\Phi_N|_{in} = {}^{(m)}(\Phi_{0,N} + I_N R_{p,N}) - {}^{(m-1)}(\Phi_{0,N} + I_N R_{p,N}) \qquad [5]$$

where ${}^{(m)}\Phi_{0,N}$ is the potential at the interior side of the fictitious dividing junction in the absence of intercell current ${}^{(m)}I_N$, and $R_{p,N}$ is the impedance to intercell current at the entrance port. To evaluate this difference and express it in terms of battery operation and design, we make use of the following relationships, Eq. [6]-[11], where the module index has been suppressed

$$\Phi_{0,N} = V_{c,N} - U_{c,N} + (U_N - V_N)\frac{\sigma}{\sigma_{c,N}} \qquad [6]$$

Furthermore, we have

$$(U_N - V_N) = \left(I_{a,N} + I_N \frac{\sigma_N}{\sigma_{c,N}}\right) R_{c,N} \qquad [7]$$

$$I_{a,N} = J_1 + J_{N-1} \qquad [8]$$

$${}^{(m-1)}I_N = {}^{(m-1)}J_N - {}^{(m-1)}J_{N-1} \qquad [9]$$

$${}^{(m)}I_N = {}^{(m)}J_N - {}^{(m)}J_{N-1} \qquad [10]$$

and

$$\sigma^{-1} = \sigma_a^{-1} + \sigma_c^{-1} \qquad [11]$$

Equations [9] and [10] are obtained from Eq. [r.4].

Upon substitution of these relationships into Eq. [5] and combining with Eq. [4], after some algebraic manipulations, we obtain the matching conditions at the (+/+) interface, Fig. 3a

$${}^{(m)}U_{c,N} - {}^{(m+1)}U_{c,N} = {}^{(m+1)}(J_{N-1}R^*_{f,N}) - {}^{(m)}(J_{N-1}R^*_{f,N}) + {}^{(m)}\left(J_1 R_{z,N}\frac{\sigma_N}{\sigma_{c,N}}\right) - {}^{(m+1)}\left(J_1 R_{z,N}\frac{\sigma_N}{\sigma_{c,N}}\right) + {}^{(m)}J_N \cdot {}^{(m)}\left(R^*_{f,N} + R_{z,N}\frac{\sigma_N}{\sigma_{c,N}}\right) + {}^{(m)}J_N {}^{(m+1)}\left(R^*_{f,N} + R_{z,N}\frac{\sigma_N}{\sigma_{c,N}}\right) + {}^{(m)}J_N R_{(m),(m+1)} \qquad [12]$$

where $R^*_{f,N} = R_{f,N} + R_{p,N} - R_{z,N}\sigma_N^2/\sigma_{a,N}\sigma_{c,N}$.

Matching conditions for the (−/−) interface, shown in Fig. 3b, are calculated in an analogous manner. Following the same procedure with due attention to the direction of current flow, we have

$${}^{(m+1)}U_{a,1} - {}^{(m)}U_{a,1} = {}^{(m+1)}(J_1 R^*_{f,1}) - {}^{(m)}(J_1 R^*_{f,1}) + {}^{(m)}\left(J_1 R_{z,1}\frac{\sigma_1}{\sigma_{a,1}}\right) - {}^{(m+1)}\left(J_1 R_{z,1}\frac{\sigma_1}{\sigma_{a,1}}\right) + {}^{(m+1)}J_0 \cdot {}^{(m)}\left(R^*_{f,1} + R_{z,1}\frac{\sigma_1}{\sigma_{a,1}}\right) + {}^{(m+1)}J_0 {}^{(m+1)}\left(R^*_{f,1} + R_{z,1}\frac{\sigma_1}{\sigma_{a,1}}\right) + {}^{(m+1)}J_0 R_{(m),(m+1)} \qquad [13]$$

where $R^*_{f,1} = R_{f,1} + R_{p,1} - R_{z,1}\dfrac{\sigma_1^2}{\sigma_{a,1}\sigma_{c,1}}$.

Intramodule Equations

In addition to the above $(M - 1)$ intermodule equations, M sets of equations corresponding to Eq. [r.15] and [r.17], which were needed to calculate the distribution of intercell and circulating currents in a single module, are required for an assembly of modules. Thus, for each of the modules, Eq. [14], corresponding to [r.15], applies

$$\sum_{i=1}^{N} U_i = V + \sum_{i=1}^{N-1} (J_i R^*_{z,i}) + J_1 \sum_{i=1}^{N} R_{z,i} + \left(J_0 R_{z,1} \frac{\sigma_1}{\sigma_{a,1}}\right) + \left(J_N R_{z,N} \frac{\sigma_N}{\sigma_{c,N}}\right) \quad [14]$$

while Eq. [r.17] remains unchanged except for the addition of an implied module index.

Method of solution.—The solution of these equations for large N and M on small computers is facilitated by considering the coupling-loop currents at each module interface as well as at the module load currents as undetermined coefficients. Then by solving separately for each module, the tridiagonal banded sets of Eq. [r.17] with $2M$ appropriately chosen sets of these coefficients, a set of $(2M - 1)$ linear equations for the coefficients is obtained. The solutions of these $(2M - 1)$ equations and the subsequent substitution of this solution into Eq. [r.17] provides M sets of $(N - 1)$ equations to be solved for the remaining loop currents.

Only minor differences in handling the changes in cell parameters upon discharge from those in Ref. (1) are introduced here. Instead of using Eq. [r.48] and [r.49] to describe the change in the electrolyte conductivity near the positive electrode of a cell and in the feed line into a cell, we now employ Eq. [15] and [16], respectively, for the time-dependent $\kappa_c(t)$ and $\kappa_f(t)$

$$\kappa_c(t) = \frac{w\kappa\epsilon_z}{1 + (Q_c(t)/Q_c)^{\xi_c}} \quad [15]$$

and

$$\kappa_f(t) = \epsilon_f\left[\kappa_d + \frac{\kappa - \kappa_d}{1 + (Q_f(t)/Q_f)^{\xi_f}}\right] \quad [16]$$

where

$$Q_c(t) = \int_0^t I_c dt \quad [17]$$

$$Q_c = \frac{wTNU}{MR_l + NR_z} \quad [18]$$

in which R_z is the nominal cell internal impedance

$$Q_f(t) = -\int_0^t I_a(r_o) dt \quad [19]$$

and

$$Q_f = \frac{\epsilon_f V_f \mathbf{F}}{2V_d} \quad [20]$$

The minus sign in Eq. [19] arises because $I_a(r_o)$ represents a reversed current on the negative electrode.

The forms of Eq. [15] and [16] permit the conductivities $\kappa_f(t)$ and $\kappa_c(t)$ to vary smoothly over their allowed ranges. The adjustable parameters, ξ_f and ξ_c, are chosen to provide module discharge characteristics approximating observed behavior. The effect of reversed anode current is noticeable throughout the module discharge period. On the other hand, the discharge current affects the internal cell impedance only after a significant amount of charge has been transferred. For these reasons, ξ_f is chosen to be of the order of unity while ξ_c was assigned a much larger value, *e.g.*, on the order of ten.

The meaning of $Q_f(t)$ and $Q_c(t)$ is as follows: $Q_f(t)$ represents the charge transferred by reversed current on a cell negative electrode in the time interval t. The quantity Q_f denotes the amount of charge transferred by the reversed current required to half-fill the feed tube volume, V_f, with a reaction product, *e.g.*, metallic Li, having a volume per equivalent weight, V_d, and conductivity, κ_d. The quantity $Q_c(t)$ is the actual amount of charge transferred to the positive electrode of a cell within the same time period, t, while Q_c, with $w = 1$, represents the amount of charge that would be transferred to the positive of a nominal cell in the time interval T under conditions of no intercell current flow and no changes in cell parameters during the discharge. The factor w, which is always less than unity, is introduced to account for the faradaic inefficiency within a particular cell.

If a battery contains more than one manifold-feed tube in parallel, a case often seen in practice, it is necessary to replace, for the purpose of calculation only, the actual assembly with an equivalent set of parallel assemblies, each having one manifold feed tube, and an equivalent load resistance, R_l, equal to the actual load resistance multiplied by the number of feed tubes. Similarly, the equivalent load current in the mth module, ${}^{(m)}J_l$, equals the actual load current divided by the number of feed tubes. Furthermore, the outer electrode radius is calculated from an effective electrode area which equals the actual area divided by the number of feed tubes. However, the manifold tube radius and the inner electrode radius remain the actual values. These assumptions appear reasonable because reversed currents occur only near the manifold fill tube so that the cell geometry away from the manifold tube is much less important than that near the fill tube.

Illustrative Examples

Two aspects of a Li/$SOCl_2$ battery scale-up, *i.e.*, the addition of modules, are presented: First, the discharge characteristics of a three-module battery that are experimentally accessible (2), are compared with calculated nodal and load currents on individual modules. Second, the reversed intercell currents are examined for a three-module battery. The latter is considered to illustrate how the number of modules may affect the integrity of functional elements, and whether or not battery size may contribute to the initiation of catastrophic events (3). The computer input data are tabulated in Table I.

Experimental discharge characteristics of a three-module assembly.—As illustrated in Fig. 4, the delivery of the total current is smooth. The current supplied by individual modules, however, varied during the discharge (2). In particular, the current labeled I_{a+} was measured at the positive collector plate of the first module, and current I_{b-} was measured at the negative collector plate between modules 1 and 2. Current I_{b+} was measured at the positive collector plate between modules 2 and 3, and I_{a-} was measured at the negative collector of module 3. The I_{b+} and I_{b-}

Table I. Data for modeling of intercell currents in assembly of modules

Input Data		
Electrolyte conductance	κ, S cm^{-1}	0.01
Deposit conductance	κ_d, S cm^{-1}	100.0
Electrode polarization-anode	κ_a, S cm^{-2}	5.0
Electrode polarization-cathode	κ_c, S cm^{-2}	1.0
Open-circuit potential	U, V	3.74
Deposit volume (equiv.)	V_d, cm^3	25.0
Fill tube-length	l_t, cm	0.04
Feed path-thickness	d, cm	0.05
Electrode-separation (nominal)	δ^*, cm	0.04
Feed path porosity-separator	ϵ_f	0.8
Cell porosity-separator	ϵ_z	0.5
Radius-fill tube	r_t, cm	0.3
Electrode inner radius	a, cm	1.3
Electrode outer radius (equiv.)	b, cm	8.7
Number feed tubes/module		2
Cell lifetime	T, s	480.0
Coupling factor	α	1.0
Number cells/module	N	50
Factor (cf. text)	ξ_c	13.0
Factor (cf. text)	ξ_f	1.0
Load resistance	R_l, Ω	3.0

Coupling factor: $\alpha = R_{(m),(m+1)}/R_l$ with R_l given by Eq. [r.34].

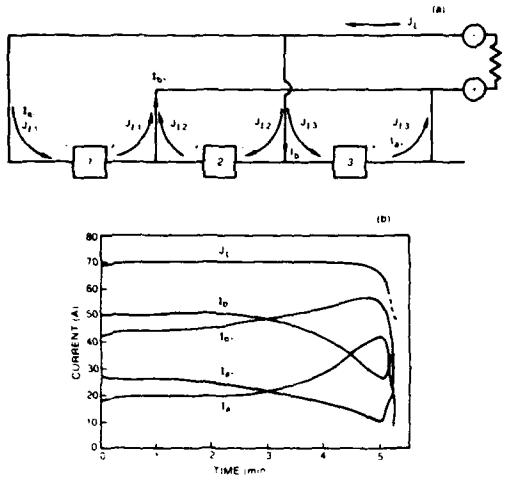

Fig. 4. Nodal load current variation in an experimental three-module assembly: (a) electric circuit analog of a three-module battery, and (b) measured current variation during discharge.

currents are initially about twice that of the I_a currents because two modules share these plates.

Calculated load and nodal currents.—We limit the discussion to well-designed and constructed batteries with the following restrictive conditions; (*i*) all modules contain the same number of cells, and (*ii*) the construction of the cells and their performance are statistically reproducible, *i.e.*, $w = 1$, in Eq. [15] and [18]. The statistical variations of module parameters is introduced in two ways. First, the porosities of the matrix in the cell, ${}^{(m)}\epsilon_{c,i}$, and in the feed line, ${}^{(m)}\epsilon_{f,i}$, are assumed to vary from cell to cell throughout the assembly, and are derived from a normally distributed random variable, $N_s{}^{(m)}\epsilon_{\alpha,i}$, having the mean value $N_s\epsilon_\alpha$ and standard deviation $[N_s\epsilon_\alpha(1 - \epsilon_\alpha)]^{0.5}$, where N_s is an arbitrary scale factor and $\alpha = c, f$ designates the cell and feed lines, respectively. Second, the electrode separation for all cells in a module, ${}^{(m)}\delta^*$, is taken to have a uniform random distribution from module to module.

A technologically important aspect of a battery scale-up is its effect on the distribution of load currents from individual modules. As illustrated in Fig. 5, the addition of modules reduces the individual load current while maintaining a smooth delivery to the main line, except toward the end of battery discharge when a crossover, indicating

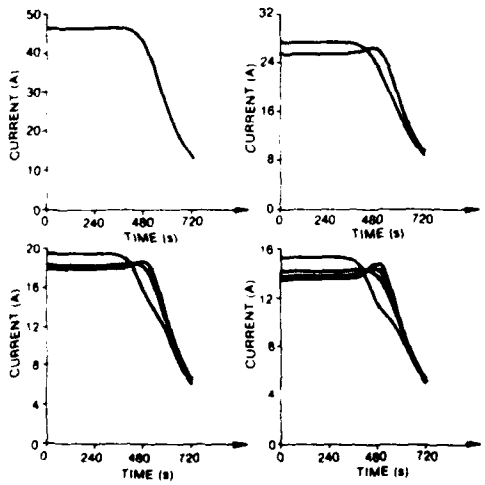

Fig. 5. Calculated load current profiles in a multimodule battery assembly; $N_s = 10$; $\delta^* = \text{const}$. Design time, T, based on an anticipated lifetime of the whole assembly. Input data is given in Table I. Configuration: even number of modules is + . . . + on battery end terminals.

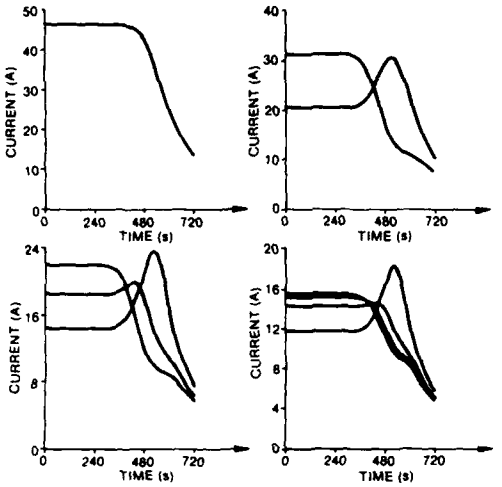

Fig. 6 Load current profiles in a multimodule battery assembly. Input parameters and configuration as in Fig. 5 except that the variation in $\delta^* = \pm 6\%$.

current sharing, occurs. It is noteworthy that the load sharing does not interfere with the power output. Thus, an increase in number of well-constructed modules is an acceptable procedure. However, if the process control is inadequate, serious problems may arise. For example, if the electrode-to-electrode spacing, δ^*, is allowed to vary by, *e.g.*, $\pm 6\%$, a significant effect on the distribution of module load current is observed, especially toward the end of discharge, Fig. 6. The current fed to the working network is not affected but the battery lifetime is somewhat reduced.

The validity of the proposed model is supported by the agreement between the time behavior of experimental and computed nodal currents for a three-module battery, shown in Fig. 4 and 7, respectively. The small variations in the measured nodal currents at the beginning of the discharge are attributed to small variations in cell construction that are not accounted for in the computed values, *i.e.*, the constant parameters in the model do not reflect the reality of experimental cells. However, toward the end of the battery lifetime, agreement with the behavior is better. The sharing of load current is evident by crossing of the currents from the various individual modules. Again, total currents, both observed and computed, show good stability.

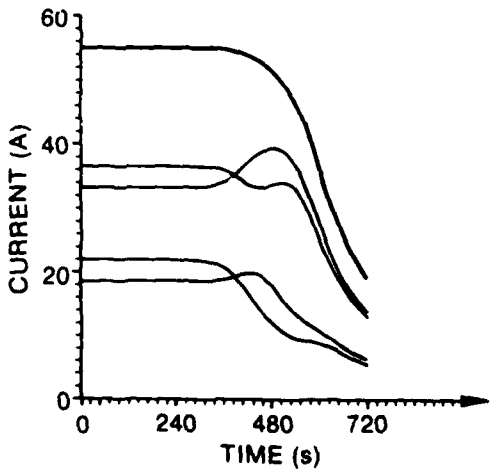

Fig. 7. Calculated load current variation for three-module battery asembly. $N_s = 10$, $\delta^* = \pm 6\%$. Input parameters and configuration as in Fig. 5.

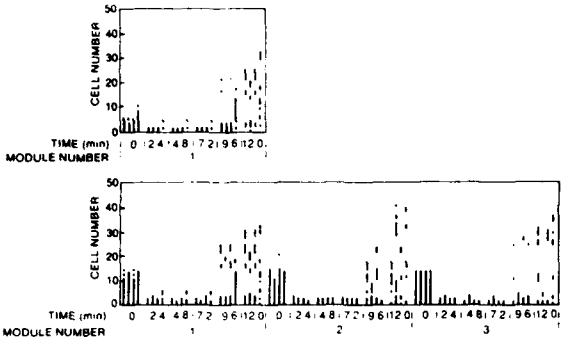

Fig. 8. Time development of the distribution of reversed intercell currents in an assembly of modules. The four vertical bars in each time frame indicate the cells experiencing reversed currents during the time interval between the specified time and the previous time, e.g., those bars at 7.2 min are for the interval from 4.8 to 7.2 min. The conditions of the calculations are from left to right: (a) N_s = 10, δ^* = const.; (b) N_s = 10, δ^* = const. with different seed in random number generator; (c) N_s = 10, δ^* = ±6%; (d) N_s = 5, δ^* = const. Other parameters taken from Table I.

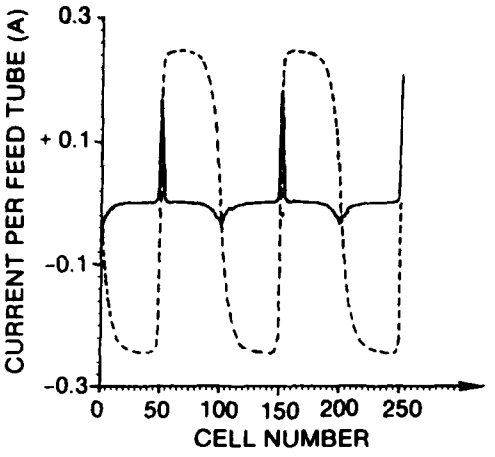

Fig. 9. The circulating (dashed line) and intercell (solid line) currents in an assembly of five modules after 2.4 min of discharge. Input parameters taken from Table I with N_s = 10, δ^* = const. Battery negative terminal on the right. The current distributions remain essentially the same throughout the lifetime, T.

Reversed intercell currents.—The distribution of the intercell currents affects the utilization of reactants, structural integrity of cells, and, as in the case of Li/$SOCl_2$ technology, may have some impact on the safety of operation. The underutilization of reactants, primarily in the terminal cells of a module, arises from the difference in the cathodic and anodic currents caused by the intercell current. If the intercell current exceeds its critical value, which depends on the load current, electrode current is reversed over a part of an electrode. If current reversal occurs at the negative, it promotes the growth of Li dendrites, which, in turn, may generate hot spots.

Of interest from both academic and practical points of view, is the examination of the effect of scale-up, i.e., how additional modules sharing a common electrolytic path affect the distribution of intercell currents. In particular, how many cells suffer from underutilization and how the degree of underutilization changes with time during the discharge. Calculations for as many as five modules were carried out. Typical results are illustrated in Fig. 8a and b for one and three modules, respectively. It is seen that the addition of modules does not substantially affect the distribution of the intercell currents. Just as with a single module, the number of cells suffering reversed intercell current diminishes shortly after the initiation of the module discharge and remains essentially uncharged throughout the rest of the battery's design lifetime, T. Evidently, the initial decrease in the number of cells affected is due to the dendritic growth of metallic Li at cell entrances which reduces their feed tube resistances, and, in turn, increases the magnitude of the intercell current. An increase in the intercell current has two effects: it reduces the number of cells affected by shunting intercell current away from more centrally located cells and promotes the underutilization of active material. The first effect, occurring early in the discharge, is the appearance of a spike in the intercell current at the negative end of a module, illustrated in Fig. 9 for a five-module battery. The second effect appears in the form of an increased number of central cells experiencing reversed current toward the end of the battery lifetime. Thus, for times greater than T, the number of cells experiencing reversed current increases markedly.

Concluding Remarks

Calculated load, nodal, and intercell currents exhibit features that are in agreement with observation, cf., Fig. 4 and 7. The scale-up (the addition of modules) of a well designed and constructed multimodule assembly, which shares a common electrolytic path, does not appear to increase safety concerns, i.e., does not inherently cause an increase in the imbalance of intercell currents. The model, however, implies that quality control plays an increasingly important role as the number of modules is increased, as illustrated in Fig. 5 and 6.

Acknowledgment

This work was supported, in part, by both the Office of Naval Research and NOSC Independent Exploratory Development program and constitutes a fraction of a program to establish a technology base for high discharge rate Li/$SOCl_2$ batteries.

Manuscript submitted May 8, 1989; revised manuscript received Aug. 25, 1989.

Naval Ocean Systems Center assisted in meeting the publication costs of this article.

LIST OF SYMBOLS

I	intercell current, A
J	current, A
N	number of cells in a module
M	number of modules in a battery
R	resistance, Ω
Q	charge density, C
T	cell lifetime, s
U	cell voltage at zero current, V
V	cell voltage, V
w	faradaic inefficiency factor

Greek Letters

δ^*	distance between electrodes, cm
ϵ	porosity
κ	conductivity, S cm^{-2}
μ, ν	running indexes
Φ	potential, V
σ	conductivity, S cm^{-2}
ξ	defined in text

Subscripts

a	anode
c	cathode
f	feed line
i, m, n	running indexes
l	load
o	initial condition
p	cell entrance port
t	fill tube
z	cell internal

REFERENCES

1. S. Szpak, C. J. Gabriel, and J. R. Driscoll, *This Journal*, **131**, 1996 (1984).
2. S. Szpak and J. R. Driscoll, "Assessment of Li/$SOCl_2$ Battery Technology: Reverse, Thin Cell Design," NOSC TR 1154 (April 1987).
3. S. Szpak, C. J. Gabriel, and J. R. Driscoll, *Electrochim. Acta*, **32**, 239 (1987).

EFFECT OF ELECTRODE MATERIAL ON $SOCl_2$ REDUCTION

P. A. Mosier-Boss and S. Szpak

Naval Ocean Systems Center, San Diego CA 95152-5000

J. J. Smith

Department of Energy, Washington DC 20545

and

R. J. Nowak

Office of Naval Research, Arlington VA 22217-5000

Abstract

The effect of electrode material on the elementary processes associated with the electroreduction of the $SOCl_2-AlCl_3$ system is examined by three techniques: IR- reflectance spectroscopy, linear scan voltammetry and galvanostatic pulsing. The results of spectroscopic examination indicate the same reaction path, *i.e.*, independent of electrode material, while the shape of voltammograms clearly show the effect of electrode material on the reaction kinetics. The latter result is further supported by galvanostatic pulse experiments.

List of Symbols

c - concentration, $mol\ cm^{-3}$

C - capacitance, $A\ s\ V^{-1}$

D - diffusion coefficient, $cm^2\ s^{-1}$

E - potential, V

F - Faraday constant, 96487 $C\ mol^{-1}$

j - current density, $A\ cm^{-2}$

k - rate constant, defined in Fig. 4

l - running index

m - running index

n - running index

R - gas constant, $J\ K^{-1}\ mol^{-1}$

t - time, s

T - temperature, K

x - coordinate, cm

Γ_m - maximum surface concentration , $mol\ cm^{-2}$

η - overpotential, V

θ - surface coverage

λ - parameter, defined in 3.2.1

ξ - parameter, defined in 3.2.1

1.0 Introduction

A technologically important $Li/SOCl_2$ electrochemical power source, exhibiting a high theoretical energy density, was discovered in the late 60's and reduced to practice, for low discharge rates, in the 70's. A decade later, a new requirement was imposed, that of maximizing its power density. To accomplish this, two design approaches were suggested: the construction of a module containing in-series connected thin cells, as one choice, and the employment of a flowing electrolyte, as the other. Seeking an improvement in performance in each of the proposed designs, modifications of both the electrode structure and composition were undertaken, unfortunately, with mixed results. Some of the difficulties were resolved through cell modeling. The conclusions reached by Tsaur and Pollard [1], Smith *et al* [2] and Nowak *et al* [3] showed that, in general, good agreement exists between the theory and practice and that the important factor in determining the cell lifetime is the form of the local current density/overpotential relation and the ensuing changes associated with the

reaction path. Examination of this system by cyclic voltammetry indicated a complex reaction path suggesting that more than one species participates in the charge transfer process, *via* an adsorption step [4,5]. Consequently, information on the form and content of the polarization equation and the structure and properties of the electrolyte and the electrode/electrolyte interphase, are of immediate interest.

In this communication, we examine the effect of electrode material on the form of the $j = j(\eta)$ relationship. We limit the discussion to events occurring at Au ,$C-glassy$ and, to a lesser degree Si electrode surfaces; the smooth Pt electrode is used as a standard for comparison. Emphasis is on the qualitative aspects of the charge transfer process. Subject to geometrical constraints, the events occurring on smooth surfaces describe the behavior of the porous structure found in practical batteries [6].

2.0 Experimental

Experimental details were presented elsewhere [7,8]. Here, for convenience, we provide a brief summary only.

2.1 *Materials /procedures.*

An analytical grade of thionyl chloride was distilled and the middle fraction was collected and stored under argon. C. P. grade aluminium chloride and lithium chloride were used as received. All solutions were prepared in a glove bag in an inert atmosphere of Ar by dissolving known amounts of Al_2Cl_6 and $LiCl$ in $SOCl_2$.

2.2 *Electrode preparation.*

Before each experiment, the Pt, $C-glassy$ and Au working electrodes were polished with an Al_2O_3 aqueous slurry on a polishing cloth. After rinsing with water the electrodes were sonicated for 5 minutes to remove residual alumina particles. After a second aqueous rinse, Au and Pt elec-

trodes were rinsed with methanol and allowed to air dry. After sonication, the $C-glassy$ electrode was rinsed with 0.05 M H_2SO_4 followed by an aqueous rinse and a methanol rinse. In the voltammetry and galvanostatic pulsing experiments the areas of the electrodes are 0.181 cm^2 for Pt and Au and 0.071 cm^2 for $C-glassy$. The electrodes were of the same degree of roughness.

2.3 *Instrumentation.*

The IR – spectra were obtained on a Nicolet 5 DXB FT-IR spectrometer (with the resolution of 2 cm^{-1}). The external reflectance spectro-electrochemical cell, patterned after that of Foley and Pons [9], was constructed from a machineable ceramic material and provided with a variable distance between the $AgCl$ window and the working electrode surface. The potential/time sweep rate and the electrode galvanostatic pulsing were controlled by the computer driven potentiostat, PAR model 173, with a 276 IEEE computer interface.

3.0 Results and discussion

3.1 *Methodology*

The electroreduction of $SOCl_2$ in practical batteries, as well as on smooth electrode surfaces, comprises a set, (perhaps more than one set), of consecutive processes occurring within the interphase region. The analysis of these processes, given in [5], is based on the van Rysselberghe concept of the interphase region [10], which is based on an open system whose structure is generated by, and responds to, the demands imposed by the dominating process(es). This concept is retained and, when coupled with three experimental techniques, *viz.* IR - spectroscopy, cyclic voltammetry and galvanostatic pulsing, is used to illustrate the effect of the electrode material on the charge transfer process, its mechanism and kinetics.

3.1.1 IR – *spectroscopy*. In- situ reflectance infrared spectroscopy is a powerful tool in probing the electrode/electrolyte interphase [11]. By varying the electrode potential, it is possible to determine, from changes in the spectra, the species undergoing electroreduction as well as their

orientation on the electrode surface. However, before such experiments can be correctly interpreted, a thorough understanding is necessary regarding the species present in the bulk solution and the equilibria between them. The examination of the $LiCl-AlCl_3-SOCl_2$ ternary system [7,8] revealed that (i) $SOCl_2$ is a weakly associated liquic (ii) Al_2Cl_6 dissolves dissociatively with the formation of a 1 : 1 adduct, $Cl_3Al\leftarrow OSCl_2$; (iii) th se adducts undergo an internal exchange reaction to form $AlCl_4^-$ and onium ion, $[Cl_2Al(\leftarrow OSCl_2)_2]^+$; and (iv) the addition of $LiCl$ breaks up the adduct and onium ion to form $AlCl_4^-$ and solvated Li^+ ion, $Li(\leftarrow OSCl_2)_2^+$.

Of interest in the analysis of the electrode/electrolyte interphase is the spectral region 925 - 1400 cm^{-1} where the $S-O$ stretching vibrations of neat $SOCl_2$, solvated Li^+ ion, adduct and onium ion occur at 1231, 1202, 1117 and 1065 cm^{-1}, respectively. Within this region, the $S-O$ vibrations, which are very sensitive to any changes in the molecular structure, are not obstructed by other absorptions [7]. A typical spectrum of the $Au/SOCl_2-AlCl_3$ interphase is shown in Fig. 1. It reveals the preferrential adsorption on the electrode surface and enrichment within the interphase of both onium ions and 1 : 1 adducts. This enrichment can be demonstrated in two ways: by using a polarized beam or by varying the spacing between the electrode and window [5]. For practical reasons, the latter has been employed. The de-convolution of the bands into Voigt profiles, shown in Fig. 1, provides additional information on the composition of the interphase. Besides the two bands due to adduct and onium ion, two additional bands appear at 1132 and 1102 cm^{-1}. These two bands, which disappear upon cathodic polarization, were tentatively assigned earlier as either (i) the symmetric and asymmetric vibrations of the adsorbed onium ion or (ii) the $S-O$ stretching vibrations of onium ion and adduct, respectively [5]. The most probable assignment is to the adsorbed onium ion. Reduction of the onium ion occurs as the initial step in the overall reduction process and may well be the only species directly reduced (*vide infra*). The disappearence of the 1132 and 1102 cm^{-1} peaks upon polarization appear to be coupled suggesting that they are derived from the same species. The shift to higher frequency indicates that adsorption is through the $S-$ atom [5].

3.1.2 *Cyclic voltammetry*. Mosier-Boss *et al* [5] postulated a set of events comprising the charge transfer process which is represented by the scheme, Eq. (I)

$$\ldots R(d) \rightarrow R(r) \rightarrow R(a) + e^- \rightarrow P_1(a) + e^- \rightarrow P_2(a) \rightarrow \ldots \qquad \text{(I)}$$

Reacting molecules, $R(d)$, are brought to the electrode surface through the reaction zone, (r), by diffusion. The adsorbed molecules, $R(a)$, undergo the charge transfer, accepting one or more electrons, yielding products $P_1(a)$, $P_2(a)$, $\cdots$. The reaction layer is formed when the product species interact with the oncoming R molecules. This layer is sandwiched between the diffusion and adsorption layers thus constructing an interphase region consisting of a number of layers populated by the interacting species. This type of system has been examined by, among others, Saveant and Vianello [13]. In such systems, the current/time dependence, $j(0,t)$, for a charge transfer process involving N electroactive species and M adsorption processes, is given by Eq. (1).

$$j(0,t) = F\left[\sum_{n=1}^{N} z_n D_n \frac{\partial c_n}{\partial x} + \sum_{m=1}^{M} \Gamma_m \frac{d\theta_m}{dt}\right] \qquad (1)$$

The right hand side of Eq. (1) accounts for contributions due to diffusional flux *via* the sum of concentration gradients and the kinetics of adsorption, expressed in terms of the change in the surface concentration summed over the number of adsorption processes. The concentration gradient(s) of the electroactive species is obtained from the mass balance equation, Eq. (2)

$$\frac{\partial c_n}{\partial t} = D_n \frac{\partial^2 c_n}{\partial x^2} - f_n(\xi,\lambda) \qquad (2)$$

which is solved subject to boundary conditions reflecting the experimental constraints. The function, $f_n(\xi,\lambda)$, is formulated for a specific set of events occurring within the interphase in the course of charge transfer. In particular, ξ refers to thermodynamic aspects, *e.g.*, equilibria between species populating the interphase, while λ contains information on the rate of relevant processes, including the forcing perturbation, *e.g.*, potential scan rate. An example of the effect of kinetic factors on the voltammogram is illustrated in Fig. 2. In particular, a change in the forcing function, through the $\lambda-$

parameter, affects the reducing current of the voltammogram more than its oxidizing current. Mass transport controlled features of the interphase response to potential perturbation, *e.g.*, autocatalysis, adsorption and desorption, are more sharply defined at lower scan rates.

3.1.3 *Galvanostatic pulsing*. Additional information can be extracted by changing the nature of the forcing function, $f_n(\xi,\lambda)$. For a class of electrode processes where adsorbed species dominate, the electrode potential can be written in a general form, Eq. (3)

$$E = E(\theta_1, \theta_2, \ldots; j) \tag{3}$$

and its time dependence can be obtained by formal differentiation which, for a galvanostatic pulse, yields Eq. (4)

$$\frac{dE}{dt} = \sum_n \frac{\partial E}{\partial \theta_l}\Big|_{j,n\neq l} \frac{d\theta_l}{dt} \tag{4}$$

Equation (4) indicates that, for $n > 1$, only rarely should a constant potential be observed during charge transfer because of the accumulation of adsorbed species. It is of interest to note, however, that Eq. (4) applies also on interruption of current; it follows, therefore, that qualitative information concerning the number of adsorbed species and the relative magnitude of the respective rate constants may be inferred from the examination of $E(t)$ measured across the relaxing interphase. An example of the electrode potential response to a 0.0011 $A\ cm^{-2}$ galvanostatic pulse and the return to rest potential is shown in Fig. 3. The changing conditions on the electrode surface are clearly displayed.

3.2 *Reaction path*.

Most recently, Mosier-Boss *et al* [12] examined the IR - spectra and linear scan voltammetry in greater detail. The rather crude formulation of the reaction scheme, Eq. (I), was refined to include additional activities, *viz.* desorption processes and catalytic events, illustrated in Fig. 4. In Fig. 4, A_0, A_1 and A_2^+ refer to neat $SOCl_2$, 1:1 adduct and onium ion, respectively. The reformulated

reaction scheme shows clearly the interplay between the thermodynamic and kinetic aspects of the $SOCl_2$ reduction on the electrode surface. This representation also aids in the interpretation of experimental data, especially when such data are obtained under transient conditions. The effect of the electrode material will enter through the kinetically controlled part of the overall process, denoted as the $\lambda-$ region and, only peripherally involving thermodynamic considerations contained within the $\xi-$ region. Thus, the effect of electrode material will appear as a change in the rate constant of the processes in the adsorbed state.

3.2.1 *IR −spectra : species present*. Determination of the effect of electrode materials on the reduction of $SOCl_2-$ bearing species by the potential perturbation technique requires that the reaction path remains unchanged. The constancy of the reaction path is manifested by identical species populating the electrode/electrolyte interphase, *i.e.*, irrespective of the electrode material. To ascertain this, the spectral region 925 - 1400 cm^{-1} was examined by in-situ IR- spectroscopy for each electrode material.

Figures 5a to 5d show this region reflected from the $Au-$, $Pt-$, $n-Si-$ and $C-$ *glassy* surfaces at rest potential (dashed lines) and while cathodically polarized (solid lines). The general similarity of the spectra show that the species present at and near the surface are the same for each of the electrode materials which, in turn, indicates that the reduction path is the same for each surface. The concentration of reactant(s) and product(s) within the interphase, however, depends on the electrode material because adsorption phenomena are highly specific. We have previously shown that at low overpotentials the primary effect is a potential dependent shift in the equilibria between the $SOCl_2-$ bearing species (*e.g.*, onium ion and adduct) occurring within the confines of the interphase region. A further increase in overpotential commences the reduction and produces new peaks in the infrared spectrum at 1331, and *ca* 1150 cm^{-1} due to the formation of SO_2, and at 1190 and 1170 cm^{-1}, assigned to an as yet, unidentified, intermediate species containing $S-O$ bond(s).

Concurrently, there is a decrease in the concentration of the 1 : 1 adduct, as well as the onium ion. It cannot be determined from the IR spectroscopy whether both the onium ion and 1 : 1 adduct are reduced simultaneously or whether only onium ion participates in the charge transfer process. The chemical equilibrium between onium ion and the 1 : 1 adduct always causes their concentrations to vary proportionally. Additional experiments are underway to resolve this ambiguity.

3.2.2 *Linear scan voltammetry : rate constants*. Equations (1) and (2) indicate that certain conditions must be met to show the effect of electrode material: one is the specified scan rate, as illustrated in Fig. 2, the other is the composition of the bulk phase, Figs. 6a and 6b. It is seen that the change in the composition *e.g.*, by addition of iron phthalocyanine or an increase in $AlCl_3$ concentration substantially changes the shape of the voltammograms.

Earlier [5], we concluded that the electroreduction of $SOCl_2$ is a two-electron transfer in which the first one, Eq. (II), is irreversible and the second, Eq. (III), is quasi-reversible

$$A^+_2 + e^- \rightarrow P_1 \qquad \text{(II)}$$

$$P_1 + e^- \rightarrow P_2 \qquad \text{(III)}$$

P_1 and P_2 are intermediate species which desorb from the electrode surface into the reaction layer where they react with other species to form the products of electroreduction Cl^- , S , SO_2. The charge transfer reactions, Eqs. (II) and (III), can be cast into corresponding rate equations. To illustrate, the rate of the charge transfer involving the first electron, Eq. (II), neglecting diffusion, is

$$\Gamma_m \frac{d\theta_1}{dt} = k_a c_{A^+_2}(1 - \Sigma\theta_i)F - k_d\theta_1 - k^{(1)}\theta_1 \exp(\alpha F \eta_1/RT) - k^{(c)}\theta_1\theta_3 \qquad (5)$$

where

$$\eta = E - E_{rev} \ ;$$

similar statements for the time change in other adsorbed species can be likewise written. The rate

constants and $\theta's$ are defined in Fig. 4. The right hand side contains the rate constants k_a , $k^{(1)}$, $k^{(c)}$ and k_d for the adsorption, electron transfer, autocatalysis and desorption processes. Equation (5) then accounts for the various processes experienced by the reacting molecules as they traverse the interphase, cf. Fig. 4 for notation. Depending on conditions of concentration, applied potential and surface coverage, the relative importance of the terms in Eq. (5) will change.

It is known [13] that, for a given set of experimental constraints, the linear scan voltammetry delineates regimes of the dominance of specific processes. In the present case, constraints applied in Fig. 2 produced a balanced set, *i.e.*, where no single process dominates the voltammogram. The first electron appears in the lsv as a current plateau, suggesting the presence of a coupled chemical reaction either preceeding or paralleling the charge transfer process. This is, of course, consistent with our observation of the equilibrium between onium ion and 1 : 1 adduct [7]. Thus the first electron transfer appears to involve the reduction of the onium ion with a corresponding reformation from the 1 : 1 adduct (as depicted in the left hand portion of Fig. 4). Changing the composition of the electrolyte phase by either the addition of a small amount of $Fe-Pc$, (*e.g.*, 2 $mg\ cm^{-3}$), Fig. 6a, or by increasing the $AlCl_3$ concentration, Fig. 6b, substantially alters the shape of the voltammogram, *vide supra* , Fig. 2. In the first case, as we increase the concentration of $AlCl_3$, and thus, the concentration of onium ions, an autocatalytic effect, manifested by a cross-over behavior, is observed. Moreover, since the cross-over point occurs at the juncture between the plateau and the cathodic peak at all scan rates, the species being regenerated on the electrode surface, *via* Eq. (IV), is P_1.

$$P_2 + A^+_2 \rightarrow 2\ P_1 \qquad \text{(IV)}$$

Addition of $Fe-Pc$, to the electrolyte solution produces a voltammogram indicative of a catalytic effect [14,15]. The catalysis masks contributions due to strongly adsorbed species, the coupled chemical equilibrium and the charge transfer. In terms of the reaction path illustrated in Fig. 4, the addi-

tion of $AlCl_3$ has no effect on any rate constant – the autocatalytic effect enters through an increase in the concentration of $A^+_2(a)$ while in the second case ($Fe-Pc$ addition), the $k^{(1)}$ is faster for the $Pt/SOCl_2-(Fe-Pc)$ than for $Pt/SOCl_2$. This is not the only effect, however: the less prominent anodic peak due to the re-oxidation of $P_2 \rightarrow P_1$, means that the rate constant, $k^{(c)}_{Fe-Pc}$, is increased in the presence of dissolved $Fe-Pc$.

The effect of the electrode material on the rate constants is illustrated in Figs. 7a to 7c. In particular, Fig. 7a shows the effect of surface modification of the $Pt-$ electrode by a chemisorbed $Fe-Pc$. Comparison of voltammograms in Figs. 2 and 7a shows a significant increase in the rate of the charge transfer associated with the first electron, *i.e.*, $k^{(1)}_{Pt(Fe-Pc)} > k^{(1)}_{Pt}$ and a similarly notable reduction in the second peak can be interpreted as an increase in the $k^{(c)}-$ value. It is unlikely that any of the features of the cyclic voltammograms is due to the reduction of the central metal ion of $Fe-Pc$. No such waves were observed in Fig. 6a nor has any such process been observed by Melendres [18,19]. The voltammogram on $Au-$ surface, Fig. 7b, shows a substantial increase in the $k^{(1)}-$ rate constant compared to Pt, Fig. 2, thus obscurring the contributions due to adsorption. On a glassy C surface, Fig. 7c, we note a substantial auto-catalytic effect only. The auto-catalytic effects are associated with the process described by Eq. (IV) coupled with relevant equilibria.

3.2.3 *Relaxation of interphase : accumulation of adsorbed species*. An interpretation of the potential decay curves in terms of Eq. (4) involves the evaluation of both $\partial E/\partial\theta$ and $d\theta/dt$. Invoking Faraday law only, *i.e.*, neglecting the mass transport term in Eq. (1), we have $d\theta_l/dt = j_{f,l}/F\Gamma_{m,l}$ which, upon substitution into Eq. (4), yields Eq. (6)

$$\frac{dE}{dt} = \sum_n \frac{\partial E}{\partial \theta_l}\Big|_{j,l\neq n} \left(\frac{j_{f,l}}{F\Gamma_{m,l}}\right) \tag{6}$$

On the other hand [18], a general expression for the electrode response to, *e.g.*, pulse current, j_{ex}, is

$$C\frac{dE}{dt} = j_{ex} - \sum_n j_{f,n} \tag{7}$$

By comparing Eqs. (6) and (7), we have $\frac{\partial E}{\partial \theta} = -\frac{F\Gamma_m}{C}$. Thus, as a first approximation we take $\partial E/\partial\theta = const$ and examine changes in the $E(t)-$ curves in terms of partial faradaic currents, *i.e.*, we attempt to assign the observed change in the mode of interphase relaxation to a particular process.

The potential/time behavior of the electrode response to galvanostatic pulse and during its return to the rest potential, shown in Fig. 3, is in general agreement with the reaction path in Fig. 4, *vide infra*. (The low concentration of $LiCl$ present in the electrolyte did not significantly alter the shape of the curves.) In what follows, results of two sets of experiments are presented, *viz.*, the effect of pulse current density and the effect of pulse length on the shape of the $E(t)$ curves are examined. As an example, we have selected the $Pt/\ldots$ system to illustrate the effect of pulse strength, Fig. 8, and the $C-glassy\ /\ldots$ to display the change in electrode potential upon a return to the initial state, following varying pulse length, Fig. 9.

The development of characteristic features of the $E(t)$ decay curves with either pulse strength or its duration, indicates the accumulation of reaction products within the interphase. This accumulation becomes clearly evident as more charge is forced across the interphase. Qualitatively, the more charge that crosses the interphase, the more pronounced the complexity of the potential decay curve. For a small amount of charge transferred (*i.e.*, short pulsing time or low pulse current), the $E(t)$ curve is almost exponential, as could be expected from integration of Eq. (4) for one process determining the electrode potential which would yield Eq. (8)

$$e^{\frac{(E_0 - E)}{b}} = 1 + \frac{j(0)t}{bC}\ ;\ b = RT/F \tag{8}$$

At a somewhat longer current pulse, the potential decay curve develops an inflection and can be

approximated by two exponential decays. With further increase in the pulse duration, the inflection point becomes a straight line with its slope and length proportional to the pulse duration. In general, the number of exponential decays observed in the potential relaxation curve reflects the number of adsorbed species [19]. The shape of these decay curves is determined by the potential determining processes while the rate of the accumulation of reaction products is the result of the magnitude of rate constants of the partial processes illustrated in Fig. 4. Thus, it is expected that, for the same pulse duration, the degree of accumulation will depend on the electrode material. For example, with the passage of time at both Pt and $C-glassy$, a composition of the interphase is reached such that three exponentially decaying segments can be seen. This is indicative of three adsorbed species being present, *viz.*, A^{+}_{2}, P_1 and P_2. On the other hand, for the relaxing $Au/SOCl_2-AlCl_3$ or the $Pt/SOCl_2-AlCl_3(Fe-Pc)$ interphases only one exponential decay, characteristic of a strong catalytic effect, is observed.

5.0 Closing Remarks

The complexity of the reaction path, Eq. (I) or Fig. 4, indicates that the material employed in the construction of the positive electrode might affect the performance of a discharging $Li/SOCl_2$ cell. The primary reason for such a conclusion is the presence of adsorbed species whose adsorption - desorption rates, as well as catalytic activities, depend on the electrode material. The experimental approach involved the identification of adsorbed species by IR- reflectance spectroscopy of an electrode-electrolyte interphase at rest and when cathodically polarized. Examination of the 925 - 1400 cm^{-1} spectral region revealed that the surface concentrations of adsorbent molecules, but not their chemical nature, were affected by the electrode material. This is, of course, an expected result because of the specificity of adsorption.

The shape of linear scan voltammetry is determined solely by the mass balance equation, Eq. (2),

through the forcing function $f_n(\xi,\lambda)$ with ξ reflecting the thermodynamics and λ the kinetics of the system. The examination of the voltammogram shape as a function of electrode material, for an *a priori* selected set of experimental conditions, led to the following relations, Eqs. (9) and (10)

$$k^{(1)}_{Au} > k^{(1)}_{Pt(Fe-Pc)} > k^{(1)}_{C} \tag{9}$$

$$k^{(c)}_{Au} > k^{(c)}_{C} > k^{(c)}_{Pt} \tag{10}$$

This series in rate constants is further supported by the potential decay across the relaxing electrode/electrolyte interphases.

Acknowledgement

This work was, in part, supported by the Office of Naval Research, Arlington, VA.

References

1. K. C. Tsaur and R. Pollard, J. Electrochem. Soc., 133, 2296 (1986)

2. J. J. Smith, S. Szpak and W. A. West, in **Power Sources 11**, L. J. Pearce, ed., International Power Sources Symposium, Brighton UK, 1987

3. R. J. Nowak, D. R. Rolison, J. J. Smith and S. Szpak, Electrochim. Acta, **33**, 1313 (1988)

4. M. J. Madou, J. J. Smith and S. Szpak, J. Electrochem. Soc., **134**, 2794 (1987)

5. P. A. Mosier-Boss, S. Szpak, J. J. Smith and R. J. Nowak, ibid., **134**, 2455 (1989)

6. S. Szpak, Experimental Simulation of Porous Electrodes, in **Techniques for Characterization of Electrodes and Electrochemical Processes**, R. Varma and J. R. Selman, eds., John Wiley and Sons, (to be published in Fall 1989)

7. P. A. Mosier-Boss, R. D. Boss, C. J. Gabriel, S. Szpak, J. J. Smith and R. J. Nowak, J. Chem. Soc. Faraday Trans. I,85, 11 (1989)

8. P. A. Mosier-Boss, S. Szpak, J. J. Smith and R. J. Nowak, J. Electrochem. Soc.,136, 1282 (1989) ;

9. J. K. Foley and S. Pons, Anal. Chem., 57., 945A (1985)

10. P. van Rysselberghe, **Thermodynamics of Irreversible Processes**, Hermann, Paris 1963

11. K. Ashley and S. Pons, Chem. Rev., **88**, 673 (1988)

12. P. A. Mosier-Boss, S. Szpak, J. J. Smith and R.J. Nowak, Exteded Abstract Nr 345, Electrochemical Society Spring Meeting, Los Angeles, CA, 1989

13. J. M. Saveant and E. Vianello, Electrochim. Acta, **12**, 629 (1967)

14. R. S. Nicholson and I. Shain, Anal. Chem., **36**, 706 (1964)

15. R. H. Wopschall and I. Shain, ibid., **39**, 1514 (1967)

16. C. A. Melendres and F. A. Cafasso, J. Electrochem. Soc., **128**, 755 (1981)

17. C. A. Melendres, C. B. Rios, X. Feng and R. McMasters, J. Phys. Chem., **87**, 3526 (1983)

18. P. C. Milner, J. Electrochem. Soc., 107 343 (1960)

19. B. E. Conway and M. Dzieciuch, Can. J. Chem.,**41**, 21, 38, 55 (1963)

Figure Captions

Fig. 1. The 940 to 1350 cm^{-1} IR- spectral region (system: $Au/SOCl_2-AlCl_3$)

1a. - Effect of cell path length : upper - 5 μm, lower - 10 μm

$S-O$ stretching vibrations: A - in onium ion at 1065 cm^{-1}; B - in 1 : 1 complex at 1117 cm^{-1}; C - in neat $SOCl_2$ at 1228 cm^{-1}

1b - decomposition of A and B bands into Voigt profiles: A' and B' for species in bulk solution; A" and B" for adsorbed species at 1065, 1117, 1133 and 1102, respectively.

Fig. 2. Effect of scan rate on voltammogram shape

System: $Pt/SOCl_2-3.0M\ AlCl_3$; solid line - $v = 10\ mV\ s^{-1}$; dashed - 5 $mV\ s^{-1}$

Fig. 3. Potential/time behavior across charging and relaxing interphase

System: $Pt/SOCl_2-3.0M\ AlCl_3-0.1M\ LiCl$; pulse current 0.0011 $A\ cm^{-2}$

Fig. 4. Summary of $SOCl_2$ reduction path

System: $AlCl_3-SOCl_2$; processes affecting the ξ and λ components of the forcing function $f_n(\xi,\lambda)$ indicated. Rate constants identified.

Fig. 5. Effect of applied potential and electrode material on IR- reflectance spectrum.

Spectral region : 925 - 1400 cm^{-1}; system - $Me/3.0M\ AlCl_3-SOCl_2$; a -, b -, c -, and d - reflected from Au , Pt, Si, $C-glassy$,- electrode surface, respectively. Dashed line - elecrtode at rest potential; solid line - polarized to -2.5 V (Au), -3.5 V (Pt), -3.0 V (Si) and -2.0 V ($C-glassy$). Bands A, B and C refer to onium ion, 1:1 complex and neat $SOCl_2$ in the bulk solution, respectively.

Fig. 6. Effect of solution composition on linear scan voltammogram

System : $Pt/SOCl_2-AlCl_3$; scan rate - 10 mVs^{-1}

a - 3. 0 M $AlCl_3$ *in* $SOCl_2$ with added 2.0 $mg\ cm^{-3}$ $Fe-Pc$; b - 4.0 M $AlCl_3$ *in* $SOCl_2$

Fig. 7. Effect of electrode material on linear scan voltammogram;

System : $Me/3.0MAlCl_3$ *in* $SOCl_2$; scan rate - 10 mVs^{-1}

a - Pt electrode with chemisorbed Fe-Pc; b - Au electrode; c - glassy C electrode

Fig. 8. Potential/time behavior as a function of pulse strength.

System: $glassyC/2.0MAlCl_3$

Fig. 9. Potential/time behavior as a function of pulse duration.

System: $Pt/3.0MAlCl_3$

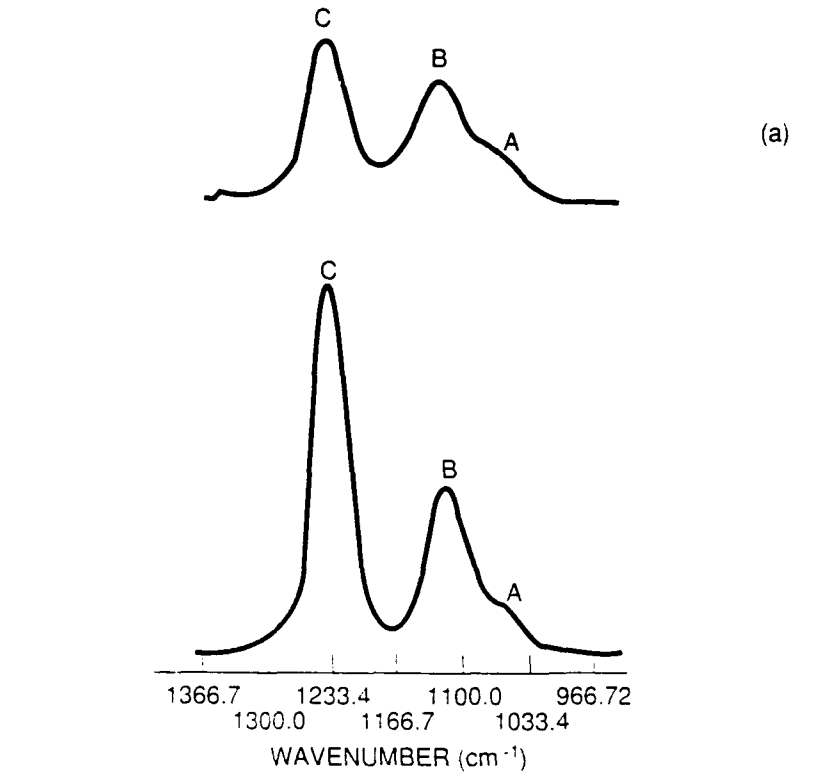
C
B
A
(a)
C
B
A
1366.7
1300.0
1233.4
1166.7
1100.0
1033.4
966.72
WAVENUMBER (cm⁻¹)

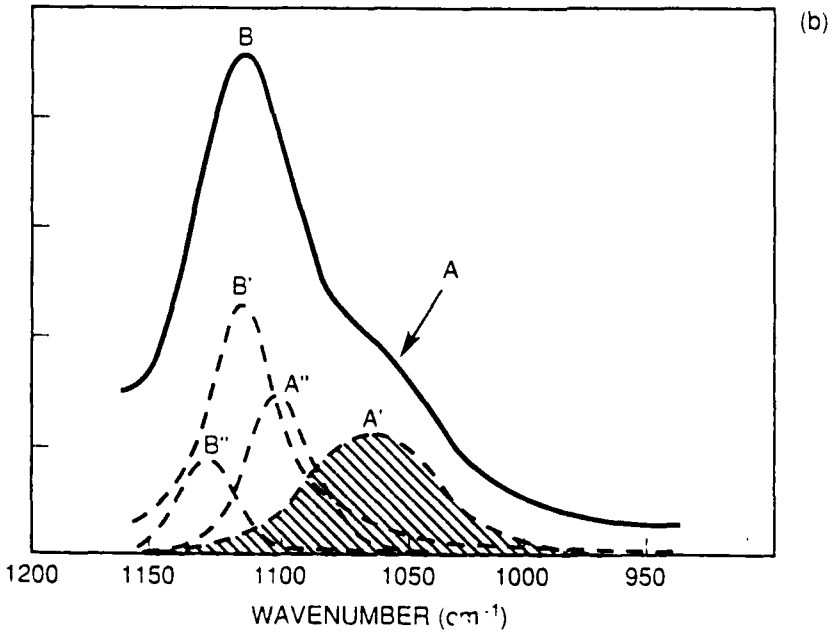
(b)
B
A
B'
A''
A'
B''
1200
1150
1100
1050
1000
950
WAVENUMBER (cm⁻¹)

Fig. 1

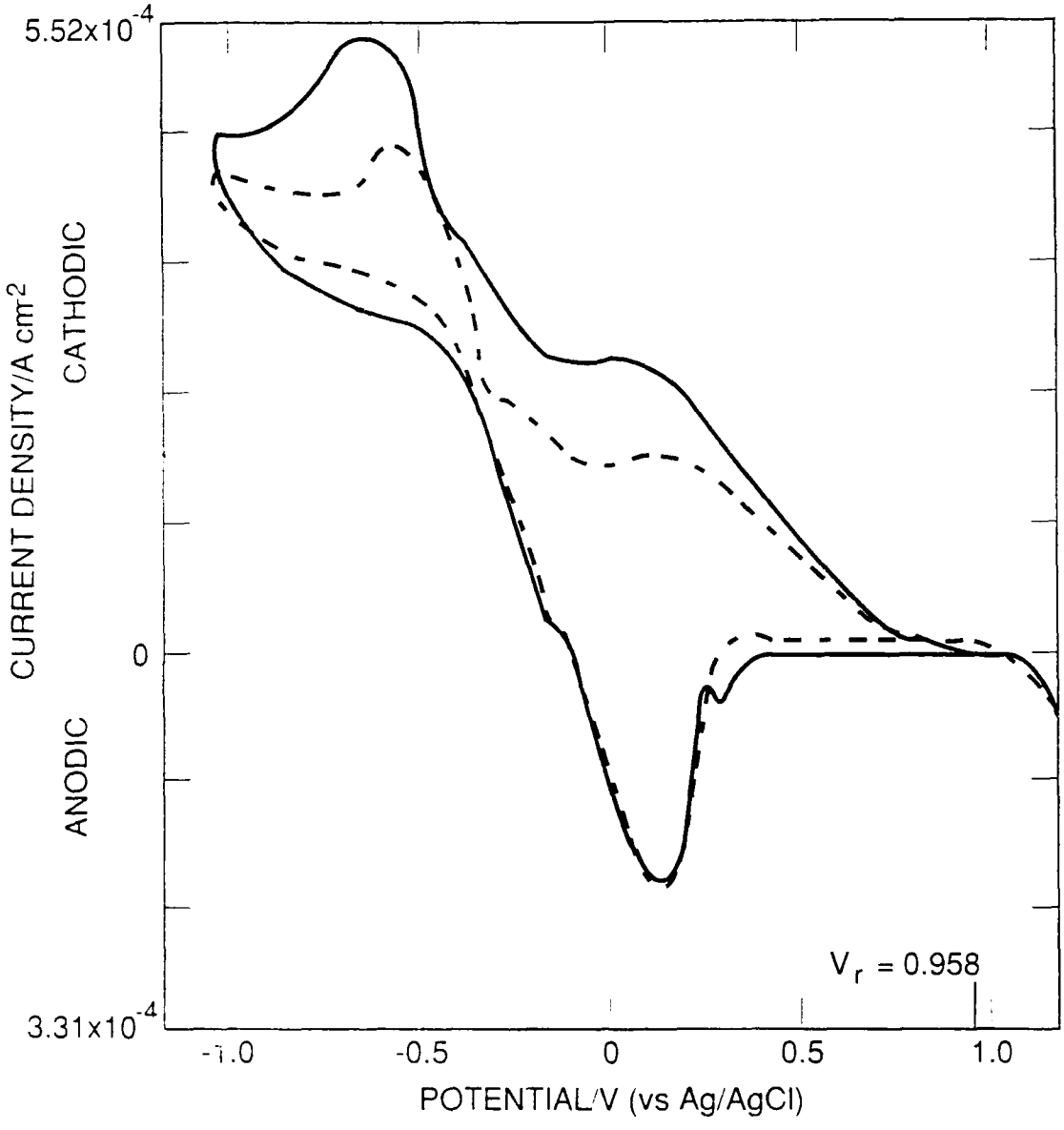
5.52x10-4
CATHODIC
CURRENT DENSITY/A cm2
0
ANODIC
3.31x10-4
Vr = 0.958
-1.0
-0.5
0
0.5
1.0
POTENTIAL/V (vs Ag/AgCl)

Fig 2

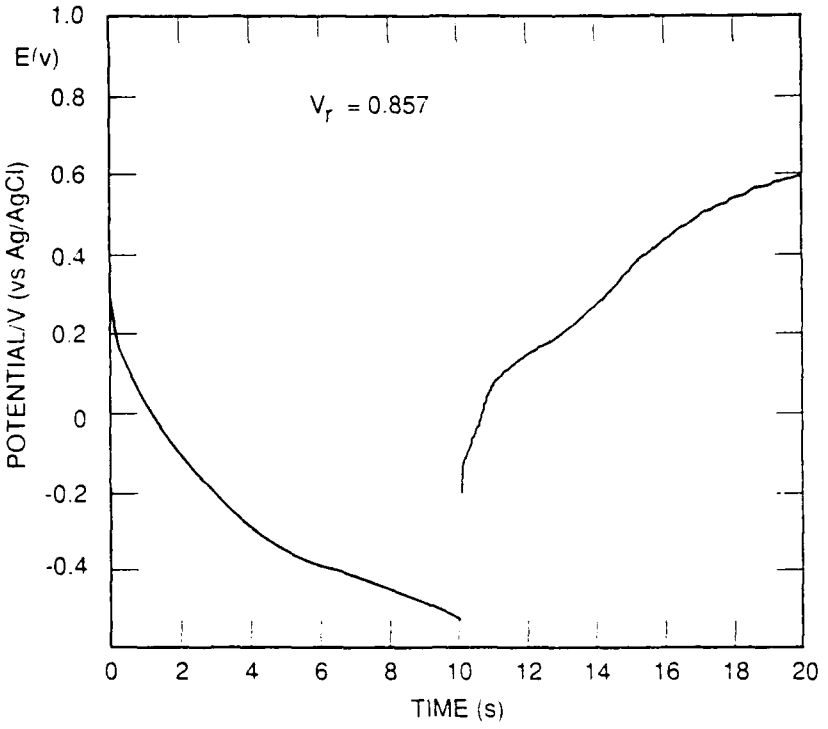
1.0
E(v)
0.8
V_r = 0.857
0.6
0.4
0.2
0
-0.2
-0.4
POTENTIAL/V (vs Ag/AgCl)
0
2
4
6
8
10
12
14
16
18
20
TIME (s)

Fig 3

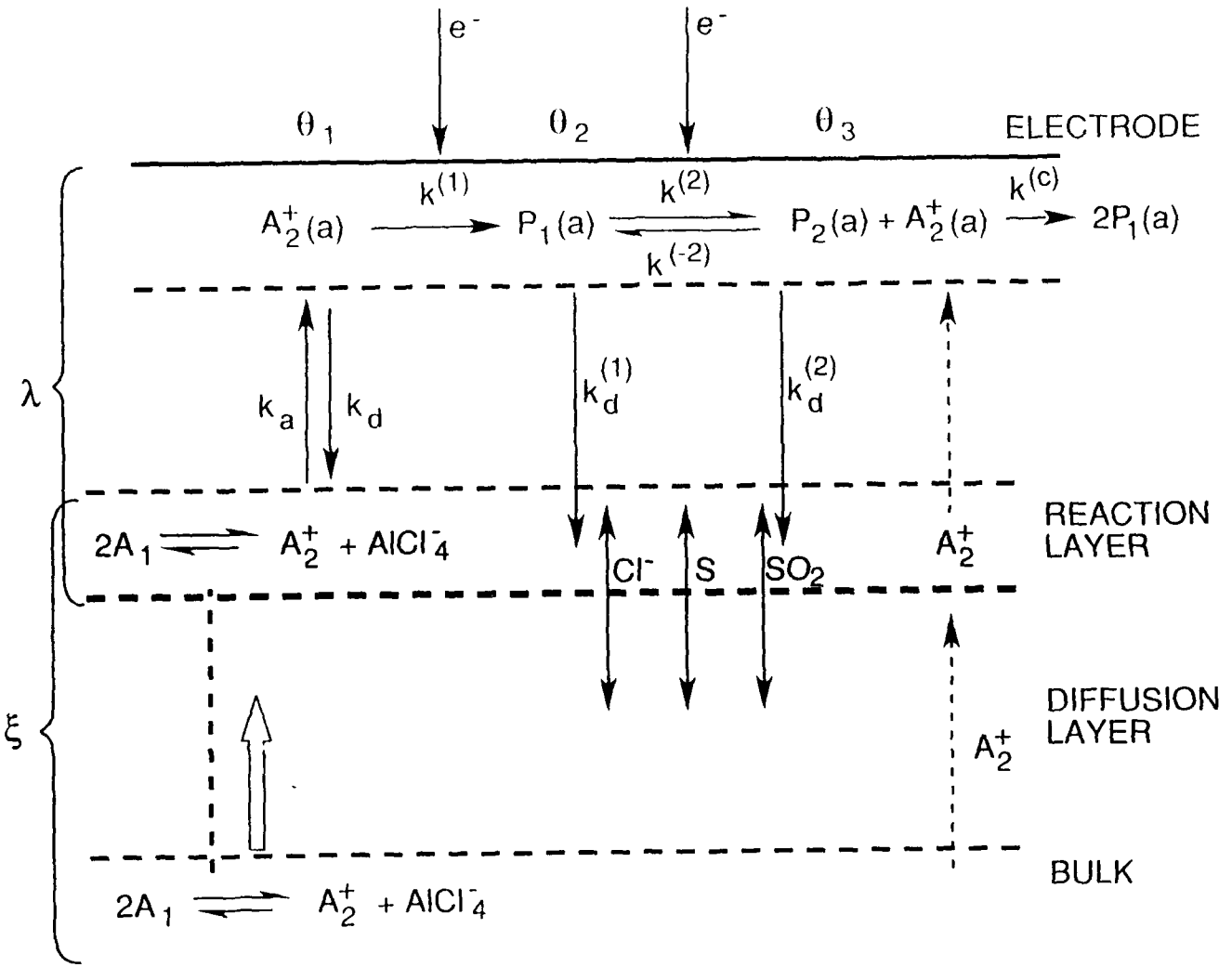
e⁻
e⁻
θ1
θ2
θ3
ELECTRODE
k(1)
k(2)
k(c)
A2+(a)
P1(a)
P2(a) + A2+(a)
2P1(a)
k(-2)
λ
ka
kd
kd(1)
kd(2)
2A1
A2+ + AlCl4-
Cl-
S
SO2
A2+
REACTION LAYER
DIFFUSION LAYER
BULK
ξ

Fig 4

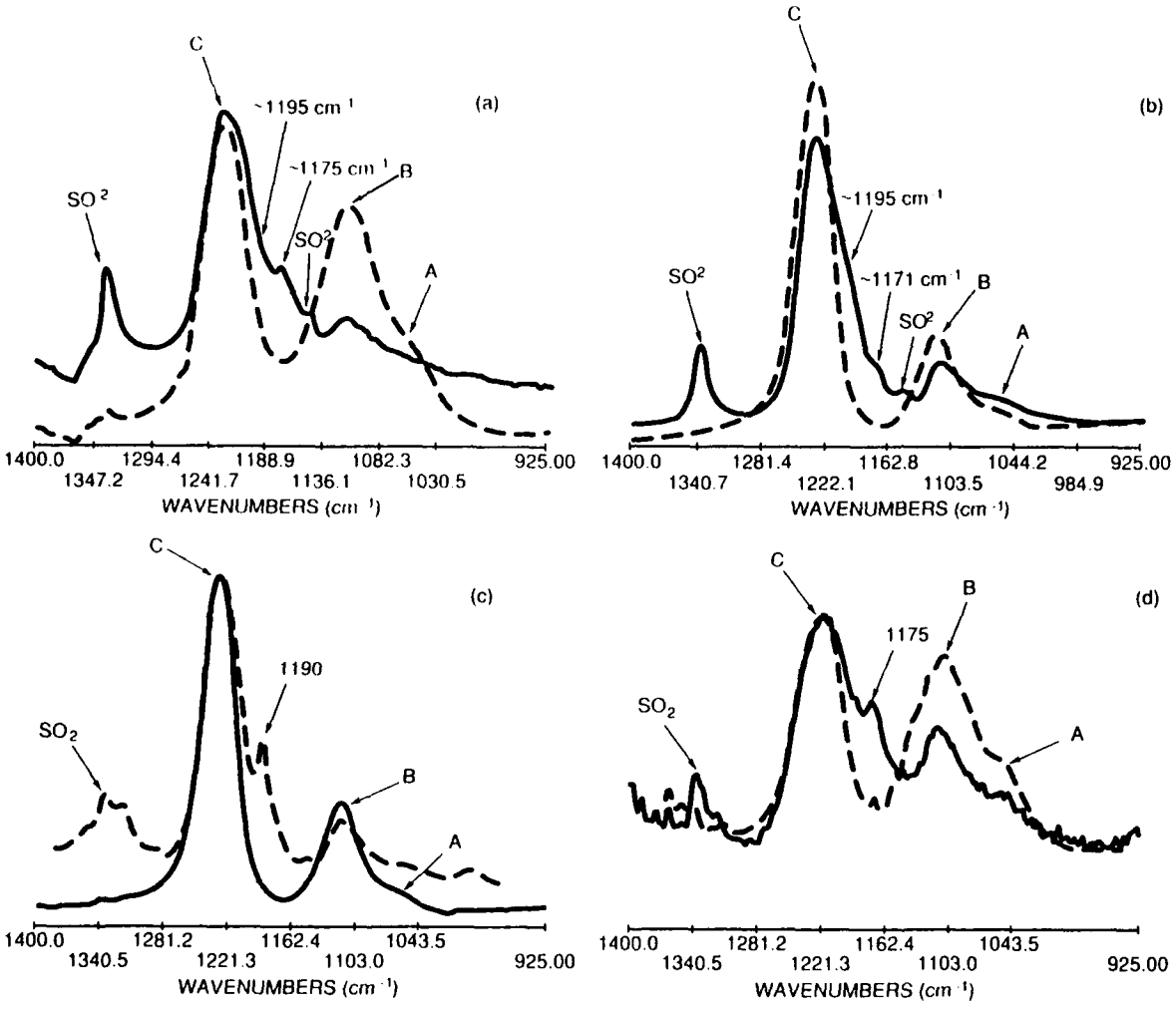
C
~1195 cm⁻¹
(a)
~1175 cm⁻¹
B
SO²
SO²
A
1400.0
1294.4
1188.9
1082.3
925.00
1347.2
1241.7
1136.1
1030.5
WAVENUMBERS (cm⁻¹)
C
(b)
~1195 cm⁻¹
SO²
~1171 cm⁻¹
B
SO²
A
1400.0
1281.4
1162.8
1044.2
925.00
1340.7
1222.1
1103.5
984.9
WAVENUMBERS (cm⁻¹)
C
(c)
1190
SO₂
B
A
1400.0
1281.2
1162.4
1043.5
925.00
1340.5
1221.3
1103.0
WAVENUMBERS (cm⁻¹)
C
B
(d)
1175
SO₂
A
1400.0
1281.2
1162.4
1043.5
925.00
1340.5
1221.3
1103.0
WAVENUMBERS (cm⁻¹)

Fig 5

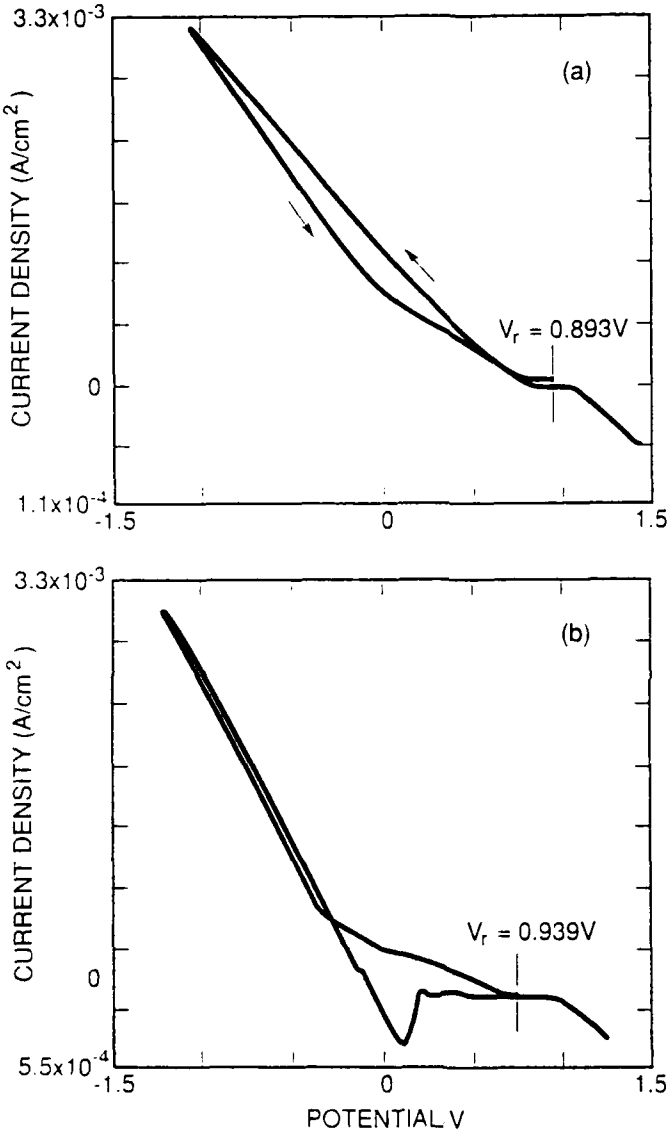
3.3x10-3
(a)
CURRENT DENSITY (A/cm2)
Vr = 0.893V
0
1.1x10-4
-1.5
0
1.5
3.3x10-3
(b)
CURRENT DENSITY (A/cm2)
Vr = 0.939V
0
5.5x10-4
-1.5
0
1.5
POTENTIAL V

Fig 6

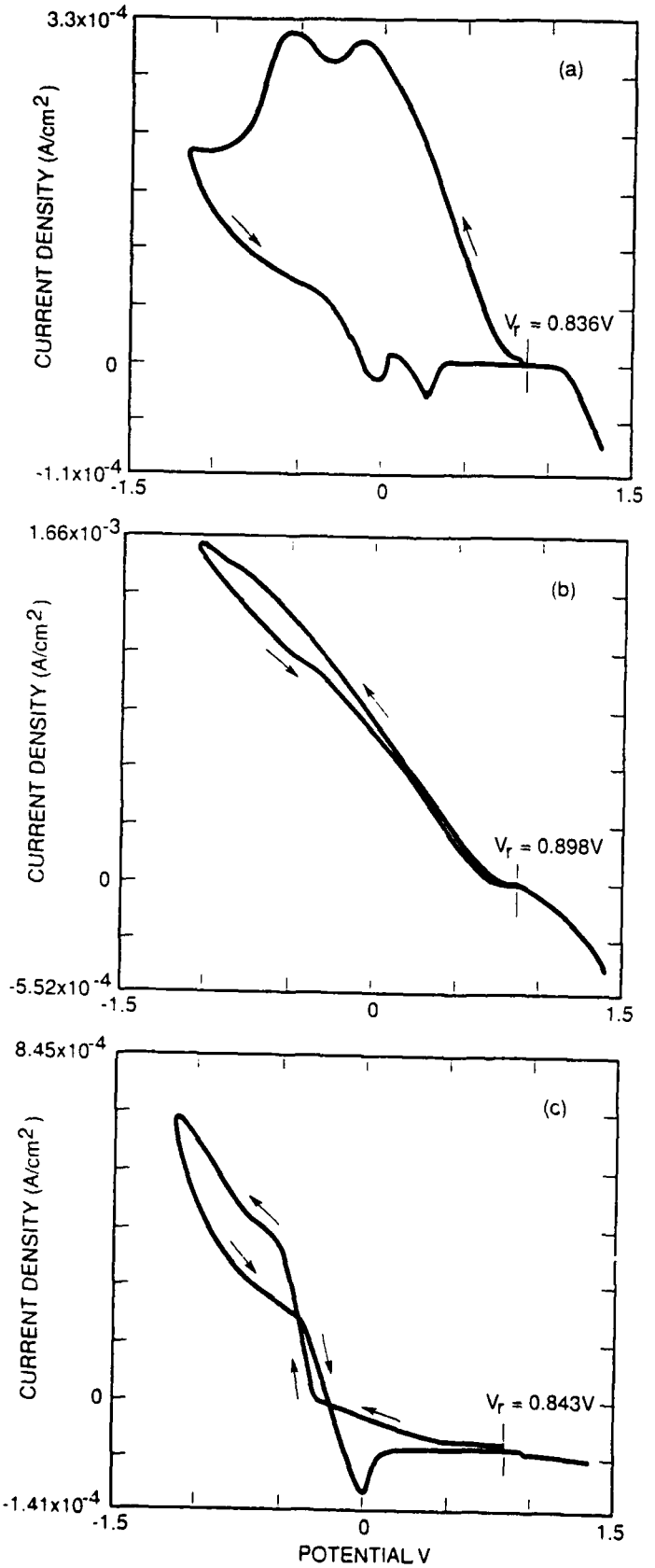
3.3x10-4
(a)
CURRENT DENSITY (A/cm2)
Vr = 0.836V
0
-1.1x10-4
-1.5
0
1.5
1.66x10-3
(b)
CURRENT DENSITY (A/cm2)
Vr = 0.898V
0
-5.52x10-4
-1.5
0
1.5
8.45x10-4
(c)
CURRENT DENSITY (A/cm2)
Vr = 0.843V
0
-1.41x10-4
-1.5
0
1.5
POTENTIAL V

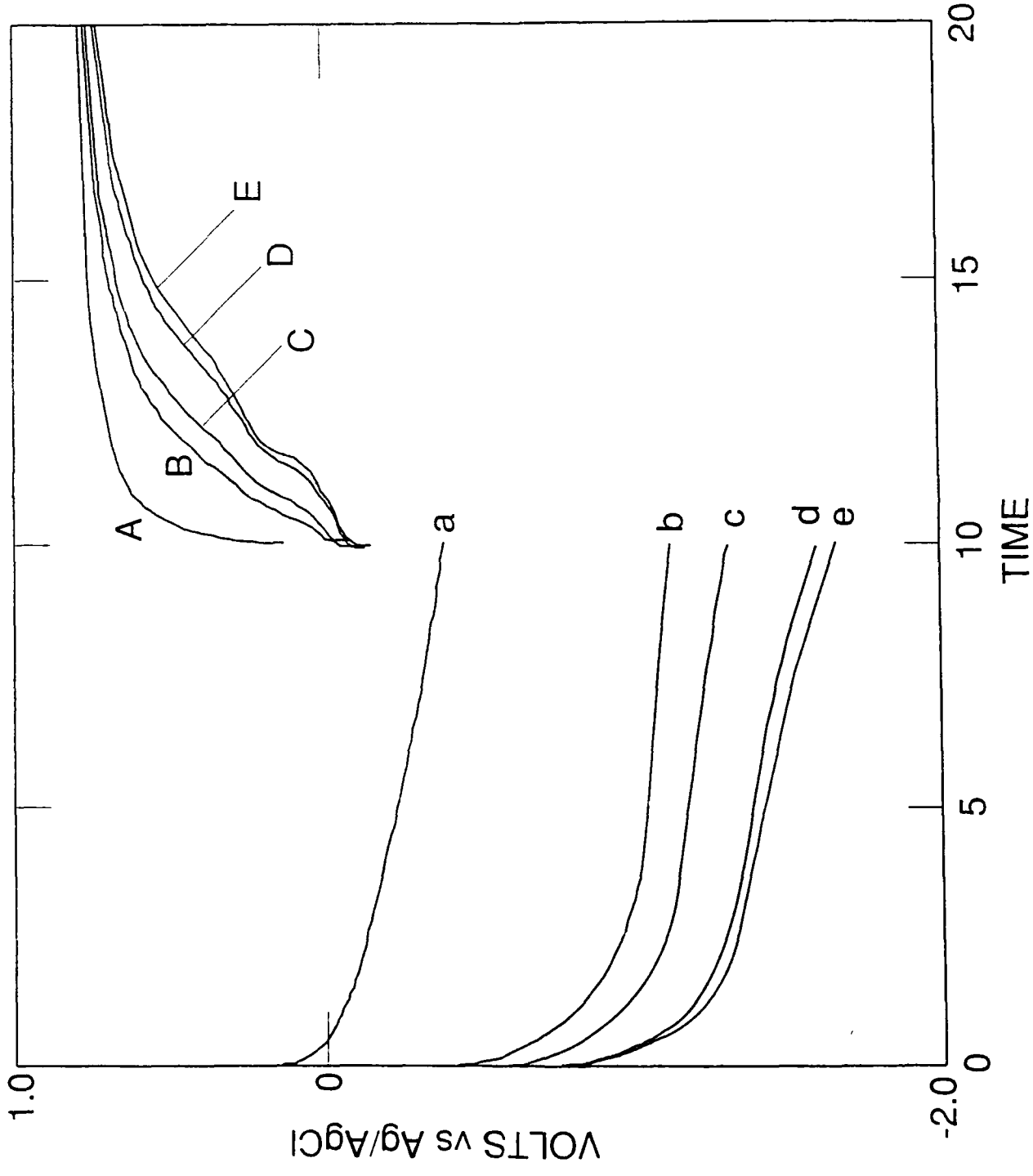

Fig 8

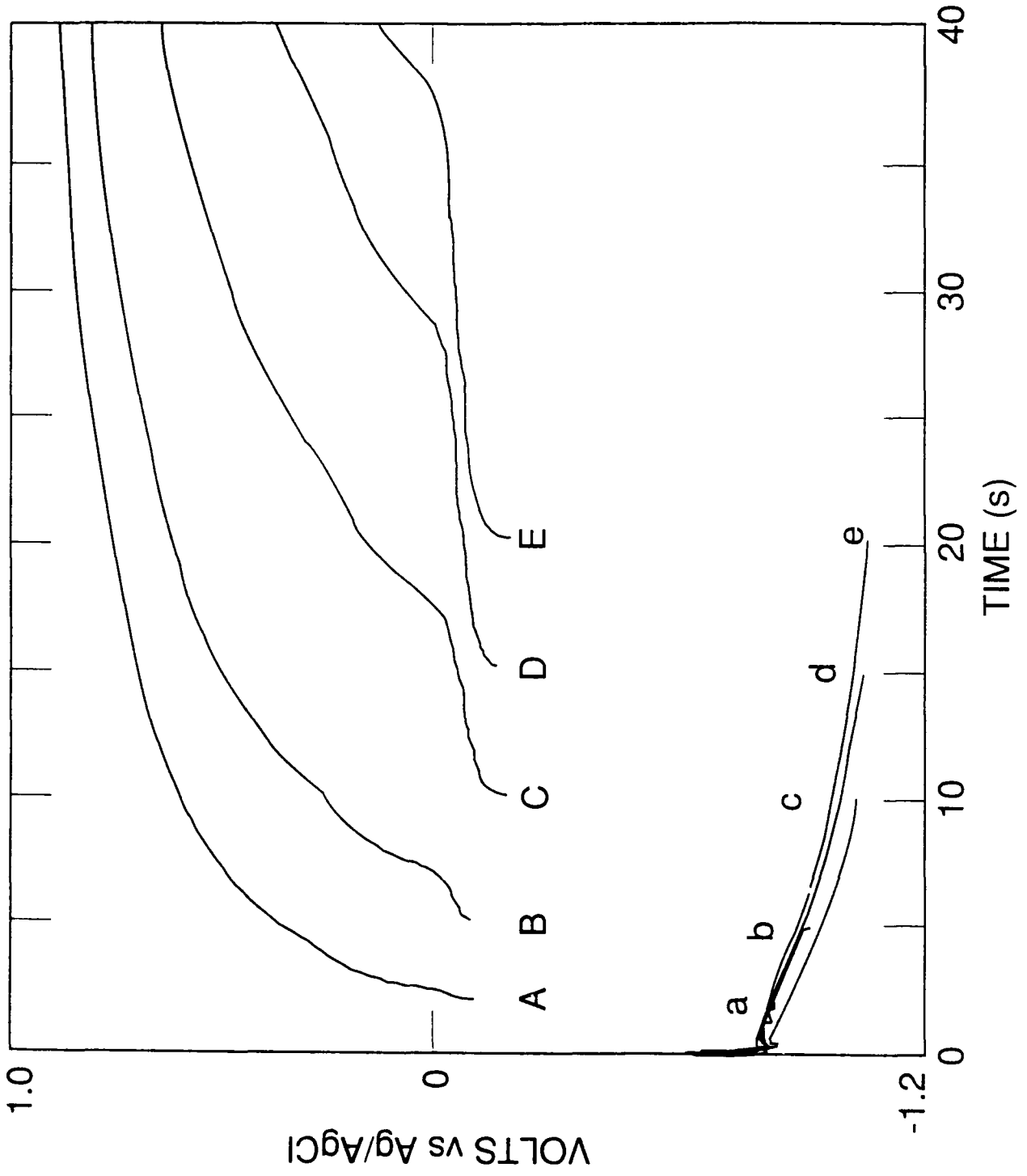
VOLTS vs Ag/AgCl
1.0
0
-1.2
0
10
20
30
40
TIME (s)
A
B
C
D
E
a
b
c
d
e

INTERCELL CURRENTS IN ASSEMBLY OF MODULES: QUALITY CONTROL CONSIDERATIONS

C. J. Gabriel, P. A. Mosier-Boss, S. Szpak

Naval Ocean Systems Center, San Diego CA 92152-5000

and

J. J. Smith

Department of Energy, Washington DC 20545

Quality control considerations in battery fabrication with regard to intercell currents in an assembly of modules is examined. The effects on battery performance of a statistical distribution in the parameters of the porous cathode structure as well as unequal compression/expansion of the module and unequal number of cells in modules are investigated. The discharge performance of modules with defective cells is also considered. Modeling methods are general, however, the examples used to illustrate pertain to the $Li/SOCl_2$ system.

1.0 Introduction

The efficient operation of equipment designed for electrochemical processing, including energy conversion devices, often requires the installation of a common electrolytic path. There are numerous advantages associated with this approach, *viz.*, bipolar cell construction, controlled supply of reactants and removal of products as well as a reliable means of thermal management. These advantages, however, are partially off-set by the parasitic shunting action of the intercell currents. In practice, these currents not only reduce the power output but often affect the structural integrity of

battery functional elements(1).

In a previous communication (2), we concluded that in well designed modules, connected electrically in parallel and hydraulically in series, an increase in their number does not inherently increase the imbalance in intercell or nodal currents. However, in an assembly of modules with one or more defective cells, or with a sufficiently large variation among the cell functional elements, a situation arises which substantially reduces the battery lifetime and, on occasion, may lead to catastrophic events. In this communication, we examine, in general terms, the effect of abnormal deviation from the average value of pertinent parameters on the performance characteristics of a multi-module battery.

2.0 Battery fabrication.

Three areas require particularly close attention during the design phase of a battery. The first relates to maximizing the extractable energy for an *a priori* given power output. The second involves minimizing the time and energy required to activate the battery or the power needed to circulate the electrolyte. The third area of concern is thermal management to realize a high power output design or to maintain the integrity of cell functional elements during operation for extended periods of time.

To minimize the power losses, a low discharge current density arrangement requiring a high potential is desired. This, in turn, requires a large number of cells in each module with several of these modules connected in parallel. To maximize the extractable energy density a compact design is needed, *i.e.*, a thin cell design (3). As a rule, the amount of electroactive material, hence the cell thickness and area, is a function of the required discharge time, usually expressed as the time needed to reach an *a priori* specified cell/battery voltage. Cells, as thin as 0.044 cm, can be fabricated (4). Of course, fabricating the very thin cells places special demands on the manufacturing and

assembly process.

2.1 Fabrication sequence.

A typical fabrication sequence of a module is summarized in the form of a block diagram in Fig. 1. The cell functional elements, *e.g.*, positive and negative electrode structures, are first fabricated. Then, other components such as separators, bipolar plates, current collectors, *etc.*, are cut to size. The assembly process consists of stacking the cells and compressing the stack to the designed thickness. Finally, means for battery activation or electrolyte circulation are provided to complete the process of module assembly.

2.2 Quality control (QC) measures.

Quality control measures are closely connected with fabrication steps and the dynamics of the cell/module operation. Thus, in the course of component fabrication, not only must the amount of stored electroactive material be controlled but also the geometrical constraints of the porous structure. The control of the purity and amount of the electroactive material, presents no special problem. On the other hand, the control of geometrical constraints is a serious and, as yet, unresolved problem. Porous electrodes are usually made by sintering or by a combination of rolling and/or pressing of the particles comprising the electrodes. Thus, the fabrication of porous electrodes incurs statistically spread deviations in structural parameters such as specific surface area, porosity, tortuosity, particle and pore size. According to Dunning (6), the description of the interplay between elementary processes associated with the charge transfer and the geometry of the electrode structure requires consideration of three averages: an average over the volume of the electrolyte phase in pores, an average over the interfacial area between the electrode matrix and electrolyte and an average over the cross section exposing electrode matrix and pores.

It is not our purpose to suggest or promote any particular form of QC activities; rather to indicate the need for such activities and discuss the consequences of their absence in terms of power loss (5),

thermal management, and the integrity of functional elements. The relevant properties are indicated in Fig. 1 alongside the fabrication sequence.

3.0 Electric circuit analog.

The characteristic features of an operating electrochemical cell can be, and are often, simulated by an electric circuit analog. Examples with regard to battery technology are numerous(7).

3.1 Assumptions and definitions.

In the present discussion, we retain all of the definitions and assumptions of refs. (1) and (2). In particular: (i) an intercell current is an ionic current that originates in one cell and terminates in another; (ii) the current distribution is adequately simulated by an electric circuit analog, Fig. 2; (iii) the phenomenological coefficients associated with the ionic current are replaced by resistances; (iv) the potentials in the electrolyte phase at the entrance port to the cell, Φ_i, are uniform; (v) the bipolar plates are equipotential; (vi) the intercell current, I_i, is equal to the difference between circulating currents, *i.e.*, $I_i = J_i - J_{i-1}$; (vii) circulating currents at the coupling interfaces between modules have finite values while those at battery terminal cells are zero. The replacement of the phenomenological coefficients by the lumped resistances implies uniform current distributions on the cross sections of the associated segments.

3.2 The $\lambda-$ parameter

An analysis of the electric circuit analog, representing a single module, is given in ref. (1) while that for an assembly of modules is given in ref. (2). In both cases, it is convenient to introduce the parameter λ. This parameter depends on the battery design, the properties of the electrolyte employed and the kinetics of the charge transfer reaction(s) occurring within the confines of the porous structures of the electrodes. For the special case, where all cell parameters are uniform throughout the modules, the expression for the intercell currents can be obtained in a closed form(1),

with λ given by Eq. (1)

$$\lambda = 1 + X + \sqrt{X(2 + X)} \tag{1}$$

in which $X = (R_t + R_z)/2R_f{}'$ where $R_f{}' = R_f + R_p - R_z\sigma^2/\sigma_a\sigma_c$. Physically, the $\lambda-$ parameter indicates the ratio of intercell currents in adjacent cells, *i.e.*, I_{i+1}/I_i. In particular, for modules with large number of cells, *e.g.*, $N > 50$, $I_{i+1}/I_i = \lambda^{-1}$ as $i \rightarrow 1$, and $I_{i+1}/I_i = \lambda$ as $i \rightarrow N$. [ref. 1, Eqs. (36) and (37)]

A cursory analysis of Eq. (1) reveals that the constancy of the $\lambda-$ parameter is assured only if the devices are capable of a steady-state operation (this implies the constancy of power output and not of electrochemical processes), *e.g.*, fuel cells and electrolyzers, providing, however, that the inert structures are not modified by passivation or corrosion. In other cases, its constancy cannot be assumed. The time dependence of the $\lambda-$ parameter is specific for a given battery system and can be, at least, qualitatively assessed with the aid of the electric circuit analog, Fig. 3. Thus, the R_t can be regarded as being constant throughout the discharge period, the R_z are functions of the transferred charge and the R_p are determined by the geometry of the entrance port and the nature of the electrochemical system.

In analogy with the special case, Eq. (1), we can define the parameter ${}^{(m)}\lambda_i -$, Eq. (2)

$${}^{(m)}\lambda_i = 1 + {}^{(m)}X_i + \sqrt{{}^{(m)}X_i(2 + {}^{(m)}X_i)} \tag{2}$$

where ${}^{(m)}X_i$, is defined similarly to X (*vide supra*), except that here the parameters R_t , R_z and $R_f{}'$ are identified with the $i-$ *th* cell in the $m-$ *th* module. In contrast to the special case, Eq. (1), here, the ${}^{(m)}\lambda_i -$ parameter characterizes the time dependent behavior of groups of cells as they degrade in the course of battery discharge rather than a complete module.

As illustrated in Fig. 4a, initially the $\lambda-$ parameter is statistically uniform throughout the multi-module battery. Its numerical value ranges between 1.16 and 1.18 and the distribution among cells

reflects the statistical variation of the functional elements. However, as the battery discharges, the individual cell functional elements undergo changes principally due to the contribution of intercell currents. The groups of cells at the negative end of modules are substantially affected, as seen in Fig. 4b. It is noted that changes in the $\lambda-$ parameter and the behavior of these cells should be examined in conjunction with Figs. 5a and 5b where it is also seen that changes have occurred at the module negative end.

3.3 Quality control (QC) points.

The cell internal resistance is, first and foremost, a function of the discharge rate and duration. To analyze the time dependence it is convenient to represent the cell processes in terms of components of an electric circuit analog. The situation within a single cell is illustrated in Fig. 3. The time-dependent component is principally located within the porous structure of the positive electrode where a precipitation of the solid phase occurs, *i.e.*, in the shaded area. The rate of change of the cell internal resistance is a function of the initial porosity and the rate at which the reaction front penetrates the electrode structure. This rate, expressed here by the combination of an effective electrode separation, δ^* , and the time dependent electrolyte conductivity, in general, varies during the cell discharge in a complex way (2). We shall not dwell into this relationship only to indicate which input parameters are affected and their physical significance.

The statistical variation in R_z arising from unequal compression of individual cells is here associated with both a variation of the cell porosity, ϵ_z , and a variation of the effective cell electrode spacing, δ^*, [see Eq. (13), ref. (1) and Eq. (15), ref. (2)]. The cell porosity is derived from the distribution of random variables y, where y is chosen from the binomial distribution having a probability of success $(\epsilon_{z,n} - \epsilon_{\min})/(\epsilon_{\max} - \epsilon_{\min})$ and a number of trials N_s, according to the relationship $y/N_s = (\epsilon_z - \epsilon_{\min})/(\epsilon_{\max} - \epsilon_{\min})$. This choice produces a distribution for $\epsilon_{\min} < \epsilon_z < \epsilon_{\max}$ having a mean $\eta_\epsilon = \epsilon_{z,n}$ and a standard deviation $\sigma_\epsilon = \sqrt{(\epsilon_{z,n} - \epsilon_{\min})(\epsilon_{\max} - \epsilon_{z,n})/N_s}$. The varia-

tion of δ^* is introduced as an arbitrarily chosen percentage deviation from design point for each module. In this communication we limit the discussion to the above mentioned variation in cell impedance and the occurrence of different numbers of cells in the module of multimodule assemblies. The latter arising from an operator error, which is a rare but not unheard of, incident in assembling modules containing 100 or more cells.

The time dependent, $R_z(t)$, associated with the dynamics of the battery discharge is introduced via the rate of change of the cathode conductance, $\kappa_c(t)$, Eq. (3)

$$\kappa_c(t) = \frac{w\,\kappa\epsilon_z}{1 + (Q(t)/Q)^{\xi_c}} \tag{3}$$

with $Q(t) = \int_0^t Idt$ and $Q = w\tau NU/(MR_l + NR_{z,n})$, where w is the deficiency factor(1). Here, $Q(t)$ is the actual amount of charge transferred to the positive electrode within the time period t, while Q represents the charge that would be transferred within the battery lifetime, τ, under conditions of no parasitic current flow. The adjustable parameter, ξ_c, is related to the morphology of the solid reaction products; here, it is chosen so that the calculated module discharge characteristics approximate observed behavior. The time variation of the feed tube resistance, R_f, affects the operation of a battery and the distribution of intercell currents, but is essentially a design factor rather than a QC issue. The time dependency and statistical variation of R_f is included here in a manner reported in ref. (2)

3.4 Construction of solution.

Figure 6 shows a flowchart of the solution program used to calculate the intercell currents within an assembly of modules. First, the geometry and physical properties of the module(s) are defined. The system parameters include the number of modules (maximum of 5), the number of cells per module (maximum of 90), porosity fineness of the cathodes, cathode use factor, anode reversed current factor, and load resistance as defined in ref. (2). The cell and feed tube porosities are

assigned from the same distribution, as described in section 3.3, using a random number generator. The porosities were chosen from the range 0.3 to 0.9 corresponding to limitations imposed by heat evolution (8) and practical considerations of cell construction. In the case of deficient modules, the number, location and deficiency factor of the affected cells are defined. In these calculations, the effective electrode spacing is assumed to be the same for each cell within the module.

Once the system parameters have been established, the starting cell and feed tube conductivities are calculated and the time step loop calculations are started. Within the time loop the port input resistances are calculated, [Eq. (1), ref. (1)], and the banded matrix for each module's loop currents are set-up. The module coupling equations for the coupling currents are computed from tridiagonal sets of linear equations - one set for each module. The reversed current for each cell is then computed as is the charge transferred by the reversed current, [Eq. (23), ref. (1)]. The loop currents are used to calculate the charge transferred to each cathode. Using the charges transferred during the time increment, the new cell and feed tube conductivities are calculated, [Eq. (15), ref. (2)]. The time is advanced by the incremental amount and the time loop calculations are done from the new time.

4.0 Results and discussion.

Previously (1), we pointed out that when a module contains only a few cells, all cells contribute to the parasitic currents. However, as the number of cells in a module increases, the centrally located cells contribute less and the involvement is shifted to the terminal cells. A similar effect is expected to govern the behavior of an assembly of modules. For this reason, calculations were carried out for modules with ten (10) and fifty (50) cells and the results examined against the quality control requirements. Calculations presented here and the input data assembled in Table I pertain to the $Li/SOCl_2$ battery. For other systems, the procedure is the same; however, the relevant input data must be secured and the needed expressions formulated accordingly.

4.1 Scale-up effects

The effect of the battery size on the discharge characteristics is examined from two viewpoints: (i) the module size (*ie*, the number of cells in a module) and (ii) the battery size *ie*, the number of modules in an assembly). Well fabricated modules are assumed.

As illustrated in Fig. 7, the load current increases with an increase in the number of modules. For example, scaling-up from two 50 - cell modules to five 50- cell modules, discharged through the same external resistance, increased the load current by *ca* 10 %. This is an expected behavior since the increase in the number of modules reduces the discharge current density in the individual modules which, in turn, reduces their polarization.

Practically all battery systems employ porous structures; thus, their fabrication incurs statistically spread deviation in *e. g.*, pore size, tortuosity factor and catalytic activity. Cumulatively, this statistical variation is identified here with the porosity variation and is controlled by N_s, the fineness factor(1). The effect of the binomial distribution of the porosity described in section 3.3 on the module load currents is shown in Figs. 8 - 10. It is seen that within 85 % of the designed discharge time, each module delivers uniformly a fraction of current that is determined by the statistical aspects of the individual modules. Within the remaining 15 %, there is a clear manifestation of load sharing in which the already depleted modules deliver less current and other modules compensate by increasing their contribution as evidenced by a a cross-over of the load currents. This load sharing presents no problems if the modules contain a large number of cells. If fewer cells comprise a module, local heating may occur toward the end of discharge, as indicated by the shaded area in Fig. 10 d. Examining Figs. 9 and 10, we note that, for modules having a large number of cells, the effect of the fineness factor on the load distribution is minimal. For an assembly of modules with only a few cells, the effect is more pronounced.

4.2 Effect of variation in module compression/expansion

A typical assembly sequence is as follows: the individual cells are stacked with due attention to alignment. When a predetermined number of cells are in place, then the module is compressed to the desired thickness. In one procedure, a variation of 4% in either compression or expansion is acceptable (4). From the QC point of view, we need to examine the effect of cell compression and/or expansion on the load current as well as currents delivered by individual modules. As expected and confirmed in Fig. 11, modules in compression, *i.e.*, decreased δ^*, contribute more to the load current than those in expansion. Our model implies that a variation of up to 10 % is acceptable. It is noteworthy that the battery load current is not affected throughout the duration of the discharge. Any correlation between porosity and compression has been omitted.

4.3 Unequal numbers of cells in modules.

Large $Li/SOCl_2$ power sources, *eg*, 10 kW, contain *ca* 100 cells per module. This large number of cells increases the probability of constructing modules with fewer or greater than the specified number of cells. The effect of such an error is illustrated in Fig. 12. It is seen that missing or additional cells in the amount of 2 % affect the battery lifetime and load delivered to the external ciruit. Specifically, the effect of fewer cells is similar to that resulting from an expansion in module thickness (*i.e.* increased δ^*) while the effect of extra cells corresponds to a compression. In either case, the deficient module may generate excess heat.

4.4 Modules with defective cells.

Defective cells in a module are cells that fail prematurely. The measure of their deficiency is introduced through the computational factor w, see Eq. (3), which varies between zero and unity, and affects both the conductivity in the cathode and the total charge deliverable by a cell(1). The smaller this factor, the more serious the defect. The occurrence of these defects in the $Li/SOCl_2$ system is associated with cathode fabrication.

For illustration of the effect of defective cells in an assembly of modules, we selected central cells

of the second module and assigned the deficiency factor $w = 0.5$. It is seen that half-way through the discharge process, the battery load current became less, Fig. 13a, due to the failure of the first module. It is also seen that the remaining modules were not able to compensate completely, Fig. 13b. Moreover, as illustrated in Figs. 13c and 13d, local heat sources are generated by the intercell currents in addition to an excessive heat production due to an increase in the load currents generated by the well functioning modules.

5.0 Concluding remarks.

QC aspects of the fabrication of a multimodule $Li/SOCl_2$ battery employing common electrolyte are examined with regard to (i) tolerances on compression and/or expansion (thickness of a module), (ii) missing or extra cells and (iii) the presence of defective cells. Present calculations confirm earlier findings that the addition of well constructed modules introduces no special difficulties. Our model also predicts that tolerances in module thickness up to ca 10 % are acceptable. The variation in the number of cells in a module up to 2 % can be tolerated. Modules with missing cells behave as if they were in expansion. The most serious problem arises from the construction of deficient cells thus suggesting a strict enforcement of the control measures in the fabrication of positive electrodes.

Acknowledgement.

This work was performed as a part of the Naval Ocean Systems Center Independent Exploratory Development program and constitutes a fraction of a program to establish a technology base for high discharge rate $Li/SOCl_2$ batteries.

Symbols.

i - running index

I - intercell current, A

J - current, A

M - number of modules in a battery

N - number of cell in a module

R - resistance, Ω

t - time, s

w - faradaic inefficiency factor

X - dimensionless resistance (defined in text)

y - random variable

δ' - effective distance between electrodes, cm

ϵ - porosity

ϵ_{max}; ϵ_{min} - see section 3.3

Φ - potential, V

λ - defined in text (Eqs. 1 and 2)

η - mean value

σ - standard deviation

subscripts

f - feed line

l - load

n - nominal

p - cell port entrance

t - fill tube

z - cell internal

superscript

(m) - module identification

References

1. S. Szpak, C. J. Gabriel and J. R. Driscoll, J. Electrochem. Soc., 131, 1996 (1984)

2. S. Szpak, C. J. Gabriel, J. J. Smith and J. R. Driscoll, ibid., 137, march issue (1990)

3. C. J. Gabriel and S. Szpak, J. Power Sources, 25,215 (1989)

4. S. Szpak and J. R. Driscoll, **Assessment of $Li/SOCl_2$ Battery Technology: Reserve, Thin Cell Design**, NOSC-TR 1154, vol. I, 1987

5. J. R. Driscoll and S. Szpak, J. Power Sources, 14, 285 (1985)

6. J. S. Dunning, Ph D Dissertation, UCLA 1970

7. R. de Levie, **Porous and Rough Electrodes**, in **Advances in Electrochemistry and Electrochemical Engineering**, vol. 6, P. Delahay and C. W. Tobias, eds., Interscience Publishers, 1967 and references therein.

8. L. A. Parnell and S. Szpak, Electrochim. Acta, 30, 913 (1985)

Figure captions

Fig. 1 - A block diagram indicating the fabrication sequence for module/battery assembly and QC requirements. l - thickness; N - number of cells; R_f and R_t - feed line and fill tube resistances, respectively; w - deficiency factor; δ^* - electrode separation; ϵ - porosity.

Fig. 2 - The module and module/module coupling representation by an electric circuit analog. J_i - circulating current; I_i - intercell current; Φ - potential at manifold inlet; R_f manifold feed resistor; R_t - equivalent feed tube resistor; R_z - internal cell impedance. Both (+/+) and (-/-) interfaces are indicated.

Fig. 3 - An electric circuit analog representation of an operating $Li/SOCl_2$ cell. Shaded areas indicate the locations of the time dependent circuit elements relevant to the computed results.

Fig. 4 - The time evolution of $\lambda-$ parameter calculated for each cell in an assembly of four fifty-cell modules for the input data listed in Table I, with $N_s = 10.0$.

4a - initial distribution

4b - distribution after 288 seconds of battery discharge. The insert is the expansion to the same scale as in 4a of the interface between the first and second module.

Fig. 5 - The time evolution of intercell currents. Conditions as in Fig. 4.

Fig. 6 - A flow chart for calculation of characteristics of the multi-module battery discharge.

Fig. 7 - The external load current in an assembly of 50- cell modules with $N_s = 10$. The other input data listed in Table I. The number of modules in an assembly is indicated alongside the curves.

Fig. 8 - The portion of the load current supplied by individual modules. Conditions as in Fig. 7. Figs. 8a - 8d for assemblies of 2, 3, 4 and 5 modules, respectively.

Fig. 9 - The portion of the load current supplied by the individual modules. Conditions as in Fig. 7 except that $N_s = 5$. Figs. 9a - 9d, for assemblies of 2, 3, 4 and 5 modules, respectively.

Fig. 10 - The portion of the load current supplied by the individual modules. Conditions as in Fig. 7. Figs. 10a - 10d, for assemblies of 2, 3, 4 and 5 modules, respectively.

Fig. 11 - The portion of the load current supplied by each module in a 3 - module assembly. Conditions as in Fig. 7, except for δ'. Fig. 11a - 4 % compression; 11b - 4 % expansion.

Fig. 12 - The portion of the load current supplied by each module in a 3- module assembly. Conditions as in Fig. 7, except for the number of cells in the first module. Fig. 12a - 49 cells; Fig. 12b - 48 cells.

Fig. 13 - The effect of a group of defective cells on battery performance. The deficient cells are numbers 29 through 32 of the second module, corresponding to numbers 69 through 72 of the complete assembly. Conditions as in Fig. 7, except that the defective cells have a deficiency factor $w = 0.5$.

Fig. 13a - external load current

Fig. 13b - load current supplied by the individual modules

The evolution of the intercell current distribution: Fig. 13c at 4.8 min; Fig. 13d - at 7.2 min.

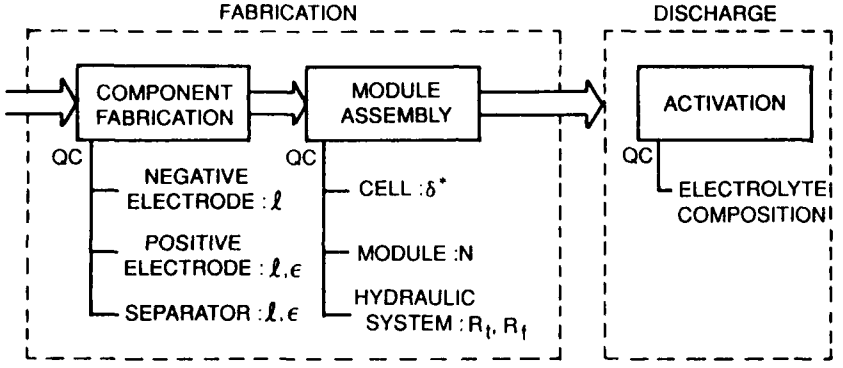
FABRICATION
DISCHARGE
COMPONENT FABRICATION
MODULE ASSEMBLY
ACTIVATION
QC
QC
QC
NEGATIVE ELECTRODE : ℓ
POSITIVE ELECTRODE : ℓ, ϵ
SEPARATOR : ℓ, ϵ
CELL : δ*
MODULE : N
HYDRAULIC SYSTEM : R_t, R_f
ELECTROLYTE COMPOSITION

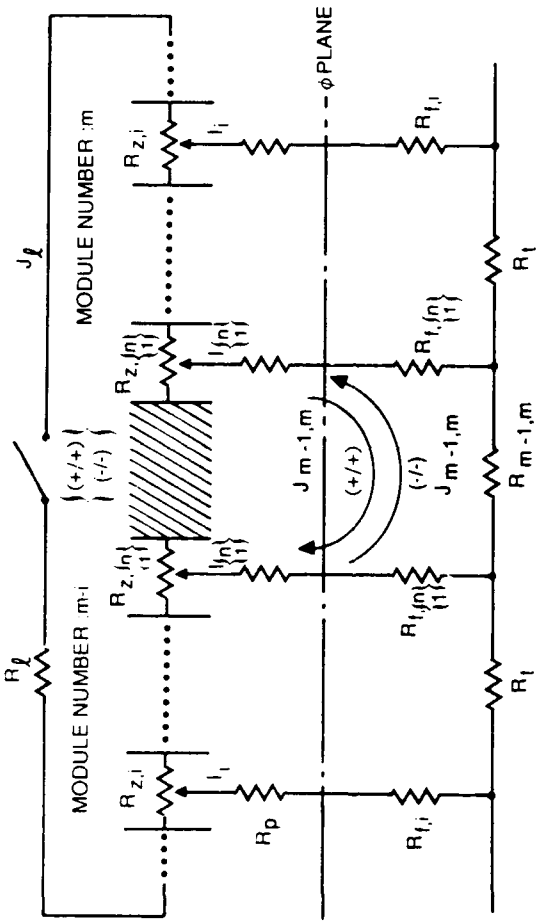
MODULE NUMBER m
MODULE NUMBER m-1
J_ℓ
R_ℓ
$R_{z,j}$
I_j
$R_{z,j}\{n\}_{(1)}$
$I_j\{n\}_{(1)}$
$R_{z,1}\{n\}_{(1)}$
$I_1\{n\}_{(1)}$
$R_{z,1}$
I_1
R_p
(+/+)
(-/-)
$J_{m-1,m}$
$J_{m-1,m}$
(+/+)
(-/-)
ϕ PLANE
$R_{t,j}$
R_t
$R_{t,j}\{n\}_{(1)}$
$R_{m-1,m}$
$R_{t,1}\{n\}_{(1)}$
R_t
$R_{t,1}$

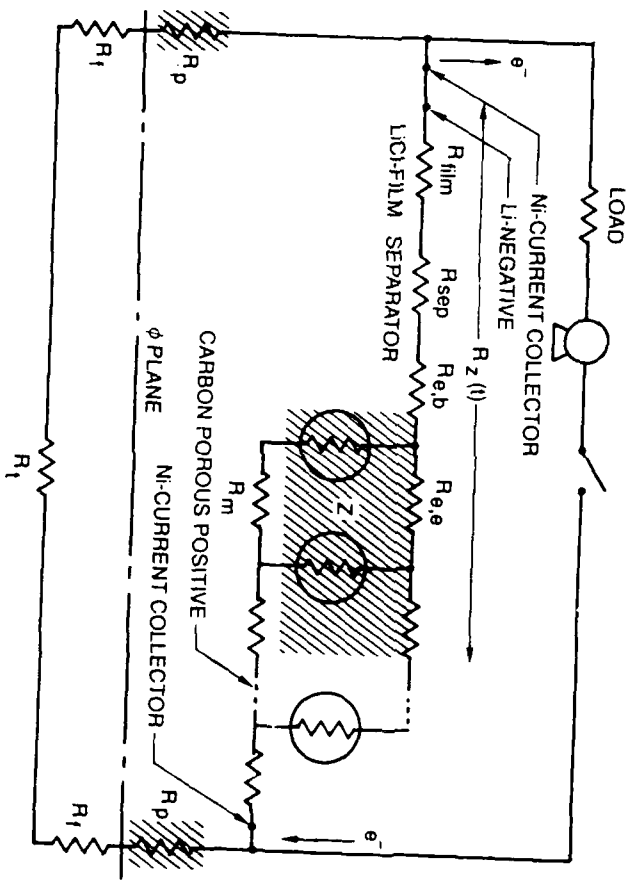
LOAD
Ni-CURRENT COLLECTOR
Li-NEGATIVE
e⁻
R film
LiCl-FILM SEPARATOR
R sep
R e,b
R z (l)
R e,e
Z
R m
CARBON POROUS POSITIVE
ϕ PLANE
Ni-CURRENT COLLECTOR
R p
R t
R t
R t
R p
e⁻

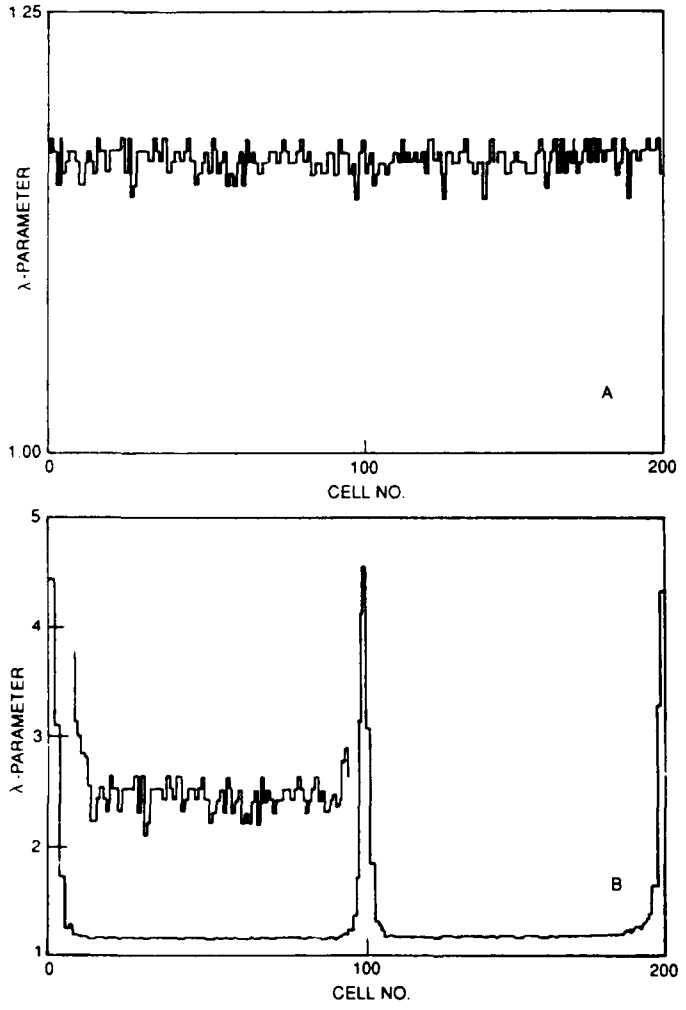
1.25
1.00
λ-PARAMETER
A
0
100
200
CELL NO.
5
4
3
2
1
λ-PARAMETER
B
0
100
200
CELL NO.

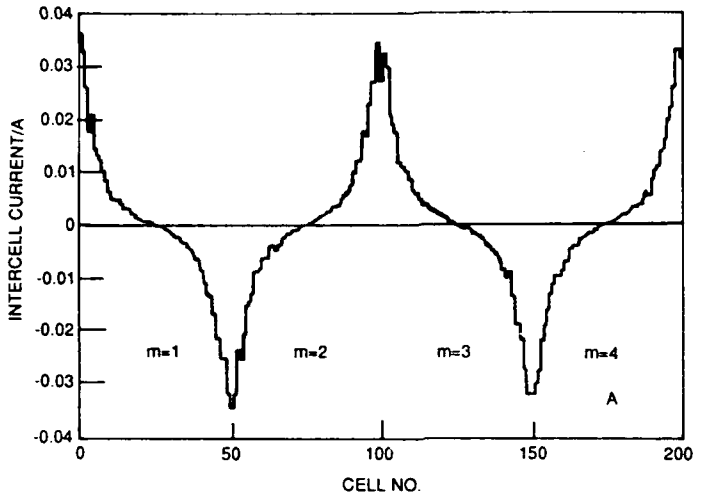
0.04
0.03
0.02
0.01
0
-0.01
-0.02
-0.03
-0.04
INTERCELL CURRENT/A
m=1
m=2
m=3
m=4
A
0
50
100
150
200
CELL NO.

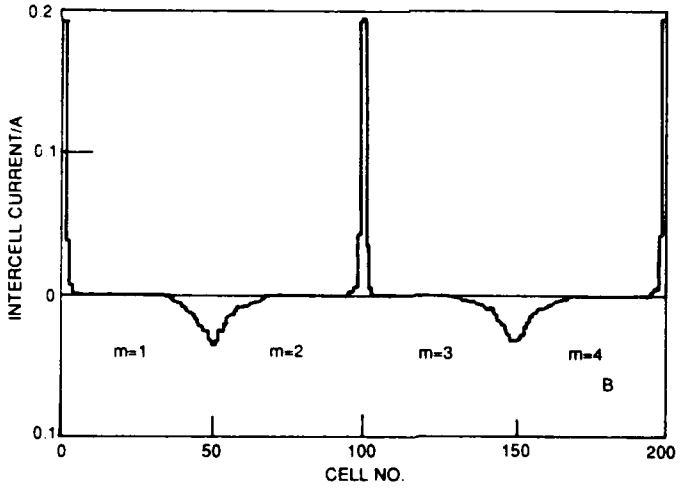
0.2
0.1
0
0.1
INTERCELL CURRENT/A
m=1
m=2
m=3
m=4
B
0
50
100
150
200
CELL NO.

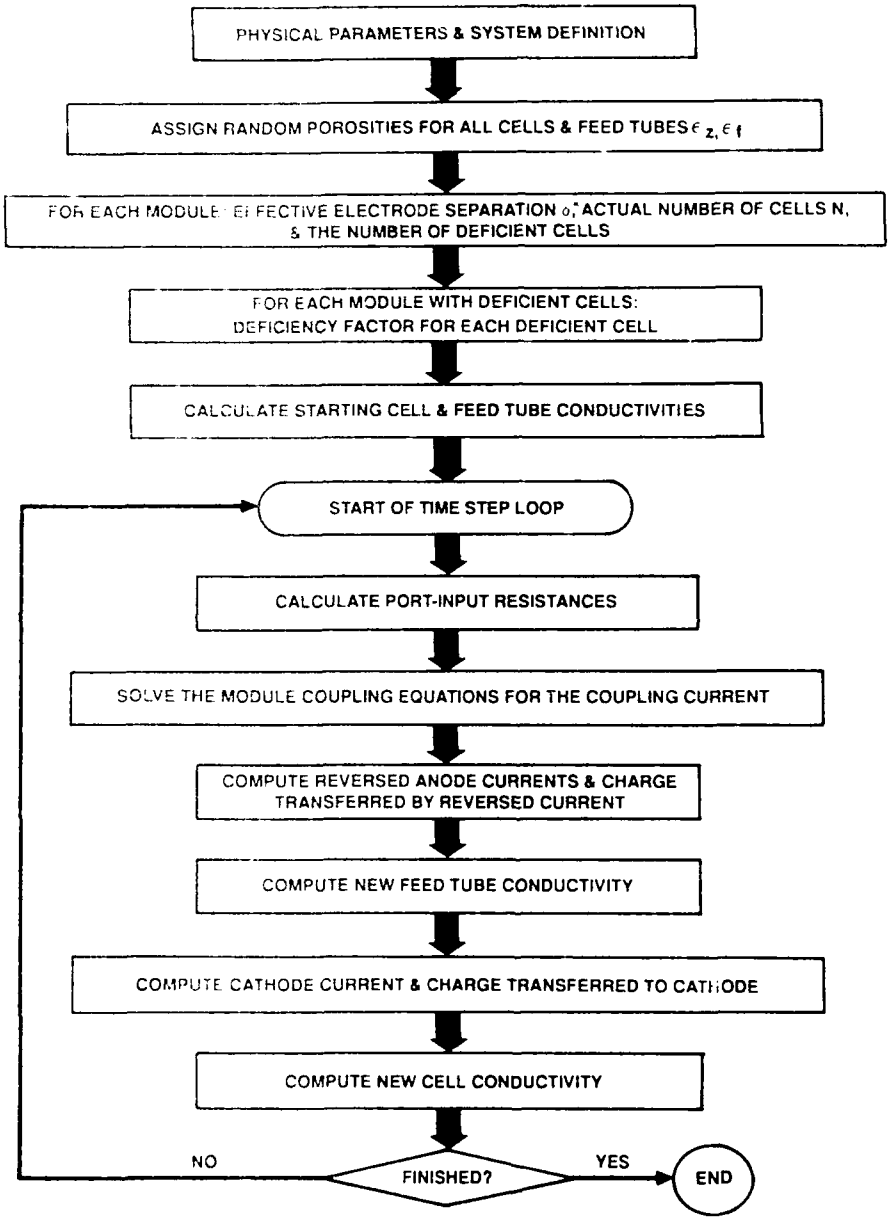
PHYSICAL PARAMETERS & SYSTEM DEFINITION
ASSIGN RANDOM POROSITIES FOR ALL CELLS & FEED TUBES ϵ_z, ϵ_f
FOR EACH MODULE: EFFECTIVE ELECTRODE SEPARATION o_i, ACTUAL NUMBER OF CELLS N, & THE NUMBER OF DEFICIENT CELLS
FOR EACH MODULE WITH DEFICIENT CELLS: DEFICIENCY FACTOR FOR EACH DEFICIENT CELL
CALCULATE STARTING CELL & FEED TUBE CONDUCTIVITIES
START OF TIME STEP LOOP
CALCULATE PORT-INPUT RESISTANCES
SOLVE THE MODULE COUPLING EQUATIONS FOR THE COUPLING CURRENT
COMPUTE REVERSED ANODE CURRENTS & CHARGE TRANSFERRED BY REVERSED CURRENT
COMPUTE NEW FEED TUBE CONDUCTIVITY
COMPUTE CATHODE CURRENT & CHARGE TRANSFERRED TO CATHODE
COMPUTE NEW CELL CONDUCTIVITY
NO
FINISHED?
YES
END

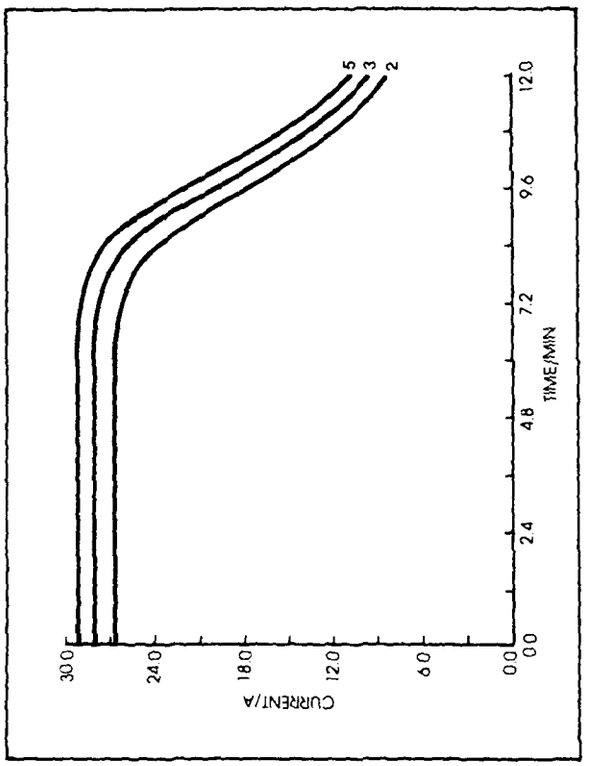
5
3
2
30.0
24.0
18.0
12.0
6.0
0.0
CURRENT/A
0.0
2.4
4.8
7.2
9.6
12.0
TIME/MIN

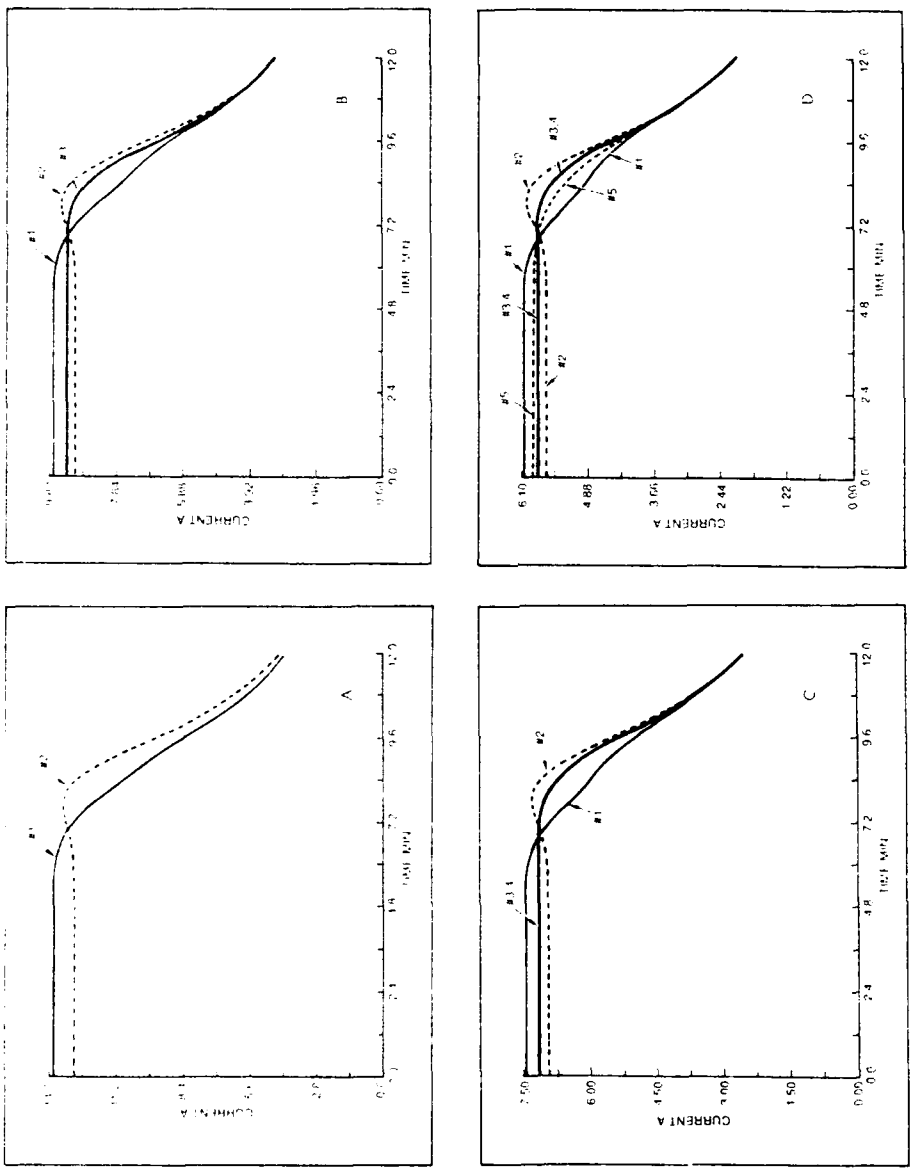
A
B
C
D
CURRENT A
TIME MIN
#1
#2
#3
#4
#5
#6
0.00
1.22
2.44
3.66
4.88
6.10
6.00
4.50
3.00
1.50
0.0
2.4
4.8
7.2
9.6
12.0

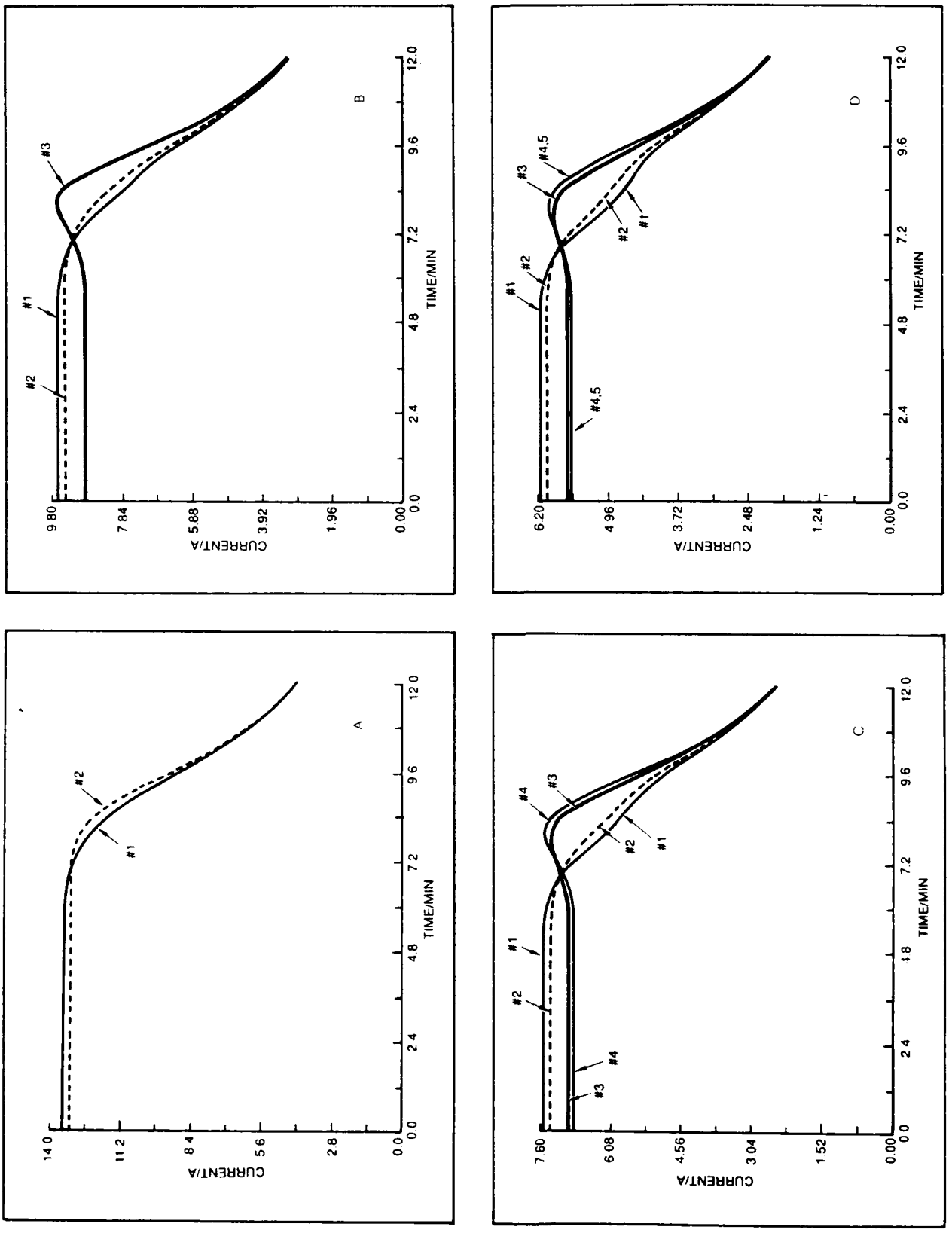
A
B
C
D
CURRENT/A
TIME/MIN
#1
#2
#3
#4
#4.5
0.0
2.4
4.8
7.2
9.6
12.0
1.52
3.04
4.56
6.08
7.60
1.24
2.48
3.72
4.96
6.20
1.96
3.92
5.88
7.84
9.80
2.8
5.6
8.4
11.2
14.0

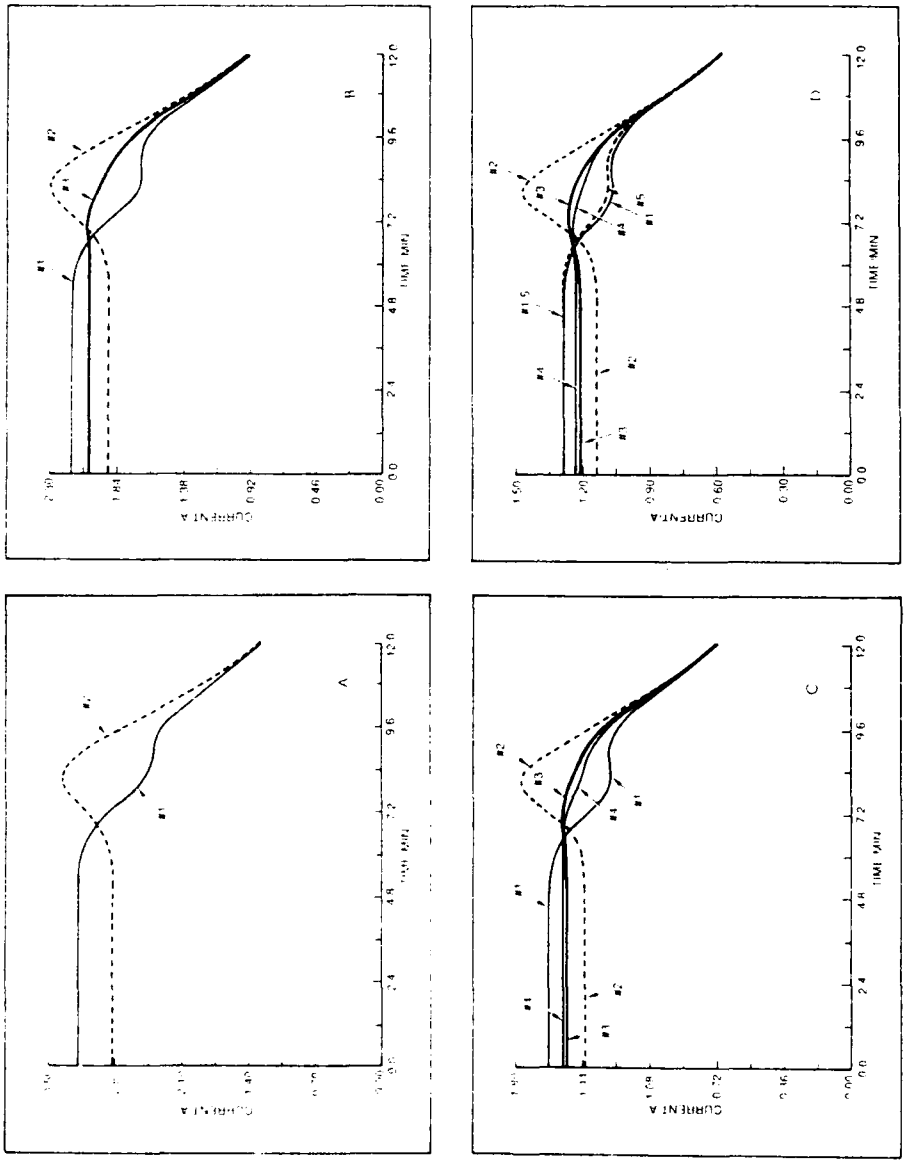
A
B
C
D
CURRENT A
TIME MIN
0.0
2.4
4.8
7.2
9.6
12.0
0.00
0.46
0.92
1.38
1.84
2.30
0.30
0.60
0.90
1.20
1.50

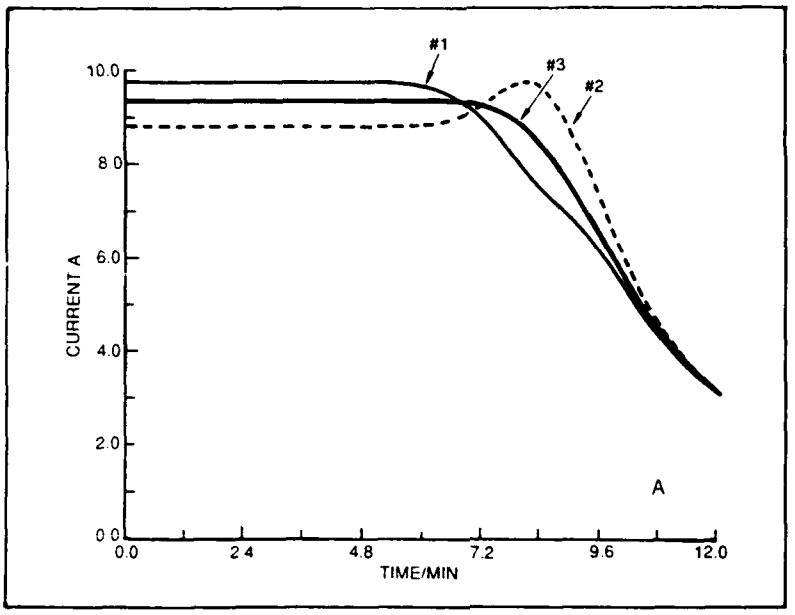
#1
#3
#2
10.0
8.0
6.0
4.0
2.0
0.0
CURRENT A
0.0
2.4
4.8
7.2
9.6
12.0
TIME/MIN
A

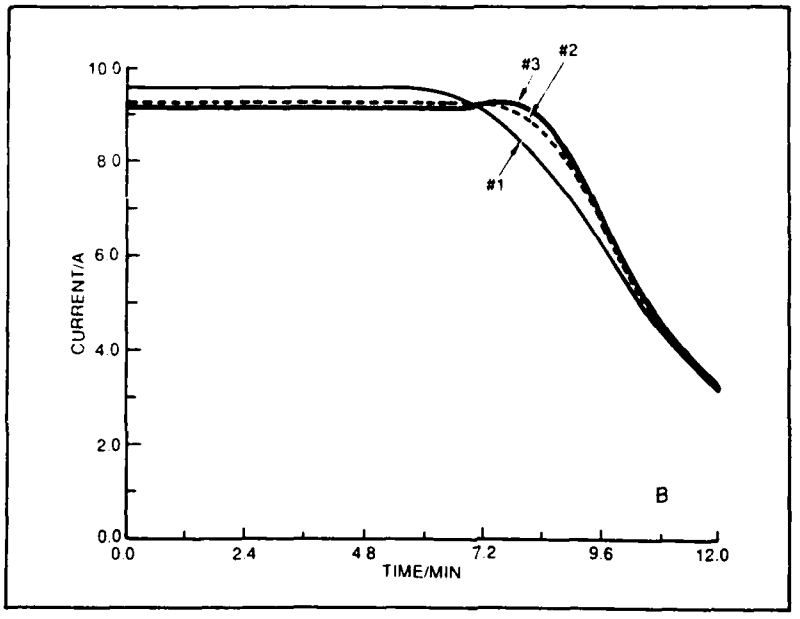
#2
#3
#1
10.0
8.0
6.0
4.0
2.0
0.0
CURRENT/A
0.0
2.4
4.8
7.2
9.6
12.0
TIME/MIN
B

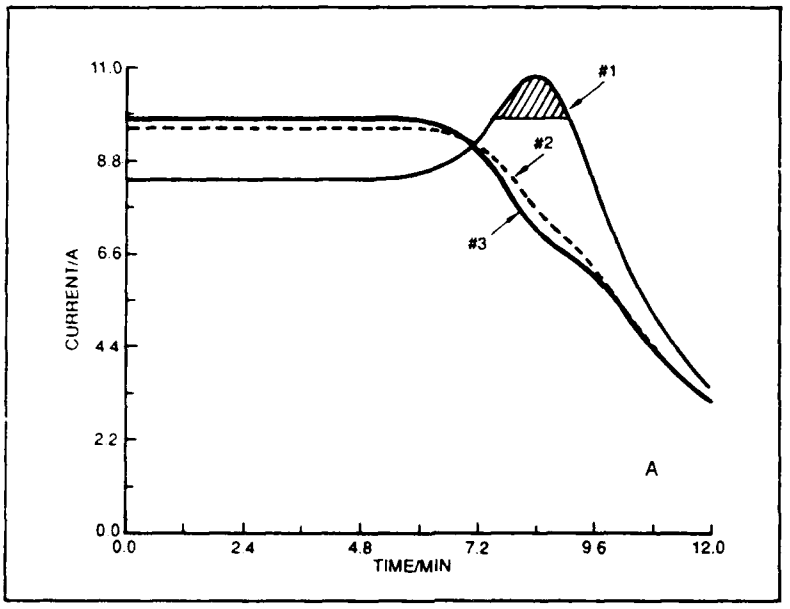
11.0
8.8
6.6
4.4
2.2
0.0
CURRENT/A
#1
#2
#3
A
0.0
2.4
4.8
7.2
9.6
12.0
TIME/MIN

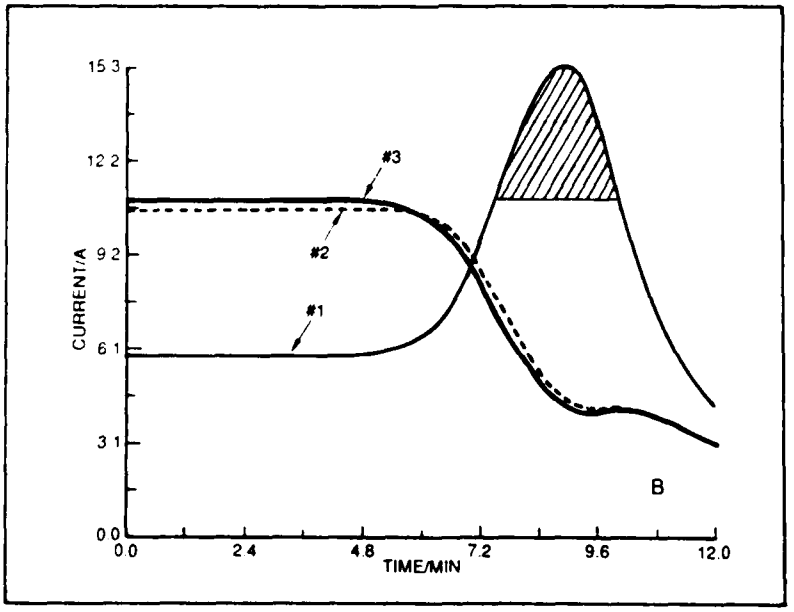
15.3
12.2
9.2
6.1
3.1
0.0
CURRENT/A
#3
#2
#1
B
0.0
2.4
4.8
7.2
9.6
12.0
TIME/MIN

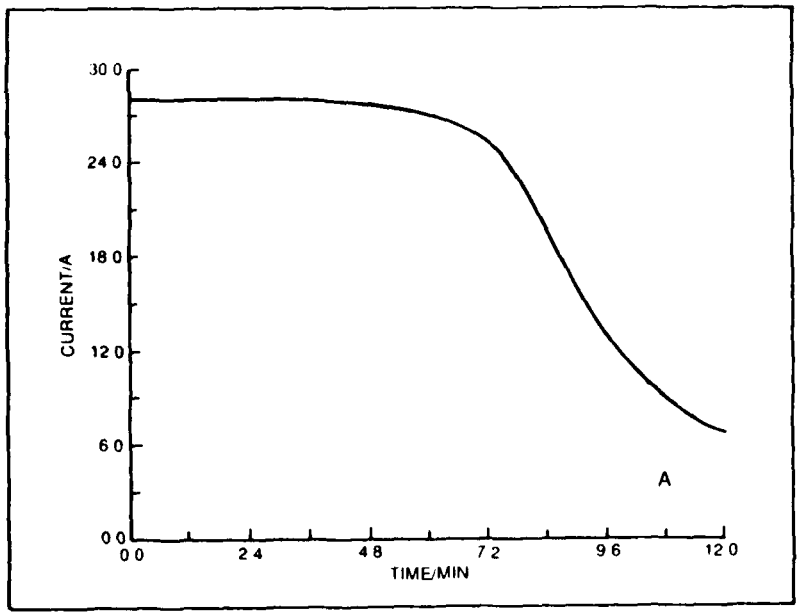
30 0
24 0
18 0
12 0
6 0
0 0
CURRENT/A
0 0
2 4
4 8
7 2
9 6
12 0
TIME/MIN
A

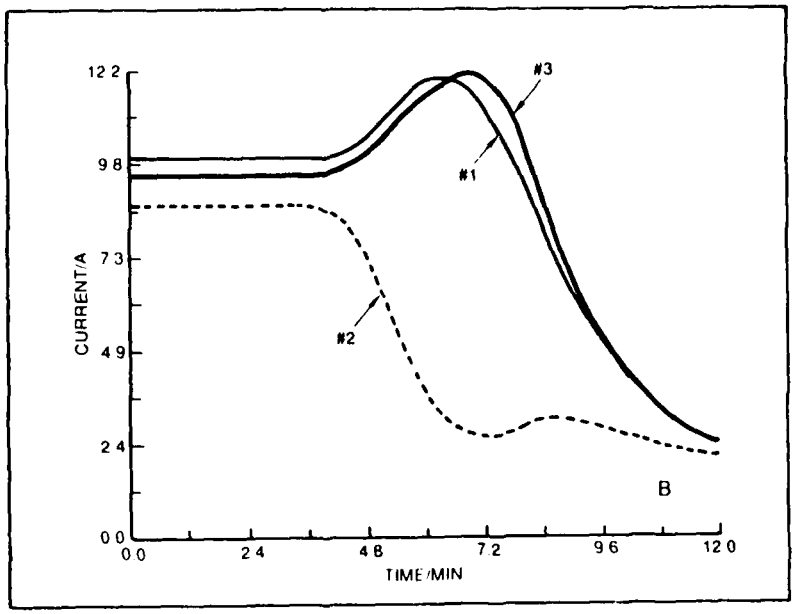
12 2
9 8
7 3
4 9
2 4
0 0
CURRENT/A
#3
#1
#2
0 0
2 4
4 8
7 2
9 6
12 0
TIME/MIN
B

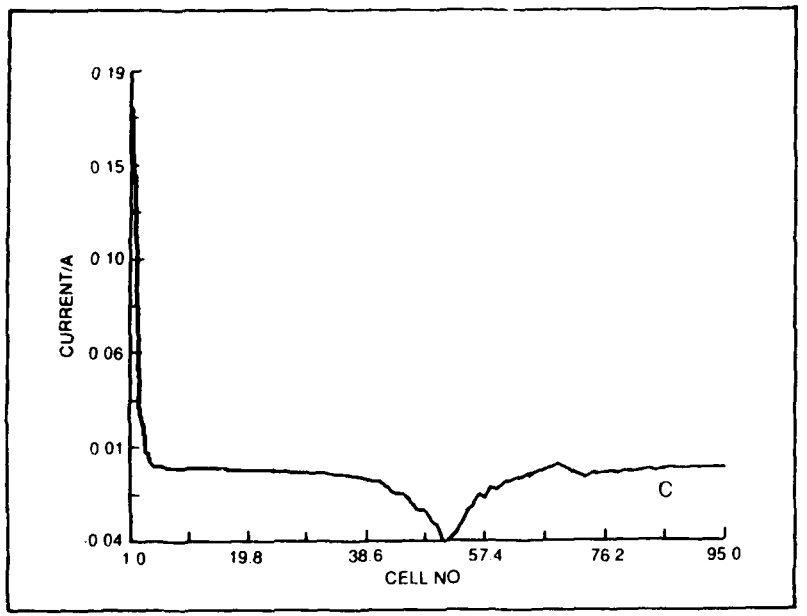
0 19
0 15
0 10
0 06
0 01
-0 04
CURRENT/A
1 0
19 8
38 6
57 4
76 2
95 0
CELL NO
C

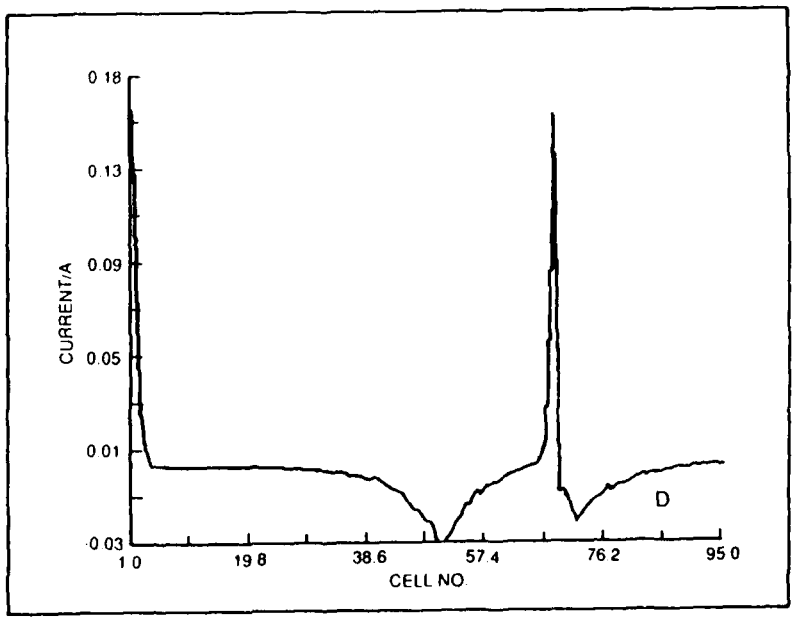
0 18
0 13
0 09
0 05
0 01
-0 03
CURRENT/A
1 0
19 8
38 6
57 4
76 2
95 0
CELL NO
D

ELECTROCATALYSIS STUDIES ON THE CATHODIC REDUCTION OF THIONYL CHLORIDE

M. Madou, K. Kinoshita, M.C.H. McKubre
SRI International
333 Ravenswood Avenue
Menlo Park, CA 94025
S. Szpak
Naval Ocean Systems Center
San Diego, CA 92117

ABSTRACT

The electrocatalytic activity of carbon electrodes and additives such as Fe-, Co-, Cu-phthalocyanines and $AlCl_3$ on the cathodic reduction of $SOCl_2$ was investigated by cyclic voltammetry and AC impedance techniques. Results obtained by cyclic voltammetry indicate that cathodic reduction of $SOCl_2$ is enhanced by Fe- and Co- phthalocyanines but remains relatively unaffected by the presence of Cu-phthalocyanine. The enhancement of the $SOCl_2$ reduction in the presence of $AlCl_3$ is substantially different than with phthalocyanines. The effect of electrocatalysts on the cathodic reduction of $SOCl_2$ and possible mechanisms for enhanced activity are discussed.

An accelerated progress in electrochemical technology can be realized only with better understanding of electrocatalysis and the development of catalysts for specific charge transfer reactions. Electrocatalysis may be viewed as a special case of heterogeneous catalysis inasmuch as the catalyst must be in contact with an electronically conductive substrate which functions as either electron source or sink. Moreover, if the catalyst is applied in the form of a thin film, it must be sufficiently conductive to avoid substantial ohmic losses. Alternatively, the electrocatalytic substance may be dissolved in the electrolyte. In such a case, active sites may be created on an otherwise inactive substrate by chemisorbed active material.

Important theoretical and practical developments in the field of electrocatalysis have occurred in the past two decades, particularly in enhancement of hydrogen and oxygen electrode reactions (1,2). Most recently, concepts advanced and catalysts developed for fuel cells were adapted to other energy conversion devices, e.g., to the highly energetic $Li/SOCl_2$ cells with the intent to increase their discharge rate capability. To accomplish this goal, the porous Shawinigan black electrodes are being modified by incorporation of finely divided metal particles, e.g., Pt (3), Cu (4), transition metal halides (5) and transition metal complexes with N_4 chelates, e.g., Co-, Fe-, Cu- phthalocyanines (6,7).

In this communication we examine the effect of $AlCl_3$ and of phthalocyanine complexes on the reduction of $SOCl_2$ taking place on a surface of glassy carbon electrodes.

EXPERIMENTAL RESULTS

Data on catalytic activities of transition metal phthalocyanines are based on cyclic voltammograms and AC impedance measurements. The description of the electrochemical cell and apparatus employed in this investigation as well as procedures used, have been described previously (8,9).

Effect of Catalysts on V_{oc}. The effect of addition of $AlCl_3$ and of Co- phthalocyanine (CoPc) on the rest-potential was examined in an U- cell provided with two compartments separated by a fritted glass disc. In this cell, one compartment contained a Li reference electrode immersed in neutral electrolyte, the other, a test electrode immersed in an electrolytye modified by addition of either $AlCl_3$, CoPc or both.

The results presented in Table I, show that, upon addition of $AlCl_3$, the rest-potential of carbon and molybdenum electrodes became 300 mV more positive while the Li electrode remained at the same potential. The addition of CoPc also shifted the rest-potential in the positive direction, but only by 100 mV. It is noteworthy that when both substances were added simultaneously, the potential shift was 400 mV, i.e, the observed potential displacement was additive. The Li electrode always remained at the same potential irrespective of solution composition, thus it can serve as a good reference electrode, while both C and Mo behave as electrodes of the first kind (9).

Effect of $AlCl_3$ Addition. The effect of the addition of $AlCl_3$ on the current/potential relationship is illustrated in Fig. 1. In particular, curve a is a voltammogram recorded in a 1M $LiAlCl_4$ solution in $SOCl_2$. Curves b and c, are voltammograms in solutions containing 0.07 M $AlCl_3$ + 0.93 M $LiAlCl_4$ in $SOCl_2$, and 0.6 M $AlCl_3$ + 0.4 M $LiAlCl_4$ in $SOCl_2$ respectively.

Evidently, the addition of $AlCl_3$ even in small amounts generates a new peak, peak A, located in this case approximately 200 mV positive with respect to the $SOCl_2$ reduction peak in neutral solutions, peak B. The height and position of peaks A and B depend, in a complex way, on amount and ratio of $AlCl_3$ concentration, peaks A and B become broader, their separation larger and displaced in the cathodic direction, curve c. At much higher concentrations, e.g., in 1.9 M $AlCl_3$ + 2.2 M $LiAlCl_4$ in $SOCl_2$, only one broad peak is observed.

Effect of Phthalocyanine Addition. The addition of phthalocyanine complexes to a neutral solution increases the peak current

and shifts the peak potential in the anodic direction. The magnitude of the peak current and its position depend on the selection of the complexed central metal ion. This dependence is illustrated in Fig. 2, where voltammograms obtained in electrolyte containing CuPc and FePc are shown alongside the voltammogram in 1 M $LiAlCl_4$ only, curves b, c and a, respectively.

Similar behavior is observed upon the addition of CoPc, Fig. 3. Here, a twofold increase in the peak current and a 250 mV displacement of the peak in the anodic direction is evident. However, the total charge transferred in the period between the initiation of reduction and passivation of the electrode surface, is about the same. The small displacements in the peak current on three successive scans on a repolished electrode in curves 1, 2 and 3 are probably due to an increase in the CoPc concentration of the slowly dissolving CoPc.

The mechanical removal of passivating films from the electrode surface is more difficult when such films are formed in the presence of the dissolved CoPc. The removal of passive films can also be accomplished by holding the electrode at potentials positive to the V_{oc}, e.g., at +4.5 V as illustrated in Fig. 4. Here, curves 1 and 2 are repetitive voltammograms covering the range between +3.6 V to +1.85 V and return. The return sweep to +3.6 V did not remove the passive film. However, by extending the return sweep to +4.5 V, the electrode surface was restored to its original condition, curve 3.

Nyquist Plot. Figure 5 shows a Nyquist plot for a neutral solution, curve a, and for a neutral solution containing CoPc, curve b. Evidently, the addition of CoPc yields also a semicircle, but its radius is substantially smaller than in the presence of the catalyst indicating that the interfacial charge transfer resistance is less in the presence of a catalyst.

DISCUSSION

The necessary condition for the initiation of an electrochemical process is the intimate contact between the reactive species and a phase boundary where the charge transfer occurs. This requirement implies that an adsorption process must precede the charge transfer step and, furthermore, it suggests that an electrocatalyst may affect more than one of the elementary processes comprising the overall reaction pathway.

The evaluation of electrocatalytic activities in a system as complex as the reduction of $SOCl_2$, is not straightforward. First, the reaction is kinetically controlled within only a narrow range of overpotentials, η, because at higher overpotentials the formation of prepassive LiCl films prevents an unambiguous interpretation of results. Second, the physicochemical properties of $SOCl_2$ based electrolytes further complicate the matter on account of the formation of

various complexes whose properties are not at present entirely known, e.g., complexation with reaction products such as SO_2 cannot be excluded.

Rest potential. An Evans type representation of the log i vs V curves for the reduction and oxidation of the $SOCl_2$-$LiAlCl_4$ solutions, implies that the rest potential observed on glassy carbon electrodes is an example of a mixed potential (9). The displacement of this potential upon the addition of CoPc is in agreement with such a conclusion inasmuch as a catalyst should not affect a true thermodynamic potential.

The displacement of the rest potential upon the addition of $AlCl_3$ to a neutral solution, arises from a change in the reactant and the products, as illustrated in a diagram, Fig. 6. In the presence of an excess of $AlCl_3$, a potential displacement is expected because of the formation of a more stable product, $LiAlCl_4$, in contrast with the formation of LiCl that occurs in neutral solutions. Theoretical calculations (10) predicted the displacement of ΔEp(= b-a) between 530 and 630 mV, depending upon the value of the equilibrium constant, K, for the reaction

$$LiCl + AlCl_3 \overset{K}{\rightleftharpoons} LiAlCl_4 \qquad (I)$$

As indicated in Fig. 6, in acid solutions it is the adduct $AlCl_3 \cdot SOCl_2$ that is the reactant, i.e., the rest-potential will be less by ΔE_r(= b-c) arising from the reaction

$$SOCl_2 + AlCl_3 \overset{K}{\rightleftharpoons} AlCl_3 \cdot SOCl_2 \qquad (II)$$

with ΔE_r given by

$$\Delta E_r = 0.0148 \log \frac{[LiAlCl_4]^4}{[AlCl_3 \cdot SOCl_2]^2 [AlCl_3]^2} \qquad (1)$$

Unfortunately, the K value for reaction, Eq. (II), is not known, but clearly since by taking the complexation of $SOCl_2$ into account a more stable reactant is made, ΔG and also ΔE will be lowered with respect to the situation where no complexation is taken into account (compare c with b in Fig. 6).

Effect of Addition of $AlCl_3$ on i/η Curves. The appearance of a second reduction peak, peak A Fig. 1, was first noted by Doddapaneni (11) for a neutral solution. However, he observed this peak under special circumstances, namely; (i) on stress annealed graphite electrodes, (ii) on dry surfaces and (iii) during the first cycle. Such a set of observations would suggest that the appearance of an additional peak is related to the state of the electrode surface. Nevertheless, he ascribed their existence to a two step process in the reduction of $SOCl_2$.

The present investigation attributes the formation of two peaks in an acid solution to the change in the properties of the electrolyte phase, primarily to the formation of the $AlCl_3 \cdot SOCl_2$ adduct. This conclusion is based on the behavior of voltammograms with a change in the concentration of $AlCl_3$. It is noteworthy that, in contrast with Doddapaneni's results, the peaks in acid solutions were reproducible in successive voltammograms.

The complicated dependence of the voltammograms on $AlCl_3$ concentration is expected in view of the complexity of the Li-$AlCl_3$-$SOCl_2$ system (12). With the addition of $AlCl_3$, not only the conductivity of the electrolyte changes but also its structure. The ion-ion and ion-solvent interactions, as well as formation of yet unidentified aggregates, makes a definite interpretation of the voltammograms impossible at the present time. Nevertheless, certain conclusions can be formulated: (i) the appearance of an additional peak in acid solutions is not due to two step reduction of $SOCl_2$ because in that case we would not see a merger of these peaks at higher $AlCl_3$ concentrations and (ii) peak A is not responsible for the observed step in the voltage-time curves of a discharging Li/$SOCl_2$ cell, i.e., to the exhaustion of $AlCl_3$ in a cell being discharged at constant load (13) since in our case consecutive cycles reproduced peak A, indicating that our cell is not exhausted of $AlCl_3$ when peak A arises.

Effect of Phthalocyanines. The electrocatalytic effect of metal-phthalocyanines (Me-Pc) where Me = Co, Fe, Cu is assumed to be through the weakening of the S=O double bond attributed to the interaction of the catalyst with the central metal ion of the N_4 chelates. In contrast to the electrocatalytic reduction of O_2 (1,2), details of the reaction pathway for the reduction of $SOCl_2$ are not known; the proposed reaction mechanisms (7, 14, 15) have not been sufficiently justified. However, if the arguments presented for catalytic reduction of O_2 also apply here, then electrocatalytic activity should decrease in the following order: Fe > Co >> Cu >> Li (with no activity associated with Li). Comparing the amount of cathodic reduction current in the presence of different phthalocyanines at a fixed potential within the range of kinetic reaction control [e.g. at +3V versus Li, see ref. (9)] reveals that the observed catalytic activities in the reduction of $SOCl_2$ are the same as for O_2 thus suggesting that the process of weakening of the S=O bond is essentially similar to that for the reduction of O_2. A word of caution: because $SOCl_2$ is a weak donor [0.4 on the Gutmann scale (16)] it may form complexes with the reaction products, and catalytic activities may not be limited to the charge transfer reaction but directly or indirectly affect other elementary processes as well. We observed that the nature of the passivating film on the carbon electrode is altered by the presence of catalysts in solution. This observation was also made on porous carbon electrodes in batteries in the presence of the same catalysts and is currently the subject of intensive investigation with different types of surface analysis techniques.

Comparing Fig. 1 with Figs. 2-4, we note that the contribution of $AlCl_3$ differs fundamentally from that of phthalocyanines. In the first case, the change in V_{oc} is attributed to the change in reactants and products while in the second case it is due to lower energy of activation for the reduction of $SOCl_2$ complexed with MePc.

An interesting feature in Fig. 3 is the slight displacement in the peak current in the anodic direction. This effect seems to be associated with an increasing concentration of the slowly dissolving CoPc. This interpretation is an agreement with earlier results of Venkatasetty (17) that the quasi-exchange current density increases with the increase in CoPc concentration.

In determining the electrocatalytic activities, we must choose a suitable reference point. (18) Here, this is very important because the kinetically controlled region is rather narrow. Up to now we have compared the catalytic activity of the different MePc by comparing currents at a fixed potential in a region where currents are under kinetic control. Another way of examining catalytic effects is by determining the influence of various additives on the electron transfer resistance (R_p) at the open circuit potential. A catalyzed reaction will lead to a smaller R_p and thus via

$$R_p = \frac{\vec{\beta}\ \overleftarrow{\beta}}{i_o(2.303)(\vec{\beta} + \overleftarrow{\beta})A}$$

where $\vec{\beta}$ and $\overleftarrow{\beta}$ are the Tafel coefficients for the forward and reverse reactions, to a larger exchange current density (19). R_p can be obtained as the low frequency limit in a Nyquist plot (see Fig. 7). In a previous paper (9) we did show that at the open circuit potential different processes occur simultaneously: reduction of Cl_2 and $SOCl_2$ and oxidation of $SOCl_2$, $AlCl_4^-$ or LiCl. Therefore a decrease in R_p or an increase in i_o might not be a good indication for faster kinetics of $SOCl_2$ reduction. Possibly the Cl_2 reduction or one of the oxidation processes is catalyzed. On the other hand, it is known that Cl_2 reduction is a fast reaction and from our previous work we know that at +3 V only $SOCl_2$ is reduced and since we do see an increase in reduction current there, it seems reasonable to assume that also at the V_{oc} the observed decrease in R_p indicates an increased effectiveness of reduction of $SOCl_2$. The R_p is about a factor of 2 smaller for the catalyzed process or i_o a factor of two bigger.

REFERENCES

1. E. Yeager, J. Electrochem. Soc., 128, 160 (1981).
2. G. Sandstede, "From Electrocatalysis to Fuel Cells", Univ. of Washington Press, Seattle-London, 1972.
3. K. A. Klinedinst, J. Electrochem. Soc., 128, 2507 (1981).
4. L. R. Giattino, US Patent No. 4,167,608 (1979).

5. W. K. Behl, J. Electrochem. Soc., 128, 939 (1981).
6. H. V. Venkatasetty, US Patent. No. 4,279,973 (1981).
7. N. Doddapaneni, Extended Abstracts No. 360, Electrochem. Soc. Fall Meeting, Detroit, MI, 1982.
8. M. J. Madou and M.C.H. McKubre, J. Electrochem. Soc., 130, 1056 (1983).
9. M. J. Madou and S. Szpak, Ibid., submitted.
10. J. Devynck, A. Petit, M. C. Brage and J. P. Descroix Electrochem. Soc. No. 263, Fall Meeting, Detroit (1982).
11. Doddapaneni, Eradcom-TR-81-0381-F Final Report.
12. S. Szpak and H. V. Venkatasetty, J. Electrochem. Soc. submitted.
13. K. A. Klinedinst and M. J. Domeniconi, J. Electrochem. Soc., 127, 530 (1980).
14. B. Carter, R. Williams, F. Isay, A. Rodrigues and H. Frank, 17th IECEC Conference paper No. 829110 (Vol.II), Los Angeles, CA., 1980.
15. W. A. Bowden and A. N. Dey, J. Electrochem. Soc., 127 1419 (1980).
16. V. Gutmann, Coordination Chemistry in Non-Aqueous Solutions, Springer Verlag, Wien New York, 1968.
17. H. V. Venkatasetty, unpublished private communication, 1981.
18. J. O'M. Bockris and A.K.N. Reddy, "Modern Electrochemistry," Vol. 2, Chap. 10, Plenum, New York, 1973.
19. D. D. Macdonald and M.C.H. McKubre, Chapter 2 in "Modern Aspects of Electrochemistry", J.'OM. Bockris, B. E. Conway and R. E. White, Eds., Vol. 14, Plenum, New York, 1982.

Table I

	1.6 M $LiAlCl_4$	1.6 M $LiAlCl_4$ + di-Li-Pc	1.6 M $LiAlCl_4$ + CoPc	1.6 M $LiAlCl_4$ +$AlCl_3$	1.6M $LiAlCl_4$ + $AlCl_3$ + CoPc
Li/Li	0	0	0	0	0
Li/C Li/MO	3.6	3.6	3.7	3.9	4

Table I. Open circuit potential measurements in a U-type cell between two Li electrodes and between Li and C and Li and Mo.

KEY WORDS

Page 1	electrocatalysis, phthalocyanine
Page 2	cyclic voltammograms, thionyl chloride
Page 3	Nyquist plot, passivating films
Page 4	glassy carbon, rest potential
Page 5	batteries, electrocatalytic activity
Page 6	electron transfer resistance, quasi-exchange current density

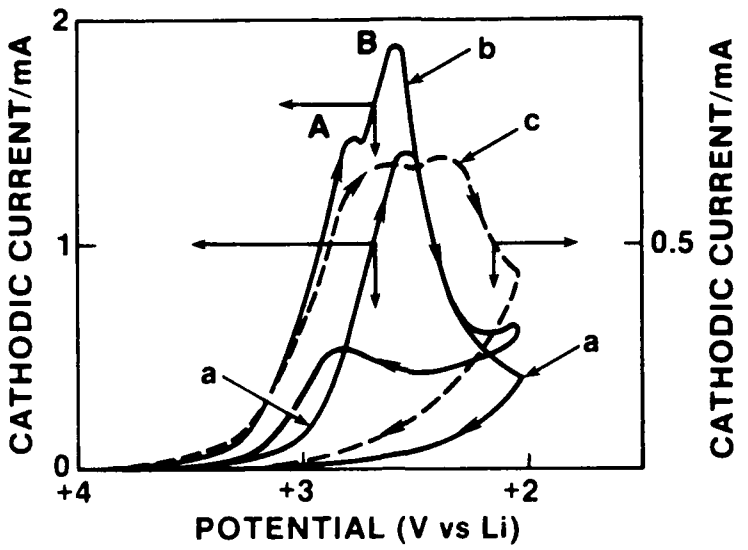

Fig 1 Cyclic Voltammograms on Glassy Carbon. Scan Rate - 50 mV s^{-1}.
Electrode Area - 0.314 cm^2.
Electrolyte - 1M $LiAlCl_4$ in $SOCl_2$ Curve a
- 0.93 M $LiAlCl_4$ - 0.07 M $AlCl_3$ in $SOCl_2$ Curve b
- 0.4 M $LiAlCl_4$ - 0.6 M $AlCl_3$ in $SOCl_2$ Curve c.

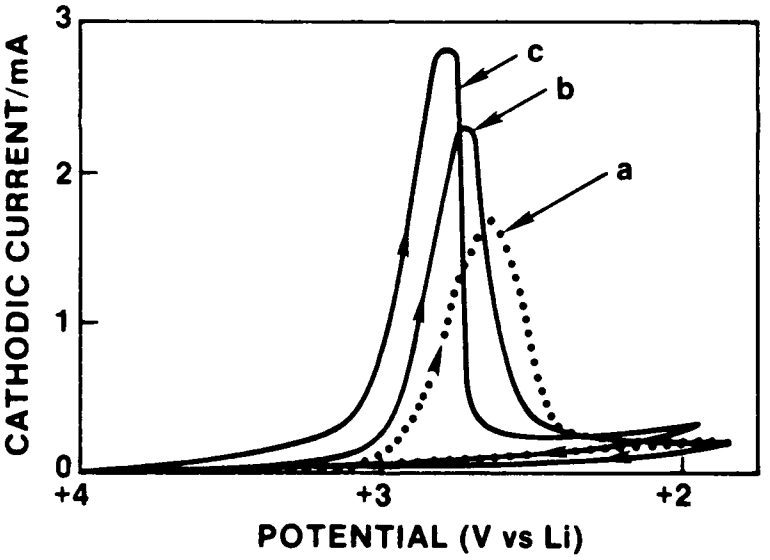

Fig 2 Cyclic Voltammograms on Glassy Carbon. Scan Rate - 50 mV s^{-1}.
Electrode Area - 0.314 cm^2.
Electrolyte - 1M $LiAlCl_4$ in $SOCl_2$ Curve a
- 1M $LiAlCl_4$ in $SOCl_2$ saturated with Cu-phthalocyanine Curve b
- 1M $LiAlCl_4$ in $SOCl_2$ saturated with Fe-phthalocyanine Curve c.

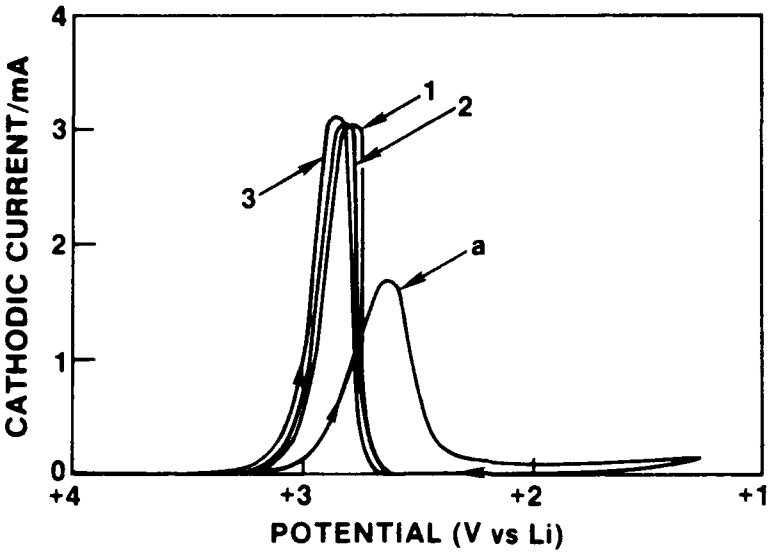

Fig 3 Cyclic Voltammogram on Glassy Carbon. Scan Rate - 50 mV s^{-1}.
Electrode Area - 0.314 cm^2.
Electrolyte - 1M $LiAlCl_4$ in $SOCl_2$ Curve a
- 1M $LiAlCl_4$ in $SOCl_2$ saturated with Co-phthalocyanine; the numbers 1, 2 and 3 refer to consecutive runs in between which the electrode was repolished.

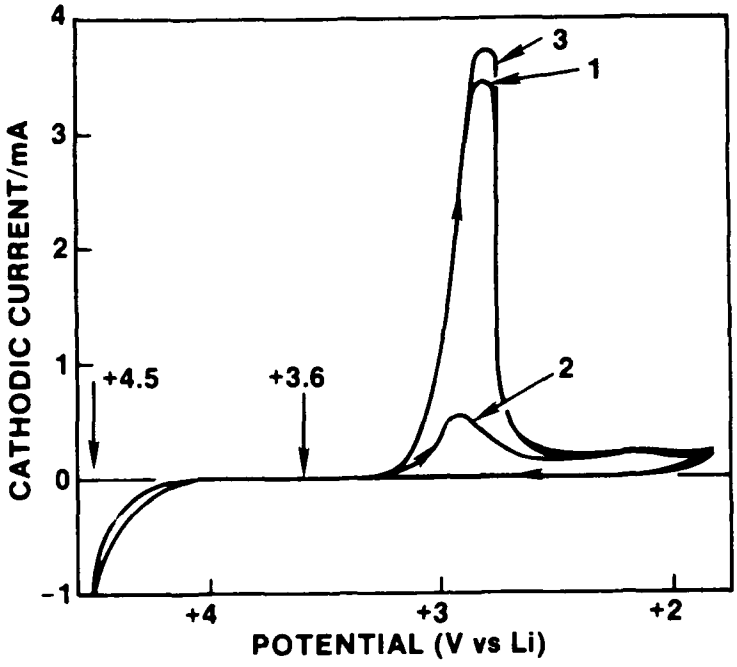

Fig 4 Cyclic Voltommogram on Glassy Carbon. Scan Rate - 50 mV s^{-1}.
Electrode Area - 0.314 cm^2.
Electrolyte - 1M $LiAlCl_4$ in $SOCl_2$ saturated with Co-phthalocyanine.
Scan Initiation - Curve 1 and 2 consecutive curves from +3.6 V on.
- Curve 3 after Curve 2 from +4.5 V on.

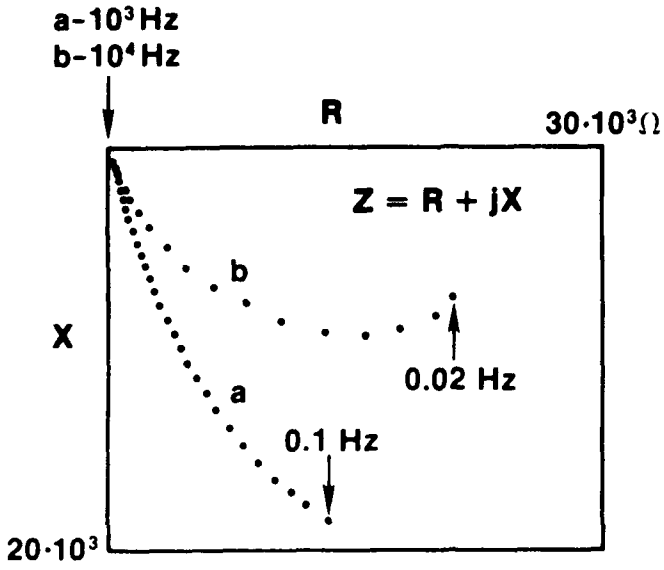

Fig 5 Nyquist Plot. Electrode - Glassy Carbon; Area - 0.316 cm^2.
Electrolyte - 1M $LiAlCl_4$ in $SOCl_4$ for Curve a
1M $LiAlCl_4$ in $SOCl_2$ saturated with Fe-phthalocyanine for Curve b.

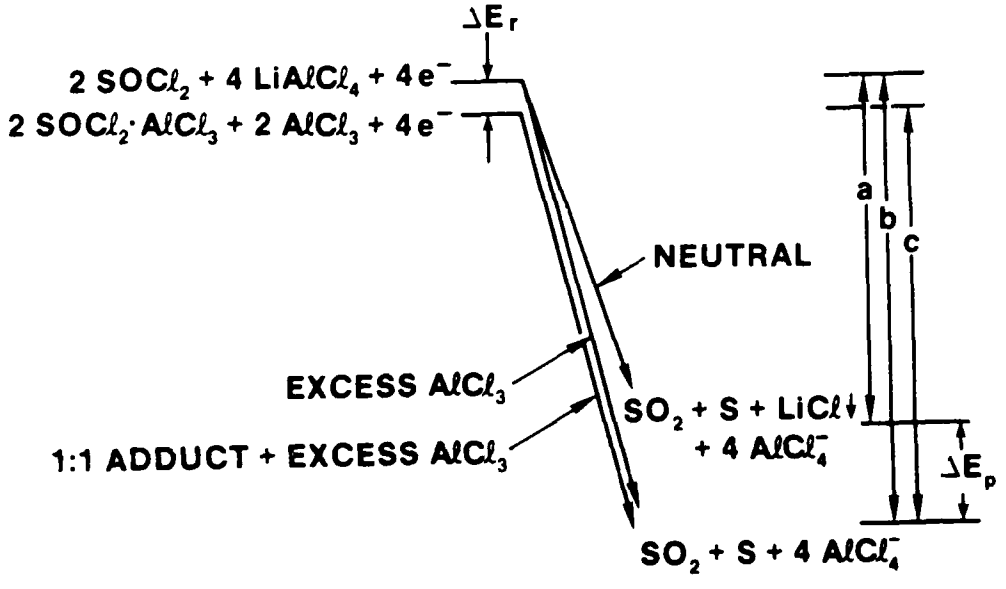

Fig 6 Energetics of the $LiAlCl_4$ - $AlCl_3$ - $SOCl_2$ - System.

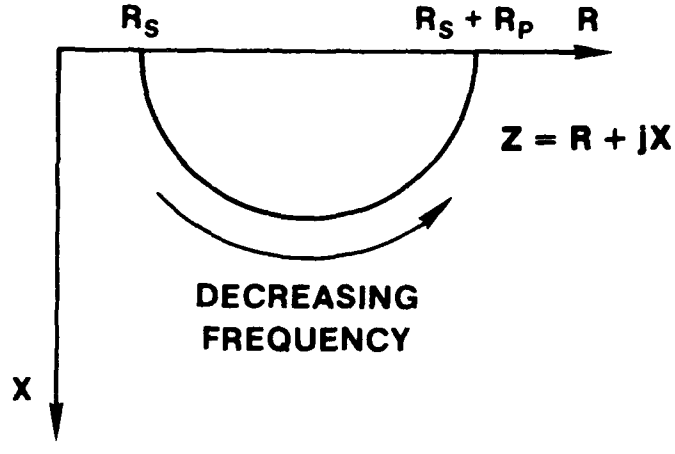

Fig 7 Nyquist Plot.
R_S = Solution Resistance.
R_P = Electron Transfer Resistance.

ON THE MECHANISM OF $SOCl_2$ REDUCTION IN LITHIUM CELLS

S. Szpak and P. A. Mosier-Boss
Naval Ocean Systems Center, San Diego CA 95152-5000
J. J. Smith
Department of Energy, Washington DC 20545
R. J. Nowak
Office of Naval Research, Arlington VA 22217-5000

The reaction path of the $SOCl_2$ reduction from electrolytes containing dissolved $AlCl_3$, with and without the addition of LiCl, is examined by IR-reflectance spectroscopy and cyclic voltammetry. The IR- spectroscopic investigation provides information on the sequence the various $SOCl_2$ - bearing species are reduced. In particular, onium ions accept electrons at low overpotentials while the $Li(\leftarrow OSCl_2)_2^+$ species require an overpotential in excess of 1.0 V for the reduction to occur. The importance of the interplay between participating processes and the charge transfer is indicated by the scan rates and the shape of voltammograms as a function of concentration of the electroactive species. This interplay emphasizes the need for a better understanding of the role of the electrode/electrolyte interphase during cell/battery discharge.

Thermodynamic considerations prescribe metallic lithium and elemental fluorine as the active elements to assure the construction of the highest energy density electrochemical power source. Although the use of lithium as the negative electrode is generally accepted, the use of fluorine as the positive electrode is not yet technologically feasible. The search for the positive electrode material has resulted in the proliferation of *Li* - cells, among them the $Li/SOCl_2$ battery. Historically, the $Li/SOCl_2$ system has evolved from the exploration of new concepts in liquid lasing rather than from thermodynamic reasoning.

The $Li/SOCl_2$ system exhibits a high theoretical specific energy density and the cell is easy to construct. Thus, it is not surprising that, shortly after its discovery, an intense development effort was undertaken, followed by claims and counterclaims. Some of these claims were of a promotional nature, others arose from a lack of a fundamental understanding of the discharge processes occurring within the cell interior. Similarly, theories on the mechanism(s) of the charge transfer process(es) have been advanced without substantial evidence offered in support(1-4). Indeed, the extent of solid information available was very meager when a question was posed as to whether or not the $Li/SOCl_2$ system can sustain a current density of *ca* 100 mA cm^{-2} for about 10 minutes. Today, the answer is yes; However, a much broader question remains unanswered, *viz.* what is the system operational capability with regard to power output and extractable energy content for an *a priori* selected discharge rate?

This communication attempts to provide a partial answer to this question through the discussion of the mechanism of the $SOCl_2$ electroreduction from practical electrolytes, *i.e.*, from electrolytes containing $LiAlCl_4$ and $AlCl_3$ dissolved in an excess of $SOCl_2$. The

discussion is limited to the systematic examination of the reduction of $SOCl_2$ from the binary and ternary systems containing $AlCl_3$ and *LiCl* and consider only the Pt/$SOCl_2$–$AlCl_3$ and the Pt/$SOCl_2$ - $AlCl_3$ - LiCl interphases.

Technology issues and method of analysis

The starting point in the identification of relevant technology issues is through cell modeling. Following the conclusions reached by Tsaur and Pollard(5), Smith *et al.* (6) showed that, in general, good agreement exists between the theory and practice and that the important factor in determining the cell lifetime is the form of the local current density/ overpotential relationship and the ensuing changes associated with the precipitation and growth of LiCl crystallites. This problem was recently examined in greater detail by Nowak *et al.* (7) in connection with the role played by the addition of Fe–Pc in a discharging Li/$SOCl_2$ cell.

Measurements of transport properties (*i. e.*, viscosity and conductivity) of $SOCl_2$- bearing electrolytes, commonly used in practical cells, indicated the concentration dependent structure of the liquid phase, whose pertinent features were deduced from the analysis of the Walden product(8). Since the electrolyte concentration changes in the course of cell discharge, it is necessary to assess the structural changes as the discharge progresses and to determine their effect on the cell performance. Furthermore, a rather cursory examination of the $j = f(E)$ curves by cyclic voltammetry has led to the conclusion that more than one $SOCl_2$ - bearing species participates in the charge transfer process(9).

In what follows, we outline suitable experimental procedures, in particular, IR- reflectance spectroscopy and cyclic voltammetry to determine which $SOCl_2$ species undergo the charge transfer process and the sequence of events associated with the energy conversion. In the case of cyclic voltammetry, we take into account the restrictions imposed by the low conductivity of the $AlCl_3$–$SOCl_2$ bulk electrolyte.

Vibrational spectroscopy. The formulation of tasks usually determines the experimental technique of choice. Thus, structural aspects of both the bulk electrolyte and the electrode/electrolyte interphase are best studied by vibrational spectroscopy, in particular, by Raman and IR spectroscopy(9). The molecular interactions were examined by decomposition of spectral bands into their Voigt profiles(10) aided and supported by molecular orbital (MO) calculations. Information on bond properties as well as inter- and intramolecular interactions can be assessed from frequencies and their shifts, band intensities, depolarization ratios and excitation profiles. The MO calculations were performed using AMPAC, a general purpose, semi-empirical molecular orbital package developed at the University of Texas at Austin, TX. These calculations yield information on the size, shape and charge distribution within moleules and complexes.

Cyclic voltammetry. Cyclic voltammetry was employed to assess and resolve the complexity of charge transfer process. This experimental technique was selected because the shape of a voltammogram is determined by two parameters only, namely the thermodynamic parameter, $\chi = Kc$, and the kinetic parameter, $\lambda = (RTc/nF)(k/v)$, where c is the concentration of the electroactive species, K the equilibrium constant, k the appropriate rate constant and v is the scan rate. These two parameters form the source/sink term in the expression for mass balance and reflect a specific set of events associated with the charge transfer reaction taking place under selected experimental conditions, Eq. (1)

$$\frac{\partial c_i}{\partial t} = D_i \frac{\partial^2 c_i}{\partial x^2} - f_i(\chi,\lambda) \qquad (1)$$

The current/time relationship, *j(0,t)* , for a linear potential scan, $E(t) = E_i^0 + |v|t$, for the N electroactive species and M adsorption processes, is given by Eq. (2)

$$j(0,t) = F\left[\sum_{i=1}^{N} n_i D_i \frac{\partial c_i}{\partial x} + \sum_{m=1}^{M} \Gamma_m \frac{d\theta_m}{dt}\right] \qquad (2)$$

where Γ_m denotes the maximum surface concentration of the *m*- th species and θ is the surface coverage. The right hand side of Eq. (2) contains contributions due to the diffusional flux *via* the sum of concentration gradients of electroactive species and the kinetics of adsorption, expressed in terms of the time rate of change in the surface coverage summed over the number of adsorption processes. Which set of processes dominates the charge transfer reaction depends, among other factors, on the rate of linear scan. In general, slow scan rates relate to the diffusional processes while fast rates expose the adsorption characteristics.

Structural aspects of $SOCl_2$ - bearing systems

The preferred composition of practical electrolytes for the discharge at 80 mA cm^{-2} is about 1.9 M $LiAlCl_4$ with a slight excess of $AlCl_3$(5). This means that, initially, most of the $SOCl_2$ remains free, *i. e.*, not complexed. However, in the course of the charge transfer reaction, the concentration of free $SOCl_2$ diminishes; thus, it is of interest to examine first the structural aspects of neat $SOCl_2$ and see how this structure is affected by the addition of $AlCl_3$ and LiCl. The effect of reaction products,in particular, SO_2 and elemental sulfur will be reported at a later date.

Neat thionyl chloride. The $SOCl_2$ molecule is of the ZXY_2 type and a member of the C_s symmetry point group. It has six normal modes of vibration, all Raman and IR active. The S–O bond of $SOCl_2$ has partial double bond character which results from the superposition of $p\pi \rightarrow d\pi$ back- bonding from O to S upon the S→O σ bond. This property will be used as a diagnostic factor in determining the various molecular interactions the $SOCl_2$ molecule undergoes in its changing environment. The S–O stretching vibration is very sensitive to changes in the charge distribution within the $SOCl_2$ molecule and, in addition, is not obstructed by other bands. The sensitivity of this vibrational mode is illustrated by studying the effect of temperature. As seen in Fig. 1, the S–O vibrational band of $SOCl_2$ recorded at 25°C is composed of two Voigt profiles at 1246.6 and 1230.5 cm^{-1} while the same band at −20°C consists of three profiles with the third profile at 1221.5 cm^{-1}. These observations suggest that neat $SOCl_2$ is a weakly associated liquid which, in turn, implies that the $SOCl_2$ molecule is amphoteric, *i. e.*, it acts simultaneously as a donor and an acceptor, Eq. (I)

$$n\ SOCl_2 \rightarrow (SOCl_2)_n;\ n = 2,3,... \qquad (I)$$

In principle, $(SOCl_2)_n$ with $n \geq 2$ may associate in two ways: *via* sulfur to oxygen bonding in either a cyclic form, for n=2, or an open- chain form, for $n \geq 2$. Dilution experiments, supported by MO calculations, indicate the presence of dimers with the open- chain spatial structure(10). The lone pair of electrons of the sulfurs are directed away from one another which, in turn, implies that the repulsion between the lone pair of electrons on the sulfur atom is chiefly responsible for the molecular structure of the dimers. At lower temperatures, dimers associate further to form higher molecular aggregates of $SOCl_2$.

The $SOCl_2$–Al_2Cl_6 system. With the addition of Al_2Cl_6, a covalent compound containing halogen bridges, a new set of Raman vibrations appears. The progressive changes in the Raman spectra are shown in Fig. 2. In addition to bands at 1108, 523, 383, 217, 167 and 114 cm^{-1}, a band at *ca* 1055 cm^{-1} emerges and gains intensity with increasing $AlCl_3$ concentration. It is noteworthy that the appearence of this band is accompanied by an increase in solution conductivity(8).

An examination of the 1000 - 1300 cm^{-1} spectral region suggests the formation of, at least, two distinct species. The first species, exhibiting a peak at 1108 cm^{-1} has been attributed to the 1 : 1 adduct, $Cl_3Al{\leftarrow}OSCl_2$. The identification of the species characterized by the broad band at 1055 cm^{-1} is less certain. For example, the broadness of this peak and the shift to lower frequency could indicate the formation of a 2 : 1 complex, $(Cl_3Al)_2{\leftarrow}OSCl_2$. But molecular adducts are neutral molecules; thus, the observed increase in the solution conductivity upon addition of $AlCl_3$ requires the formation of ionic species. The formation of ions from the 1:1 adduct can occur in two ways: (i) *via* the halide transfer, Eq. (II)

$$Cl_3Al{\leftarrow}OSCl_2 \rightarrow AlCl_4^- + SOCl^+ \qquad \text{(II)}$$

or (ii) *via* the internal exchange route, Eq. (III)

$$2\ Cl_3Al{\leftarrow}OSCl_2 \rightarrow [Cl_2Al(\leftarrow OSCl_2)_2]^+ + AlCl_4^- \qquad \text{(III)}$$

No spectroscopic evidence has been presented for the positively charged $SOCl^+$ species, as required by Eq. (II) and suggested by others(11). On the other hand, the evidence for the existance of the onium ion is quite convincing(10). Furthermore, the results of MO calculations of relative stabilities of the mono- and di-solvated onium ion favor the latter as the dominant species responsible for the increase in the solution conductivity.

The $SOCl_2$–$AlCl_3$–LiCl system. The addition of LiCl to the binary $SOCl_2$ - $AlCl_3$ system results in the destruction of the $Cl_2SO{\rightarrow}AlCl_3$ adduct, Eq. (IV)

$$n\ SOCl_2 + Cl_2SO{\rightarrow}AlCl_3 + LiCl \rightarrow (n-1)\ SOCl_2 + [Li(\leftarrow OSCl_2)_2]^+ + AlCl_4^- \qquad \text{(IV)}$$

In particular, for n = 1, *i.e.*, for the 1 : 1 : 2 molar ratio of LiCl : $AlCl_3$: $SOCl_2$, no free $SOCl_2$ should be present. Accordingly, as illustrated in Fig. 3, the spectral bands associated with the $Cl_2SO{\rightarrow}AlCl_3$ complex disappear and those characteristic of $AlCl_4^-$ and solvated Li^+ ion are present. Also, absent is the 1055 cm^{-1} peak due to the onium ion, as required by Eq. (III).

Computer generated structures and the strength of S - O bond. Computer optimized structures of $SOCl_2$- bearing species are shown in Fig. 4. These calculations suggest only slight structural changes upon complexation of $SOCl_2$ with itself, Fig. 4a, or $AlCl_3$, Fig. 4b. Significant changes do occur when forming the onium ion, Fig. 4c, where each of the complexed $SOCl_2$ molecules is affected differently. Also, of interest is to note that, except for the S–O stretch, the vibrational modes of Li^+ complexed $SOCl_2$ occur at higher frequencies than those in neat $SOCl_2$(12), which is consistent with complexation through the oxygen atom of $SOCl_2$ (11,12). Although calculations reproduce the structures of $SOCl_2$, $AlCl_3$ and $AlCl_4^-$ within 5 % on all bonds and angles, they probably are not accurate enough for unequivocally establishing the structure of complexes and related properties, nevertheless the comparison among the various species is, most likely, valid.

Structural changes can be summarized as follows: $SOCl_2$ in the liquid state, forms open-

chain dimers and/or oligomers having a zig-zag structure. The dissolution of Al_2Cl_6 occurs dissociatively with the formation of adducts which, at higher concentration, yields onium ions and $AlCl_4^-$. The addition of LiCl causes the destruction of $Cl_3Al{\leftarrow}OSCl_2$ with the formation of solvated Li^+. By comparing the frequencies of the S–O stretching vibration of the various species, the strength of the S–O bond of the interacting $SOCl_2$ molecule can be arranged in the following order of diminishing strength: $Cl_2SO > (Cl_2SO)_n$ with $n > 2 > Li(\leftarrow OSCl_2)_2^+ > Cl_3Al{\leftarrow}OSCl_2 > [Cl_2Al(\leftarrow OSCl_2)_2]^+$. Spectral data, results of MO calculations and measurements of transport properties are in agreement.

Elementary processes and the reaction path

Since the structural features of the electrolyte phase are concentration dependent, it follows that they will change in the course of the cell discharge. Consequently, the form of the current/potential relationship is expected to change. This conjecture is further supported by the observed change in the strength of the S–O bond of the various species which, in turn, depends on the composition of the bulk and the nature of the electrode/electrolyte interphase.

Electrode/electrolyte interphase. An interphase is a region formed whenever, at least, two immiscible phases are placed in contact with each other, *e.g.* , whenever an electrode is immersed in an electrolyte. This region, whether in equilibrium or not, influences the charge transfer process. During the charge transfer process the interphase consists of a series of layers, each associated with a participating elementary process. In this representation, the interphase region is an open system in which a number of consecutive processes takes place. A typical set of events is as follows: reactant molecules are brought from the bulk, b, to the electrode surface, s, by diffusion, d, followed by adsorption, a, and, after the charge transfer, products are returned back to the bulk.

The interphase region of the $AlCl_3$–$SOCl_2$ system was examined by *in situ* IR- reflectance spectroscopy. This examination revealed preferrential adsorption of onium ions on the electrode surface and a region of enrichment of both onium ions and the 1 : 1 complex in contact with the adsorption layer and the bulk, Fig. 5. This, rather significant enhancement in the concentration of onium ions in the vicinity of the electrode surface is observed both at rest potential and while cathodically polarized. Evidently, at low overpotentials the major event is the potential dependent shift in equilibria between the $SOCl_2$ -bearing species occurring within the confines of the interphase region. With a further increase in overpotential, cf. Fig. 6,new peaks appear, *viz.* at 1331 and *ca* 1150 cm^{-1} due to the formation of SO_2 and at 1190 and 1170 cm^{-1} asigned to, as yet, unidentified product(s) containing S–O bond(s). Concurrently, there is a loss in the concentration of free and complexed $SOCl_2$. It is not clear whether these species are simultaneously reduced or if only one species participates in the charge transfer process. This ambiguity cannot be resolved by kinetic arguments alone; however the MO calculations favor the discharge from the adsorbed onium ion.

Shape of voltammograms. A typical voltammogram for the $SOCl_2$ - $AlCl_3$ system is shown in Fig. 7. The characteristic feature of the reductive scan is the appearance of current plateaus, with the first j_A, extending over a considerable range of overpotentials, followed by a narrow, second plateau, j_B. The development of such plateaus suggests coupling of chemical reaction(s) to the charge transfer process. The occurrence of current plateaus and, in general, the shape of the voltammograms can be explained by the consideration of a reaction

zone, sandwiched between the adsorption and diffusion layers, under the added stipulation that the interphase region operates as an open system(9).

The shape of the voltammograms as a function of scan rate, $AlCl_3$ concentration and the scan reversal potential(13) is consistent with the reaction path, Eqs. (V) and (VI)

$$A_2^+ + e^- \rightarrow P_1^{(a)};\ k_+,\ \alpha,\ E_1^0 \qquad (V)$$

$$P_1^{(a)} + e^- \rightarrow P_2^{(a)};\ k_+ \ll k_-\alpha,\ E_2^0 \qquad (VI)$$

Thus, the reduction of $SOCl_2$ in the $AlCl_3$ - $SOCl_2$ electrolyte occurs *via* the two-electron transfer, of which the first is irreversible while the second is quasi-reversible with $k_+ \ll k_-$ and E_2^0 more positive than E_1^0. Furthermore, as illustrated in Fig. 8, adsorption processes play a key role in the reaction mechanism giving rise to mild auto-catalytic effects. Also, diffusional processes modify the adsorption characteristics. It is noteworthy that both $P_1^{(a)}$ and $P_2^{(a)}$ species are stable in the adsorbed state but not in the environment of the adjacent layers where they undergo chemical reaction(s) creating the reaction layer, r, and yielding Cl^-, elemental sulfur and SO_2. Figure 8 illustrates the structure of the interphase and summarizes the process of electroreduction of the $SOCl_2$–$AlCl_3$ system,where symbols A_0, A_1 and A_2^+ are substituted for neat $SOCl_2$, the 1:1 complex and the onium ion, respectively. At rest potential, j=0, the interphase is at equilibrium, [*i. e.* , the question of reversibility of the open circuit potential(9) is disregarded, since it cannot be confirmed by IR- reflectance spectroscopy(10)] and consists of two layers: an adsorption and enrichment layers in contact with the bulk electrolyte, identified by superscripts a, i and b, respectively. The structure of the polarized interphase is more complex. As illustrated in Fig. 8b, we find two additional layers: the reaction layer, r, sandwiched between the enrichment and the adsorption layer and the diffusion layer.

Effects of LiCl addition. The addition of LiCl to the electrolyte phase is expected to modify the j=f(E) relationship for, at least, two reasons: first, the presence of Li^+ tends to change the structure of electrolyte thus affecting the characteristic features of the electrode/electrolyte interphase both, initially and in the course of the charge transfer process. These changes include the displacement of $SOCl_2$ molecules by SO_2 to yield $Li(OSCl_2SO_2)^+$ and $Li(SO_2)_3^+$(14). Second, because there is a substantial increase in the electrical conductance which, *nota bene*, is also the result of structural changes of the electrolyte phase.

The effect of LiCl addition on the shape of voltammograms is illustrated in Figs. 10 and 11. In particular, Fig. 10 shows the effect of LiCl concentration on the shape of the reductive and oxidative parts of the voltammogram while Fig. 11 illustrates the effect of changing the scan rate. A cursory examination of Fig. 10 shows that the presence of Li^+, even at small concentrations, has a profound effect on the magnitude of the charge transfer current density except at very low overpotentials. Of interest is the fact, however, that no change in the shape of voltammograms has occurred which means that the participating events are likely the same but their rate(s) is (are) accelerated.

Examination of the Pt/$SOCl_2$–$AlCl_3$–LiCl interphase by IR- reflectance spectrosopy offered some insight into the compositional changes associated with the prsence of Li^+. In particular, as illustrated in Fig. 12, a new peak due to $Li(\leftarrow OSCl_2)_2^-$ appears. Unfortunately, the S–O stretching frequency of the $SOCl_2$ complexed with Li^+ obscurs peaks at 1171 and 1195 cm^{-1} observed upon cathodic polarization. Consequently, it is not possible to assess the degree of interaction, if any, between products P_1 and/or P_2 and Li^+ - bearing species. On the positive side, the IR- reflectance spectroscopy supports an earlier suggestion

concerning the reduction of complexed $SOCl_2$ in successive order with that complexed to Li^+ occurring at the highest overpotentials.

Concluding Remarks

The studies on the mechanism of $SOCl_2$ electroreduction are not yet completed. Nevertheless a somewhat clearer picture has emerged that provides a better insight into the nature and complexity of events occurring within the confines of a discharging cell. In closing, we address the importance of the structure and composition of the electrode/electrolyte interphase.

The results clearly indicate that $SOCl_2$ is a reactive molecule. In the liquid state $SOCl_2$ forms dimers and higher molecular aggregates. It also forms both neutral complexes as well as ionic species arising from an internal exchange reaction with $AlCl_3$, Eq.(III), and interacts with Li^+. Thus, a practical electrolyte is characterized by a complex set of equilibria in which the degree of interaction varies, as evidenced by the strength of the S–O bond. Consequently, the electroreduction most likely involves a set of complex consecutive events.

The difference in the energy states of $SOCl_2$ molecules in the $SOCl_2$ - complexes, *e. g.*, A_1, A_2^+, $Li(\leftarrow OSCl_2)_2^+$, etc., suggests the potential dependent sequence of the charge transfer. In acidic solutions, the $SOCl_2$ in A_2^+ is reduced first while the reduction of $Li(\leftarrow OSCl_2)_2^+$ occurs at overpotentials in excess of 1 V. The composition and structure of the interphase changes with the passage of current: the reacting species are used-up thereby shifting the chemical equilibria to produce more of the electroactive species. Furthermore, the reaction products modify the interphase , *i. e.* , Cl^- reacts with the 1 : 1 complex to form $AlCl_4^-$ and SO_2 displaces $SOCl_2$ in the Li - complex to yield $Li(OSCl_2SO_2)^+$ - species. As a result, there is a complicated coupling between the charge transfer process and the chemical equilibria.

The effect of concentration and scan rate on the shape of voltammograms further illustrates the interplay between the processes at the electrode surface with those within the interphase and the bulk. Thus, the importance of the interphase region cannot be overemphasized and the interplay between the various processes cannot be ignored.

Acknowledgement

This work was supported, in part, by the Office of Naval Research.

References

1. N. Doddapaneni, *Extended Abstract Nr 360* , Electrochemical Society Fall Meeting, Detroit MI 1982
2. B. Carter, R. Williams, F. Tsay, A. Rodriques and H. Frank, *Proc. 17 th IECEC Conf., paper Nr N 829110* , Los Angeles CA 1980
3. W. A. Boden and A. N. Dey, J. Electrochem. Soc., 127, 1419 (1980)
4. W. K. Istone and R. J. Brodd, ibid., 129, 1863 (1982)
5. K. C. Tsaur and R. Pollard, ibid., 131, 975 (1984); 131, 984 (1984); 133, 2296 (1986)

6. J. J. Smith, S. Szpak and W. A. West, *Function of Electrocatalysis on the Reduction of* $SOCl_2$ *at Porous Electrodes* , in Power Sources 11, L. J. Pearce, ed., International Power Sources Symposium, 1987
7. R. J. Nowak, D. R. Rolison, J. J. Smith and S. Szpak, Electrochim. Acta, 33, 1313 (1988)
8. S. Szpak and H. V. Venkatasetty, J. Electrochem. Soc.,131, 961 (1984)
9. M. Madou and S. Szpak, ibid.,131, 2471 (1984)
10. P. A. Mosier - Boss, R. D. Boss. C. J. Gabriel, S. Szpak, J. J. Smith and R. J. Nowak, J. Chem. Soc. Far. Trans. I, in press
11. D. A Long and R. T. Bailey, Trans. Far. Soc., 59, 594 (1963)
12. P. A. Mosier-Boss, S. Szpak, J. J. Smith and R. J. Nowak, J. Electrochem. Soc., submitted (Jan 1988)
13. P. A. Mosier-Boss, S. Szpak, J. J. Smith and R. J. Nowak, J. Electrohem. Soc., submitted, Sept. 1988
14. G. Mairesse, *Doctoral Dissertation* , Lille, 1978

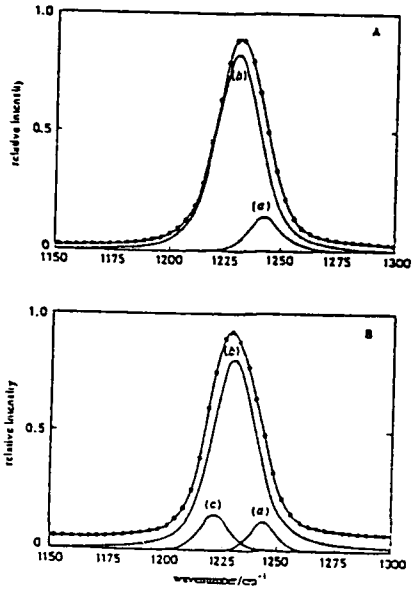

Fig. 1. Decomposition of S-O stretching band of neat $SOCl_2$ into Voigt profiles: A at 23.5°C; B at -20°C.

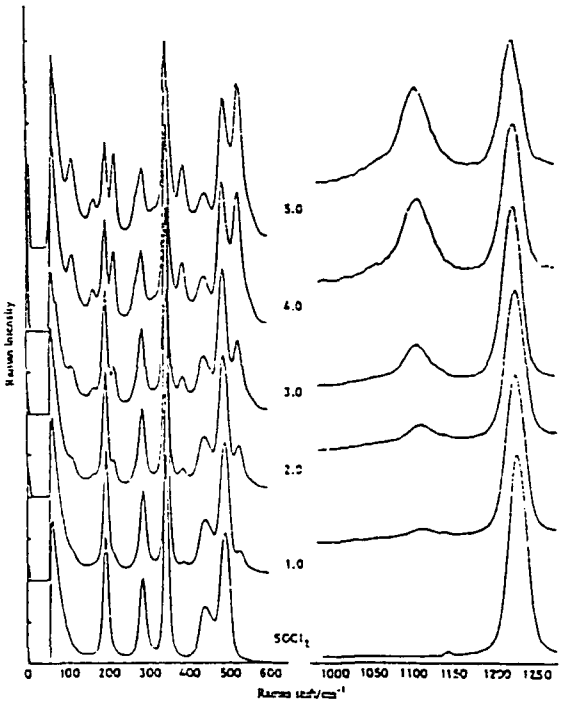

Fig. 2. Evolution of Raman spectra as a function of concentration (mol l^{-1}). 1:1 complex at 1108 cm^{-1} and onium ion at 1055 cm^{-1}.

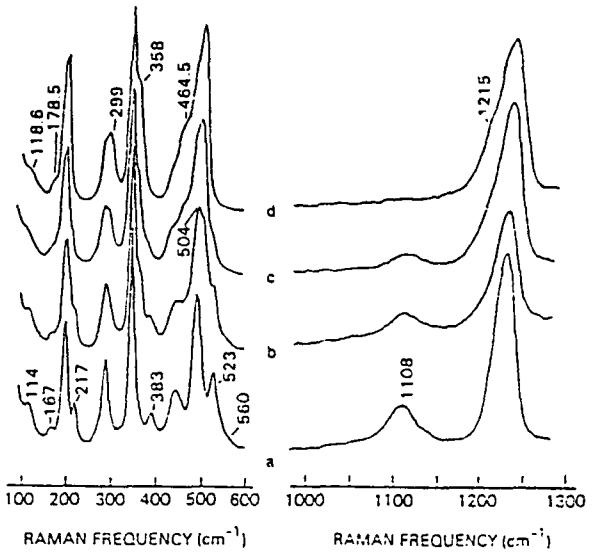

frequency/ cm^{-1}	vibrational mode
114	$AlCl_3$ rocking of $Cl_3Al{-}OSCl_2$
119	Cl-Al-Cl bend of $AlCl_4^-$
167	$AlCl_3$ bend of $Cl_3Al{-}OSCl_2$
178	Cl-Al-Cl bend of $AlCl_4^-$
217	SCl_2 bend of $Cl_3Al{-}OSCl_2$
299	$OSCl_2$ torsion of $Li(-OSCl_2)_2^+$
358	Al-Cl sym. stretch of $AlCl_4^-$
383	Al -O stretch of $Cl_3Al{-}OSCl_2$
464	S -Cl asym. stretch of $Li(-OSCl_2)_2^+$
504	S -Cl sym. stretch of $Li(-OSCl_2)_2^+$
523	S -Cl sym. stretch of $Cl_3Al{-}OSCl_2$
560	$AlCl_3$ stretch of $Cl_3Al{-}OSCl_2$
1108	S -O stretch of $Cl_3Al{-}OSCl_2$
1215	S - O stretch of $Li(-OSCl_2)_2^+$

Fig. 3. Raman spectra of $LiCl-AlCl_3-SOCl_2$ system:
a. 3.0 M $AlCl_3$ in $SOCl_2$
b, c, and d. 3.0 M $AlCl_3$ + x M LiCl in $SOCl_2$, with x = 1.0, 2.0 and 3.0, respectively.

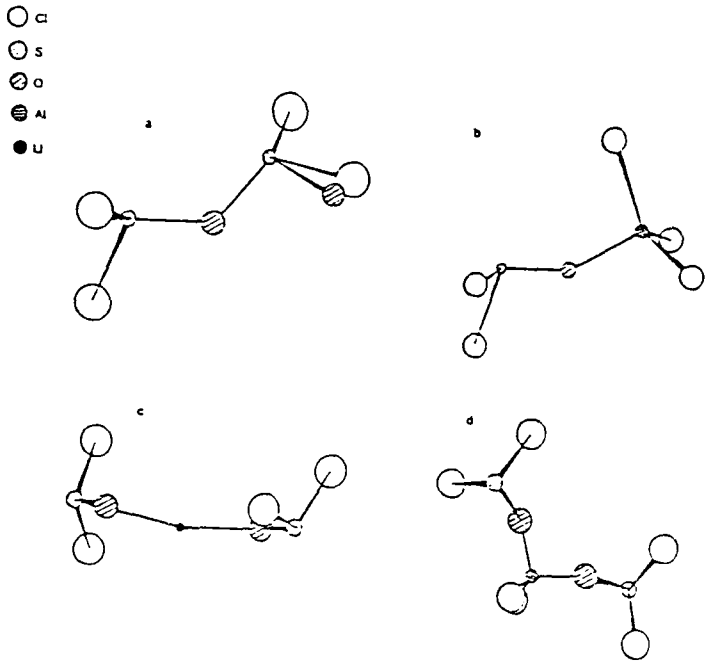

Fig. 4. Computer generated structures:
a. dimer, $(SOCl_2)_2$
b. 1:1 complex, $Cl_3Al\text{-}OSCl_2$
c. 1:2 complex ion, $Li(\text{-}OSCl_2)_2^+$
d. onium ion, $[Cl_2Al(\text{-}OSCl_2)_2]^+$

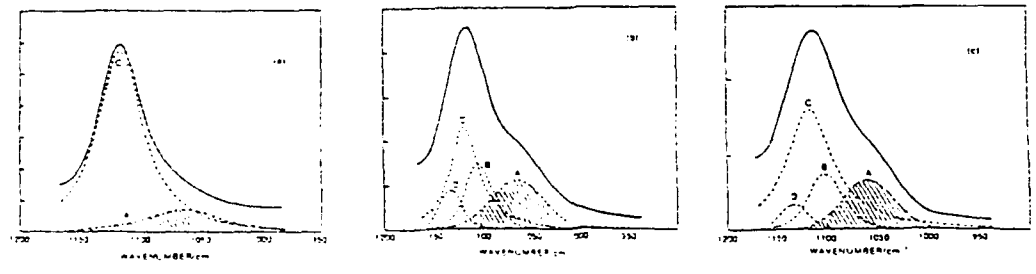

Fig. 5. The 950 - 1150 cm^{-1} IR-spectral region decomposed into Voigt profiles (electrolyte = 4.0 M $AlCl_3$ in $SOCl_2$):
a. trasmittance spectrum
b. reflectance spectrum from Au electrode
c. reflectance spectrum from Pt electrode

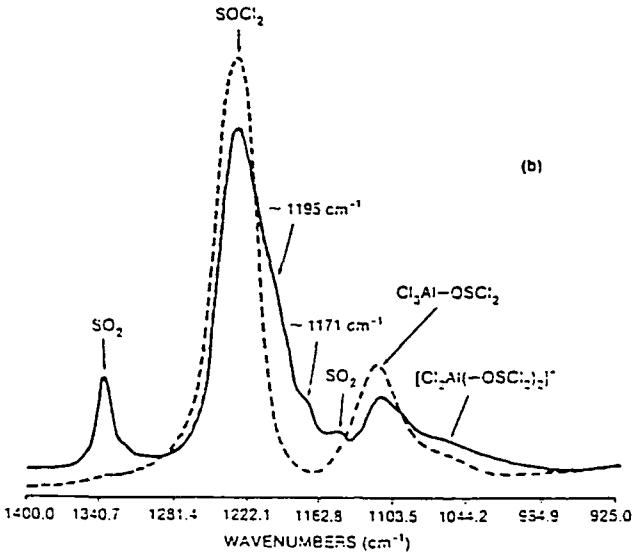

Fig. 6. The 950 - 1150cm^{-1} spectral region of the Pt/$SOCl_2$-4.0 M $AlCl_3$ interphase: dashed line - at rest potential; solid line - cathodically polarized at η = -3.5 V.

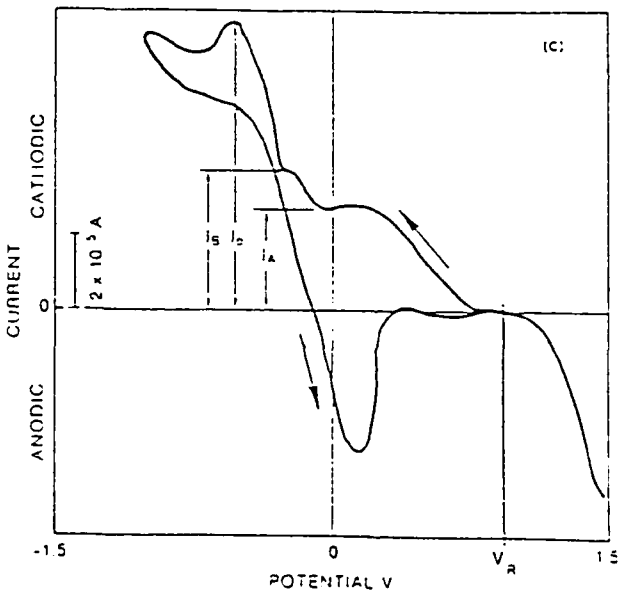

Fig. 7. Typical shape of a voltammogram. Electrolyte - 3.0 M $AlCl_3$ in $SOCl_2$; E_i^o = 900 mV v5 Ag/AgCl ref.; scan rate = 5 mV sec^{-1}.

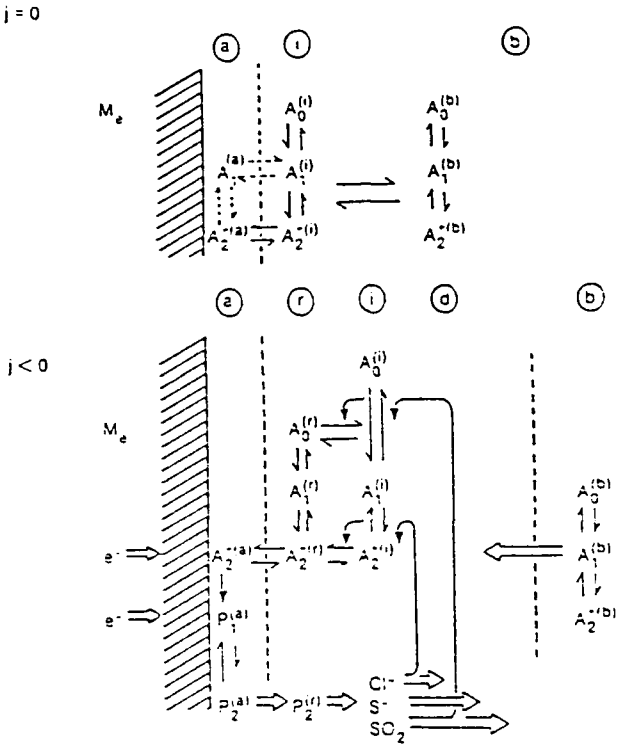

Fig. 8. Structure of, and processes within, the Pt/$SOCl_2$-$AlCl_3$ interphase: upper for j = 0; lower for j < 0. a-adsorption layer; b-bulk phase; d-diffusion (transport) layer; i-enrichment layer; r-reaction layer; A_0 - neat $SOCl_2$; A_1 - 1:1 complex; A_2^+ - onium ion.

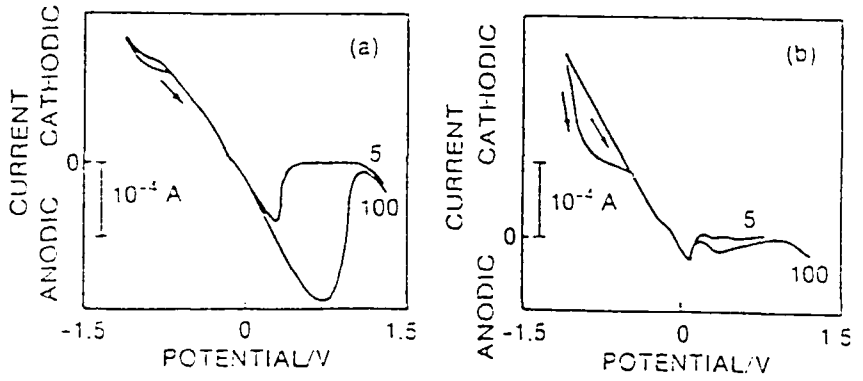

Fig. 9. Effect of reductive scan rate on the composition/adsorption features of the interphase illustrated by an oxidative scan. a. v_{red} = 10 mV s^{-1}; b. v_{red} = 100 mV s^{-1}; oxidative scan rate = indicated; Electrolyte = 3.0 M $AlCl_3$ in $SOCl_2$.

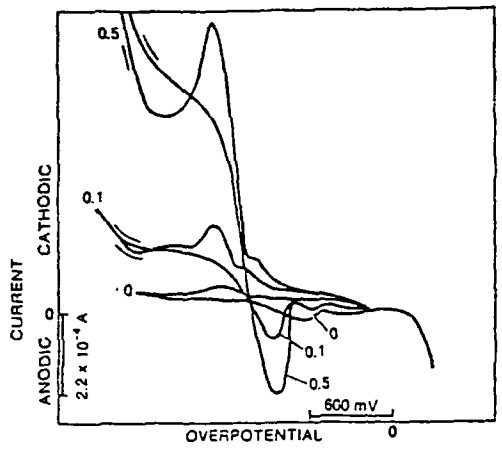

Fig. 10. Effect of LiCl concentration on the shape of the voltammograms. Electrolyte - x M LiCl and 3.0 M $AlCl_3$ in $SOCl_2$ with x = 0, 0.1 and 0.5; scan rate - v = 10 mV^3s^{-1}.

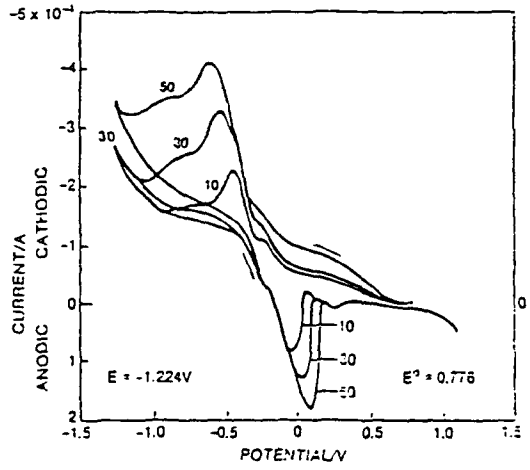

Fig. 11. Effect of scan rate on the shape of voltammograms. Electrolyte - 0.1 M LiCl and 3.0 M $AlCl_3$ in $SOCl_2$; scan rates in mV s^{-1} indicated.

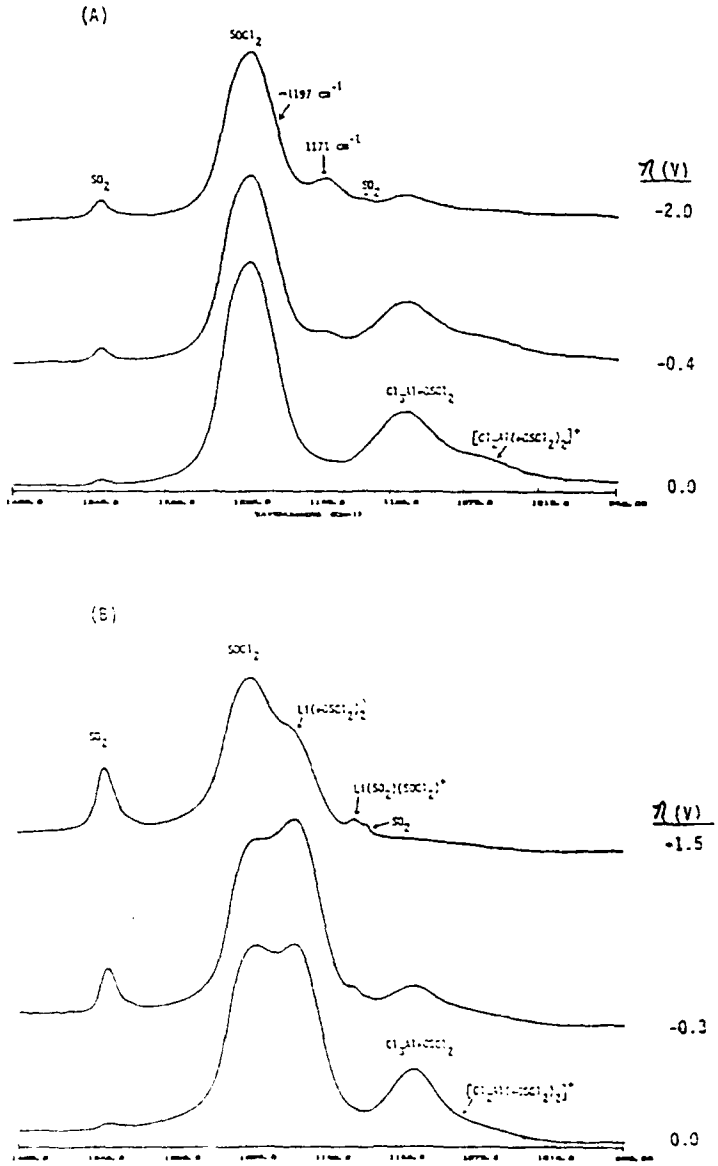

Fig. 12. The 950 - 1400 cm^{-1} IR spectral region of cathodically polarized Pt/electrolyte interphase.
upper (A) - electrolyte: 4.0 M $AlCl_3$ in $SOCl_2$
lower (B) - electrolyte: 4.0 M $AlCl_3$ and 1.0 M LiCl in $SOCl_2$
overpotentials - indicated

ELECTRIC PROPULSION: SELECTION OF A POWER SOURCE

S. Szpak and L. A. Parnell
Naval Ocean Systems Center, San Diego Ca 92152-5000

Abstract

Methods and considerations relevant to selection of power sources for use in electric propulsion systems are discussed. Electrochemical power sources are assessed generically with respect to both thermodynamic and kinetic considerations. A brief comparison is also made with thermochemical energy conversion, showing that energy desities of these two competing approaches to propulsion are quite comparable. As functional requirements and constraints are imposed on the power source and electrical propulsion system for, say, small undersea vehicles such as torpedos, the advantages/disadvantages of any particular system become much more difficult to ascertain. However, it is clear that static chemical systems are more easily evaluated than flowing and it is observed that there are no "free of charge" features.

Introductory remarks

For many years, the merits of thermal *vs* electric power sources for propulsion of underwater weapon systems have been debated. In spite of, at times, spirited discussions, the matter has not been resolved. It is not our purpose to generate more arguments for or against one or the other of the propulsion concepts. Rather, we arbitrarily selected for discussion an electric propulsion system and intend to focus on methods leading to a rational selection of the most appropriate power source from among the many electrochemical systems that are capable of meeting the mission requirements.

A general form of an expression for the energy-to-work conversion, $E \rightarrow W$, is Eq. (1)

$$\delta E = P \delta K \qquad (1)$$

where the energy gain/loss, δE, equals the quantity transported, δK, multiplied by the corresponding potential, P. The quantities associated with the energetic process that are transported, are: *volume*, V, *entropy*, S, *electric charge*, q, and *the amount* of chemical substance, n. The corresponding potentials are, respectively: negative pressure, $-p$, temperature, T, electric potential, Φ, and chemical potential, μ. In addition, Eq. (1) defines a system where the energy conversion is localized.

The selection process implies a comparison. For comparison of power sources to be meaningful, it must start from the same form of energy and terminate with the same useable form. The starting form is invariably the chemical energy stored in the reactants and the useable form is the torque needed to turn the propeller. In thermal power sources, the chemical energy, $-\Delta H$, is converted into the torque by the following set of events, Eq. (I)

$$-\Delta H \rightarrow Q_t \rightarrow W(pV) \rightarrow Torque \qquad (I)$$

The intermediate step, $W(pV)$, is necessary because the direct conversion of heat to another form is impossible. The inefficient step is the $Q_t \rightarrow W(pV)$ conversion because thermal energy can only be utilized through its transfer to an auxiliary system which, in turn, is capable of delivering work, *e.g.*, mechanical compression of a stored gas from which heat is rejected at lower temperature. The corresponding set of events for a direct conversion is as follows, Eq (II)

$$-\Delta H \rightarrow q\Phi \rightarrow Torque \qquad (II)$$

The omission of the Q_t term enormously improves the conversion efficiency. Physically, the Q_t – term represents a chaotic motion of molecules while the $(q\Phi)$ – term is the work done by an orderly flow of electrons in an external circuit. In electrochemical systems, apart from parasitic reactions taking place in *the cell interior*, the chaos of chemical reaction occurs at well defined positions within the reaction space, *i.e.*, at the electrode surfaces. In particular, the negative electrode is an electron source while the positive electrode functions as an electron sink thereby causing the flow of electrons in an external circuit without any additional ordering process.

An item of interest: The first electrochemical energy conversion device, a $H_2 - O_2$ fuel cell, was constructed in 1839. The enormous gain in the efficiency of the direct conversion was, of course, recognized and, at the turn of century, Ostwald advocated the use of the conversion *via* electrochemical processes. Although sound advice and given with authority (after all, Ostwald was a leading scientist of that period), no real progress has been made until *ca* 1950, because of the lack of understanding of the electron transfer process .[1]

Battery vs reciprocating engine

One of the criteria to select a power source is to assure the power output for the required time of operation. As shown in Fig. 1, for missions of short duration reciprocating engines deliver substantially more power than batteries. However, the difference in power output between the reciprocating engines and batteries diminishes with increasing delivery period, becoming insignificant at *ca* 30 minutes. Figure 1 also indicates that for longer missions cryogenic engines are capable of delivering more power than batteries. Unfortunately, their size and refrigeration requirements preclude them from further considerations, at least, in the context of the present communication. The remainder of this presentation will discuss the selection in general terms rather than any particular system. Following this, however, the various electrochemical systems will be compared. We will also present arguments that for, *e.g.* , torpedo propulsion, batteries appear to be not only acceptable, but preferable power sources, especially when other operational requirements, *e.g.*, noise level, are taken into consideration.

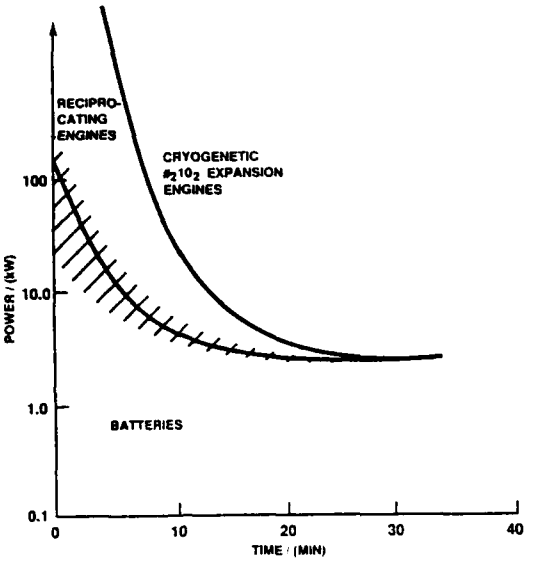

Fig. 1 - Power *vs* mission duration: a rough guide to system selection

Selling a program - Facts vs fiction

It is customary to use charts, diagrams and tables to promote the selection of a particular system as the best suited and/or most appropriate for a given mission. For the case of electric propulsion, one often hears statements such as: system A has the highest energy density yet reduced to practice, system B makes its own electrolyte, system C is the safest or least expensive, etc. In most cases such statements are correct but, are they relevant? Obviously, claims concerning the power/energy density can only be supported after construction and demonstration of a power source. The advantage provided by "making its own electrolyte" must be examined in terms of additional control devices needed to maintain the electrolyte composition within the acceptable range. Finally, the safe use of any energy dense system requires an understanding of the triggering mechanism that leads to an uncontrolled release of the stored energy.

In what follows, we attempt to separate facts from fiction, reality from imagination, and construct a set of arguments for an unbiased selection of an electric system through the use of thermodynamic criteria, kinetic considerations, as well as engineering reasoning, where the penalties for "free of charge features" are addressed.

Thermodynamic criteria

A primary battery converts chemical energy, stored in the reactants, into electrical. A spontaneous production of electricity is initiated by the removal of constraints imposed upon the system. In this sense, a primary battery is a driving system where the thermodynamic potential is the active force and the external load is the independent variable. Thermodynamic functions give the measure of the energy avilable from the system, *viz.* the enthalpy of the reaction, ΔH, which is the total energy released, and the Gibbs' free energy of reaction, ΔG, which represents the maximum amount of energy that can be converted to electrical energy. They are related by Eq. (2)

$$\Delta G = \Delta H - T \Delta S \qquad (2)$$

In summary, thermodynamics, *via* Eq. (2), provides information on the extractable energy content and such cell properties as the open cell potential, V_o, and the so-called thermoneutral potential, V_t. The V_o of a galvanic cell is a potential measured between positive and negative battery terminals under the condition of no current flow, *i.e.*, $V_o = V^{(+)} - V^{(-)}$. It is always a positive quantity and depends, as indicated by Eq. (3), only on the system chemistry and not on the physical size or shape of a cell.

$$V_o = -\frac{\Delta G}{nF} \qquad (3)$$

The other quantity of interest in the battery technology is the thermoneutral potential, V_t, Eq. (4).

$$V_t = -\frac{\Delta H}{nF} \qquad (4)$$

This quantity, also independent of the physical size or shape of the device, provides a basis for calculating the efficiencies of a discharging cell. The quoted energy contents are either calculated or obtained under near zero discharge current conditions and expressed as specific energy density, Wh/kg or Wh/dm^3, in terms of equivalent weight or volume, $kg/equiv.$ or $dm^3/equiv.$, respectively. They can be calculated provided that stoichiometry of reaction is known. The appropriate expressions are: $-\Delta G/\Sigma w$ and $-\Delta G/\Sigma v$, where Σw and Σv, denote the sum of weights and volume of reactants involved in the overall process of battery discharge. If the stoichiometry is not known, the energy content argument based on the energy density should not be used.

Pourbaix diagrams

A convenient overview of advantages and disadvantages of a galvanic cell, especially that using an aqueous electrolyte can be obtained by an examination of respective Pourbaix diagrams .[2,3] These diagrams provide a summary of thermodynamic data on conditions assuring the stability of a metal and its oxides/hydroxides as a function of the pH value of solution (composition of solution). Three examples of Pourbaix diagrams are provided in Figs. 2a, b and c; they illustrate the stability of water and aqueous electrolytes, Fig. 2a, as well as the $Al-$, and $Ag-$ potential/ pH relationships, in a somewhat simplified form, Figs. 2 b and c, respectively.

Fig. 2 - Pourbaix diagrams

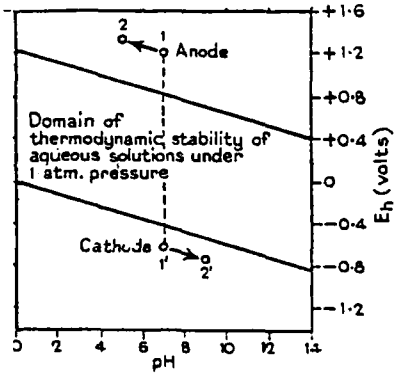

a - stability of water and aqueous electrolytes

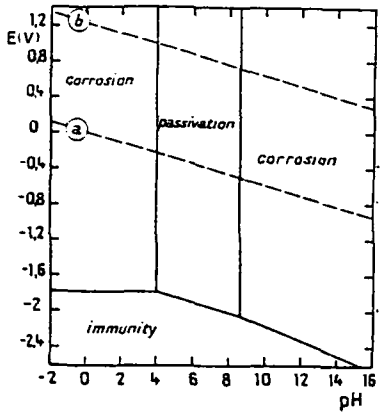

b - the Al/H_2O syystem

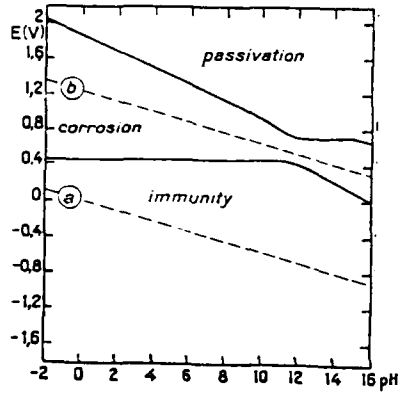

c - the Ag/H_2O system

The pH/E diagram, Fig. 2a, illustrates conditions governing the thermodynamic stability of water and aqueous solutions at 1 atm. pressure. Aqueous solutions are stable within the potential region, Eq. (5)

$$1.228 - 0.0591\ pH < E < -0.0591\ pH \qquad (5)$$

with potentials, in volts, measured *vs* the standard hydrogen reference electrode. At potentials $E > 1.228 - 0.0591pH$ water decomposes with oxygen evolution (oxidizing condition) while at $E < -0.0591pH$ it evolves hydrogen (reducing condition). The pH value denotes the acidity or alkalinity of solutions; $pH < 7.0$ for the former, and $pH > 7.0$ for the latter.

In the second example, Fig. 2b, the stability conditions for the system Al/H_2O are displayed. Here, four regions can be identified: the region of immunity, *i.e.*, the region where Al will not corrode, provided that cathodic polarization is maintained; the region of passivation, where the electrode surface is covered with oxides (hydroxides); and the regions of corrosion activities in an acid medium and in an alkaline solution. Of practical interest is the region $13.0 < pH < 16.0$. Typically, this region represents the alkalinity of electrolytes used in Al/AgO and other alkaline batteries. If not cathodically polarized, the Al electrode immersed in such electrolytes will corrode with the evolution of hydrogen. Obviously, the deleterious effects of hydrogen evolution with regard to safety cannot be overlooked. Furthermore, corrosion is a parasitic process which substantially affects the conversion efficiency. The resulting potential will be found somewhere between -2.4 and -1.2 V *vs* the hydrogen reference electrode, depending on specific circumstances.

The thermodynamic stabilty of the Ag/H_2O system is illustrated in Fig. 2c. As in the Al/H_2O system, here also the regions of immunity, corrosion and passivation are delineated. The difference, however, is that corrosion of silver occurs within the potential range where water is stable, *i.e.*, silver corrodes without the evolution of hydrogen, and the electrode passivation requires an oxidizing medium, (*e.g.* , anodic polarization).

The construction of a Pourbaix diagram for the $Al/H_2O/AgO$ cell cell is shown in Fig. 3. Conditions governing the cell stability are obtained by superimposing the respective diagrams and matching their potential scales. A set of conclusions can be drawn immediately, *viz*: the $Al-$ electrode will corrode with the evolution of hydrogen; the stability of the AgO electrode should be examined carefully; the cell potential is the difference between the AgO/H_2O electrode and the corrosion potential of the Al electrode, *i.e.*, the cell potential is expected to vary with the electrode material and solution composition; the

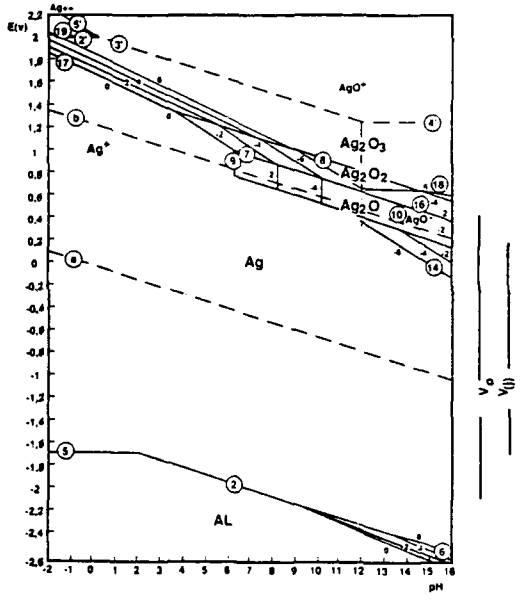

Fig. 3 - Pourbaix diagram for the $Al/H_2O/AgO$ cell

gas evolution will occur as a results of water decomposition caused by immersed Al; and the change in the pH of the electrolyte may cause electrode passivation. These observations should alert both the developer and the user to seek information on the rate of these processes in order to assess their significance in affecting mission requirements. Of special interest is the evolution of hydrogen generated by the parasitic corrosion as well as the passivation of the electrode surface. Note that if Li is substituted for Al, as in the Li/AgO battery, the evolution of hydrogen is roughly six to eight times higher thus, in practice, presenting serious problems.

Kinetic considerations

Thermodynamic considerations provide information on what is possible but not what can be realized in practice. Convenient as

they are, Pourbaix diagrams do not and cannot predict the behavior of a discharging cell/battery, because of its dynamic character which is illustrated in Figs. 4a and 4b. In particular, Fig. 4a shows a cross section of an electrochemical cell - here the $Li/SOCl_2$ cell - and lists the elementary processes while Fig. 4b presents these processes in terms of components of an equivalent electric circuit.

Fig. 4 - Functional elements of a galvanic cell and their representation

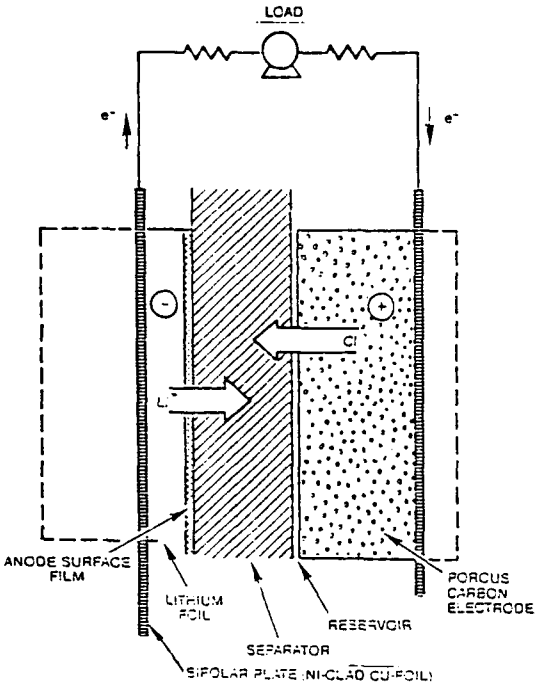

a - cross section of the $Li/SOCl_2$ cell

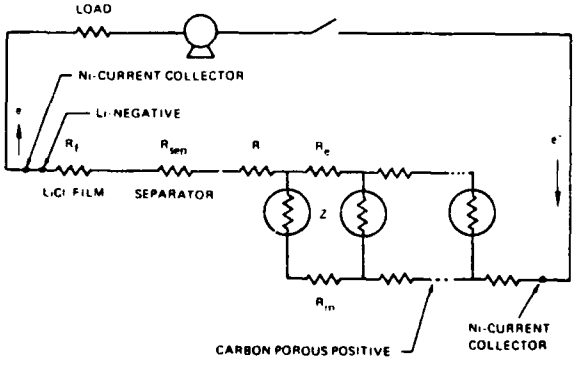

b - equivalent electric circuit analog

As indicated in Fig. 4a, any galvanic cell contains four basic functional elements that, together with the participating elementary processes, fully describe the cell discharge process, and provide a basis for comparison and selection. These four functional elements are: the negative electrode which functions as a seat for the generation of electrons *via* the oxidation reaction; the positive electrode where the reduction reaction consumes electrons generated at the negative; the separator which prevents direct contact between electrodes ; and an electrolyte which permits ionic conductance. The elementary processes occurring within the cell interior, are: the diffusion of reactants toward the electrode surface; the adsorption on the electrode surface; the charge transfer; the desorption of reaction products; the diffusion of products away from the electrode surface; the ion conduction through an electrolyte; and, to complete the cycle, the flow of electrons in an external circuit where the electrical work is delivered. This set of elementary processes consumes energy which, in turn, reduces the open circuit potential, V_o, to an operating cell potential, V, *i.e.*, the working cell potential is the open circuit potential less all of the losses associated with the cell operations.

A characteristic feature of a discharging cell is that the elementary processes occur consecutively. The slowest process, known as the rate determining step (rds), controls the overall rate and, consequently, is primarily responsible for the loss of the cell potential. Kinetic considerations deal with the examination of factors affecting the rds and, therefore also, the operational capabilities of the system under selection.

In the simplest approach, we write for the rate of a reaction an expression in the form of Ohm's law, *i.e.* , $r = kX$, where r is the reaction rate, k is the phenomenological coefficient, and X is the driving force. In terms of an electric circuit analog, the coefficient k is the resistive component and X is the equivalent potential drop across it associated with the current flow, Fig. 4b. For a set of consecutive reactions (resistive elements in series), the internal cell resistance, R_z, is, in fact, a sum of individual resistances, Eq. (6)

$$R_z = R_s + \sum_i Z_i \qquad (6)$$

Here, R_s is the resistance in the electrolyte phase; It is separated out in Eq. (6) because it can be easily calculated from the transport properties and the physical conditions in the neighborhood of the electrode surface. The second term, the electrode impedance, ΣZ_i, denotes impedances associated with individual elementary processes that take place within the immediate vicinity of the electrode surface, defined as the electrode/electrolyte interphase. In fact, it is this impedance that is the focal point and requires detailed analysis because of its specificity and non-ohmic character. Further complications arise because these processes occur within the confines of a porous structure which is always present in practice. Thus, instead of $Z_i = const.$, we have, for any discharging cell, $Z_i = Z_i(j,t)$ where j is the current and t is time. The time dependence enters through changes in the physico-chemical properties as well as the kinetics associated with the passage of charge across the interphase.

Power into load

A factor of utmost importance for propulsion technology is the power delivered to load, *i.e.*, the $jV-$ product. The potential of a discharging cell can be expressed in terms of the resistive load, R_l, alternatively the discharge current, j, by relatively simple formulas, Eqs. (7a) and (7b), respectively.

$$V(R_l) = V_0\left(\frac{R_l}{R_s + R_l}\right) \tag{7a}$$

$$V(j) = V_0 - jR_s \tag{7b}$$

with the corresponding expressions for power, P, Eqs. (8a) and (8b)

$$P = \left(\frac{V_0}{R_s + R_l}\right)^2 R_l \tag{8a}$$

$$P = jV_0 - j^2R_s \tag{8b}$$

A graphical representation of the functional dependence, Eqs. (8a) and (8b), shown in Figs. 5a and 5b, respectively, reveal the existence of a power maximum, P_{max}, when R_s equals R_l. Specifically, Fig. 5a shows the effect of load resistance on the power output while Fig. 5b displays the effect of cell internal resistance. It is seen that, as the R_s is increased, the cell power output decreases and occurs at lower discharge currents. In principle, either form can be used for further discussion. However, from a practical point of view, it is more convenient to employ Eq. (8b). This choice reflects the fact that changes in the physico-chemical properties of the cell functional elements are directly related to the amount of charge transferred, $Q = jt$, *i.e.*, to the discharge current, j. These changes arise from either the depletion of the electro-active material or the precipitation of non-conductive reaction products. In practical cells employing porous electrodes, the distribution of the charge transfer current density is highly non-linear. As a consequence, the term ΣZ_i is usually a complex function of time. The cell resistance, governing the power output is no longer constant, *i.e.*, Eq. (8b) is valid only within short period of time. In many instances, the functional dependence can be expressed analytically ;[4,5] for example, the rate of penetration, under condition of total depletion of the electro-active material, is given by Eq. (9)

$$x(t) + \lambda \tan\left(\frac{l - x(t)}{\lambda}\right) = lt/t_m \tag{9}$$

where $\lambda = (Z/\rho)^{0.5}$, indicates the degree of non-linearity of the secondary current density distribution, $x(t)$ is the time dependent position of the advancing front within the porous structure and $t_m = Q/j$ is the cell lifetime. The cell power output is accordingly given by Eq. (10)

$$P = j[V_0 - jR_s] - j^2\rho\left[x(t) + \lambda\coth\frac{l - x(t)}{\lambda}\right] \tag{10}$$

where the first term on the right hand side is the expression for a cell without porous electrodes, Eq. (8b) and the second term indicates the time dependent contribution to power loss associated with the processes occurring within the porous structure of cell electrodes. Consequently, Eq. (10) together with concepts summarized in Fig. 4b, can be used to argue the relative merits of electrochemical power systems under consideration.

Two sets of factors determine the discharge characteristics of a porous electrode: The first set, collected in ρ, accounts for those factors that contribute to the ionic transport in the direction normal to the electrode frontal surface. These factors are: diffusion, migration and convective flow. The second set, denoted by Z, represents processes occurring within the electrode/electrolyte interphase. In reality, processes of the first set interact with the processes of the second set so that a clear distinction is not always possible. In particular, in battery electrodes, both sets of parameters change in the course of charge/discharge, either because of change in the reaction path or in the electrode structure. In either case, the numerical value of the λ – parameter is affected.

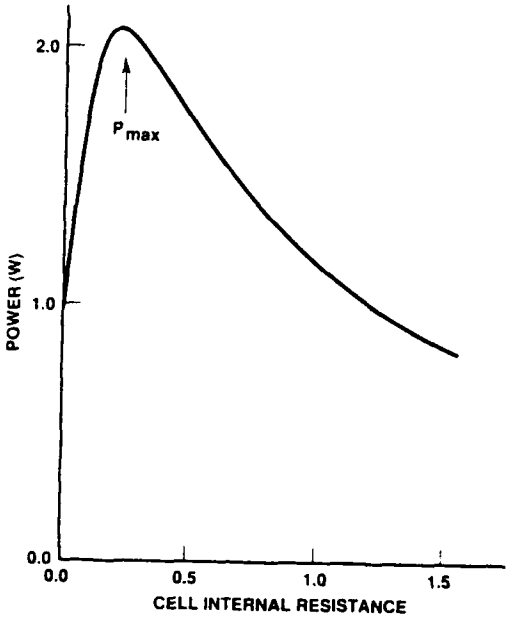

Fig. 5 - Effect of load and internal resistance on cell power output

a - effect of load resistance, R_l

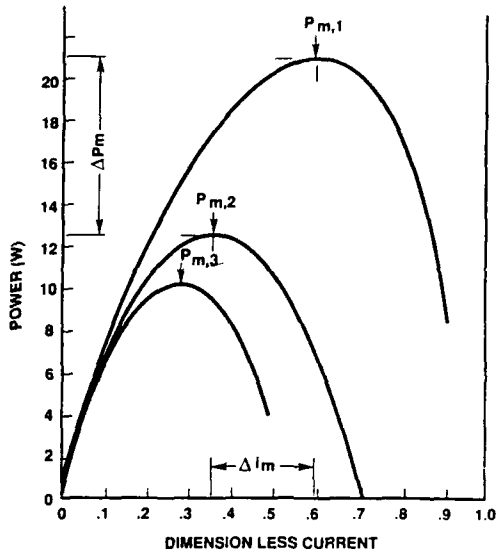

b - effect of cell internal resistance, R_s

A plot of cell power as a function of the discharge rate and the λ − parameter, Eq. (10), is shown in Fig. 6 a -d for t/t_m = 0.1, 0.3, 0.5 and 0.8, respectively. It is seen that the cell power is sensitive to this parameter within a rather narrow range. In the example considered here, to obtain P_{max} requires that λ = 0.5. This value indicates the need for an open structure with large pore size. However, if lower power output are desired, the λ − parameter should be increased.

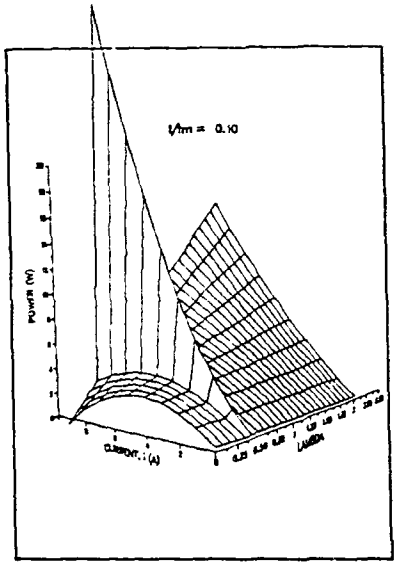

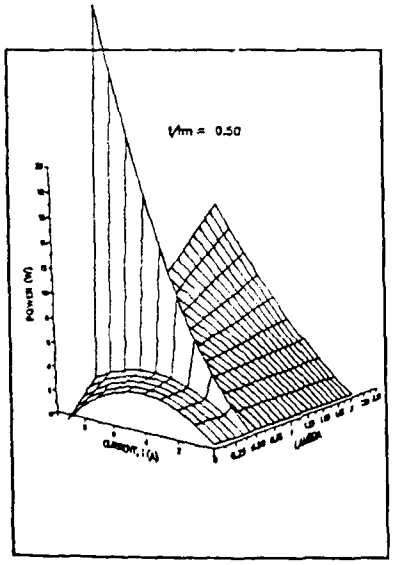

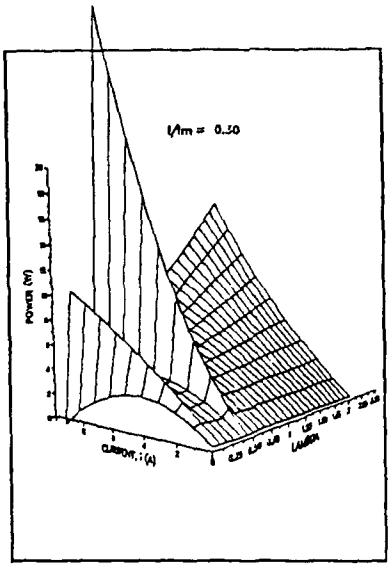

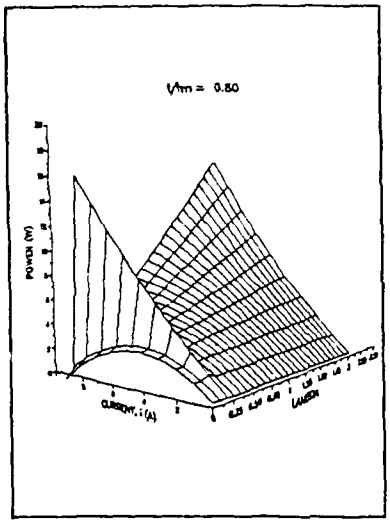

Fig. 6 - Combined effect of charge transfer kinetics and changes in electrode porous structure on cell power output at indicated discharge times

Evidence for the interplay between the first and second set of events , *i.e.* between the various processes, is provided by the plot at t/t_m = 0.3, Fig. 6b. Here, a significant increase in the cell power is observed at two values of the λ − parameter which indicates that conditions satisfying maximization of cell power can be realized.

Torpedo propulsion systems

Both volumetric and gravimetric energy densities of competing torpedo propulsion systems have been reported by numerous interested parties. Two approaches have been used: one based

on weights of reactants, and one based on a complete system. The difficulty with any of these approaches is that, in the first case, the hardware is ignored and in the second case, projections are made using without factual information. To date, only the SCEPS system provides data on complete and operational system. ADSCEPS and most, if not all, electrochemical power sources are under development and have yet be reliably produced and demonstrated.

Best estimates of energy densities of competing systems are tabulated in TABLE I. As the energy densities of advanced thermal and electrical propulsion systems are projected to be approximately equal, other relative merits of these systems should be examined. Of those usually considered, perhaps the most significant difference between SCEPS and the battery is in speed change, which clearly favor the electric propulsion. Other comparisons one might make include the following: radiated noise characteristics, which would tend to favor battery systems; turnaround cost, which is probably equal; and reliability, which currently favors SCEPS but could well favor electrochemical power sources after a comparable development period.

Table I : Comparison of propulsion systems

System	efficiency	utilization	Wh/kg- pract.
Li/SF_6	0.21	0.88	665
Adsceps	0.27	0.9	875
Li/AgO	0.41	0.7	390
Al/AgO	0.44	0.7	320
$Li/SOCl_2$	0.77	0.6	680

Concluding remarks

In a simplest case of a single cell with flat, non-porous electrodes, the selection process is straight forward. The use of porous structures for electrode matrix, a common feature in all practical batteries, introduces the first difficulty in the selection. The series-connected assembly of cells adds further difficulties due to the generation of intercell currents. These additional difficulties can be, in principle, handled but, in practice, they are the main source of disagreement among proponents of particular sytems .[6]

In short, as added features are required or constraints imposed, the advantages/disadvantages of any particular system are less clearly defined. Two comments that can be made without reservation are that there is no "free of charge feature" and that it is easier to evaluate a chemical reactor (static design) than a chemical plant (flowing electrolyte design).

Acknowledgement

This work was supported by NOSC IED program.

References

1. J. O'M. Bockris and A.K.N. Reddy, **Modern Electrochemistry**, Plenum Press, New York, 1972
2. M.N.J. Pourbaix, **Thermodynamics of Dilute Aqueous Solutions**, Edward Arnold & Co., London, 1949
3. M. Pourbaix, **Atlas of Electrochemical Equilibria in Aqueous Solutions**, Pergamon Press,1966
4. S. Szpak and G.E. McWilliams, J. Electrochem. Soc.,120, 635 (1973)
5. S. Szpak, A.K. Nedoluha and T. Katan, ibid., 122, 1054 (1975)
6. C. J. Gabriel and S. Szpak, J. Power Sources, in press

THE $Li/SOCl_2$ PROPULSION SYSTEM: RESEARCH TO DEVELOPMENT TRANSITION ISSUES

J. J. Smith
Department of Energy
Washington DC 20545
and
S. Szpak
Naval Ocean Systems Center
San Diego CA 92152-5000

Abstract

Issues normally encountered in the transition from pure through applied research to construction of engineering models (breadboard models) are discussed in general terms. Emphasis is on the interaction between technical personnel and organization rather than administrative staff. For a vehicle to identify and convey transition issues, we selected the $Li/SOCl_2$ system designed and tested for discharge rates compatible with requirements of the light weight torpedo propulsion.

Introductory remarks

The usual argument for the employment of an electrochemical power source is an efficient energy conversion from chemical to electrical, *i.e.* , a conversion free from Carnot limitations. This argument is usually amplified by a set of claims, such as: easy start-up, simple swim-out procedure, uncomplicated speed change, quiet operation, etc. The opponents of electric propulsion counter with statements concerning the "state-of-the-art" of this technology, prior commitments and expenditures and inevitably, in the case of $Li-$ systems, safety issues, after conveniently forgetting that any energy dense system is potentially dangerous if triggered and allowed to proceed in an uncontrolled manner. The $Li/SOCl_2$ system exhibits such significant advantages in energy density that the key is not to abandon it but rather to understand the operational limitations of this system and to determine triggering mechanisms so that preventive measures can be employed.

In principle, the decision to select a class of power sources from among the available ones should be based solely on technical merits. In reality, other factors are often decisive. Recently, newspaper articles provide ample evidence of procurement activities, some of which may be regarded as questionable. Here, we limit our discussion to problems associated with technical issues confronting both the management and engineering community engaged in the process of developing an electrochemical power source for torpedo propulsion and view it from the perspective of a contract monitor. Although the intent is a general presentation, the example used is very specific, *i.e.* the development of the $Li/SOCl_2$ battery.

Concept of transition

The period for a typical R & D project, from inception to production, is from 5 to 10 years, depending upon the maturity of technology at the point of initiation, the complexity of the system and the specific design requirements. Present day fiscal constraints, military considerations and international competition place great demands on scientists and engineers to accelerate and optimize development programs. Since the almost exponential growth of funding of the past decades has leveled off, much greater effort must be exercised to match opportunities presented by scientific inquiries with requirements of applications. One way to accomplish this is through a smooth transition from the concepts of fundamental research to specific technology issues and into the construction of engineering models. To achieve such a transition requires the identification and solution of problems, both technical and procedural, impeding the process.

Transition is defined as a passage from one stage to another and it can be viewed as a set of events that can be illustrated by, what is known in chemistry as, the donor-acceptor concept. For the transition to occur, ideas or results generated within the context of activities of one stage must satisfy the constraints imposed by the next stage. The nature of these constraints may vary from case to case, but, in general, they can be reduced to human factors, including management philosophy and technical considerations. The transition process is completed when an equilibrium is reached whereby conflicting interests are satisfied. These interests cannot be satisfied unless the issues are clearly defined. In practice, we are confronted with reaching an equilibrium between requirements, specifications and private interests.

Human/organizational factors

Factors affecting the transition are not exclusively of a technical nature. The attitudes of individuals and the infrastructure of the performing or supporting organizations may either facilitate or hinder the transition process. Individual attitudes can include boredom, zeal and proprietary, as well as genuine, interest in accelerated development. Obviously, the latter is no problem as long as it does not advance to overzealousness. Boredom is often encoutered: Many researchers loose interest in a problem once a solution has been identified or a feasibility demonstrated. In this case, care must be taken to maintain sufficient interest without excessive zeal which might inhibit the transition process by pur-

suing technology beyond the point necessary for a smooth transition. The situation may be further aggravated by the proverbial arrogance of which scientists are often accused. Obviously, such a perception is counter-productive. There is a natural tendency for individuals and, collectively, organizations to favor technologies discovered or proposed from within. Alternatively, individuals or organizations may seek to pursue the development produced from within, even though others are better equipped to effect the transition. The merits of technological advancement and professional judgement often surrender to misplaced priorities and decisions made long in the past. When evaluating a proposal, one often examines the organizational structure, Fig. 1a. It usually represents rational assignments and balanced division of duties, responsibilities and authorities. On-site inspection, however, often reveals that, in the meantime, changes have occurred of the type illustrated in Fig. 1b. Of course, proper organizational infrastructure and attitude can prevent these becoming issues.

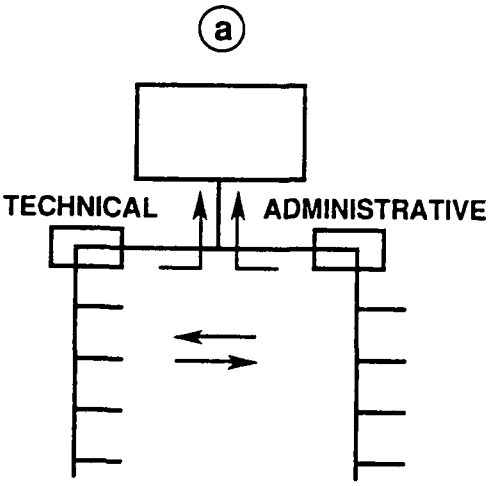

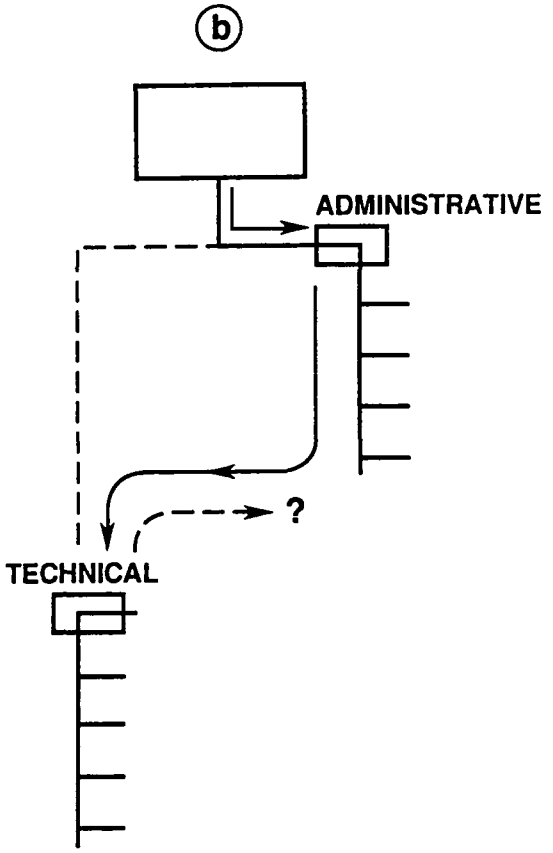

Fig. 1 - Organizational infrastructure
a - parallel (dual) system of responsibilities and authorities
b - common operational infrastructure under "load" conditions

Technical factors

Before discussing the factors affecting the transition process, we should consider the scope of each catergory of activities. Research, broadly defined, includes investigations aimed at discovery and/or interpretation of facts, revision of existing theories in light of new facts and the practical applications of such facts. The dominant feature of pure research is seeking an extension of existing knowledge for its own sake. Applied research, on the other hand, examines the use of new theories and observations for practical ends. Its prime interest is to identify the technology issues and propose their reduction to practice. The transition process provides the necessary coupling even though the boundary between them is quite nebulous. On the other hand, the boundary between applied research and development is, generally, better defined. In particular, the development phase of the transition process is the conversion of technology into a product which, at minimum, demonstrates the practicability of the technology.

A preferred transition process is illustrated in Fig. 2. A certain observation, not necessarily related to the intent of original research, gives rise to a technologically important situation. To exploit full potential of this observation, a transition from 6.1 to 6.2 is undertaken and analyzed. In particular, constraints imposed by the 6.2 activities are examined. Such examination requires a set of consultative interactions. In the same manner, further transition activities are examined.

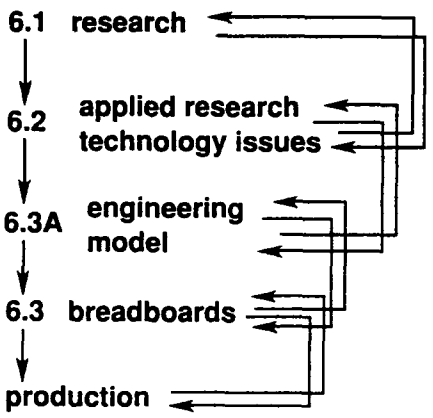

Fig. 2 - Idealized model for transition activities

Propulsion requirements-an early period

The $Li/SOCl_2$ system was first disclosed in 1973 .[1] Following that, considerable research, including applied research and exploratory development led to the transition of the technology to engineering development about 1980 and, somewhat later, a full scale effort was authorized. In 1981, the Naval Sea Systems Command funded the engineering development of the $Li/SOCl_2$ – battery at the Altus Corp., San Jose, CA and monitored by Naval Ocean Systems Center (NOSC). The transition problems and associated technology issues are summarized against this background. A word of caution: the present discussion is not intended to be a criticism of past practices nor endorsment of our views but simply a vehicle to illustrate the power of rational transition.

A great deal of enthusiasm and a rather rapid progress in the development of the low discharge rate $Li/SOCl_2$ cells prompted an immediate transition to 6.3A activities in the area of high discharge rates, *i.e.*, a jump from 6.1 to 6.3A. This jump created a new situation, a situation where the starting point in the development process was the construction of an operational 87 cell module, delivering 9 kW for eight minutes. Thus, the engineering development commenced without an existing 6.2 effort directed at high rate applications. As a result, the existing technology base 6.1 and 6.2 projects only indirectly contributed to the 6.3A effort. Figure 3 illustrates this situation in a pictorial manner. To assure the required power output, a thin cell design was adapted with the negative to positive electrode spacing on the order of a fraction of a millimeter and the discharge current density of 80 $mAcm^{-2}$. This requirement alone consituted what might be called, a "quantum jump" in this technology.

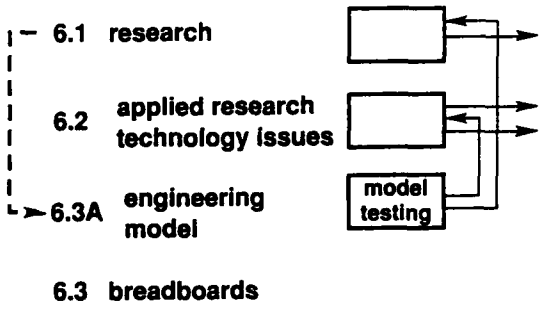

Fig. 3 - Transition activities for high discharge rate $Li/SOCl_2$ battery

To understand the consequences of this jump and to illustrate the power of rational transition, we examine Fig. 4 - a history of testing program .[2] The failure analysis is based on data from two series of tests: the 300 series, which was aimed at a discharge of 80 $mA\ cm^{-2}$ for eight minutes, and the 781 series, discharged at 60 $mA\ cm^{-2}$ for 12.7 minutes. These failures can be grouped into three broad categories: failures that occurred (i) during the manufacturing cycle, (ii) during battery discharge, and (iii) in performance. The first two categories refer to modules that failed to function as a unit at some point in the electrical test (*i.e.*, during activation, discharge or depletion). Consequently, these failures will not be considered here, inasmuch as they are not transition issues but rather the quality control (QC) requirements.

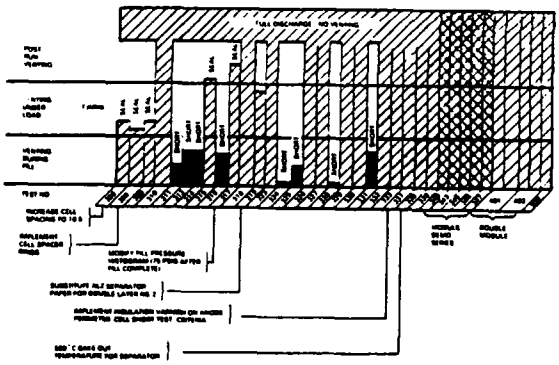

Fig. 4 - History of testing

Failures during discharge were due to electrical shorts and arose from the contradictory nature of system requirements. To meet power density requirements, a thin cell design was needed which, in practice meant a total separator thickness of *ca* 2 mils. The separator must be highly porous to minimize the iR – drop across the cell and permit rapid filling with electrolyte. In addition, the separator must be sufficiently strong to prevent distortion and tearing during assembly and activation. It also must provide a barrier to exclude the migration of carbon particles from the positive to the negative electrode. This is illustrated quite dramatically by the fact that incorrect selection of separator

material in the early phase of the development was the cause of internal shorts and fires in several modules tested (see Fig. 4). Here, again transition issues are not involved - the solution depends on better QC.

Identification of transition issues

Only performance failures, *i.e.* those failures that refer to modules that successfully completed the test procedure but failed to meet performance goals are considered. Figure 4 illustrates the unpredictibility of module performance, in general, while Table I concentrates on the cell lifetime. It is seen that modules, originally designed for eight minutes of operation at 80 $mA\ cm^{-2}$, failed the design goals. Clearly, a variation of 17 % in performance is not acceptable for any weapon system. To

TABLE I
300 series electrical performance

Electrical performance				
Test Nr	V (V)	I (A)	P (kW)	t (min)
329	277	30.3	8.38	7.90
330	278	30.3	8.42	7.85
332	278	30.7	8.53	7.30
333	280	30.9	8.65	8.20
338	279	30.6	8.54	7.60
339	281	31.0	8.71	7.30
340	279	30.7	8.56	7.00
343	279	31.0	8.65	7.50
345	275	30.3	8.33	8.00
346	280	30.9	8.66	6.80
347	279	30.7	8.57	7.10

identify the technology issues that must be resolved, we consider a discharging cell, as noted earlier ,[3] a dynamic system of interacting processes occurring within the confines of a porous structure. In a system as complex as $Li/SOCl_2$, collection of all information necessary to understand and characterize the battery is impossible so that the development of an accurate predictive model is a high priority. In fact, the rational approach to any development of this type requires an underlying model to leverage the experimental results.

Cell/battery modeling

The first modeling of the dynamics of the discharging $Li/SOCl_2$ cell was presented by Tsaur and Pollard .[4] The governing equations involved material balances, flux relations for species in the electrolyte phase, Faraday's law, Ohm's law (modified for the electrolyte phase), polarization equation, active specific surface area in the cathode and the thickness of protective film at the anode. The input data required for modeling are: initial temperature and concentration of the electrolyte, conductivities and densities of solid phases, open circuit potential and its temperature dependence and the kinetic parameters of the charge transfer reaction. Formulation of the conservation and transport equations is straight forward. On the other hand, developing expressions for the electrode kinetics requires more care and attention. This is so because the rate determining step (rds), *i.e.*, an elementary process that controls the overall rate, will change with change in potential, cathode composition and length of discharge. The usual exponential form of the kinetic relationship applies only within a rather narrow range of overpotentials. All these changes are incorporated in the model by modifying the specific surface area while retaining the Tafel-like form for the charge transfer kinetics.

Results of modeling

A typical galvanostatic discharge curve of a $Li/SOCl_2$ cell employing an acid electrolyte is shown in Fig. 5. The hump at the beginning of the discharge is due to $SOCl_2$ – reduction in an acid electrolyte, ie, the width of this hump is proportional to the excess of $AlCl_3$ initially present in the discharging cell. The slope of the central region of the $V(t)$ curve depends primarily on the properties of the $LiCl$ film at the negative electrode surface. Toward the end of the discharge, the $V(t)$ curve is governed by the events within the porous structure of the positive electrode. Qualitatively, neither the slope nor cell voltage are sensitive to the aj_o product, *i.e.* the product of the specific surface area and the exchange current density. In contrast to cell voltage, the cell lifetime is very sensitive to it. With an increase of the aj_o product, the reaction zone is shifted toward the front face of the porous structure, thus favoring rapid plugging. As indicated in Fig. 5, other factors can significantly affect the predicted cell lifetime. Thus, with small values of exponent p, the effective surface area available for the charge transfer reaction falls rapidly with $LiCl$ deposition, the reaction zone penetrates deeper into the electrode structure, and the cell operates for a longer period of time before the cathode face

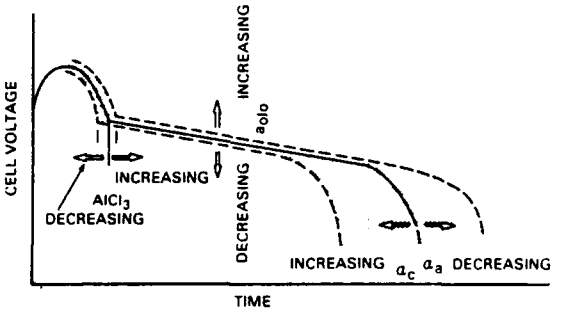

Fig. 5 - Schematic representation of a galvanostatic discharge curve; effect of change in kinetic parameters

becomes blocked. Smaller α_a and α_c also extend cell lifetime. In contrast to the effect of a change in the p parameter, this extension is due to a change in the reduction mechanism rather than a change in the electrode's physical structure.

Other observations, *e.g.* the effect of morphology and growth habits of the $LiCl$ precipitated within the porous structure, as well as the unexpected behavior upon addition of $Fe-Pc$[5], form the basis for re-examination of priorities and the initiation of much needed, but neglected, consultative interactions involving basic and applied research and developmental activities.

Re-examination of issues

Manufacturing difficulties and safety concerns led to the cancellation of the engineering development program in the 1985/86

time frame. In this, as in any other energy dense system, an uncontrolled release of the stored energy produces devastating effects. The safety issue was further compounded by the lack of understanding of the basic chemical processes responsible for battery operation which, in turn, produced an uneasiness about the ability to control them. This was the net result of a decision to transition directly to the development phase without the benefit of rational transition from 6.1 to 6. 2, thence to 6.3A activities.

Since the cancellation of the engineering development program, considerable progress has been made in understanding both the technology of the $Li/SOCl_2$ system and the design features of the high discharge rate battery. This accomplishment raises several issues: it could be argued that the decision to transition was premature because the technology was insufficiently advanced to assure success. On the other hand, it could be said that that the research and exploratory development phases were improperly addressed. Alternatively, the development community might have failed to exploit the available information and technology base in their project definition. The complexity of the system undoubtedly contributed to this shortcomings. As we see it now, there were no shortcuts then nor are there now. Consequently, it was necessary to resort to the slower but surer systematic development of understanding the basic physical and chemical properties of the individual components followed by a construction of a model to demonstrate the behavior of the final product. To this end, we set out to define a research program which would address those aspects of the technology which were impeding the construction of the high discharge rate battery as well as the most interesting scientific questions of a fundamental nature relevant to the electroreduction of oxyhalides. What follows is a brief summary of the resultant program which we, the authors of this communication, have pursued.

In the course of our research, we examined a number of issues, among them: *thermal management* [6], initiation of catastrophic events [7], magnitude of parasitic currents [8], and selected scale-up problems.[9] These problems were treated with simple models which agreed rather well with observation. The most important modeling, offering predictive capabilities, is that of Tsaur and Pollard.[4] Its range depends on how well the mechanism of $SOCl_2$ electroreduction is known. To this end, we elucidated the structural properties of the eletrolyte phase from transport properties [10], refined them by spectroscopic examination, and resolved ambiguities by theoretical calculations.[11,12] Although these studies are not completed, a somewhat clearer picture has emerged that provides better insight into their nature and complexity. A more complete discussion of these activities in the context of the $Li/SOCl_2$ high rate battery transition process can be found elsewhere.[13]

Dissemination of information is one of the essential activities aiding a rational development of the tchnology base. It encourages a free exchange of ideas and promotes discussion. It also prevents accumulation of so-called "proprietary" information, (i.e. information developed, often at public expense, for private exploitation). Review papers,[14-16] published at more or less equal intervals, were designed to summarize the progress made and identify the unresolved technology issues.

Closing remarks

Scientific development promotes its own acceleration: ideas are converted into factual observations, observations lead to applications and applications create products. But, there are also obstacles. A most common obstacle attributed to human factors is the decision to authorize the transition step. Once the decision has been reached, allocation of sufficient resources is necessary. A systematic approach to the establishment of a sound technology base is the best approach. Construction of engineering models based on "know- how" should be discouraged as too expensive. As an example, the cost to demonstrate performance of just one $Li/SOCl_2$, 9 kW module was *ca* 30 thousand dollars, while the cost of above mentioned research and exploratory development activities, summarized in 25 publications, was but a small fraction of the millions of dollars spent *via* the demonstration route.

References

1. J. J. Auborn, K. W. French, S. I. Lieberman, V. K. Shaw and A. Heller, J. Electrochem. Soc., 120, 1613 (1973)
2. S. Szpak and J. R. Driscoll, NOSC - TR 1154, vol. I, 1987
3. S. Szpak and L. A. Parnell, Joint Propulsion Conference, communication: 89-2826, Monterey CA, June 1989
4. K. C. Tsaur and R. Pollard, J. Electrochem. Soc., 131, 975 (1984); ibid., 131, 984 (1984)
5. R. J. Nowak, D. R. Rolison, J. J. Smith and S. Szpak, Electrochim. Acta, 33, 1313 (1988)
6. L. A. Parnell and S. Szpak, Electrochim. Acta, 30, 913 (1985)
7. S. Szpak, C. J. Gabriel and J. R. Driscoll, Electrochim. Acta, 32, 239 (1987)
8. S. Szpak, C. J. Gabriel and J. R. Driscoll, J. Electrochem. Soc., 131, 1996 (1984)
9. P. A. Mosier-Boss, L. A. Parnell and S. Szpak, 23-rd Joint Propulsion Conf., San Diego Ca ,1987
10. S. Szpak and H. V. Venkatasetty, J. Electrochem. Soc., 131, 961 (1984)
11. P. A. Mosier-Boss, R. D. Boss, C. J. Gabriel, S. Szpak, J. J. Smith and R. J. Nowak, J. Chem. Soc. Faraday Trans. I,85, 11 (1989)
12. P. A. Mosier-Boss, S. Szpak, J. J. Smith and R. J. Nowak, J. Electrochem. Soc., 136, 1282 (1989)
13. S. Szpak and J. J. Smith, Naval Research Reviews, to be published
14. S. Szpak and H. V. Venkatasetty, Power Sources 9, Brighton (UK) 1982
15. J. R. Driscoll, R. Pollard, J. J. Smith and S. Szpak, Power Sources 10, Brighton (UK) 1984
16. J. J. Smith, W. A. West and S. Szpak, Power Sources 11, Brighton (UK) 1987

TRANSITION ISSUES ASSOCIATED WITH THE DEVELOPMENT OF THE $Li/SOCl_2$ BATTERY TECHNOLOGY

S. Szpak

Naval Ocean Systems Center, San Diego CA 92152-5000

and

J. J. Smith

Department of Energy, Washington DC 20545

The period for a typical R&D project, from inception to production is from 5 to 10 years, depending on the maturity of technology at the point of project initiation, the complexity of the system and the specific design requirements; although occasionally longer periods may be required. Present day fiscal constraints, military considerations (*e.g.* , the fear of obsolescence of hardware) and international competition place great demands on scientists and engineers to accelerate and optimize development programs. Since the almost exponential growth of funding of the past decades has leveled off, much greater effort must be exercised to match opportunities presented by scientific inquires with requirements of applications. One way to accomplish this objective is through a smooth and expeditious transition from the concepts of fundamental research to specific technology issues and into the construction of engineering models. To achieve such a transition requires the identification and solution of problems, both technical and procedural, impeding the process. We present here a synopsis of the development of the $Li/SOCl_2$ battery technology and use this development as an example to emphasize both positive and negative aspects of the transition process.

The $Li/SOCl_2$ battery development is an excellent example because it illustrates two important points. First, a significant technological advancement was born unexpectedly as a "spin-off" from

fundamental research; a result, which in itself confirms the value of a fundamental technology-base research program. Second, it brings into focus consequences of an attempt to parallel research and engineering, *i.e.*, to accelerate the development by producing an engineering model without adequately solving the underlying technical problems and fully utilizing the power of rational transition.

Historically, the $Li/SOCl_2$ technology originated from a small Office of Naval Research (ONR) contract on new concepts in liquid lasers; a concept quite unrelated to battery technology. The careful analysis of the processes observed led to the discovery and the construction of this powerful battery system. It possesses the highest energy density of any commercially produced battery and is a leading contender for numerous military applications. Largely as a result of the latter, an intense development effort, both in this country and abroad, has been undertaken to provide the needed power sources. Some of these efforts are nearing completion, whereas others are still on-going. Among the latter is the development of a high discharge rate battery. It is upon this development activity that we focus our attention relative to the transition process.

Concept of a transition

Transition is defined as a passage or evolution from one stage to another. It is not a one-step process; rather, it consists of a set of events that can be illustrated by a donor-acceptor concept. For the transition to occur, ideas or results generated within the context of activities of one stage must satisfy the constraints imposed by the next stage. The nature of these constraints may vary from case to case, but, in general, they can be reduced to human factors, including management philosophy, and technical considerations. The transition process is completed when a kind of equilibrium is reached whereby conflicting interests are satisfied. But equilibrium conditions cannot be satisfied unless the issues are clearly defined. Using the analogy of a pendulum, an oscillatory behavior of ever decreasing amplitude is sought by identifying and dealing with driving forces as well as the opposing factors. In practice, we are confronted with reaching a compromise between requirements,

specifications, and private interests.

Before discussing the factors affecting the transition process, we should consider the scope of each category of activities. Research, broadly defined, includes investigations aimed at discovery and/or interpretation of facts, revision of existing theories in light of new facts and the practical application of such facts. The dominant feature of pure research is in seeking an extension of knowledge for its own sake. Applied research, on the other hand, examines the use of new theories and observations for practical ends. Its prime interest is to identify the technology issues and propose their reduction to practice. The transition process provides the necessary coupling even though the boundary between them is quite nebulous. On the other hand, the boundary between applied research and development is, generally, better defined. In particular, the developmental phase of the transition process is the conversion of the technology into a product which, at a minimum, demonstrates the practicality of the technology.

Factors affecting the transition process are not exclusively of a technical nature. The attitudes of individuals and the infrastructure of the performing or supporting organization may either facilitate or hinder a transition. Individual attitudes can include boredom, zeal and proprietary, as well as genuine, interest in expeditious development. Obviously, the latter is no problem as long as it does not advance overzealousness. Boredom is often encountered: Many researchers lose interest in a problem once a solution has been identified or a feasibility demonstrated. In this case, care must be taken to maintain sufficient interest without excessive zeal which might inhibit the transition process by pursuing technology beyond the point necessary for a smooth transition. The situation may be further aggravated by the proverbial arrogance of which scientists are often accused. Obviously, such perception is counter-productive. There is a natural tendency for individuals and, collectively, organizations to favor technologies discovered or proposed from within. Alternatively, individuals or organizations may seek to pursue the development produced from within, even though others are

better equipped to affect the transition. The merits of technological advancement and professional judgement often surrender to misplaced priorities and decisions made long in the past. Proper organizational infrastructure and attitude can prevent these becoming issues.

Mechanism of transition.

A conceptual representation of the transition process is summarized in Fig. 1. A certain observation, often unrelated to the intent of original research, gives rise to a set of interesting conclusions, A_j . Among them is the technologically important spin-off situation, $A_j{}^0$. To exploit the potential of $A_j{}^0$ and assess its practicability, a transition to $B_j{}^0$ must be undertaken. In practice, relevant issues must be clearly defined and solutions outlined. In terms of the donor - acceptor concept, the $A_j{}^0 \rightarrow B_j{}^0$ transition is analyzed and, in particular, constraints imposed by $B_j{}^0$ are examined. This examination requires a set of consultative interactions to secure additional fundamental information, $B_j{}^0 \rightarrow B_{j,m}{}^0$, as well as those needed for design purposes, $B_j{}^0 \rightarrow B_{j,n}$. The expected net result is a clear definition of issues as well as preferred solutions.

The sequence of activities presented in Fig. 1 is over-simplified. We considered an ideal situation, just as the theoretical scientist would choose controlled environment for his work. However, transitions from pure to applied research are diffuse because theorists formulate their problems in the simplest way and try to arrive at a clear conclusion and a well defined physical model. The reality is quite different. Only rarely can the situation be described by mathematical equations that allow solutions in closed form. The interplay occurring between the various participating processes demands highly developed computational skills to sort out the relevant from the irrelevant.

Restating, theoretical scientists deal with individual phenomena/processes which are observed under simple and controlled conditions while developmental-type persons consider the same problem in a real world environment. The process under investigation is not an isolated event but a set of events occurring simultaneously. Consequently, the mathematical treatment involves the interplay

between the various processes, with feedback conditions, usually leading to a set of nonlinear equations. Today, because of availability of fast computers, realistic modeling becomes an accessible and powerful tool to guide developmental efforts.

The development program: An early period

The $Li/SOCl_2$ battery development program was running pretty much on the 10 year R&D project life up until about 1980. Realistically, however, the completion time of the project would likely have exceeded the 10 year period, since the high discharge rate battery under development presented technical problems not yet encountered by the battery community.

The $Li/SOCl_2$ system was first disclosed in 1973. Following that, considerable research, including applied research and exploratory development were applied to the system leading to a decision to transition the technology to engineering development about 1980 with the subsequent call to develop a high discharge rate battery required for propulsion. Several proposals were reviewed, but upon review, all were rejected and the program was effectively cancelled. The technology reverted back to exploratory development, where it remains today.

A summary of activities in the early period were as follows: Much of the fundamental research was performed under the original ONR contract and subsequently in some industrial laboratories. The initial transition within the Department of Defense occurred through ONR when the Naval Ocean Systems Center (NOSC) was tasked with a small exploratory development project for a sonobouy battery. Shortly thereafter, both the Army and Air Force initiated development programs of their own. As a consequence, the characteristic feature of this period was a proliferation of military development programs and an attempt of rapid transition from applied research to engineering development.

On somewhat closer examination of this period, one negative result emerges: The objectives in each case were different. Consequently, the cross communication as well as the establishment of a common data base were inadequate. A duplication of effort was common-place with solutions of little generic value to other workers investigating this system. On the positive side, however, the technology advanced to the stage where we knew that we could build $Li/SOCl_2$ batteries. We had some understanding of the chemistry, cell design and, likely limits of performance. Also during this period, the technology was commercialized with the production of a $Li/SOCl_2$ heart pacemaker battery, a very low discharge rate system. More importantly, however, this technology spawned the formation of new companies whose objectives were to produce $Li/SOCl_2$ batteries. The expected payoff from this high energy density system for military applications led to numerous development projects. In fact, these activities drove the expansion of the field.

Development of the power dense $Li/SOCl_2$ system.

Several reasons can be cited as being responsible for the decision to cancel the engineering development transition. In general, these can be collected under the topics of safety and manufacturing. In this, as in any other very high energy density system, an uncontrolled release of the energy produces effects similar to explosives. Moreover, events with other lithium batteries had emphasized the need to ensure safe operation. The safety issue was further compounded by a general lack of understanding of the basic chemical processes responsible for battery operation which, in turn, produced an uneasiness about the ability to control the discharge.

Manufacturing uncertainties took the form of a concern as to whether the battery designs produced in the exploratory development phase could actually be scaled to the appropriate size, subject to the volume/weight specifications of the application. Issues such as thermal management, quality control, shunt current effects, and, here also safety, were involved. An additional factor contributing to cancellation of the development program was a competing technology, the so-called lithium/water

system. The exact role that this competition played in the decision to delay the transition cannot be determined. It should be noted, however, that this technology has now been abandoned altogether. Also involved in the decision was the parallel development of a thermally-based system for propul sion which, to date (and at the time of the proposed transition), is the official power source of choice for torpedo propulsion. While the latter has an overall impeding effect on acceptance of a battery power source, the effect is that of reducing time criticality, that is, relieving the pressure to develop.

Re-examination of issues

In the interim period since the cancellation of the engineering development program, considerable progress has been made in understanding both the technology of the $Li/SOCl_2$ system and the design features of the high discharge rate battery. This progress raises several issues about the transition process, presented here in a form of "Monday morning quarterbacking". It can be argued that the decision to transition was premature because the technology was insufficiently advanced to assure success. Moreover, it could be said that the research and exploratory development phases were improperly pursued either in terms of the issues addressed or in the applicability of the results produced. Alternatively, the developmental community might have failed to exploit the available information and technology base in their project definition. Reality is a combination of these factors. Again, in retrospect, the issues of safety and manufacturing along with the technical components were inadequately treated in the exploratory development phase. This was not for lack of identification, or even effort. Rather, we believe, it was due to a failure to address successfully the technical problems necessary to overcome the issues. The complexity of the system undoubtedly contributed to this shortcomings; definitive experiments were difficult to conceive and perform. As we see it now, there were no shortcuts then nor are there now. Consequently, it was necessary to resort to the slower but surer systematic development of understanding; first, of the basic physical and chemical properties of the individual components and second, of the systems as a whole followed by the con-

struction of a model to demonstrate the behavior of the final product.

Because of the attractive performance parameters for the system, we never considered dropping the technology. Rather, we set out to define a research program which would address both the aspects of the technology which were impeding the development of a high rate system and the most interesting unanswered scientific questions fundamental to $Li/SOCl_2$ and other oxyhalide electrolyte systems. What follows is a brief summary of the resultant program which we, the authors, have pursued.

Modeling. An individual cell in a battery may be viewed as an electrochemical reactor operating in response to imposed demands. When at rest, it is a constrained system that reacts spontaneously as the constraints are removed. Thus, the operation of a battery, a single cell, or even a selected functional element, is a dynamic event where the participating processes occur within a well defined reaction space. These processes, inclusive of interactions among them, can be cast into a set of precise mathematical statements. It follows, therefore, that cell modeling is among the first tasks to be undertaken when attempting the transition: ${A_j}^0 \rightarrow {B_j}^0$. In practice, difficulties arise in the formulating of an acceptable model, *i.e.*, a model that reflects the physical reality and yet, where the mathematical expressions are simple so that, at least in the preliminary stages, they yield solutions in a closed form. The modeling exercises may be of the 6.1 type, here the ${B_{j,m}}^0$ series, or the 6.2 type, here the ${B_{j,n}}^0$ series, depending upon their complexity and our current level of understanding.

In the course of our research effort, we examined a number of issues: thermal management(A.6), initiation of catastrophic events(F.4), magnitude of parasitic (intercell) currents(F.3) and selected scale-up problems(R.5). These problems were treated with simple models which agreed rather well with observation. However, the most important modeling, offering predictive capabilities, is the cell modeling by Tsaur and Pollard under a small ONR contract (F.13 and ref. therein). This relatively modest undertaking yielded information of enormous value - it focused on the fundamental issue of

the reaction path and catalytic effects, and clearly showed that the formation and growth of precipitated $LiCl$ within the porous structure must be addressed(F.8).

Mechanistic studies. Equations that describe the behavior of $Li/SOCl_2$ cell include material and energy balances, conservation of volume, Ohm's law and kinetic relationships. Formulation of the conservation and transport equations is straightforward. On the other hand, developing the expressions for the electrode kinetics requires care and attention. It is here that reliable information is of utmost importance: the input parameters for modeling exercizes, as well as proposed models, must reflect the realism of the discharging cell. To this end, we elucidated the structural properties of the electrolyte phase from the transport measurements(F.2), refined them by spectroscopic examination(F.9) and resolved ambiguities by theoretical calculations(F.5,F.9). The charge transfer reactions occurring within the $Li/SOCl_2$ cells are very complex, indeed. Although these studies are not yet completed, a somewhat clearer picture has emerged that provides better insight into their nature and complexity (F.1,F.6,F.11,F.12).

Dissemination of information. Timely dissemination of information is one of the essential activities aiding a rational development of the technology base. It encourages a free exchange of ideas and promotes discussion. It also prevents accumulation of so-called "proprietary" information, (*i.e.*, information developed, often at public expense, for private exploitation). For convenience, the information developed in the course of this program is divided into three groups, viz. review papers(R.1 -R.6), applied research(A.1 -A.7) and fundamental research(F.1 -F.13). Review papers, published at more or less equal time intervals, were designed to summarize the progress made and identify the unresolved technology issues. The second group offered solutions to well defined issues and the third was devoted to the discussion of selected fundamental aspects of the $Li/SOCl_2$ power source technology.

Another spin-off.

Scientific development promotes its own acceleration: ideas are converted into factual observations, observations lead to applications and applications create product. One such example is the extension of the $Li/SOCl_2$ cell lifetime arising from the study of the properties of the pre-passive and passive films formed on the electrode surface. In an earlier communication, we observed that a cathodically polarized electrode(C, Pt, Au)/electrolyte interphase behaves as a p-type semiconductor(F.7). Extending this investigation to the Si/electrolyte interphase, we noted the absence of passivation(F.6). Consequently, the incorporation of elemental Si into the cathode structure was predicted to substantially increase the cell lifetime(F.13). This has now been confirmed (P.1). This spin-off has led to new design concepts(F.14) and a new category of cells yielding an estimated 30 % increase in the extractable energy content.

Obstacles to effective transition.

The two most common obstacles to effective transition attributed to human factors are: (i) failure to take the next step, ie, to authorize the transition effort; and (ii) ***scientific chauvinism***, which simply means: if I cannot reproduce somebody's else results in the first (rough) trial, I will simply dismiss them as irrelevant or, at least, questionable.

Two points concerning transition activities in battery development can be made. First, it is customary to select the battery system having the highest Gibbs free energy, which is the measure of the available driving force. This fact alone, however, should not be taken as the central point because it provides no information on losses associated with cell operation. Hence, cell modeling is the perequisite to any discussion concerning the expected performance, especially at high discharge rates.

The second point concerns the allocation of resources (funding). The construction and testing of

special purpose batteries is expensive. In some of the above cited references, we have commented on the value of a systematic approach to the establishment of a sound technology base for $Li/SOCl_2$ batteries. A combination of this work with that of others (also cited in the above references) now provides a much more secure base for a high discharge rate $Li/SOCl_2$ development project. This enhancement has been achieved at a relatively modest cost, particularly when compared to some of the earlier efforts in which battery and module tests were used to collect data. As an example, the cost to "demonstrate" performance of a $Li/SOCl_2$, 9 kW module was *ca* 30 thousand dollars per module, while the cost of the above outlined activities, summarized in 25 publications in refereed journals, was but a small fraction of the millions of dollars spent *via* the "demonstration" route.

References

(i) Review papers,(R.)

1. S. Szpak and H. V. Venkatasetty, High rate $Li/SOCl_2$ power source: approach and progress, **Power Sources 9**, Proc. 13-th International Power Sources Symposium, Brighton, UK 1982

2. J. R. Driscoll, R. Pollard, J. J. Smith and S. Szpak, Development of high rate $Li/SOCl_2$ system: theory and practice, **Power Sources 10**, Proc. 14-th International Power Sources Symposium, Brighton, UK 1984

3. J. R. Driscoll, R. Pollard, J. J. Smith and S. Szpak, Selected aspects of high rate $Li/SOCl_2$ power sources technology, **Proc. 20-th IECEC**, Miami Beach FL, 1985

4. J. J. Smith, S. Szpak and W. A. West, Function of electrocatalysis on the reduction of $SOCl_2$ at porous electrodes, in **Power Sources 11**, L. J. Pearce, ed., International Power Sources Symposium, 1987

5. P. A. Mosier-Boss, L. A. Parnell and S. Szpak, Scale-up problems in batteries for propulsion, **AIAA/SAE/ASME/ASEE 23-rd Joint Propulsion Conference**, San Diego CA, 1987

(ii) Applied aspects, (A.)

1. J. R. Driscoll and S. Szpak, High discharge rate $Li/SOCl_2$ battery: SEM and EDAX examination of cathodes, **Proc. 30-th Power Sources Symposium**, Atlantic City, NJ 1982

2. J. R. Driscoll and S. Szpak, Investigation of positive electrode characteristics in high rate $Li/SOCl_2$ cells, J. Power Sources, **10**, 343 (1983)

3. H. V. Venkatasetty and S. Szpak, Properties of $SOCl_2$ -based electrolytes: conductivity, viscosity and density, J. Chem. Eng. Data, **28**, 47 (1983)

4. B. Carter, H. Frank and S. Szpak, Reaction products on current or potential reversal in $Li/SOCl_2$ cells, J. Power Sources, 13, 287 (1984)

5. J. R. Driscoll and S. Szpak, Thermal behavior of electrochemical cells by liquid crystal display, J. Power Sources, **14**, 321 (1985)

6. L. A. Parnell and S. Szpak, Thermal behavior of $Li/SOCl_2$ batteries of thin cell design, Electrochim. Acta, **30**, 913 (1985)

7. J. R. Driscoll and S. Szpak, Quality assessment of unactivated cells by AC impedance technique, J. Power Sources, **16**, 285 (1985)

(iii) Fundamental research, (F.)

1. M. Madou and S. Szpak, Investigation of $SOCl_2$ reduction by cyclic voltammetry and AC impedance measurements, J. Electrochem. Soc., **131**, 2471 (1984)

2. S. Szpak and H. V. Venkatasetty, Transport properties of $AlCl_3-SOCl_2$ - based electrolytes, J. Electrochem. Soc., **131**, 961 (1984)

3. S. Szpak, C. J. Gabriel and J. R. Driscoll, $Li/SOCl_2$ battery intercell currents, J. Electrochem. Soc., **131**, 1996 (1984)

4. S. Szpak, C. J. Gabriel and J. R. Driscoll, Catastrophic thermal runaway in Li batteries, Electrochim. Acta, **32**, 239 (1987)

5. C. J. Gabriel, P. A. Mosier - Boss and S. Szpak, Resolution of vibrational bands into Voigt profiles,

Spectrochim. Acta, 43A, 1293 (1987)

6. M. J. Madou, J. J. Smith and S. Szpak, Comments on electroreduction of $SOCl_2$, J. Electrochem. Soc., 134, 2794 (1987)

7. M. Madou, T. Otagawa, S. Gaisford, J. J. Smith and S. Szpak, Photoeffects on polarized electrodes in the $SOCl_2-LiAlCl_4$ system, J. Electrochem. Soc., 135, 262 (1988)

8. R. J. Nowak, D. R. Rolison, J. J. Smith and S. Szpak, Role of $Fe-Pc$ in a discharging $Li/SOCl_2$ cell, Eletrochim. Acta, 33, 1313 (1988)

9. P. A. Mosier - Boss, R. D. Boss, C. J. Gabriel, S. Szpak, J. J. Smith and R. J. Nowak, Raman and infrared spectrosopy of the $AlCl_3-SOCl_2$ system, J. Chem. Soc., Faraday Trans. I 85, 11 (1989)

10. S. Szpak, P. A. Mosier - Boss, J. J. Smith and R. J. Nowak, On the mechanism of $SOCl_2$ reduction in lithium cells, Proc. Battery Div., The Electrochemical Society, Oct. 1988

11. P. A. Mosier - Boss, S. Szpak, J. J. Smith and R.J. Nowak, $LiCl-AlCl_3-SOCl_2$ system: structures, species and equilibria, J. Electrochem. Soc., 136,1282 (1989)

12. P. A. Mosier - Boss, S. Szpak, J. J. Smith and R. J. Nowak, Electroreduction of $SOCl_2$. I: $AlCl_3-SOCl_2$ system. ibid., accepted

13. K. C. Tsaur and R. Pollard, Precipitation of solids in electrochemical cells, ibid., 133, 2296 (1986)

(iv) Patents, (P.)

1. M. Madou and S. Szpak, Navy Case - 69586 (Patent pending)

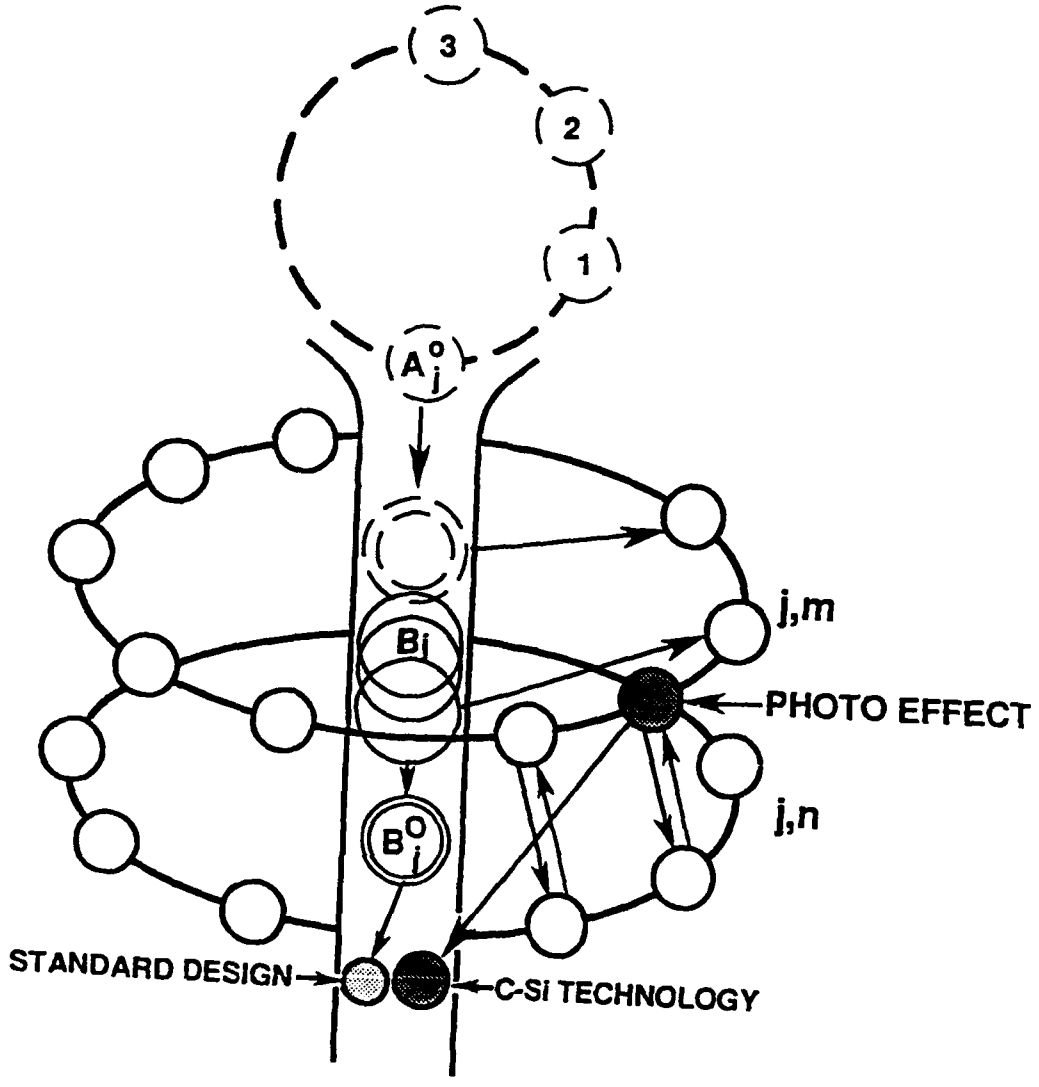
3
2
1
A^o_j
B_j
B^o_j
j,m
PHOTO EFFECT
j,n
STANDARD DESIGN
C-Si TECHNOLOGY

MECHANISTIC ASPECTS OF $SOCl_2$ ELECTROREDUCTION: EFFECT OF ELECTRODE MATERIAL

P. A. Mosier-Boss and S. Szpak
Naval Ocean Systems Center, San Diego CA 92152-5000
J. J. Smith
Department of Energy, Washington DC 20545

Abstract

The effect of electrode material on the elementary processes associated with the electroreduction of the $SOCl_2 - AlCl_3$ system is examined by three techniques: IR-reflectance spectroscopy, linear scan voltammetry and galvanostatic pulsing. The results of spectroscopic examination indicate the same reaction path regardless of material. However the shape of the voltammograms clearly show the effect of electrode material on the reaction kinetics.

INTRODUCTION

In order to maximize the power density of the $Li/SOCl_2$ electrochemical power source, two design approaches were suggested: the construction of a module containing in-series connected thin cells, as one choice, and the employment of a flowing electrolyte, as the other. To improve the performance in each of the proposed designs, modifications of both the electrode structure and composition were undertaken, with mixed results. Some difficulties were resolved through cell modeling. The conclusions reached by Tsaur and Pollard [1], Smith *et al* [2] and Nowak *et al* [3] showed that, in general, good agreement exists between the theory and practice and that the important factor in determining the cell lifetime is the form of the local current density/overpotential relation and the ensuing changes associated with the reaction path. Examination of this system by linear scan voltammetry indicated a complex reaction path suggesting that more than one species participates in the charge transfer process, *viz.* an adsorption step [4,5]. In this communication, we examine the effect of electrode material on the form of the $j = j(\eta)$ relationship. The discussion is limited to events occurring at *Au*, *C-glassy*, and *Pt* electrode surfaces. Subject to geometrical constraints, the events occurring on the smooth surfaces describe the behavior of the porous structure found in practical batteries [6].

Methodology

The effect of electrode material on the elementary processes associated with the electroreduction of the $SOCl_2 - AlCl_3$ system is examined by three techniques: IR-reflectance spectroscopy, linear scan voltammetry and galvanostatic pulsing. Experimental details have been presented elsewhere [5,7].

Electrochemical and Chemical Reactions

The electroreduction of $SOCl_2$ in practical batteries, as well as on smooth electrode surfaces, comprises one or more sets of consecutive processes occurring within an interphase region. The analysis of these processes, given in [5,7] is based on the van Rysselberghe concept of the interphase region [8], which is based on an open system whose structure is generated by, and responds to, the demands imposed by the dominating process(es). This concept is retained and, when coupled with three experimental techniques, *viz.*, IR - spectroscopy, linear scan voltammetry and galvanostatic pulsing, is used to illustrate the effect of the electrode material on the charge transfer process, its mechanism and kinetics.

The results obtained by Madou *et al* [4] showed the importance of the composition as well as the structural aspects of bulk electrolyte on the kinetics of the charge transfer process. The structural aspects of the $AlCl_3 - SOCl_2$ system were examined by vibrational spectroscopy [9]. The results of these studies revealed that (i) $SOCl_2$ is a weakly associated liquid; (ii) Al_2Cl_6 dissolves dissociatively with the formation of of a 1:1 adduct, $Cl_3Al{\leftarrow}OSCl_2$; and (iii) these adducts undergo an external exchange reaction to form $AlCl_4^-$ and onium ion, $[Cl_3Al(\leftarrow OSCl_2)_2]^+$. These conclusions were further substantiated by molecular orbital calculations [9] and solution conductivity measurements [10]. (Hereafter, for brevity, the symbols A_0, A_1, and A_2^+ will be used to denote neat $SOCl_2$, 1:1 adduct and onium ion, respectively).

An interphase region is formed whenever an electrode is in contact with an electrolyte. In-situ IR spectroscopy of the interphase region has clearly shown that there is an enrichment of 1:1 adduct and onium ion [5]. Besides the *S-O stretching vibrational bands due to* adduct and onium ion, two additional bands were observed. These bands disappear upon cathodic polarization and have been assigned to adsorbed onium ion [5,7]. Therefore at rest potential, the interphase is equilibrated with the bulk with a significant enrichment of A_1 and A_2^+ in the vicinity of the electrode surface, as shown in Figure 1. Furthermore, the interphase consists of adsorption and enrichment layers in contact with the bulk electrolyte.

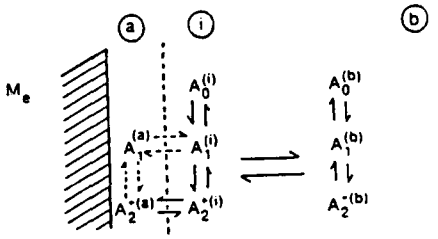

Figure 1. The $AlCl_3 - SOCl_2$ system at the rest potential. b=bulk, i=interphase and a=adsorption layer

The mechanism of $AlCl_3 - SOCl_2$ electrolyte reduction has been discussed elsewhere [5,7]. What follows is a short summary. Figure 2a shows the effect of scan rate on the shape of the linear scan voltammograms obtained for a 3.0 M solution on *Pt*. The electroreduction of $SOCl_2$ is a two-electron transfer in which the first one, Eq. (1), is irreversible and the second, Eq. (2), is quasi-reversible

$$A_2^+ + e^- \rightarrow P_1 \qquad (1)$$

$$P_1 + e^- \rightarrow P_2 \qquad (2)$$

P_1 and P_2 are unidentified intermediate species which desorb from the electrode surface into the reaction layer where they react with other species to form the products of electroreduction Cl^-, SO_2 and S. In-situ IR spectroscopy has shown that upon cathodic polarization new peaks due to SO_2 appear in the spectra as well as two additional bands assigned to, as yet, unidentified products containing a $S-O$ bond. It is likely that these unassigned bands are associated with P_1 and P_2 [5]. Furthermore, galvanostatic pulsing experiments indicate that three adsorbed species are present on the *Pt* electrode [7]. Figure 3 shows the potential/time behavior across a charging and relaxing interphase for the $Pt/AlCl_3 - SOCl_2$ system. Three exponential decays are observed in the relaxation curve. In general, the number of exponential decays observed in the potential relaxation curve reflects the number of adsorbed species [11].

The linear scan voltammograms, shown in Figure 2, also show a current plateau which is associated with the first electron transfer. This suggests a coupled chemical reaction either preceeding or parallel with the charge transfer [12]. Indeed an equilibrium does exist between onium ion and 1:1 adduct and, from the in-situ IR experiments, a loss of both these species is observed with increasing overpotential [5]. As the scan rate is decreased (Figure 2a) or the concentration of $AlCl_3$ is increased (Figure 2b), an auto-catalytic effect, manifested by a cross-over behavior in the linear scan voltammograms [12], is observed [5,7]. Increasing the $AlCl_3$ concentration increases the concentration of onium ions. Moreover, since the cross-over point occurs at the juncture between the current plateau and the cathodic peak due to the second electron transfer, the species being regenerated on the electrode surface, *via* Eq. (3), is P_1.

$$P_2 + A_2^+ \rightarrow 2P_1 \qquad (3)$$

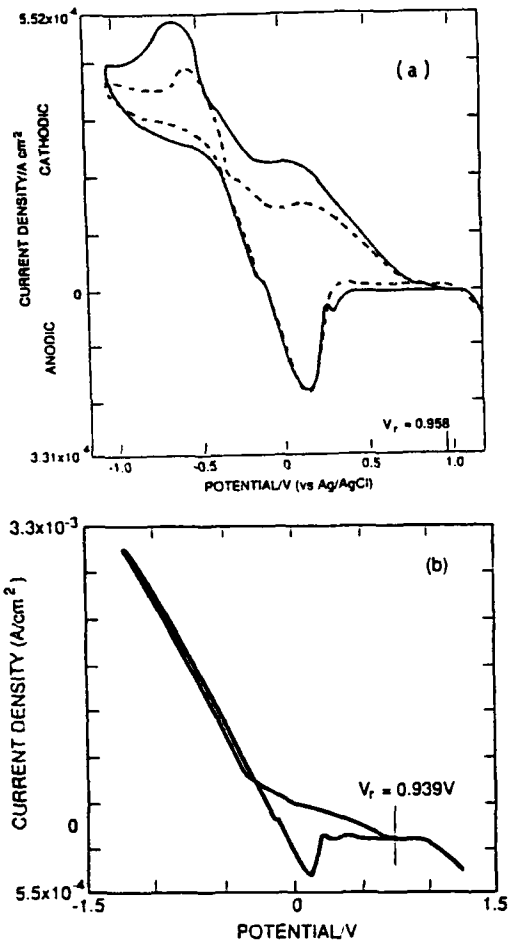

Figure 2. Effect of scan rate and concentration on voltammogram shape.
a- System: $Pt/SOCl_2 - 3.0M\ AlCl_3$; solid line-$v = 10\ mV\ s^{-1}$; dashed-$5\ mV\ s^{-1}$
b- System: $Pt/SOCl_2 - 4.0M\ AlCl_3$; $v = 10\ mV\ s^{-1}$

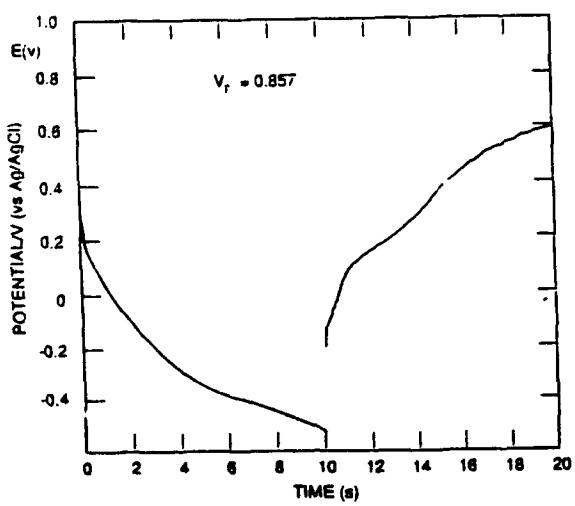

Figure 3. Potential/time behavior across charging and relaxing interphase System: $Pt/SOCl_2 - 3.0M\ AlCl_3$; pulse current 0.0011 $A\ cm^{-2}$

The remaining features in the linear scan voltammograms shown in Figure 2 are pre- and postpeaks due to adsorbed species [13]. The sequence of events occurring during $SOCl_2$ electroreduction is summarized in Figure 4. In Figure 4, ξ reflects the thermodynamics and λ the kinetics of the system. The rate constants for adsorption, autocatalysis and desorption are denoted by k_a, $k^{(c)}$ and k_d, respectively. The rate constants for the first and second electron transfers are given by $k^{(1)}$ and $k^{(2)}$. Surface coverages of A_2^+, P_1 and P_2 are defined by θ_1, θ_2 and θ_3, respectively

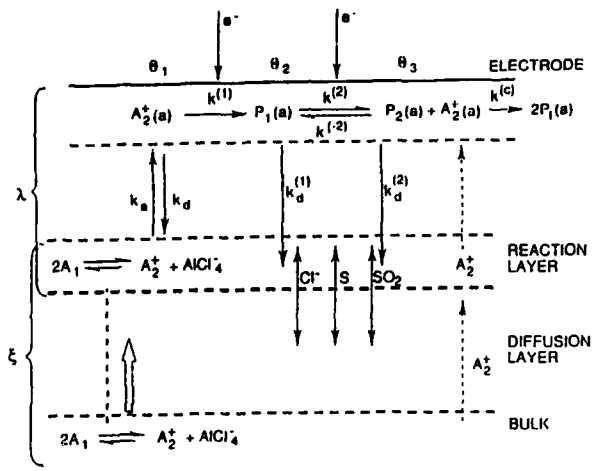

Figure 4. Summary of $SOCl_2$ reduction path.

RESULTS

Effect of Electrode Material on Electroreduction

Determination of the effect of electrode materials on the reduction of $SOCl_2$-bearing species by the potential perturbation technique requires that the reaction path remains unchanged. The constancy of the reaction path is manifested by identical species populating the electrode/electrolyte interphase, *i.e.*, irrespective of the electrode material. To ascertain this, the spectral region 925-1400 cm^{-1} was examined by in-situ IR spectroscopy for each electrode material.

Figures 5a to 5d show this region reflected from the *Au*-, *Pt*-, *n-Si*- and *C-glassy* sufaces at rest potential (dashed lines) and while cathodically polarized (solid lines). The general similarity of the spectra show that the species present at and near the surface are the same for each of the electrode materials which, in turn, indicates that the reduction path is the same for each surface. The concentration of of reactant(s) and products(s) within the interphase, however, depends on the electrode material because adsorption phenomena are highly specific.

It is known [14] that, for a given set of experimental constraints, the linear scan voltammetry delineates regimes of the dominance of specific processes. In the case of the *Pt* electrode, constraints applied in Figure 2 produced a balanced set, *i.e.*, where no single process dominates the voltammogram. Changing the composition of the electrolyte phase by the addition of a small amount of *Fe-Pc* (*e.g.*, 2 *mg* cm^{-3}), Figure 6a, substantially alters the shape of the voltammograms, *vide supra*, Figure 2. Addition of *Fe-Pc* to the electrolyte solution produces a voltammogram indicative of catalytic effect [12,13]. The catalysis masks contributions due to strongly adsorbed species, the coupled chemical equilibrium and the charge transfer. Furthermore, the relaxation curve obtained from galvanostatic pulsing experiments shows only one exponential decay which is characteristic of a strong catalytic effect. In terms of the reaction path illustrated in Figure 4, the $k^{(1)}$ is faster for the $Pt/SOCl_2$-(*Fe-Pc*) than for $Pt/SOCl_2$. Furthermore, the less prominent anodic peak due to the re-oxidation of $P_2 \rightarrow P_1$, means that the rate constant, $k^{(c)}_{Pt-Pc}$, is increased in the presence of dissolved *Fe-Pc*.

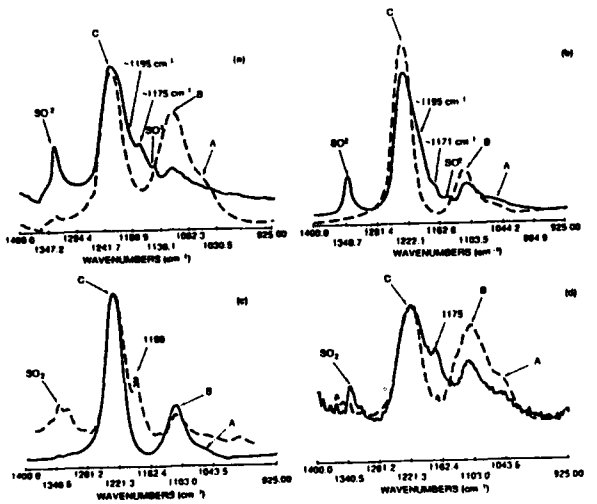

Figure 5. Effect of applied potential and electrode material on IR-reflectance spectrum.
Spectral region: 925-1400 cm^{-1}; System:*Me* /3.0*M* $AlCl_3 - SOCl_2$a-, b-, c-, and d- reflected from *Au*, *Pt*, *Si*, *C –glassy* -electrode surface, respectively. Dashed line-electrode at rest potential; solid line- polarized to -2.5 *V* (*Au*), -3.5 *V* (*Pt*), -3.0 *V* (*Si*) and -2.0 *V* (*C –glassy*). Bands A, B, and C refer to onium ion, 1:1 adduct and neat $SOCl_2$ in the bulk solution, respectively.

The effect of the electrode material on the rate constants is illustrated in Figures 6b to 6d. In particular, Figure 6b shows the effect of surface modification of the *Pt*-electrode by a chemisorbed *Fe –Pc*. Comparison of voltammograms in Figures 2 and 6b shows a significant increase in the rate of the charge transfer associated with the first electron, *i.e.*, $k_A^{(1)}(Fe-Pc) > k_A^{(1)}$ and a similarly notable reduction in the second peak can be interpreted as an increase in the $k^{(c)}$-value. It is unlikely that any of the features of the linear scan voltammogram shown in Figure 6b is due to the reduction of the central metal ion of *Fe –Pc*. No such waves were observed in Figure 6a nor has any such process been observed by Melendres [15,16]. The voltammogram on *Au*-surface, Figure 6c, shows a substantial increase in the $k^{(1)}$-rate constant compared to *Pt*, Figure 2, thus obscurring the contributions due to adsorption. Likewise the relaxation curve obtained during galvanostatic pulsing experiments shows only one exponential decay. On a *glassy C* surface, Figure 6d, a substantial auto-catalytic effect is observed. The auto-catalytic effects are associated with the process described by Eq. (III) coupled with relevant equilibria. As with *Pt*, three exponentially decaying segments are observed in the galvanostatic relaxation curves indicative of three adsorbed species.

CONCLUSIONS

The complexity of the reaction path, Figure 4, indicates that the material employed in the construction of the positive electrode might affect the performance of a discharging *Li* /$SOCl_2$ cell. The primary reason for such a conclusion is the presence of adsorbed species whose adsorption-desorption rates, as well as catalytic activities, depend on the electrode material.

The examination of the voltammogram shape as a function of electrode material led to the following relations, Eqs. (4) and (5)

$$k_{Au}^{(1)} > k_{A}^{(1)}(Fe-Pc) > k_{C}^{(1)} \quad (4)$$

$$k_{Au}^{(c)} > k_{C}^{(c)} > k_{A}^{(c)} \quad (5)$$

This series in rate constants is further supported by the potential decay across the relaxing electrode/electrolyte interphases.

ACKNOWLEDGEMENT

This work was funded, in part, by the Naval Ocean Systems Center Independent Exploratory Development program.

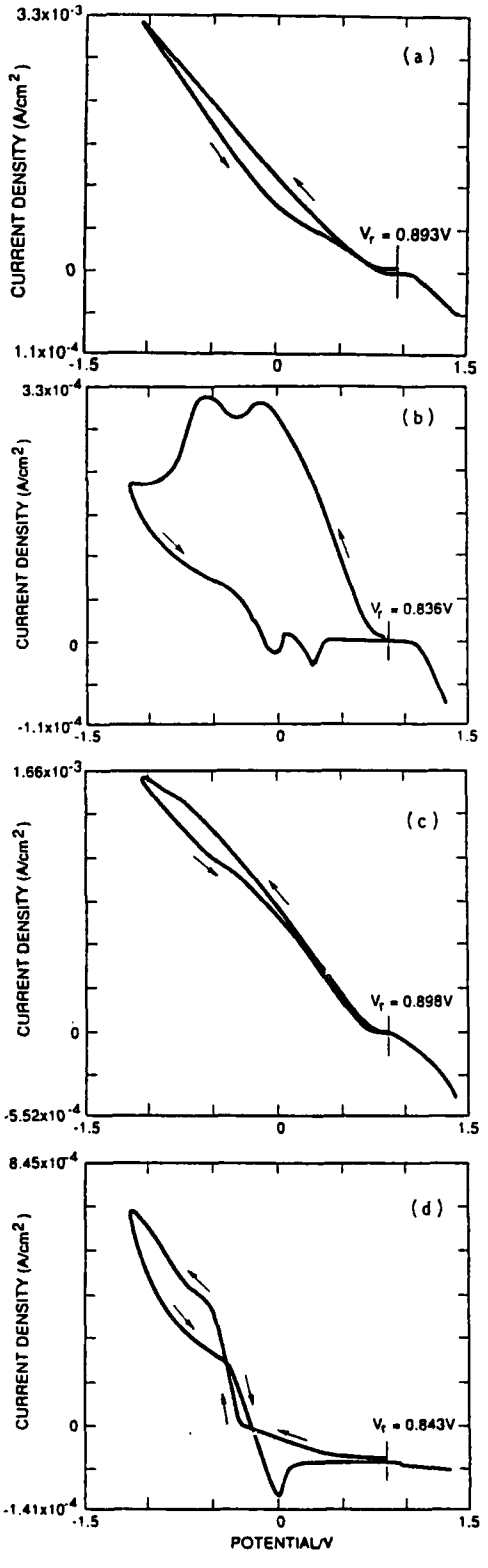

Figure 6. Effect of solution composition and electrode material on linear scan voltammograms; Scan rate-10 $mV\ s^{-1}$; System: a-*Pt* /$SOCl_2$ – 3.0*M* $AlCl_3$ with added 2.0 *mg* cm^{-3} *Fe –Pc*, b through d- *Me* /$SOCl_2$ – 3.0*M* $AlCl_3$ where b- *Pt* electrode with chemisorbed *Fe –Pc*; c- *Au* electrode; d- *glassy –C* electrode

REFERENCES

[1] K. C. Tsaur and R. Pollard, "Precipitation of Solids in Electrochemical Cells", J. Electrochem. Soc., vol. 133, pp. 2296-2308, Nov. 1986.

[2] J. J. Smith, S. Szpak and W. A. West, "Function of Electrocatalysis on the Reduction of $SOCl_2$ at Porous Electrodes", Power Sources 11. Brighton UK: Taylor and Francis (Printers) Ltd., 1987, ch. 31, pp. 441-453.

[3] R. J. Nowak, D. R. Rolison, J. J. Smith and S. Szpak, "Role of $Fe-Pc$ in a Discharging $Li/SOCl_2$ Cell", Electrochim. Acta, vol. 33, pp. 1313-1319, Oct. 1988.

[4] M. J. Madou, J. J. Smith and S. Szpak, "Comments on Electroreduction of $SOCl_2$", J. Electrochem. Soc., vol. 134, pp. 2794-2798, Nov. 1987.

[5] P. A. Mosier-Boss, S. Szpak, J. J. Smith and R. J. Nowak, "Electroreduction of $SOCl_2$ I. $AlCl_3 - SOCl_2$ System on Pt Electrode", J. Electrochem. Soc., vol. 136, pp. 2455-2462, Sept., 1989.

[6] S. Szpak, "Experimental Simulation of Porous Electrodes", Techniques for Characterization of Electrodes and Electrochemical Processes John Wiley and Sons, Inc., to be published in Fall 1989.

[7] P. A. Mosier-Boss, S. Szpak, J. J. Smith and R. J. Nowak, "Effect of Electrode Material on $SOCl_2$ Reduction", Electrochim. Acta, in press.

[8] P. van Rysselberghe, Thermodynamics of Irreversible Processes. Paris: Hermann, 1963.

[9] P. A. Mosier-Boss, R. D. Boss, C. J. Gabriel, S. Szpak, J. J. Smith and R. J. Nowak, "Raman and Infrared Spectroscopy of the $AlCl_3 - SOCl_2$ System", J. Chem. Soc. Faraday Trans. I, vol. 85, pp. 11-21, Jan. 1989.

[10] S. Szpak and H. V. Venkatasetty, "Transport Properties of Aluminum Chloride-Thionyl Chloride-Based Electrolytes", J. Electrochem. Soc., vol. 131, pp. 961-968, May 1984.

[11] B. E. Conway and M. Dzieciuch, "New Approches to the Study of Electrochemical Decarboxylation and the Kolbe Reaction", Can. J. Chem., vol. 41, pp. 21-67, Jan. 1963.

[12] R. S. Nicholson and I. Shain, "Theory of Stationary Electrode Polarography: Single Scan and Cyclic Methods Applied to Reversible, Irreversible, and Kinetic Systems", Anal. Chem., vol 36, pp. 706-723, April 1964.

[13] R. H. Wopschall and I. Shain, "Effects of Adsorption of Electroactive Species in Stationary Electrode Polarography", Anal. Chem., vol. 39, pp. 1514-1534, Nov. 1967.

[14] J. M. Saveant and E. Vianello, "Potential-Sweep Voltammetry: General Theory of Chemical Polarization", Electrochim. Acta, vol. 12, pp. 629-646, Dec. 1967.

[15] C. A. Melendres and F. A. Cafasso, "Electrochemical and In-Situ Laser Raman Spectroscopy Studies on Carbon-Supported Iron Phthalocyanine Electrodes", J. Electrochem. Soc., vol. 128, pp. 755-760, April 1981.

[16] C. A. Melendres, C. B. Rios, X. Feng and R. McMasters, "In-Situ Laser Raman Spectra of Iron Phthalocyanine Adsorbed on Copper and Gold Electrodes", J. Phys. Chem., vol. 87, pp. 3526-3531, Sept. 1983.

INTERCELL CURRENT IN A MULTIMODULE ASSEMBLY

($Li/SOCl_2$ System:Design, Manufacturing and QC Considerations)

S. Szpak and P. A. Mosier-Boss

Naval Ocean Systems Center, San Diego CA 95152-5000

and

J. J. Smith

Department of Energy, Washington DC 20545

1.0 Introductory Remarks

Often power sources for military applications are designed to operate within relatively narrow limits - these limits being on the edge of the system capabilities. This requirement results in serious difficulties in the fabrication, *ie*, it imposes strict quality control (QC) measures to prevent failures, such as the reduced cell-battery lifetime or the initiation of a catastrophic event. Here, we limit the discussion to one aspect only, *viz.*, to the QC steps that affect the intercell currents of the high energy/power density batteries. Specifically, we consider QC implications with regard to the $Li/SOCl_2$– power source designed for propulsion. This system, as well as other power dense systems, have some common features, namely: compact design, multimodule construction and reserve configuration operating either under static or flowing electrolyte conditions. Although the design and methods of assembly may vary from system to system and from manufacturer to manufacturer, nevertheless, in general, QC procedures are most likely employed at the same points in the assembly

process and to the same cell/module functional elements.

2.0 Dynamics of operation, Fabrication and QC points.

A high power output $Li/SOCl_2$ battery is usually assembled by connecting a number of modules. As an example, in one design twenty modules connected in parallel, each containing approximately 100 cells, have been employed (1). Obviously, this enormous number of thin cells - and the need for high reliability - imposes stringent requirements on the manufacturer.

The basic block in the construction of a module is the galvanic cell. It contains four functional elements that, together with the participating processes, fully describe the cell discharge processes. These elements are: the negative electrode which functions as a seat for the generation of electrons *via* the oxidation reaction; the positive electrode where the reduction reaction consumes electrons generated at the negative; the separator which prevents direct contact between electrodes and, yet, permits ionic conductance. The elementary processes occurring within the cell interior are: the diffusion of reactants toward the electrode surface; the adsorption on the electrode surface; the charge transfer; the diffusion of products away from the electrode surface; the ion conduction through an electrolyte; and, to complete the cycle, the flow of electrons in an external circuit where the electrical work is delivered. Because porous electrodes are used, their fabrication incurs statistically spread deviation in *eg.*, surface area, porosity, tortuosity and particle and pore size. The dynamics of the cell/module operation involves the interaction between elementary processes and the electrode structure. Thus, it follows that all porous functional elements must conform to standards.

The battery is manufactured by stacking modules and interconnecting them hydraulically. The basic module assembly involves: (i) stacking the individual elements, (ii) compressing the stack to final dimension and sealing the outer and inner cell edges. The compliance with specification demands (i) counting the number of cells in a module, (ii) measuring the cell/module thickness and

inspecting the quality of seals. As indicated in Fig. 1, the QC measures are connected to the fabrication steps and the dynamics of the cell operation; their effect on the intercell currents form the main body of this presentation.

3.0 Concept of Equivalent Analogs.

If we write for the rate of reaction an expression in the form of Ohm's law, *ie.*, $r = kX$, where r is the reaction rate, k is the phenomenological coefficient, and X is the driving force, then an electric circuit analog can be easily constructed. In terms of the electric circuit analog the coefficent k is the resistive component and X is the equivalent potential drop associated with the current flow. For a set of consecutive reactions (*ie*, resistive elements in series), the internal cell resistance, R_z, is the sum of individual resistances, Fig. 2 - upper left. Thus, the cell impedance comprises all impedances associated with individual processes occurring within the confines of electrode interior. Consequently, it is the focal point that requires a detailed analysis because of its specificity and non-ohmic character and because it is generally time-dependent (2).

A module consists of N cells connected in series. Because energetic systems, as a rule, are constructed in a reserve configuration, means for cell activation and/or electrolyte circulation must be provided. The corresponding electric circuit analog consists of $NR_{z,i}$ with added resistive components, R_t and R_f, which are associated with the continuous electrolytic path must. An example of a multimodule assembly is shown in Fig. 2. A multimodule assembly may contain either an even or an odd number of modules which, when connected in parallel, share positive/positive, (+/+), and negative/negative, (- / -), interfaces (3).

4.0 Circulating and intercell currents

The intercell current is an ionic current that originates in one cell and terminates in another. It does not perform any useful work; on the contrary, it is a parasitic current resulting in the loss of

power and capacity (4) and may contribute to the catastrophic thermal runaway(2,5). Both these currents can be calculated using either a continuous (6) or discrete model (2).

Qualitatively, circulating currents exhibit a maximum at the central cells whereas the largest intercell currents are found in the end cells where they change sign from positive (at the negative end) to negative (at the positive end). For modules with small number of cells, all cells generate intercell currents (2). As the number of cells increases the centrally located cells contribute less. When an intercell current exceeds its critical value, current reversal occurs causing electrodeposition at the negative electrodes and corrosion at the positive. A characteristic number reflecting the distribution of these currents is the $\lambda-$ parameter (2). This parameter depends on battery design, electrolyte properties and the charge transfer reaction. Its most desirable value, $\lambda = 1.0$, is closely related to QC measures.

5.0 Illustrative examples

To illustrate the effect of QC measures, we first examine the behavior of a well designed and constructed multimodule battery. In particular, we consider the time evolution of the load current in an external circuit, the load sharing by individual modules and the changes in the $\lambda-$ parameter. Second, we evaluate the behavior of defective cells by comparing performance of defective modules with that of well constructed.

5.1 Scale-up effects of well designed battery.

Figures 3 to 5 show the results of modeling of a well constructed multimodule battery. As illustrated in Fig. 3, the load current increases with an increase in the number of modules. For example, the scaling up from a two 50 cell module battey to a five module battery which is discharged through the same resistance, increases the load current by *ca* 10 %. This is an expected behavior since the increase in the number of modules reduces the current density and, therefore also their

polarization.

The effect of normal distribution of the relevant properties of the porous structures of cell components on the current delivered by individual modules is illustrated in Figs. 4a - 4d. It is seen that within 85 % of the battery lifetime each modules delivers uniformly a fraction of the current that is determined by the statistical aspects of modules. Within the remaining 15 %, there is a clear manifestation of load sharing. The already depleted modules deliver less current and other modules compensate by increasing their contribution. The time evolution of the distribution of intercell currents and the $\lambda-$ parameter is shown in Figs. 5a - 5d, respectively.

5.2 Effect of variation in module compression/expansion

Typically, the process of module assembly involves the placement of a predetermined number of cells with due attention to their alignment followed by compression to the designed thickness. In practice, the variation of $+-$ 4 % is acceptable (1). Such a degree of variation in thickness does not substantially affect either the total load current or contribution by individual modules, as seen from comparison of Figs. 6 with 4b. However, as expected, modules in compression contribute more to the load current than those in expansion. Our model predicts that variation up to 10 % are acceptable

5.3 Unequal numbers of cells in modules.

The large number of cells in a module, *eg.* , 100 cells for a 10 kW module, increases the probability of constructing modules with fewer or greater number of cells than specified. The effect of such an error is shown in Fig. 7. As indicated, the effect of fewer cells is similar to that resulting from expansion in module thickness, while the extra cells corresponds to a compression. Missing one cell in a 50 cell module can be tolerated - missing two cells, however, seriously affects the battery performance, as shown in Fig. 7b.

5.4 Modules with defective cells

Defective cells are those that fail to function prematurely. The source of defective cells can be traced to cathode fabrication. The measure of the deficiency is introduced in our model through the computational factor reflecting both the conductivity in the cathode and the total charge deliverable by a cell (2). Its numerical may value vary between zero and unity - the smaller this factor, the more serious the defect. To illustrate the effect of defective cells, we selected central cells of the first module and assigned the deficince factor, $w = 0.5$. It is seen that approximately half-way through the discharge process, the battery load current became less due to the failure of the first module. It is also seen that the remaining modules cannot compensate completely. Moreover, as illustrated in Figs. 8c and d, local heat sources are generated by the intercell currents in addition to the excessive heat generation by the increase in load current by the still functioning modules.

6.0 Concluding remarks

Present calculations confirm, what has been found in practice, that the addition of well constructed modules introduces no special operational difficulties. Our model predicts that tolerances in module thickness up to ca 10 % and the variation in the number of cells in a module up to 2 % are acceptable. The most serious problem, however, arises from the deficient cells thus suggesting a strict enforcement of the QC measures especially in the fabrication of positive electrodes.

Acknowledgement

This work was performed as a part of the Naval Ocean Systems Center Independent Exploratory Development program.

References

1. S. Szpak and J. R. Driscoll, **Assessment of $Li/SOCl_2$ Battery Technology : Reserve, Thin Cell**

Design, NOSC TR 1154, April 1987

2. S. Szpak, C. J. Gabriel and J. R. Driscoll, J. Electrochem. Soc., **131**, 1996 (1984)

3. S. Szpak, C. J. Gabriel, J. J. Smith and J. R. Driscoll, J. Electrochem. Soc., **137**, 849 (1990)

4. C. J. Gabriel and S. Szpak, J. Power Sources, **25**, 215 (1989)

5. L. A. Parnell and S. Szpak, Electrochim. Acta, **30**, 913 (1985)

6. O. S. Ksenzhek and N. D. Koshel, Elektrokhimyia, **6**, 1587 (1970); ibid., **7**, 353 (1971)

Figure captions

Fig. 1 - A flow chart indicating fabrication sequence and QC inspection stations.

Fig. 2 - Electric circuit analogs.

a - cell (upper left)

b - module and module/module interface

Fig. 3 - Load current in external circuit delivered by well constructed multimodule battery. Number of modules indicated alongside.

Fig. 4 - Sharing of load currents by individual modules for: 2 - (4a), 3- (4b), 4 - (4c) and 5- (4d) module battery.

Fig. 5 - Time evolution of the distribution of intercell currents and the $\lambda-$ parameter.

5a and 5b - intercell currets at $t = 0$ and $t = 288$ seconds

5c and 5d - $\lambda-$ parameter at $t = 0$ and $t = 288$ seconds (insert drawn to the same scale as in 5c)

Fig. 6 - Portion of load current supplied by individual modules in a 3- module assembly.

6a - module Nr 2 in expansion by 4 %

6b - module Nr 2 in compression by 4 %

Fig. 7 - Effect of unequal numbers of cells on load current in a three - 50 cell module battery.

7a - module Nr 1 - 49 cells

7b - module Nr 1 - 48 cells

Fig. 8 - Effect of defective cells on battery performance

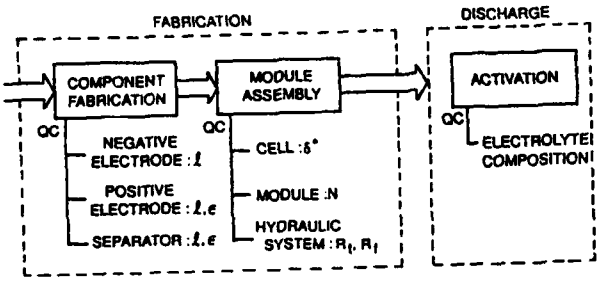

Fig. 1

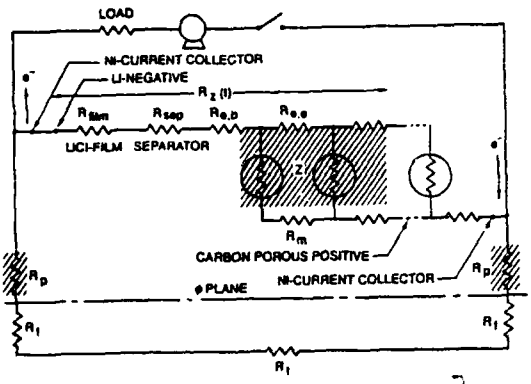

a

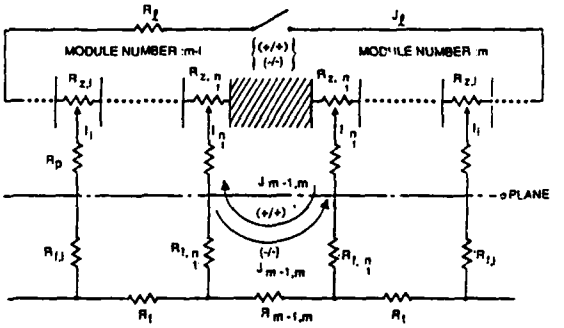

b

Fig. 2

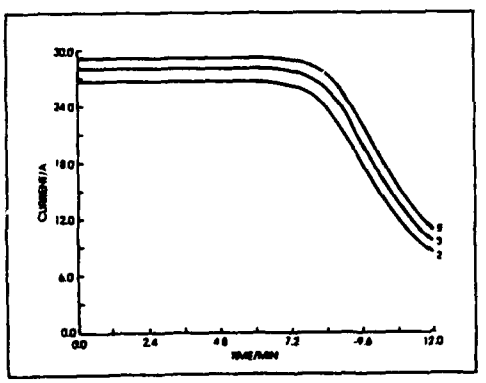

Fig. 3

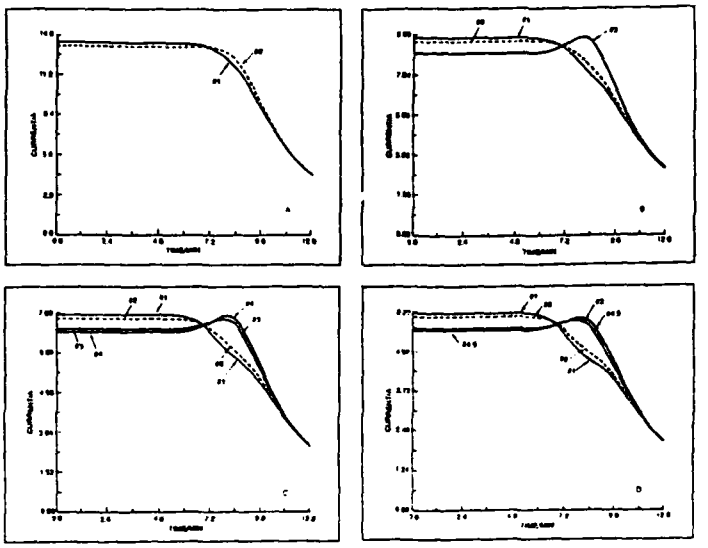

Fig 4

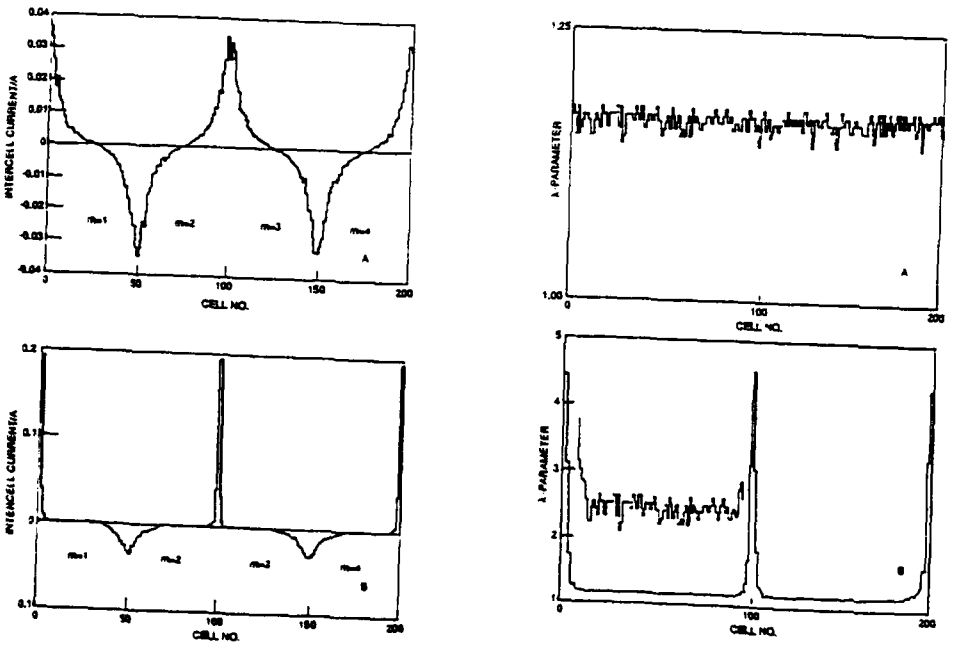

a

b

c

d

Fig 5

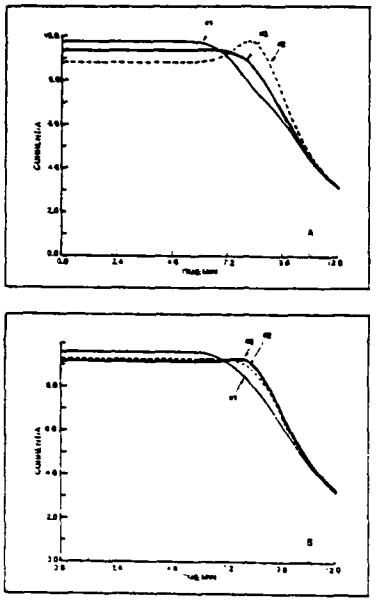

Fig. 6

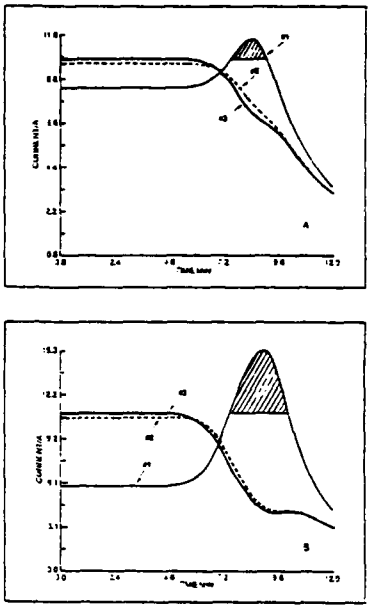

Fig 7

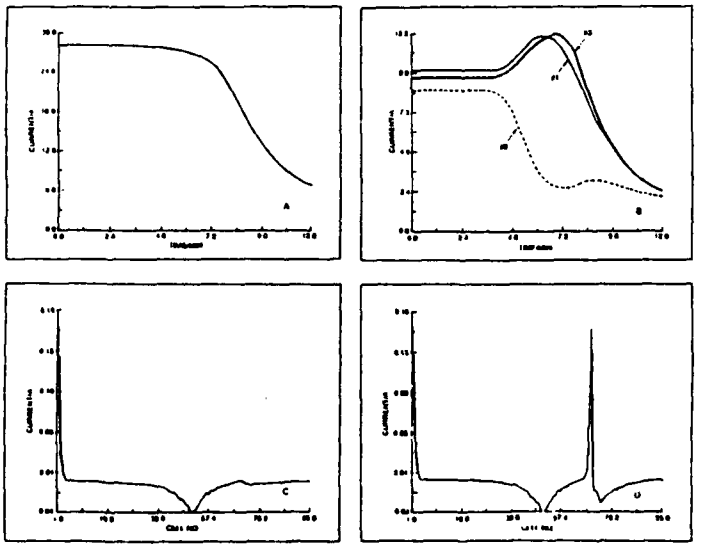

Fig. 8

3.0 PRESENTATIONS

This section contains presentations given at Electrochemical Society National meetings, International Power Sources Symposiums, and International Conference on Li Batteries from May 1987 through June 1990.

75-Word Abstract Form

Extended Abstract must be submitted with the 75-Word Abstract by December 1, 1986

Philadelphia, Pennsylvania—May 10-15, 1987

Submit to: The Electrochemical Society, Inc.
10 South Main Street, Pennington, NJ 08534-2896
With a copy to the Organizing Chairman

Abstract No. .....
(to be assigned by the Society)

Schedule for Nonaqueous Electrochemistry
(Title of Symposium)

Sponsored by Physical Electrochemistry and Battery Divisions
(Division/Group)

Title of paper Effect of Illumination on the Electroreduction of Thionyl Chloride

Authors (Underline name of author presenting paper.) Dr. Marc Madou, T. Otagawa, G. Gaisford, S. Szpak

Business affiliation and address SRI International
333 Ravenswood Avenue
Menlo Park, CA USA 94025 (415) 859 4066
(State or Country) (ZIP Code) (Telephone No.)

(Type abstract in this area—double-spaced.)

The effect of illumination on the electroreduction of $SOCl_2$ on Pt, Au, C, and n- and p-type Si electrodes was studied in a 1M $LiAlCl_4$ solution in $SOCl_2$. Two types of photoeffects could be distinguished, one associated with the presence of reaction products of the electroreduction on the electrode, and one, in the case of the Si electrodes, associated with the presence of a space charge inside the electrode. It was also found that the well-known blocking of the electrode surface by reaction productions of the electroreduction of $SOCl_2$ was delayed considerably when using Si electrodes (in other words the electrode capacity improved). The energetics of the $Si/SOCl_2$ interface are discussed in detail. The implications for the construction of a novel type of non-passivating electrode are given.

Do you require any audiovisual equipment?

- ☐ **35 mm (2 x 2 in.) slide projector**
- ☒ **Overhead projector**
- ☐ **Specify other (subject to availability and cost)**

Has the information in this abstract been presented verbally, submitted for publication, or published?
☒ **Yes** ☐ **No**
If the answer is yes, please provide the reference (except in the case of invited review presentations). _____

Is a full length paper on this work to be submitted for Society Journal publication? ☒ **Yes** ☐ **No**

Papers presented before a Society technical meeting become the property of the Society and may not be published elsewhere without written permission of the Society. Papers presented at Society technical meetings must be authored by a member or sponsored by an active member.

Insert name of Society member author or sponsor

EFFECT OF ILLUMINATION ON THE ELECTROREDUCTION OF THIONYL CHLORIDE

M. Madou, T. Otagawa, G. Gaisford
SRI International, Menlo Park, CA

S. Szpak
Naval Oceans Systems Center
San Diego, CA 92152-5000

Introduction

It is well known that the current of neutral thionyl chloride (1 M $LiAlCl_4$) electroreduction rapidly diminishes with time because of blocking of the electrode by reaction products (e.g. 1-2). Chakhov et al. (3) reported that such a "blocked" electrode in the case of vitreous carbon or pyrolytic graphite, exhibits a pronounced cathodic photoeffect in which the electroreduction of $SOCl_2$ is enhanced significantly. They attributed this to the fact that vitreous carbon as well as pyrolytic graphite, when immersed in $SOCl_2$, behaves like a p-type semiconductor with a 2 eV bandgap. Such a p-type semiconductor behaviour, they argue, comes about because of the formation of a surface compound, presumably a solid film involving carbon corrosion products, leading to the electrode passivation through a decrease in the free electron concentration in the surface layers. Upon illumination of the surface, there is an increase in the concentration of free electrons, and hence an increase in the reduction currents of $SOCl_2$.

In this work we studied photoeffects on different electrode materials (C, Au, Pt, and n- and p-Si) with the aim of better understanding the nature of the reported photoeffects and also to better understand the kinetics of the $SOCl_2$ reduction by applying semiconductor electrochemistry models such as the isoenergetic charge transfer model (4) to our results on the $Si/SOCl_2$ interface.

An unexpected result from this work that has possible practical applications, is the observation that Si electrodes do not passivate ("block") as fast as, for example, carbon electrodes.

Results and Discussion

1. Photoeffects on C, Pt, and Au

In Figure 1 we show the electroreduction currents on vitreous carbon, Pt, and gold electrodes in a solution of 1 M $LiAlCl_4$ in $SOCl_2$ as a function of time while chopping the light that strikes the electrode surface. The light source used was a tungsten microscope lamp. The electrode potential in Fig. 1 is given with respect to a Li reference electrode and all potentials are within the range of electro-reduction of $SOCl_2$. The photoeffect reported by Chakhov et al. (3) for vitreous carbon is reproduced here but obviously the same effect of enhanced electroreduction by illumination is observed for Pt and Au electrodes.

The deeper into the passivating potential range (and presumably the thicker the passivating film) the more pronounced the photoeffect. The explanation for the photoeffect on vitreous carbon, given by Chakhov et al. (3) involved carbon corrosion products, the above results indicate that any model relying exclusively on involvement of carbon corrosion products is incomplete Our results, reported further below, indicate that the observed photoeffect is more probably associated with the presence of LiCl on all these electrodes.

2. The $Si/SOCl_2$ Interface

Cyclic voltammograms on n- and p-type Si electrodes ($\rho = \pm 1$ Ωcm) in a solution of 1 M $LiAlCl_4$ in $SOCl_2$ in the dark, exhibit "diode" characteristics associated with a Schottky barrier at the interface $Si/SOCl_2$. From the isoenergetic charge transfer model (4) it follows that; 1) because of the absence of a large anodic current in the case of n-type Si in the dark, no electron injection by $SOCl_2$ into the Si conduction band takes place, and 2) because of the absence of a large cathodic current in the case of p-type in the dark, no hole injection by $SOCl_2$ in the Si valence band takes place. If hole injection would proceed at a fast rate it would typically lead to fast corrosion of the Si by $SOCl_2$ even at open circuit.

The onset of the reduction of $SOCl_2$ on n-Si in the dark exhibits a large overpotential compared to C, Pt, and Au. Because of the low conductivity of the Si used here and the existence of a space charge at the interface $Si/SOCl_2$, such a large overpotential is not unexpected. For a practical battery electrode, highly conductive, degenerate Si would have to be used.

The type of photoeffects observed on the C, Pt and Au (see Fig. 1) electrodes was not observed on Si. Only in the voltage range where a substantial space charge is present at the $Si/SOCl_2$ interface, in both n- and p-type, did we observe the typical space-charge-dominated semiconductor-type photoeffects. These photoeffects are much larger than the ones shown in Fig. 1 and the response time is also much faster.

3. Delayed Passivation on Si Electrodes

A 1 cm^2 Pt and an n-Si electrode were subjected to a cathodic current of 100 $\mu A/cm^2$ in a solution of 1 M $LiAlCl_4$ in $SOCl_2$ (using a galvanostat). Meanwhile the voltage of the Pt and the n-Si were measured with respect to a Li reference electrode as a function of time. At the point of complete passivation such curves show an inflection towards more negative potentials. That inflection point in the case of n-Si occurs much later than for Pt (5 times as long as it takes for Pt to passivate). The above experiment indicates that Si passivates much slower than Pt (we found that Pt, C, and Au all passivated after about the same time of electroreduction current). The above experiment might also explain why the photoeffect illustrated in Fig. 1 does not occur with Si. It seems that LiCl either does not form in this case, or if it forms, it forms much slower. If LiCl is not present the photoeffect observed in Fig. 1 does not seem to occur. We speculate that on the Si electrode soluble "$SiCl_x$" species forms preferentially rather than the insoluble LiCl.

Possibly light enables e^- to be excited into the conduction band or in localized states within the LiCl bandgap providing a path for further reduction of $SOCl_2$ (5). A more practical implication of the above experiments is that Si electrodes might have a higher charge capacity in $SOCl_2$ batteries than C electrodes. Because of the high overpotential of Si one would have to use highly conductive Si and probably mix Si with carbon.

References

1. W.K. Behl, J. Electrochem. Soc. 101, 367 (1919).
2. M.J. Madou and S. Szpak, J. Electrochem. Soc. 131, 2472 (1984).
3. N.I. Chakhov, Yu. M. Povarov and Yu. V. Pleskov, Elektrokhimiya, 16, 1445 (1980).
4. H. Gericher, Surface Science, 13, 265 (1964).
5. F.M. Deinick, W.R. Cieslak, D.E. Peebles and J.W. Rogers, Jr., Ext. Abs. Fall Mtg. The Electrochem. Soc. San Diego, 1986,(October).

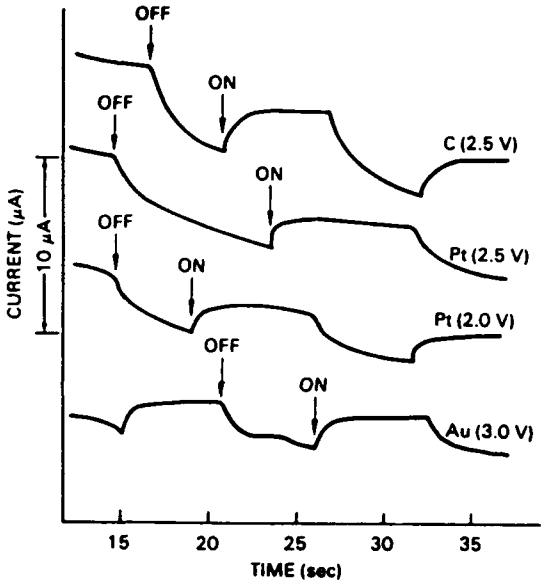

Fig. 1 Photoeffects on C, Pt, and Au in 1 M $LiAlCl_4$ in $SOCl_2$.

75-Word Abstract Form

Extended Abstract must be submitted with the 75-Word Abstract by December 1, 1986

Philadelphia, Pennsylvania—May 10-15, 1987

Submit to: The Electrochemical Society, Inc.
10 South Main Street, Pennington, NJ 08534-2896
With a copy to the Organizing Chairman

Abstract No. ..... (to be assigned by the Society)

Schedule for ..... Nonaqueous Electrochemistry .....
(Title of Symposium)

Sponsored by Physical Electrochemistry and Battery Divisions
(Division/Group)

Title of paper Structure of $AlCl_3$ - $SOCl_2$ - LiCl System by Raman Spectroscopy

Authors (Underline name of author presenting paper.) P. A. Mosier-Boss, J. J. Smith, and S. Szpak

Business affiliation and address Naval Ocean Systems Center, San Diego, CA and Naval Weapons Center, China Lake, CA

(State or Country) (ZIP Code) (Telephone No.)

(Type abstract in this area—double-spaced.)

The $AlCl_3$-$SOCl_2$-LiCl system is examined as a function of composition and temperature by Raman Spectroscopy. Structural informations are derived from S=O and S-Cl stretching frequencies recorded for pure $SOCl_2$ and their shifts observed upon addition of $AlCl_3$ and LiCl. In particular, addition of $AlCl_3$ shifts the S=O stretching vibrations to lower frequencies due to formation of $AlCl_3.SOCl_2$ complexes. As the concentration of $AlCl_3$ exceeds 3.0 M, a broad shoulder appears at still lower frequencies, tentatively assigned to the $(AlCl_3)_2.SOCl_2$ complex. Addition of LiCl breaks up the molecular complexes of $AlCl_3$ and $SOCl_2$ to form solvated Li^+ ions and $AlCl_4^-$ species. Structures of the species present in the solution and assignment of vibrational bands are discussed.

Do you require any audiovisual equipment?

☒ 35 mm (2 x 2 in.) slide projector

☐ Overhead projector

☐ Specify other (subject to availability and cost)

Has the information in this abstract been presented verbally, submitted for publication, or published?

☐ Yes ☒ No

If the answer is yes, please provide the reference (except in the case of invited review presentations). _____

Is a full length paper on this work to be submitted for Society Journal publication? ☐ Yes ☒ No

J. J. Smith and S. Szpak
Insert name of Society member author or sponsor

STRUCTURE OF $AlCl_3$-$SOCl_2$-LiCl SYSTEM BY RAMAN SPECTROSCOPY

P.A. Mosier-Boss and S. Szpak
NOSC
San Diego, CA 95152-5000

J.J. Smith
NWC
China Lake, CA 93555-6001

1. INTRODUCTION

Recent data on the performance characteristics of Li/$SOCl_2$ cells point to the importance of structural aspects of $SOCl_2$ based electrolytes (1). Evidently, performance in cells operating at high discharge rates is influenced by electrolyte structure (2). In this communication the structural aspects of the changing electrolyte composition in the course of cell discharge is examined by Raman spectroscopy.

2. RESULTS AND DISCUSSION

(i) Liquid $SOCl_2$

Changes observed in the frequencies of the S=O stretching vibration and the S-Cl symmetric and asymmetric stretching vibrations are the principal basis for the present discussion. An intense band in the S=O stretch region, at 1229 cm^{-1}, is actually a composite band of three overlapping peaks. This observation, as well as dilution studies of $SOCl_2$ in CCl_4, C_6H_6, CH_2Cl_2, n-C_6H_{14} and $CH_3C_6H_5$, indicate that $SOCl_2$ itself is an associated liquid consisting of dimers and higher aggregates.

(ii) The $AlCl_3$-$SOCl_2$ System

With the addition of $AlCl_3$ to $SOCl_2$ a new band appears at 1103 cm^{-1} which is attributed to the S=O stretching vibration of $AlCl_3 \cdot SOCl_2$ complex, Fig. 1. With the addition of $AlCl_3$ the S-Cl symmetric and asymmetric stretches of $SOCl_2$ are shifted to higher frequency. Both of these observations support coordination through the oxygen atom of $SOCl_2$ (3,4).

At concentrations greater than 3.0 M $AlCl_3$ in $SOCl_2$, a broad shoulder appears at ca 1063 cm^{-1} which has tentatively been assigned to the $(AlCl_3)_2 \cdot SOCl_2$ complex. The shift to even lower frequency implies that both $AlCl_3$ species in 2:1 complex coordinate through the oxygen atom of $SOCl_2$. The broadness of the new band as well as the smaller shift to lower frequency as compared to the 1:1 complex indicates that the second $AlCl_3$ is weakly coordinated to $SOCl_2$. These conclusions are in agreement with earlier works (5-8).

The Raman spectrum of a 1:1 mole ratio solution of $AlCl_3$ and $SOCl_2$ shows the existence of $AlCl_4^-$, i.e. in agreement with conductance data (7,8). It is unlikely, however, that the counterion of $AlCl_4^-$ is $SOCl^+$ since no high frequency bands were observed in the S=O stretching region. The counterion is probably $[AlCl_2SOCl_2]^+$ ion in analogy to $AlCl_3$-THF (9,10) and $AlCl_3$-CH_3NO_2 (11) systems.

(iii) The $AlCl_3$-LiCl-$SOCl_2$ System

The addition of LiCl to the $AlCl_3$-$SOCl_2$ system breaks up the molecular complexes of $AlCl_3$ and $SOCl_2$ to form solvated Li^+ ions and $AlCl_4^-$ species. As illustrated in Fig. 2, the band due to the S=O stretch of the $AlCl_3.SOCl_2$ complex at 1103 cm^{-1} decreases with increasing LiCl concentration and a new band appears at ca 1200 cm^{-1}. This band is attributed to the S=O stretching vibration of $SOCl_2$ molecules in the solvation sphere of Li^+ ions. Since this band occurs at lower frequency than that of $SOCl_2$, it indicates that $SOCl_2$ solvates Li^+ ion through the oxygen atom.

(iv) Temperature Effects

In the $AlCl_3$-$SOCl_2$ system, no significant changes are observed within temperature range +25°C to -20°C except for broadening of several of the bands appearing between 100 and 600 cm^{-1} with decreasing temperature. This broadening suggests the formation of higher molecular aggregates of $AlCl_3$ and $SOCl_2$. In the $AlCl_3$-LiCl-$SOCl_2$ system, with decreasing temperature, the vibrational bands due to $AlCl_4^-$ (i.e., the Cl-Al-Cl vibrational bending modes at 119 and 179 cm^{-1} and the Al-Cl symmetric stretch at ca 358 cm^{-1}, sharpen. A sharpening of the bands of $SOCl_2$ associated with Li^+ was also observed. These changes have been attributed to the formation of ion pairs.

REFERENCES

1. M. J. Madou, J. J. Smith and S. Szpak, J. Electrochem. Soc., submitted (1986).
2. K. C. Tsaur and R. Pollard, ibid, 131, 984 (1984).
3. F. A. Cotton and R. Francis, J. Am. Chem. Soc., 82, 2986 (1960).
4. J. Selbin, W. E. Bull and L. H. Holmes, Jr., J. Inorg. Nucl. Chem., 16, 219 (1961).
5. D. A. Long and R. F. Bailey, Trans. Faraday Soc., 59, 594 (1963).
6. H. Spandau and E. Brunneck, Z. Anorg. Chem., 270, 201 (1952).
7. H. Spandau and E. Brunneck, Z. Anorg. Chem., 278, 197 (1955).
8. H. Hecht, Z. Anorg. Chem., 254, 44 (1947).
9. J. Derouault and M. S. Forel, Inorg. Chem., 16, 3207 (1977).
10. J. Derouault, P. Granger and M. S. Forel, Inorg. Chem., 16, 3214 (1977).
11. M. Dalibart, J. Derouault and P. Granger, Inorg. Chem., 21, 2241 (1982).

Figure 1. The S=O stretching region of $AlCl_3$-$SOCl_2$ solutions.

Figure 2. The S=O stretching region of solutions of $AlCl_3$ and LiCl in $SOCl_2$.

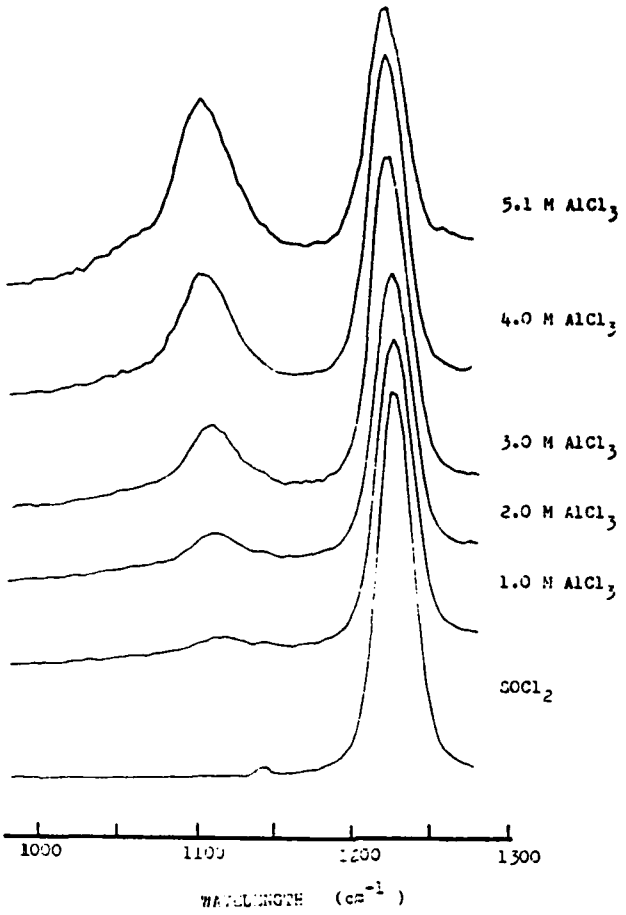
5.1 M AlCl3
4.0 M AlCl3
3.0 M AlCl3
2.0 M AlCl3
1.0 M AlCl3
SOCl2
1000
1100
1200
1300
WAVELENGTH (cm-1)

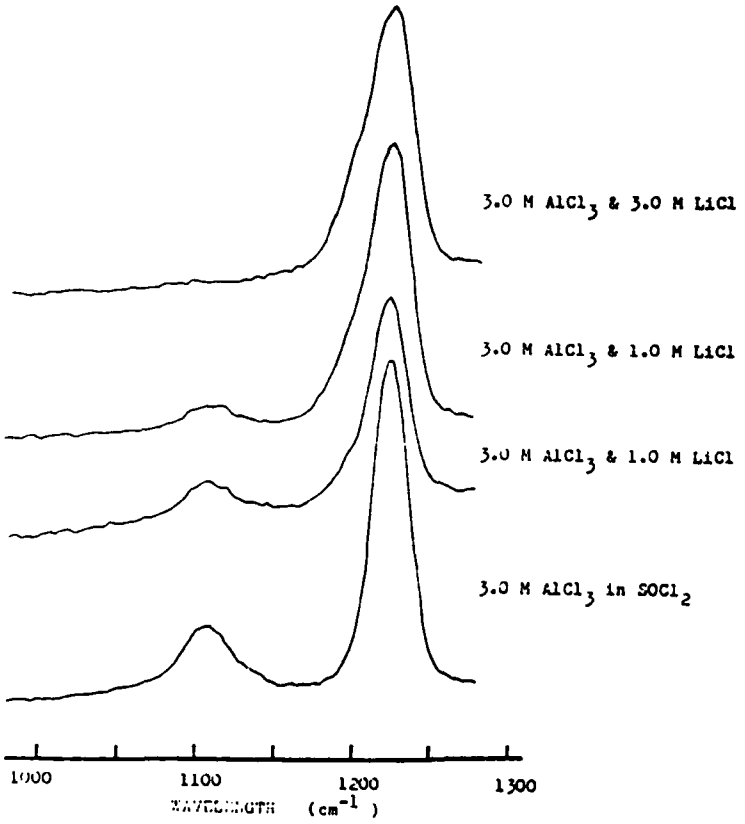
3.0 M AlCl3 & 3.0 M LiCl
3.0 M AlCl3 & 1.0 M LiCl
3.0 M AlCl3 & 1.0 M LiCl
3.0 M AlCl3 in SOCl2
1000
1100
1200
1300
WAVELENGTH (cm-1)

75-Word Abstract Form

Extended Abstract must be submitted with the 75-Word Abstract by May 1, 1987

Honolulu, Hawaii—October 18-23, 1987

Submit to: The Electrochemical Society, Inc.
10 South Main Street, Pennington, NJ 08534-2896
With a copy to the Organizing Chairman

Abstract No. .....
(to be assigned by the Society)

Schedule for .....
(Title of Symposium)

Sponsored by .....
(Division/Group)

Title of paper .....

.....

Authors (Underline name of author presenting paper.) .....

.....

Business affiliation and address .....

.....

.....
(State or Country) (ZIP Code) (Telephone No.)

(Type abstract in this area—double-spaced.)

175 **Intercell Currents in Assembly of Modules:** *S. Szpak** and *C. J. Gabriel*, Naval Ocean Systems Center, San Diego, CA 92152-5000. *J. J. Smith*, Naval Weapons Center, China Lake, CA 93555-6001

Treatment of intercell currents in electrochemical currents, *e.g.*, reserve batteries, fuel cells, and electrolyzers, consisting of a number of series connected cells having a common electrolytic path is well known. This treatment is extended to another technologically important case, that of a battery designed for high power density capabilities. The intercell/intermodule current arising on activation or during operation of a battery comprising several multicell modules connected electrically in parallel and fed from a common manifold is examined. The $Li/SOCl_2$ battery of a thin cell design is used as an example.

Do you require any audiovisual equipment?

- ☐ **35 mm (2 x 2 in.) slide projector**
- ☐ **Overhead projector**
- ☐ **Specify other (subject to availability and cost)**

Has the information in this abstract been presented verbally, submitted for publication, or published?
☐ **Yes** ☐ **No**
If the answer is yes, please provide the reference (except in the case of invited review presentations). _____

Is a full length paper on this work to be submitted for Society Journal publication? ☐ **Yes** ☐ **No**

.....
Insert name of Society member author or sponsor

INTERCELL CURRENTS IN ASSEMBLY OF MODULES

S. Szpak and C. J. Gabriel
Naval Ocean Systems Center
San Diego, CA 92152-5000
and
J. J. Smith
Naval Weapons Center
China Lake, CA 93555-6001

Qualitatively, an intercell current is an ionic current that originates in one cell and terminates in another. It is a parasitic current which not only reduces the effectiveness of an electrochemical device but in some cases, eg Li batteries of reserve type, may lead to the initiation of a catastrophic event (1). This parasitic current is present whenever a continuous electrolytic path through all cells/modules is required for either filling the battery or flowing the electrolyte.

A typical multimodule battery with the necessary accessories is shown in Fig. 1. In contrast to a single cell which can be viewed as a chemical reactor, the battery employing eg flowing electrolyte, resembles a chemical plant. Here, the discussion is limited to the "energy section" of the battery. This section contains three modules connected electrically in parallel and hydraulically in series and is represented by an equivalent electric circuit analog.

Quantitatively, the magnitude of the intercell currents as well as their effect on the battery operation, are evaluated by solving a set of equations formulated for the electric circuit analogs shown in Figs. 2a and b.

Subject to simplifying assumptions (2), the equations for the current in the external load and the circulating currents in the fill path are given by Eqs. (1) and (2)

$$J_l R_l = V_l \text{ with } J_l = \sum J_{l,i} \text{ and } V_l = \sum V_{i,j} \qquad (1)$$

and, within each module,

$$-J_{i-1}R_{f,i} + J_i(R_{f,i} + R_{f,i+1} + R_{t,i})$$

$$-J_{i+1}R_{f,i+1} = \bar{\bar{O}}_{i+1} - \bar{\phi}_i, (i = 1,2,\ldots,N-1) \qquad (2)$$

Similar equations govern the circulating currents at the interface between connecting modules. Consistent with the battery operation, the boundary and interface conditions are:

$$J_{0,1} = J_{0,N} = O; J_{N,1} = -J_{N,2}; J_{0,2} = -J_{0,3}; V_{a,N,1} = V_{a,N,3}$$

and

$$V_{c,1,2} = V_{c,1,3} = V_{c,2,3}.$$

Numerical solutions for a selected set of operating conditions of the thin cell design reserve $Li/SOCl_2$ battery, containing three 86-cell modules are presented.

References.

1. S. Szpak, C. J. Gabriel and J. R. Driscoll, Electrochim. Acta, 32, 239 (1987)

2. S. Szpak. C. J. Gabriel and J. R. Driscoll, J. Electrochem. Soc., 131, 1996 (1984)

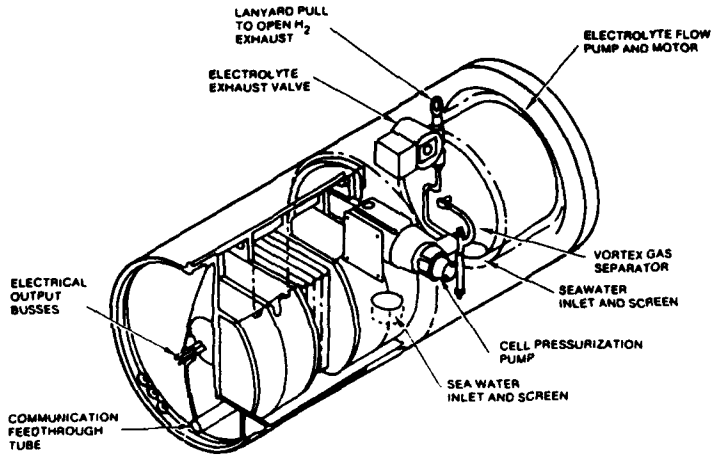

Fig. 1 Multimodule battery assembly including accessories

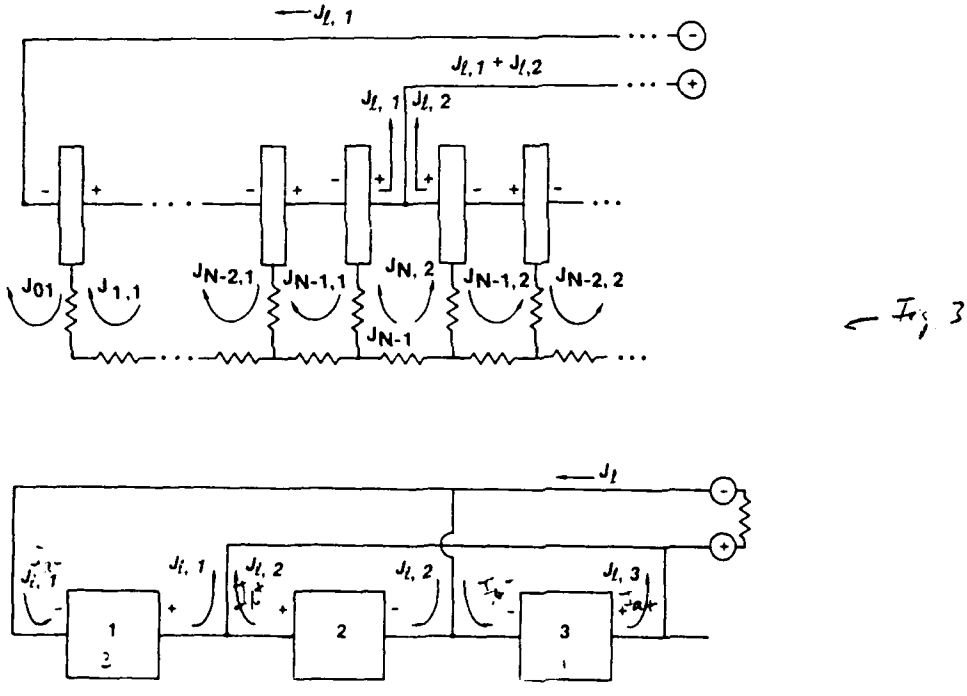

Fig. 2 Multimodule battery representation.

2a Equivalent electric circuit.

2b Intermodule connection.

(For symbol 3 identification see ref. (2)).

75-Word Abstract Form

Extended Abstract must be submitted with the 75-Word Abstract by May 1, 1987

Honolulu, Hawaii—October 18-23, 1987

Submit to: The Electrochemical Society, Inc.
10 South Main Street, Pennington, NJ 08534-2896
With a copy to the Organizing Chairman

Abstract No.
(to be assigned by the Society)

Schedule for Lithium Battery
(Title of Symposium)

Sponsored by Battery
(Division/Group)

Title of paper Properties of Thionyl Chloride Electrolytes

Authors (Underline name of author presenting paper) Jerry J. Smith[1], Stan Szpak[2], Debra Rolison[3], Pamela Mosier-Boss[2], Peter Schmidt[4], and Stan Pons[5]

Business affiliation and address [1]Naval Weapons Center, China Lake, CA 93555, [2]Naval Ocean Systems Center, San Diego, CA 95152, [3]Naval Research Laboratory, Washington, DC 20375 [4]Oakland University, Rochester, MI 48063, [5]University of Utah, Salt Lake City, UT 84112

(State or Country) (ZIP Code) 619-939-1444 (Telephone No.)

(Type abstract in this area—double-spaced.)

Electrolytes of the system $AlCl_3$-LiCl-$SOCl_2$ are complex solutions whose compositions are determined by several factors. The properties of the electrolytes, and hence the performance of the batteries containing them, are strongly influenced by their composition. Measurements of the electrolyte's physical properties, coupled with results from spectroscopic investigations show the presence of several chemical species, including complexes and ions with varying degrees of $SOCl_2$ solvation. The specific species and the factors which lead to their formation and destruction are described.

Do you require any audiovisual equipment?

35 mm (2 x 2 in.) slide projector

X Overhead projector

Specify other (subject to availability and cost)

Has the information in this abstract been presented verbally, submitted for publication, or published?

Yes X No

If the answer is yes, please provide the reference (except in the case of invited review presentations).

Is a full length paper on this work to be submitted for Society Journal publication? X Yes ☐ No

Dr. Jerry J. Smith
Insert name of Society member author or sponsor

PROPERTIES OF THIONYL CHLORIDE ELECTROLYTES

J. J. Smith,[1] S. Szpak,[2] Debra R. Rolison,[3] P. A. Mosier-Boss,[2] P. P. Schmidt,[4] and S. Pons[5]
[1]Naval Weapons Center, China Lake, CA 93555
[2]Naval Ocean Systems Center, San Diego, CA 95152
[3]Naval Research Laboratory, Washington, DC 20375
[4]Oakland University, Rochester, MI 48063
[5]University of Utah, Salt Lake City, UT 84112

INTRODUCTION

The lithium-thionyl chloride battery system has the highest practical energy density of any commercial battery. As such, it is of considerable interest for applications having weight and volume restrictions. Optimization of this system has yet to be achieved due, in part, to a lack of understanding of the system and the factors that establish its operational characteristics and determine its safety.

The electrolyte is composed of thionyl chloride solutions containing aluminum trichloride and lithium chloride, either in 1:1 concentrations for the neutral electrolyte or with excess aluminum trichloride in the case of acidic electrolyte. Concentrations of the species in excess of 1 M are common. Properties of the electrolyte are dependent on the concentrations of constituents. Likewise, the performance of the battery system is dependent on the electrolyte.

Reported here is a series of observations on the properties of thionyl-chloride electrolytes obtained from vapor pressure measurements, infrared and Raman spectroscopy, and nuclear magnetic resonance (NMR) spectrometry. The results are supported by molecular orbital calculations.

EXPERIMENTAL

Infrared experiments were performed using the SNIFTIRS technique [1]. Raman spectra were taken using a scanning double monochromator and photon-counting methods [2]. NMR spectra were obtained on a Brucker 300 MHz spectrometer.

RESULTS AND DISCUSSION

Neat thionyl chloride is a complex liquid. Raman spectra of the liquid provide evidence for association [2]. Relative stabilities of aggregated thionyl chloride have been investigated theoretically; the results are consistent with the Raman data.

The vapor pressure of an aluminum trichloride-thionyl chloride solution as a function of aluminum trichloride concentration exhibits a maximum in the vicinity of 3 M aluminum trichloride [3]. When sulfur dioxide is present in the solution, the relative magnitude of the maximum is enhanced. Infrared spectra of the aluminum trichloride-thionyl chloride solutions show a distinct change in appearance when the concentration of aluminum trichloride is increased from 1.5 to 3.0 M; whereas the spectra for 3.0 and 4.5 M aluminum trichloride solutions are quite similar. The difference is particularly evident in the absorptions near 1100 cm^{-1} -- absorptions attributed to aluminum trichloride-thionyl chloride complexes. The results are interpreted in terms of electrolyte restructuring at the higher aluminum trichloride concentrations.

At very high aluminum trichloride concentrations (1:1 $AlCl_3$:$SOCl_2$), the species $AlCl_2^+$ is formed [2]. This species appears to be complexed by two thionyl chloride molecules. The representative reaction is:

$$2AlCl_3(SOCl_2) = [AlCl_2(SOCl_2)_2]^+ + AlCl_4^-$$

Evidence is also obtained for the 2:1 aluminum trichloride-thionyl chloride complex.

^{27}Al NMR spectra of the electrolytes are relatively simple in appearance. Peaks attributable to the aluminum trichloride-thionyl chloride complexes and to the $AlCl_2^+$ species are observed. In addition, the heptachloroaluminate ion, $Al_2Cl_7^-$, has been tentatively identified. The presence of the latter suggests that both thionyl chloride and the tetrachloroaluminate ion compete for excess aluminum trichloride in the acid electrolyte.

Raman spectra show that lithium ion is complexed in the electrolytes. Molecular orbital calculations have been used to guide the interpretation of the spectral results. Lithium ion in these electrolytes is associated with thionyl chloride. When sulfur dioxide is present, the lithium ion-sulfur dioxide-thionyl chloride complex is present.

In conclusion, the results confirm the complex nature of the electrolytes. The structure of the electrolyte changes with changing composition. The species participating in the electroreduction process therefore also change.

REFERENCES

1. J. Foley, C. Korzeniewski, J. Daschbach, and S. Pons, in Electroanalytical Chemistry, Vol. 14, A.J. Bard, ed., Marcel Dekker, New York, 1986.
2. P.A. Mosier-Boss, J.J. Smith, and S. Szpak, Paper No. 496, 1987 Spring Meeting, The Electrochemical Society, Philadelphia, PA.
3. W.A. West, J.J. Smith, and S. Szpak, unpublished results; W.A. West, S. Szpak, and J.J. Smith, Paper SW-8, 3rd International Meeting on Lithium Batteries, Kyoto, Japan, May 1986.

75-Word Abstract Form

Extended Abstract must be submitted with the 75-Word Abstract by December 1, 1987

Atlanta, Georgia—May 15-20, 1988

Submit to: The Electrochemical Society, Inc.
10 South Main Street, Pennington, NJ 08534-2896
With a copy to the Organizing Chairman

Abstract No. .....
(to be assigned by the Society)

Schedule for Physical Electrochemistry - General Session
(Title of Symposium)

Sponsored by .....
(Division/Group)

Title of paper Electroreduction of $AlCl_3$ - $SOCl_2$ Solutions

Authors (Underline name of author presenting paper.) P. Mosier Boss[1], S. Szpak[1]
J. J. Smith[2] and J. R. Nowak[3]

Business affiliation and address 1 - - Naval Ocean Systems Center, San Diego, CA 92152-5000
2 - - Dept. of Energy, Washington, D.C. 20545
3 - - Office of Naval Research, Arlington, VA 22217-5000
(State or Country) (ZIP Code) (Telephone No.)

(Type abstract in this area—double-spaced.)

The electroreduction of the $AlCl_3$- $SOCl_2$ solution on Pt and Au electrodes is examined by cyclic voltanmetry and IR reflectance spectroscopy. It is shown that the reaction path is governed by the composition of the electrode/electrolyte interphase and that significant changes in the reaction path occur in ca 2.2M $AlCl_3$ in $SOCl_2$. At lower $AlCl_3$ concentrations, only the complexed species undergo reduction while at higher concentrations, free $SOCl_2$ is also reduced. The effect of the electrode material on the reaction path is minimal but not on the reduction rate, which is greater on Pt than Au electrodes.

Do you require any audiovisual equipment?

- ☒ **35 mm (2 x 2 in.) slide projector**
- ☐ **Overhead projector**
- ☐ **Specify other (subject to availability and cost)**

Has the information in this abstract been presented verbally, submitted for publication, or published?

☐ **Yes** ☒ **No**

If the answer is yes, please provide the reference (except in the case of invited review presentations). _____

Is a full length paper on this work to be submitted for Society Journal publication? ☒ **Yes** ☐ **No**

Dr. S. Szpak
Insert name of Society member author or sponsor

ELECTROREDUCTION OF $AlCl_3$ - $SOCl_2$ SOLUTIONS

P. Mosier Boss[1], S. Szpak[1]
J. J. Smith[2] and J. R. Nowak[3]

[1]Naval Ocean Systems Center, San Diego, CA 92152-5000
[2]Dept. of Energy, Washington, D.C. 20545
[3]Office of Naval Research, Arlington, VA 22217-5000

Recently, a series of investigations into the structural aspects and reduction path of $SOCl_2$-bearing electrodes have shown their strong dependence on solution composition. For example, Szpak and Venkatasetty (1) investigated transport properties of $SOCl_2$-based electrolytes, West, et al. (2) looked at the vapor pressure for $AlCl_3$-$SOCl_2$ solutions, Smith, et al. (3) examined the $SOCl_2$ electroreduction path as a function of $AlCl_3$ concentration and Mosier-Boss, et al. (4) discussed structural aspects of these electrolytes from Raman spectroscopic results. All of these investigations indicated that a substantial change in behavior occurred near an $AlCl_3$ concentration of 2M. The present investigation extends the examination of these changes to cyclic voltammetry and IR reflectance spectroscopy of the Pt and Au electrode/electrolyte interphase.

Cyclic Voltammetry - The shape of the voltammograms of the type shown in Fig. 1, depends on both solution composition and sweep rate. For the Pt electrode in 2.0M $AlCl_3$, at low sweep rates (e.g., $10mVs^{-1}$), more than one reduction peak are observed. As the sweep rate increases, the number of peaks is reduced; at $250mVs^{-1}$ only one peak at -0.82V is observed. At the highest sweep rate ($500mVs^{-1}$) the voltammogram resembles that for a 3.0M $AlCl_3$ solution, Fig. 1. Such behavior implies modification of the electrode surface by an absorbing film. The behavior of the Au electrode is similar except that the changes occur at lower concentrations and sweep rates.

IR Reflectance Spectroscopy - The spectral region, 950-1500 cm^{-1}, for 2.0M and 3.0M $AlCl_3$ in contact with a cathodically polarized Pt electrode is shown in Fig. 2. The difference between the spectra is substantial and suggests that in the 2.0M solution, the $AlCl_3$-$SOCl_2$ adduct and the onium complex are preferentially reduced to form SO_2, while in 3.0M solution, the free $SOCl_2$ also undergoes reduction. Similar observations pertain to the Au electrode.

In conclusion, the electroreduction of $SOCl_2$ is a complex process in which the composition of the electrode/electrolyte interphase plays a major role.

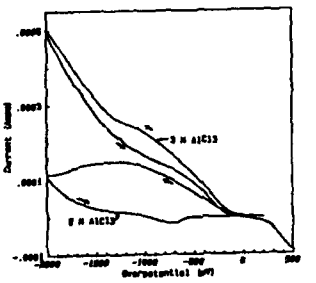

Fig. 1 Cyclic Voltammograms of 2.0M and 3.0M $AlCl_3$ in $SOCl_2$ on Pt at 50 mV s^{-1}.

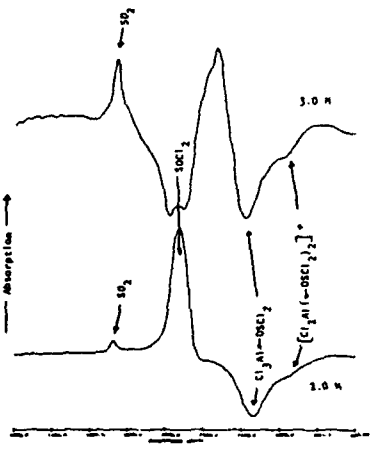

Fig. 2 Infrared Difference Spectra of 2.0M and 3.0M $AlCl_3$ in $SOCl_2$ on Pt at η = -1.0 V vs Ag/Ag Cl.

REFERENCES
1. S. Szpak and H. Venkatasetty, J. Electrochem. Soc.131, 961 (1984)
2. W. West, J. J. Smith and S. Szpak, presentation SW-8, Third International Meeting on Li-Batteries, Kyoto (Japan) May 1986
3. J. J. Smith, S. Pons, J. Li, W. West and S. Szpak, presentation SW-2, Ibid
4. P. A. Mosier-Boss, R. O. Boss, C. J. Gabriel, S. Szpak, J. J. Smith and R. J. Nowak, Trans.Far. Soc. I, submitted

Chicago, Illinois—October 9-14, 1988

Submit to: The Electrochemical Society, Inc.
10 South Main Street, Pennington, NJ 08534-2896
With a copy to the Organizing Chairman

Abstract No. ..... (to be assigned by the Society)

Schedule for Materials and Processes for Lithium Batteries
(Title of Symposium)

Sponsored by .....
(Division/Group)

Title of paper Electroreduction of $SOCl_2$: The Pt/LiCl - $AlCl_3$ - $SOCl_2$ System

Authors (Underline name of author presenting paper.) P. A. Mosier-Boss[1], S. Szpak[1], J. J. Smith[2] and R. J. Nowak[3]

Business affiliation and address (1) Naval Ocean Systems Center, San Diego, CA 92152-5000
(2) Dept. of Energy, Washington, DC 20545
(3) Office of Naval Research, Arlington, VA 22217-5000
(State or Country) (ZIP Code) (Telephone No.)

(Type abstract in this area—double-spaced.)

The electroreduction of $AlCl_3$ - LiCl - $SOCl_2$ solutions on Pt electrode is examined by linear scan voltammetry and IR reflectance spectroscopy. It is shown that the reaction path is governed by the composition of the electrode/electrolyte interphase. In acidic solutions, the onium ion undergoes electroreduction first followed by the solvated lithium ion. The addition of LiCl to the $AlCl_3$ - $SOCl_2$ system not only results in larger current densities but also modifies the adsorption characteristics of the electrode surface.

Do you require any audiovisual equipment?

- ☐ 35 mm (2 x 2 in.) slide projector
- ☒ Overhead projector
- ☐ Specify other (subject to availability and cost)

Has the information in this abstract been presented verbally, submitted for publication, or published?
☐ Yes ☒ No
If the answer is yes, please provide the reference (except in the case of invited review presentations). _____

Is a full length paper on this work to be submitted for Society Journal publication? ☒ Yes ☐ No

Papers presented before a Society technical meeting become the property of the Society and may not be published elsewhere without written permission of the Society. Papers presented at Society technical meetings must be authored by a member or sponsored by an active member.

..... Insert name of Society member author or sponsor

ELECTROREDUCTION OF $SOCl_2$: THE Pt/LiCl - $AlCl_3$ - $SOCl_2$ SYSTEM

P. Mosier Boss[1], S. Szpak[1]

J. J. Smith[2] and J. R. Nowak[3]

[1]Naval Ocean Systems Center, San Diego, CA 92152-5000

[2]Dept. of Energy, Washington, DC 20545

[3]Office of Naval Research, Arlington, VA 22217-5000

An optimization procedure, applied to the Li/$SOCl_2$ battery and based on sound models, falls short of expectations. The reason for this deficiency is attributed to a poor understanding of the elementary processes occurring within the porous structures of practical electrodes(1,2).

In the previous work(3,4), we examined the behavior and properties of a somewhat simpler system: Pt/$AlCl_3$ - $SOCl_2$ and concluded that the electroreduction of $SOCl_2$ in practical electrolytes follows a complex path of the cec-type. Moreover, the surface processes are modified by the selection of the electrode material. The introduction of an additional component, eg LiCl, is expected to complicate further the already complex reaction path. The increase in the complexity is demonstrated by using the ir-reflectance spectroscopy and linear scan voltammetry as the investigative tools.

IR-REFLECTANCE SPECTROSCOPY

The effect of LiCl addition on the composition of the Pt/$AlCl_3$ - $SOCl_2$ interphase both, at rest and cathodically polarized, was examined by the ir-reflectance spectroscopy. Representative results, shown in Figs. 1a and 1b, indicate an active participation of the Li^+ions in the electroreduction process. This participation involves establishment of new equilibria between the various species present at the elctrode surface as well as the corrective adjustment of elementary surface processes. A preliminary analysis suggests that, in acidic solutions, the $SOCl_2$ in the onium ion, $Cl_2Al[(\leftarrow OSCl_2)_2]^+$ is reduced first while in the $Li(\leftarrow OSCl_2)_2^+$ it occurs at $\eta > -1.2$ V. It is noteworthy that prior to its reduction, $Li(\leftarrow OSCl_2)_2^+$ accumulates in the interphase region. Furthermore, we note the formation of $Li(SO_2,SOCl_2)^+$ species at $\eta < -1.2$ V, ie, at potentials associated with the reduction of onium ions.

LINEAR SCAN VOLTAMMETRY

The tendency of $SOCl_2$ to solvate ions and form complexes, as well as the reactivity of the reaction product with other components of practical electrolytes, suggests coupling of the charge transfer to other participating processes. The shape of the lsv curve is governed by the mass balance equation, Eq.(1)

$$\frac{\partial c}{\partial t} = D\frac{\partial^2 c}{\partial x^2} - f(\chi,\lambda) \qquad (1)$$

where the source function $f(\chi,\lambda)$ depends on two parameters, viz. the thermodynamic parameter, $\chi = Kc^0$, and the kinetic parameter, $\lambda = \frac{RT}{nF}\frac{^0k}{v}$. Here, c^0 is the concentration of electroactive species, k is the appropriate rate constant, K is the equilibrium constant, and v is the scan rate. The charge transfer cd, for N electroactive species and M adsorption processes, is given by an expression, Eq.(2)

$$j(0,t) = F\left[\sum_{i=1}^{N} n_i D_i \frac{\partial c(0,t)i}{\partial x} + \sum_{m=1}^{M} \Gamma \frac{d\theta(t)}{dt}\right] \qquad (2)$$

where Γ denotes the maximum surface concentration and θ is the surface coverage.

As illustrated in Fig. 2, the addition of LiCl changes substantially the shape of the lsv curve for otherwise identical experimental conditions. The dominant effects are: (i) current densities are larger in the presence of LiCl, and (ii) the adsorption relationships are modified, especially at potentials less than - 100mV(4).

REFERENCES

1. R. J. Nowak, D. R. Rolison, J. J. Smith and S. Szpak, Electrochim. Acta, in press
2. K. C. Tsaur and R. Pollard, J. Electrochem Soc., 133,2296 (1986)
3. J. J. Smith, S. Pons, J. Li, W. West and S. Szpak, presentation SW-2, Third International Meeting on Li-Batteries, Kyoto (Japan), May 1986
4. P. Mosier-Boss, S. Szpak, J. J. Smith and J. R. Nowak, Ext. Abstr. Nr 487, Electrochem Soc. Spring Meeting, Atlanta GA, May 1988

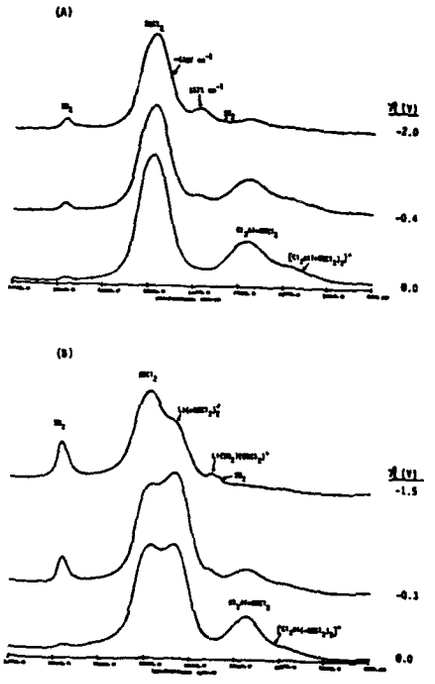

Fig. 1 The 940 - 1400 cm^{-1} spectral region of the metal/electrolyte interphase

A--Pt/4.0 M $AlCl_3$ - $SOCl_2$ interphase

B--Pt/1.0 M LiCl - 4.0 M $AlCl_3$ - $SOCl_2$ interphase

Overpotentials indicated

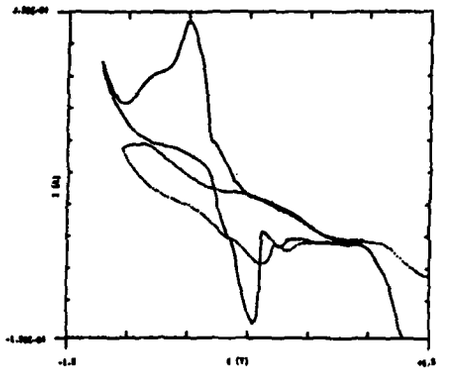

Fig. 2 Cyclic voltammograms

solid line: Pt/0.1 M LiCl-3.0 M $AlCl_3$ - $SOCl_2$ system

dashed line: Pt/3.0 M $AlCl_3$ - $SOCl_2$ system

electrode area: 0.3 cm^2

sweep rate: 30 mV s^{-1}

75-Word Abstract Form

Extended Abstract must be submitted with the 75-Word Abstract by December 1, 1988

Los Angeles, California—May 7-12, 1989

Submit to: The Electrochemical Society, Inc.
10 South Main Street, Pennington, NJ 08534-2896
With a copy to the Organizing Chairman

Abstract No. ..... (to be assigned by the Society)

Schedule for Energy Technology/Physical Electrochemistry
(Title of Symposium)

Sponsored by .....
(Division/Group)

Title of paper On the Reduction of $SOCl_2$: Effect of Electrode Material

Authors (Underline name of author presenting paper.) P. A. Mosier-Boss[1], S. Szpak[1], R. J. Nowak[2], and J. J. Smith[3]

Business affiliation and address 1. Naval Ocean Systems Center, San Diego, CA 92152-5000

2. Office of Naval Research, Arlington, VA 22217-5000

3. Department of Energy, Washington, DC 20545
(State or Country) (ZIP Code) (Telephone No.)

(Type abstract in this area—double-spaced.)

The effect of electrode material on the reduction of $SOCl_2$ is investigated by cyclic voltammetry and *in situ* IR- spectroscopy. Mechanistic features of the reaction path on *Au*, treated (oxidized and reduced) and untreated glassy carbon surfaces are compared with those observed on *Pt* electrodes. The effect of solution composition, including the addition of transition metal phthalocyanines, is examined.

Do you require any audiovisual equipment?

- ☐ 35 mm (2 x 2 in.) slide projector
- ☒ Overhead projector
- ☐ Specify other (subject to availability and cost)

Has the information in this abstract been presented verbally, submitted for publication, or published?
☐ Yes ☒ No
If the answer is yes, please provide the reference (except in the case of invited review presentations). _____

Is a full length paper on this work to be submitted for Society Journal publication? ☒ Yes ☐ No

all authors are Society members
Insert name of Society member author or sponsor

On the Reduction of $SOCl_2$: Effect of Electrode Material

P. A. Mosier-Boss and S. Szpak
Naval Ocean Systems Center, San Diego CA92152-5000
R. J. Nowak
Office of Naval Research, Arlington VA 22217-5000
and
J. J. Smith
Department of Energy, Washington, DC 20545

Earlier observations(1,2) concerning the effect of composition and structure of the positive electrode on the $Li/SOCl_2$ cell performance, suggest an involvement of the electrode material in the charge transfer process. Selected aspects of this involvement were recently discussed by Nowak et al. (3). Here, we present further evidence that the effect of the electrode material on the cell performance cannot and should not be ignored.

Briefly, the sequence of events comprising the charge transfer process in the eg, $AlCl_3$–$SOCl_2$ system, is as follows(4): (i) enrichment of the electrode/electrolyte interphase (including the adsorption) by onium ions, $Cl_2(\leftarrow OSCl_2)_2^+$, and the 1:1 adduct, $Cl_3Al \leftarrow OSCl_2$, (ii) sequential acceptance of two electrons per $SOCl_2$ molecule, of which the first is irreversible while the second is quasi-reversible, and (iii) desorption of reaction products. Molecular orbital calculations suggest the crucial role played by the $S-O$ bond strength in connection with the charge transfer as well as the stability of intermediates in the adsorbed state. These features point to possible catalytic activities of the electrode surface.

The evidence for the interaction between the electrode material and the charge transfer process can be demonstrated by viewing Fig. 1 where cyclic voltammetry curves obtained on Pt and Au electrode surfaces, under otherwise identical conditions (ie, solution composition and scan rate), are displayed. Of interest is the lack of corresponding changes in the IR-spectral region at rest potential as well as in the course of cell discharge, as illustrated in Fig. 2. This lack of correspondence suggests that the effect involves adsorbed species only, ie, it affects the rate of an individual elementary process, a process which most likely interacts with the electrode material. These observations are extended to other electrode materials; in particular, treated glassy carbon surfaces, viz. in the reduced and oxidized states, are examined. The relationship between the morphological features of the LiCl deposit, the electrode treatment and the rate of the charge transfer reaction, is presented.

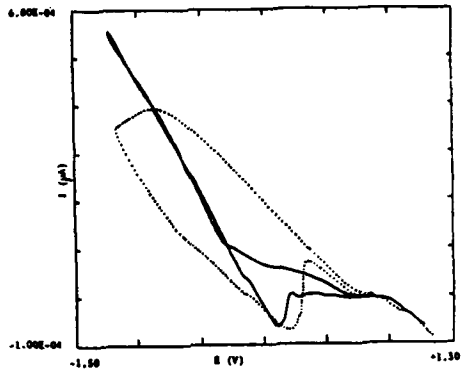

Fig. 1. Cyclic voltammagrams obtained on Pt (——) and Au (.....) at a sweep rate of 10 mV/sec.

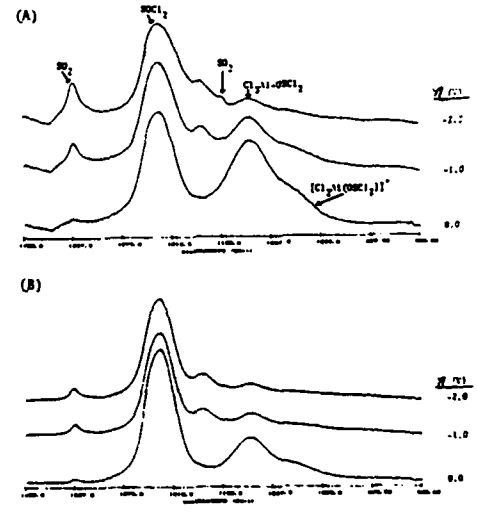

Fig. 2. The 900 to 1400 cm^{-1} spectral region of the metal/electrolyte interphase.
A) Au/4.0 M $AlCl_3$-$SOCl_2$ solution.
B) Pt/4.0 M $AlCl_3$-$SOCl_2$ solution.
Overpotentials indicated.

References

1. J.C. Bailley and G. E. Blomgren, Abstr. Nr 18, Electrochemical Society Fall Meeting, Chicago IL, Oct. 1988 and references therein
2. R. J. Nowak, D. R. Rolison, J. J. Smith and S. Szpak, Electrochim. Acta, 33, 1313 (1988)
3. P. A. Mosier-Boss, R. D. Boss, C. J. Gabriel, S. Szpak, J. J. Smith and R. J. Nowak, J. Chem. Soc. Faraday Trans.,I - in press

75-Word Abstract Form

Extended Abstract must be submitted with the 75-Word Abstract by December 1, 1988

Los Angeles, California—May 7-12, 1989

Submit to: The Electrochemical Society, Inc.
10 South Main Street, Pennington, NJ 08534-2896
With a copy to the Organizing Chairman

Abstract No. .....
(to be assigned by the Society)

Schedule for Energy Technology/Physical Electrochemistry
(Title of Symposium)

Sponsored by .....
(Division/Group)

Title of paper Examination of Pt/LiCl-$AlCl_3$-$SOCl_2$ interphase by relaxation techniques

Authors (Underline name of author presenting paper.) P. A. Mosier-Boss[1], S. Szpak[1], R. J. Nowak[2] and J. J. Smith[3]

Business affiliation and address 1. Naval Ocean Systems Center, San Diego, CA 92152-5000
2. Office of Naval Research, Arlington, VA 22217-5000
3. Department of Energy, Washington, DC 20545
(State or Country) (ZIP Code) (Telephone No.)

(Type abstract in this area—double-spaced.)

The electroreduction of $SOCl_2$ from the $SOCl_2$–$LiCl$–$AlCl_3$ system is of the cec type. Among the relevant processes are the adsorption of onium ion, $Cl_2Al(\leftarrow OSCl_2)_2^+$ and the 1:1 adduct, $Cl_3Al \leftarrow OSCl_2$. The complexity of this reaction is further increased by the interaction of the stable reaction products, viz. Cl^- and SO_2 with the electrolyte components originally present. The complexity of the interphase region is investigated by relaxation techniques and analyzed with the aid of an equivalent electric circuit analog. The interpretation of $E(t)$ and/or $i(t)$ curves arising from galvanostatic and/or potentiostatic perturbations , when combined with the IR spectra, provide a more complete picture of the interphase region.

Do you require any audiovisual equipment?

- ☐ 35 mm (2 x 2 in.) slide projector
- ☒ Overhead projector
- ☐ Specify other (subject to availability and cost)

Has the information in this abstract been presented verbally, submitted for publication, or published?
☐ Yes ☒ No
If the answer is yes, please provide the reference (except in the case of invited review presentations). _____

Is a full length paper on this work to be submitted for Society Journal publication? ☒ Yes ☐ No

all authers are Society members
Insert name of Society member author or sponsor

Examination of $Pt/LiCl-AlCl_3-SOCl_2$ Interphase by Relaxation Techniques

P. A. Mosier-Boss and S. Szpak
Naval Ocean Systems Center, San Diego, CA 92152-5000
R. J. Nowak
Office of Naval Research, Arlington, VA 22217-5000
and
J. J. Smith
Department of Energy, Washington, DC 20545

Previous studies concerning the electroreduction of $SOCl_2$ from the $SOCl_2-AlCl_3$ and $LiCl-AlCl_3-SOCl_2$ systems on Pt electrodes showed clearly the complexity of the system as well as the reaction path(1-3). The electrolyte phase contains the onium ions, $Cl_2Al(\leftarrow OSCl_2)_2^+$, $AlCl_4^-$, 1:1 adducts, $Cl_2Al\leftarrow OSCl_2$, in addition to $(SOCl_2)_2$. When in contact with metallic electrode, eg, platinum, an interphase enriched in complexed species was found. The cyclic voltammograms provided evidence for the cec type with the adsorption of electroactive species playing an important role. The charge transfer process occurs sequentially and appears to be related to the $S-O$ bond strength. The acceptance of the first electron yields a stable molecule which becomes unstable upon the insertion of the second electron and when desorbed from the electrode surface. The details of the instability and the reaction path leading to stable reaction products, ie, Cl^-, SO_2 and S, are not yet known but, most likely, they have no effect on the current/potential relationship except for changing the composition of the electrolyte phase and the associated composition changes within the electrode/electrolyte interphase. Here, additional information is sought via the potential and current relaxations arising from current and potential perturbations. The electrode response to these perturbations is analyzed with the aid of an equivalent electric circuit analog. These responses, when combined with the results of IR- spectroscopy and cyclic voltammetry, constitute yet another set of data to provide a better understanding of the interphase and its effect on the charge transfer step.

References

1. R.J. Nowak, D. R. Rolison, J. J. Smith and S. Szpak, Electrochim. Acta, 33, 1313 (1988)
2. P.A. Mosier-Boss, R. D. Boss, C. J. Gabriel, S. Szpak, J. J. Smith and R. J. Nowak, J. Chem. Soc. Faraday Trans. I - in press
3. P. A. Mosier-Boss, S. Szpak, J. J. Smith and R. J. Nowak, J. Electrochem. Soc. - in press

75-Word Abstract Form

Extended Abstract must be submitted with the 75-Word Abstract by December 1, 1989

Montreal, Quebec, Canada—May 6-11, 1990

Submit to: The Electrochemical Society, Inc.
10 South Main Street, Pennington, NJ 08534-2896
With a copy to the Organizer

Abstract No. .....
(to be assigned by the Society)

Schedule for ..... Physical Electrochemistry .....
(Title of Symposium)

Sponsored by .....
(Division/Group)

Title of paper . Electroreduction of $SO_2Cl_2/AlCl_3$ and $SOCl_2/AlCl_3$ Systems: Similarities and Differences

Authors (Underline name of author presenting paper.) ... P.A. Mosier-Boss,[1] S. Szpak[1], J.J. Smith[2], and R. J. Nowak[3]

Business affiliation and address . 1. Naval Ocean Systems Center, San Diego, CA 92152-5000
2. Department of Energy, Washington D.C. 20545
3. Office of Naval Research, Arlington, VA 22217-5000
(State or Country) (ZIP Code) (Telephone No.)

(Type abstract in this area—double-spaced.)

Electroreduction of the $SO_2Cl_2-AlCl_3$ system on Au, Pt and glassy carbon surfaces is examined. The galvanostatic and potentiostatic pulses as well as cyclic voltammetry indicate that the reaction path is more complex for the reduction of SO_2Cl_2 than for $SOCl_2$. In both cases, the IR- reflectance spectra are consistent with the charge transfer *via* the $S-$ atom. The difference in the reaction paths is attributed to the electronic structure, geometry and chemistry of the species present in solution.

Do you require any audiovisual equipment?

- ☐ 35 mm (2 x 2 in.) slide projector
- ☒ Overhead projector
- ☐ Other equipment at author's expense and subject to availability

Has the information in this abstract been presented verbally, submitted for publication, or published?

☐ Yes ☒ No

If the answer is yes, please provide the reference (except in the case of invited review presentations). _____

Is a full length paper on this work to be submitted for Society Journal publication? ☐ Yes ☐ No

ELECTROREDUCTION OF $SO_2Cl_2/AlCl_3$ AND $SO_2Cl_2/AlCl_3$ SYSTEMS: SIMILARITIES AND DIFFERENCES

P. A. Mosier-Boss and S. Szpak

Naval Ocean Systems Center, San Diego, CA 92152-5000

R. J. Nowak

Office of Naval Research, Arlington, VA 22217-5000

J. J. Smith

Department of Energy, Washington, DC 20545

A systematic study of the electroreduction of an oxychloride-aluminum chloride system has been limited to thionyl chloride(1,2). Much less effort has been devoted to the elucidation of the charge transfer processes involving SO_2Cl_2 (3,4). Our interest in the latter system is due to its potentially high energy density and somewhat higher operating cell voltages. Moreover, the Li/SO_2Cl_2 system shows promising rechargeability and is believed to be safer because no elemental sulfur is formed in the course of battery discharge. Obviously, a better understanding of the species and equilibria occurring in the $SO_2Cl_2/AlCl_3$ solutions as well as the kinetics of the charge transfer are needed. Here we present experimental evidence illustrating the similarities and differences between these two systems.

On the basis of general considerations as well as experimental evidence, the sequence of events during the electroreduction of either $SOCl_2$ or SO_2Cl_2 is: (i) enrichment of the electrode-electrolyte interphase with the reactive species, (ii) sequential acceptance of two electrons through the $S-$ atom, and (iii) desorption of reaction products. However, the examination of galvanostatic and potentiostatic perturbations as well as cyclic voltammetry data indicates a much greater complexity of the charge transfer processes involving the SO_2Cl_2 molecule. The interaction between the electrode material and the participating species is more pronounced, especially on the Au - surface. This added complexity is illustrated in Figs. 1 A and B, where the IR spectra obtained under identical conditions are displayed. In both cases, the involvement of the $S-O$ bond is evident. The identification of species and assignment of the spectral bands observed for the $AlCl_3-SO_2Cl_2$ system awaits the results of molecular orbital calculations, presently in progress. As with the $AlCl_3-SOCl_2$ system, the equilibria and geometry of the reactive species are expected to strongly influence the reaction path of SO_2Cl_2 based electrolytes.

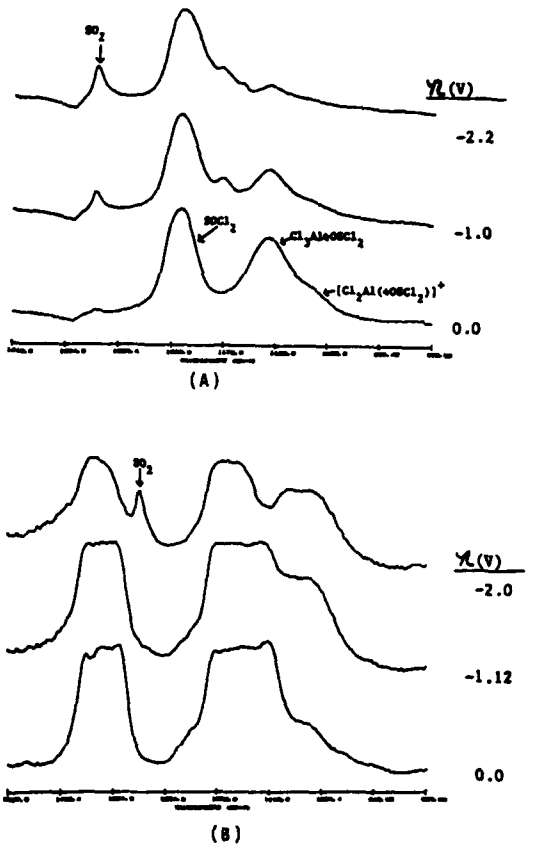

Fig. 1 The $S-O$ stretching spectral region of the metal/electrolyte interphase.
A - Au/ $SOCl_2-AlCl_3$ solution
B - Au/ $SO_2Cl_2-AlCl_3$ solution
Overpotentials indicated.

References
1. P. A. Mosier-Boss, S. Szpak, J. J. Smith and R. J. Nowak, J. Electrochem. Soc., 136, 1282 (1989)
2. P. A Mosier-Boss, S. Szpak, J. J. Smith and R. J. Nowak, J. Electrochem. Soc., 136, 3455 (1989)
3. P. H. Smith, A. A. Papanicolaou, M. H. Wilson and S. D, James, Ext. Abstract Nr 15, Fall Meeting, San Diego Ca, 1986
4. K. A. Klinedinst, Ext. Abstract Nr 33, Fall Meeting, San Diego Ca 1986

MECHANISTIC ASPECTS OF $SOCl_2$ ELECTROREDUCTION

EFFECT OF ELECTRODE MATERIAL

P. A. Mosier-Boss and S. Szpak
Naval Ocean Systems Center, San Diego CA 95152-5000
and
J. J. Smith
Department of Energy, Washington DC 20545

One approach to increase the $Li/SOCl_2$ cell lifetime and discharge rate capabilities is to modify the composition of the Shawinigan black porous structure of the positive electrode. The effect of the various additives, including metallic Pt (1) and Cu (2), the transition metal halides (3) and the transition metal N_4- chelates (4,5), have been examined in some detail. The mechanism by which these additives affect battery performance is not yet fully understood: some of these additives eg, Cu , $CuCl_2$ function as intermediates, others, *e.g.*, $Fe-Pc$ or $Co-Pc$, are thought to act as catalysts.

In this communication, we address the effect of electrode material on the rate constants of the consecutive elementary processes comprising the overall charge transfer reaction. The analysis and semiquantitative conclusions are based on the earlier results of the IR- reflectance spectroscopy and linear scan voltammetry (6) combined with the relaxation characteristics of the metal - electrolyte interphase following the application of a galvanostatic or potentiostatic pulse (7). The electrode materials selected for this discussion include: Pt , Au , Si and glassy carbon.

References

1. K. A. Klinedinst, J. Electrochem. Soc., 128R, 250 (1981)
2. L. R. Giattino, U. S. Patent Nr 4,167,608 (1979)
3. V. V. Behl, J. Electrochem. Soc., 128, 939 (1981)
4. H. V. Venkatasetty, U. S. Patent Nr 4,279,973 (1981)
5. N. Doddapaneni, Ext. Abstr. Nr 360, The Electrochem. Soc. Spring Meeting, Detroit MI (1982)
6. P. A. Mosier-Boss, S. Szpak, J. J. Smith and R. J. Nowak, J. Electrochem. Soc., 136, 1282, 2455 (1989)
7. P. A. Mosier-Boss, S. Szpak, J. J. Smith and R. J. Nowak, Electrochim. Acta, (submitted, Sept. 1989)

INTERCELL CURRENTS IN A MULTIMODULE ASSEMBLY

(Design, Manufacturing and QC considerations)

S. Szpak and P. A. Mosier-Boss
Naval Ocean Systems Center, San Diego CA 95152-5000
and
J. J. Smith
Department of Energy, Washington DC 20545

As a rule, military applications require electrochemical power sources that are both energy and power dense. Thus, systems with a large Gibbs free energy are sought, and to assure stability an electrolyte is kept in a separate container. A common path is provided to either activate cells or circulate the electrolyte.

There are many advantages associated with this approach, *viz.* bipolar cell construction, controlled supply of reactants or removal of products, and a reliable thermal management. These advantages, however, are partially off-set by the parasitic shunting action of the intercell currents. In practice, these currents not only reduce the power output but often affect the structural integrity of the battery functional elements(1).

In a previous communication (2), we concluded that an increase in the number of well designed modules, electrically in parallel - hydrolically in series, does not inherently increase the imbalance in intercell or nodal currents(2). However, in an assembly of modules with one or more defective cells, or with sufficiently large variation among the cell functional elements, a situation arises which substantially reduces the battery lifetime and, on occasion, may lead to catastrophic thermal runaways. In this communication, we will examine, in general terms, design options and the role of quality control procedures during the manufacturing of these batteries and other energy conversion devices.

References

1. S. Szpak, C. J. Gabriel and J. R. Driscoll, J. Electrochem. Soc., 131, 1996 (1984)
2. S. Szpak, C. J. Gabriel, J. J. Smith and J. R. Driscoll, ibid., in press

VIBRATIONAL SPECTROSCOPIC INVESTIGATIONS OF THIONYL CHLORIDE ELECTROLYTES

J. J. SMITH[1], S. PONS[2], J. LI[2], W. WEST[3] AND S. SZPAK[4]

[1]Office of Naval Research, Arlington, VA*
[2]University of Utah, Salt Lake City, UT
[3]Naval Surface Weapons Center, White Oak, MD
[4]Naval Ocean Systems Center, San Diego, CA

While the lithium/thionyl chloride battery has been around for over ten years, the mechanism by which thionyl chloride is reduced electrochemically is not yet established. This lack of information has inhibited the rate of progress toward the development of a safe battery capable of operating at the high energy and power densities for which the system is so attractive. Even now, the discharge reaction for the system is written

$$4Li + 2SOCl_2 = 4LiCl + S + SO_2 \qquad (1)$$

A number of investigations have been made to establish the reaction mechanism and to identify the intermediates present during the discharge process (1). Separately, Istone and Brodd (1) and Attia, et al. (2) have used infrared spectroscopy in an attempt to characterize the thionyl chloride reduction process. Several possible intermediate sulfur-oxygen-chlorine containing species, including SCl_2, S_2O, S_2Cl_2 and SO_2Cl_2, have been observed in the electrolyte during electroreduction, depending on conditions. The difficulty in using infrared spectroscopy for determining the intermediates lies in the complexity of the spectra, particularly in the region between 400 and 900 cm^{-1}, a region where most of the electrolyte components have absorptions. Recently, in situ Fourier transform infrared spectroelectrochemistry, specifically SNIFTIRS (3), has been shown to be a valuable technique for elucidating electrochemical processes. This technique has been applied to the electroreduction of $SOCl_2$ electrolytes; the results are presented here.

Lithium/thionyl chloride batteries have been produced with both neutral (lithium tetrachloroaluminate supporting electrolyte) and acidic (excess aluminum trichloride) electrolytes. Both have been investigated in this work using the experimental procedure reported earlier (4). The electroreduction was performed at a polished platinum electrode surface. Electrolyte compositions between 1.5 and 4.5M aluminum trichloride with varying amounts of added lithium chloride were investigated.

The initial thrust was to characterize the electrolyte composition. The formation of various complexes in the electrolytes and their involvement in the electroreduction are established (5). Figure 1 shows the SNIFTIRS spectra of three solutions of aluminum trichloride in thionyl chloride at the concentrations of 1.5, 3.0 and 4.5M. A significant change in appearance occurs when the concentration of $AlCl_3$ is increased from 1.5 to 3.0M; the spectra for the 3.0 and 4.5M solutions are very similar. This is evidence for a change in composition of the solution at the higher $AlCl_3$ concentrations. The strong absorption at approximately 1100 cm^{-1} is due to the $AlCl_3 \cdot SOCl_2$ complex in which the aluminum chloride is associated with the oxygen in thionyl chloride. It is likely that the absorptions in the region 500-700 cm^{-1} are also due in part to the complex. The change in spectral appearance as the concentration of $AlCl_3$ is increased is attributed to the formation of the higher adducts of $AlCl_3$ with $SOCl_2$.

Figure 2 shows the SNIFTIRS spectra taken at the potential corresponding to the maximum in the cyclic voltammetry curve for the reduction of the thionyl chloride electrolytes containing various concentrations of aluminum trichloride and lithium chloride. Increased absorption corresponds to species produced by the electrochemistry whereas reduced absorption (upward point peaks) are associated with species whose concentrations decrease as a result of the electrochemical process. For the acidic electrolytes, the major reactant is the aluminum chloride-thionyl chloride adduct(s) and the most identifiable product is SO_2 (from the strong absorption at 1335 cm^{-1}). The results for the neutral electrolytes show similarities in product species, however, the aluminum trichloride-thionyl chloride complexes are no longer involved in the reaction.

Figure 3 is the spectrum taken at a potential near -2.5 volts vs. platinum. This potential is at the center of the lowest potential reduction peak in the cyclic voltammogram. It is clear from the spectrum that this process is the electroreduction of sulfur dioxide confirming the suggestion of Istone and Brodd (1).

Collectively, the results of this investigation permit specific conclusions to be drawn about the mechanisms for the electroreduction processes in neutral and acid electrolytes. These will be presented in detail.

*Present address, Naval Weapons Center, China Lake, CA 93555

REFERENCES

1. Istone, W. K. and Brodd, R. J., J. Electrochem. Soc. 131, 2467 (1984) and references therein.

2. Attia, A. I., Sarrazin, C., Gabriel, K. A. and Burns, R. P., ibid, 131, 2523 (1984).
3. Foley, J. W. Korzeniewski, C. Daschbach, J. and Pons, S., "Electro-analytical Chemistry," A. J. Bard, Ed., Marcel Dekker, New York, in press.
4. Li, J., Pons, S. and Smith, J. J., Langmuir, in press.
5. Klinedinst, K. A., J. Electrochem. Soc., 128, 2507 (1981).

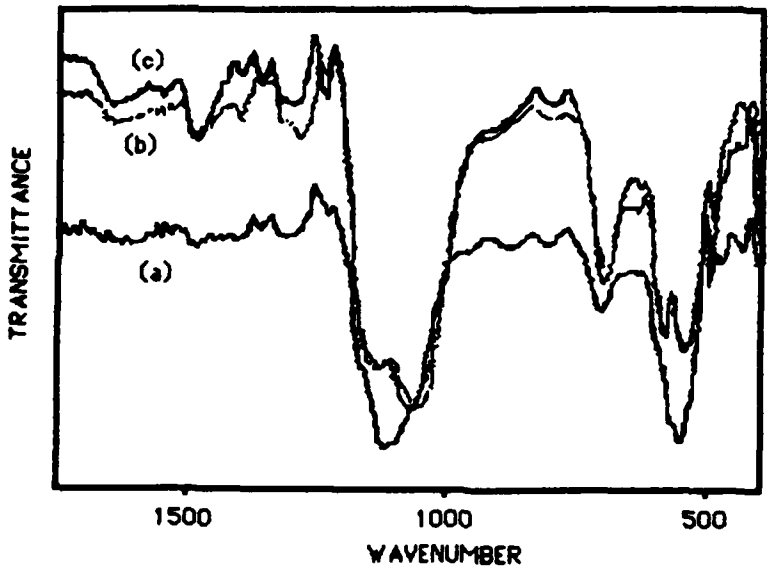

FIGURE 1. SPECTRA OF $AlCl_3$ - $SOCl_2$ SOLUTIONS (a) 1.5 M; (b) 3.0 M; (c) 4.5 M

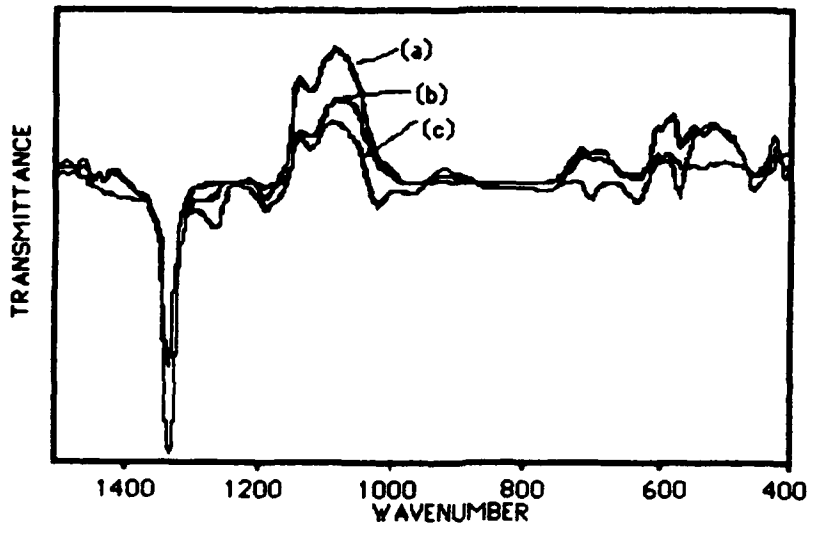

FIGURE 2. SPECTRA OF THIONYL CHLORIDE ELECTROREDUCTION
(a) 1.5 M $AlCl_3$ + 0.75 M LiCl; (b) 3.0 M $AlCl_3$ + 0.75 LiCl;
(c) 4.5 M $AlCl_3$ + 0.75 M LiCl

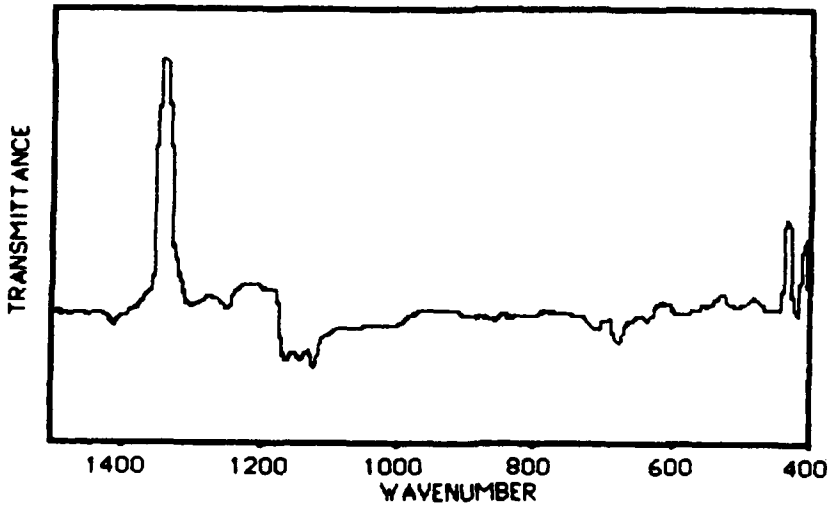

FIGURE 3. SPECTRUM OF THIONYL CHLORIDE ELECTROREDUCTION
1.5 M $AlCl_3$ + 1.5 M LiCl; V = -2.5 V vs Pt; ref at -0.9 V

4.0 TABLES OF CONTENTS

This section contains the tables of contents of Volumes I and II of this report. They serve as a quick reference.

This page intentionally left blank

Assessment of $Li/SOCl_2$ Battery Technology: Reserve, Thin-Cell Design

Technical Report 1154, April 1987, Volume I

Dr. S. Szpak

Naval Ocean Systems Center

Dr. J. R. Driscoll

Lockhead Missiles and Space Company

Palo Alto Research Laboratories

CONTENTS

Assessment of $Li/SOCl_2$ Battery Technology: Reserve, Thin-Cell Design

Technical Report 1154, April 1987, Volume II

Dr. S. Szpak

Naval Ocean Systems Center

Dr. J. R. Driscoll

Lockhead Missiles and Space Company

Palo Alto Research Laboratories

Table of Contents

2-3. **High Rate $Li/SOCl_2$ Power Source: Approach and Progress**, S. Szpak and H. V. Venkatasetty, 13th International Power Sources Symposium, 403 (1982).

2-23. **Investigation of Positive Electrode Characteristics in High Rate $Li/SOCl_2$ Cells**, S. Szpak and J. R. Driscoll, J. Power Sources, 10, 343 (1983).

2-35. **Properties of $SOCl_2$-Based Electrolytes. 1. Conductivity, Viscosity, and Density**, H. V. Venkatasetty and S. Szpak, J. Chem. Eng. Data, 28, 47 (1983).

2-41. **Determination of the Thermoneutral Potential of $Li/SOCl_2$ Cells**, N. A. Godshall and J. R. Driscoll, J. Electrochem. Soc., 131, 2221 (1984).

2-47. **Reaction Products on Current or Potential Reversal in $Li/SOCl_2$ Cells**, B. J. Carter, H. A. Frank and S. Szpak, J. Power Sources, 13, 287 (1984).

2-57. **Transport Properties of Aluminum Chloride-Thionyl Chloride-Based Electrolytes**, S. Szpak and H. V. Venkatasetty, J. Electrochem. Soc., 131, 961 (1984).

2-65. **Investigation of $SOCl_2$ Reduction by Cyclic Voltammetry and AC Impedance Measurements**, M. J. Madou and S. Szpak, J. Electrocem. Soc., 131, 2471 (1984).

2-71. **Mathematical Modeling of the Lithium, Thionyl Chloride Static Cell. I. Neutral Electrolyte**, K. Tsaur and R. Pollard, J. Electrochem. Soc., 131, 975 (1984).

2-81. **Mathematical Modeling of the Lithium, Thionyl Chloride Static Cell. II. Acid Electrolyte**, K. Tsaur and R. Pollard, J. Electrochem. Soc., 131, 984 (1984).

2-89. **$Li/SOCl_2$ Battery Intercell Currents**, S. Szpak, C. J. Gabriel and J. R. Driscoll, J. Electrochem. Soc., 131, 1996 (1984).

2-99. **Development of a High-Rate $Li/SOCl_2$ System: Theory vs. Practice**, J. R. Driscoll, R. Pollard, J. J. Smith and S. Szpak, 14th International Power Sources Symposium, 1984.

2-113. **Selected Aspects of High Rate $Li/SOCl_2$ Power Sources Technology**, J. R. Driscoll, R. Pollard, J. J. Smith and S. Szpak, pres. Nr. 859124, 20 th IECEC, Miami Beach FL, 1985.

2-123. **Thermal Behaviour of $Li/SOCl_2$ Batteries of Thin Cell Design**, L. A. Parnell and S. Szpak, Electrochim. Acta, 30, 913 (1985).

2-133. **Thermal Behavior of Electrochemical Cells by Liquid Crystal Display**, J. R. Driscoll and S. Szpak, J. of Power Sources, 14, 321 (1985).

2-141. **Precipitation of Solids in Electrochemical Cells**, K. Tsaur and R. Pollard, J. Electrochem. Soc., 133, 2296 (1986).

2-155. **Function of Electrocatalysis on the Reduction of $SOCl_2$ at Porous Electrodes**, J. J. Smith, S. Szpak ans W. A. West, 15th International Power Sources Symposium, 1986.

2-167. **Catastrophic Thermal Runaway in Lithium Batteries**, S. Szpak, C. J. Gabriel and J. R. Driscoll, Electrochim. Acta, 32, 239 (1987).

2-177. **Resolution of Vibrational Bands into Voight Profiles**, C. J. Gabriel, P. A. Mosier-Boss and S. Szpak, Spectrochim. Acta, in press.

2-185. **Scale-Up Problems in Batteries for Propulsion**, P. A. Mosier-Boss, L. A. Parnell and S. Szpak, AIAA/SAE/ASME/ASEE 23rd Joint Propulsion Conference, San DIego CA, 1987.

2-191. **Comments on Electroreduction of $SOCl_2$**, M. J. Madou, J. J. Smith and S. Szpak, J. Electrochem. Soc., in press.

REPORT DOCUMENTATION PAGE

Form Approved
OMB No. 0704-0188

1. AGENCY USE ONLY *(Leave blank)*	2. REPORT DATE	3. REPORT TYPE AND DATES COVERED
	June 1990	Final: April 1987 – June 1990

4. TITLE AND SUBTITLE
ASSESSMENT OF $Li/SOCl_2$ BATTERY TECHNOLOGY RESERVE, THIN-CELL DESIGN

5. FUNDING NUMBERS
PE: 0602936N
PROJ: ZE87-634
SUB PROJ: RV36I21
AGENCY ACC: DN309 109

6. AUTHOR(S)
P. A. Mosier-Boss and S. Szpak

7. PERFORMING ORGANIZATION NAME(S) AND ADDRESS(ES)
Naval Ocean Systems Center
San Diego, CA 92152-5000

8. PERFORMING ORGANIZATION REPORT NUMBER
NOSC TR 1154
Vol. III

9. SPONSORING/MONITORING AGENCY NAME(S) AND ADDRESS(ES)
Office of the Chief of Naval Research, Arlington, VA 22217 and
Independent Exploratory Development Programs (IED), NOSC

10. SPONSORING/MONITORING AGENCY REPORT NUMBER

11. SUPPLEMENTARY NOTES

12a. DISTRIBUTION/AVAILABILITY STATEMENT
Approved for public release; distribution is unlimited.

12b. DISTRIBUTION CODE

13. ABSTRACT *(Maximum 200 words)*

This volume is a compilation of technical papers that strengthens the technology base for high-discharge rate $Li/SOCl_2$ batteries and is a continuation of Volume II. This volume also contains abstracts of presentations given at meetings in 1986-1990 and the tables of contents of the previous two volumes.

14. SUBJECT TERMS
$Li/SOCl_2$ system
thin-cell batteries
electrode material

15. NUMBER OF PAGES
242

16. PRICE CODE

17. SECURITY CLASSIFICATION OF REPORT	18. SECURITY CLASSIFICATION OF THIS PAGE	19. SECURITY CLASSIFICATION OF ABSTRACT	20. LIMITATION OF ABSTRACT
UNCLASSIFIED	UNCLASSIFIED	UNCLASSIFIED	SAME AS REPORT